Mathematical modelling and optimization of enzymatic cascades for the synthesis of industrially valuable products

Česnik, Morana

SVEUČILIŠTE U ZAGREBU
FAKULTET KEMIJSKOG INŽENJERSTVA I TEHNOLOGIJE

Kandidatkinja **Morana Česnik**
predala je dana: 17. svibnja 2019. doktorski rad izrađen pod mentorstvom prof. dr. sc. Zvjezdane Findrik Blažević, Fakultet kemijskog inženjerstva i tehnologije Sveučilišta u Zagrebu.

Povjerenstvo za ocjenu doktorskog rada u sastavu:

Prof. emerita Đurđa Vasić-Rački, Fakultet kemijskog inženjerstva i tehnologije Sveučilišta u Zagrebu
Prof. dr. sc. Pere Clapés, Institute of Advanced Chemistry of Catalonia, CSIC, Barcelona
Prof. dr. sc. Marija Vuković Domanovac, Fakultet kemijskog inženjerstva i tehnologije Sveučilišta u Zagrebu

pozitivno je ocijenilo doktorski rad doktorandice Morane Česnik, a Fakultetsko vijeće Fakulteta kemijskog inženjerstva i tehnologije Sveučilišta u Zagrebu na sjednici održanoj dana 23. rujna 2019. prihvatilo je ocjenu i odobrilo obranu doktorskog rada pred povjerenstvom u istom sastavu.

Obrana doktorskog rada održana je dana 4. listopada 2019.

D e k a n

Prof. dr. sc. Tomislav Bolanča

University of Zagreb

FACULTY OF CHEMICAL ENGINEERING AND TECHNOLOGY

Morana Česnik

MATHEMATICAL MODELLING AND OPTIMIZATION OF ENZYMATIC CASCADES FOR THE SYNTHESIS OF INDUSTRIALLY VALUABLE PRODUCTS

DOCTORAL THESIS

Zagreb, 2019

Sveučilište u Zagrebu

FAKULTET KEMIJSKOG INŽENJERSTVA I TEHNOLOGIJE

Morana Česnik

MATEMATIČKO MODELIRANJE I OPTIMIZACIJA ENZIMSKIH KASKADA ZA SINTEZU INDUSTRIJSKI VRIJEDNIH PRODUKATA

DOKTORSKI RAD

Zagreb, 2019.

University of Zagreb

FACULTY OF CHEMICAL ENGINEERING AND TECHNOLOGY

MORANA ČESNIK

MATHEMATICAL MODELLING AND OPTIMIZATION OF ENZYMATIC CASCADES FOR THE SYNTHESIS OF INDUSTRIALLY VALUABLE PRODUCTS

DOCTORAL THESIS

Mentor:
Prof. Zvjezdana Findrik Blažević, PhD

Zagreb, 2019

Sveučilište u Zagrebu

FAKULTET KEMIJSKOG INŽENJERSTVA I TEHNOLOGIJE

MORANA ČESNIK

MATEMATIČKO MODELIRANJE I OPTIMIZACIJA ENZIMSKIH KASKADA ZA SINTEZU INDUSTRIJSKI VRIJEDNIH PRODUKATA

DOKTORSKI RAD

Mentor:
Prof. dr. sc. Zvjezdana Findrik Blažević

Zagreb, 2019.

Bibliographic facts:

UDC: 66.011:577.15:544.4(043.3)=111

Scientific area: Technical Sciences

Scientific field: Chemical Engineering

Scientific branch: Reaction Engineering

Institution: University of Zagreb, Faculty of Chemical Engineering and Technology, Department of Reaction Engineering and Catalysis

Supervisor: Prof. Zvjezdana Findrik Blažević, PhD

Number of pages: 182

Number of figures: 89

Number of tables: 49

Number of appendixes: 10

Number of references: 128

Date of defense: October 4th 2019

Members of the Committee for defense of the thesis:

1. Prof. emer. Đurđa Vasić-Rački, PhD, Faculty of Chemical Engineering and Technology, University of Zagreb, Croatia
2. Prof. Pere Clapés, PhD, Catalonia Institute for Advanced Chemistry-CSIC, Barcelona, Spain
3. Prof. Marija Vuković Domanovac, PhD, Faculty of Chemical Engineering and Technology, University of Zagreb, Croatia

Dissertation is stored at:

1. National and University Library Zagreb, Hrvatske bratske zajednice bb, Zagreb; Library of Faculty of Chemical Engineering and Technology, University of Zagreb, Marulićev trg 20, Zagreb;
2. Library of University of Rijeka, Dolac 1, Rijeka;
3. Library of University of Split, Livanjska 5, Split and
4. Library of University of Osijek, Europska avenija 24, Osijek.

Dissertation topic was accepted on 214th regular session of Council of the Faculty of Chemical Engineering and Technology, University of Zagreb held on February 26th 2018, and approved at 11th session of the Senat of the University of Zagreb held on May 15th in 349th academic year (2017/2018).

Information about the supervisor

Prof. Zvjezdana Findrik Blažević, PhD

Zvjezdana Findrik Blažević [redacted] got her diploma at the Faculty of Chemical Engineering and Technology, University of Zagreb in 2002. She was employed in 2002 at the Department of Reaction Engineering and Catalysis at the Faculty of Chemical Engineering and Technology, University of Zagreb as junior researcher – younger assistant on the project "Biocatalysts and biotransformations" led by prof. dr. sc. Đurđa Vasić-Rački. She finished her MSc thesis in 2004 and PhD in 2006 in Technical Sciences/Chemical Engineering/Reaction Engineering. The topic of her PhD study was: "Study of reactions catalysed by amino acid oxidases". She was an assistant professor from 2009, an associate professor from 2012 and is a full professor from 2018.

In 2002 she got the Rector's award for student's work, in 2005 the Award of the Society of University Teachers, Scholars and other Scientists – Zagreb, in 2006 National Science Award – Annual Award for Junior Researchers – in the field of Biotechnical Sciences, and in 2009 Award of the Academy of Engineering – award to young scientist 'Vera Johanides'.

She spent some time abroad in foreign institutions: Department of Technical Chemistry, University of Rostock, Germany, in 2002 (2 months), Institute of Biotechnology of the Research Center Jülich, Germany, in 2004 (2 months) and 2007 (1 month), and the Institute for the Advanced Chemistry, CSIC, Barcelona, Spain, in 2010 (1 month).

She was head of the Department of Reaction Engineering and Catalysis in academic years 2011/2012 and 2012/2013. From 2013 she is ECTS coordinator of the Faculty of Chemical Engineering and Technology, University of Zagreb and is currently a member of several Faculty committees.

Her work is focused on the application of biocatalysts in purified or partially purified form, and enzyme reaction engineering. She applies optimization methods on biocatalytic processes, particularly multi-enzyme systems. She also works on isolation and purification of biocatalysts from microorganisms.

She has published one book chapter, 30 scientific papers in journals cited in CC and SCI data bases, 7 papers in other journals, 7 papers in proceedings from national and international conferences. She gave four invited lectures at national and international conferences and two invited lectures at international summer school, and one plenary lecture

on a national conference. She participated in organization of eleven scientific and professional conferences, and was president of the scientific and organizing committee of one of them.

She led one international project and a research group at another international project (FP6). She is currently a project partner of the Horizon 2020 international project Carbazymes and associate in a project EnzyFluor financed by the Croatian Science Foundation. She is also a coordinator of a CEEPUS network – Chemistry and Chemical Engineering (CIII-SI-0708). She participated in realization of 7 projects financed by Ministry of Science Education and Sports of Croatia, and two projects financed by the Ministry of Education of Hungary.

She was a supervisor of 20 BSc theses, 16 MSc theses, 1 PhD thesis and is currently a supervisor of 3 PhD theses.

She is a member of the Croatian Society of Chemical Engineers, the Society of University Teachers, Scholars and other Scientists – Zagreb and the European Federation of Biotechnology, where she is a Croatian delegate in the Section on Applied Biocatalysis.

She is a member of the Editorial Board of Hungarian Journal of Industry and Chemistry. She reviewed more than 70 papers in international journals, several international projects and PhD theses from abroad.

This PhD thesis was supported by the European Union's Horizon 2020 project CarbaZymes: Sustainable industrial processes based on a C–C bond-forming enzyme platform, contract Grant Agreement No. 635595.

Acknowledgments

This work was supported by the Horizon 2020 project CarbaZymes: Sustainable industrial processes based on a C–C bond-forming enzyme platform, contract Grant No. 635595.
I would also like to acknowledge the support from COST project: CM1303 Systems Biocatalysis.

My greatest thanks go to my mentor and my dear friend prof. Zvjezdana Findrik Blažević. Thanks for all the guidelines, help and discussions throughout the whole period of my doctoral research. Your help and selflessly invested time had a great influence on the thesis outcomes as well as on my personal success and feeling of content. Thank you.

I would like to thank prof. Đurđa Vasić-Rački for her genuine interest in my work and all the given advices based on her rich scientific experience.
Thanks to Martina Sudar, PhD who was a most helpful colleague throughout my research, especially during the first period in the lab. Her advices helped me overcoming obstacles more easily.
Thanks to my colleagues Anera, Lela, Nataša, Martin, Nevena, Dino and prof. Ana for all the pleasant hours in the office and lab.
I would like to thank prof. Pere Clapés for all the advices, support, supply of the chemicals and enzymes needed for my work and for the hospitality during my stay in Barcelona at the Institute for the Advanced Chemistry. I would also like to thank Raquel, Karel and Rosér for a warm and friendly atmosphere during my stay.
I would like to thank Prozomix Ltd, Simon and Mimi in particular, for supplying numerous enzymes for my research.
I would like to thank prof. Wolf-Dieter Fessner for supplying FSA variants used in this research.
I thank prof. Aurelio Hidalgo and Sandra Bosch for supplying aldolases YfaUs used in this research.
I thank prof. Marija Vuković Domanovac for a successful cooperation during my PhD that resulted in publishing a review article.
Thanks to Marin and Matija for helping me performing LC-MS analysis of my samples and to Comprehensive Water Technology for their hospitality.
Thanks to the students Mladena, Dino, Anamarija, Lucija, Paula and Lucija for the lab work they helped me with.

Thanks to Goran for the (second time) fun times in the office and for keeping me on the „right way" together with Mladen and Martina.
Thanks to my SES group INA colleagues. Our friendship, fun times and mutual support overcome time.
Thanks to my friends and family, especially Iva, Vedran and Sonja, for their support during this challenging period of my life.
Thanks to my parents for their love and never fading support.
Thanks to Matija for his love, joy and unconditional support. Our fruitful discussions regarding our decisions easily confirm and clarify our true life goals and haven't failed us yet.

“The great book, always open and which we should make an effort to read, is that of Nature.”

Antoni Gaudí

ABSTRACT

Biocatalysis is in focus due to its use for the synthesis of pharmaceuticals making manufacturing processes more sustainable. In recent years, much interest has been shown in the use of multi-enzyme cascades as a tool in organic synthesis. Reaction engineering methodology was used in this thesis for describing and optimizing three separate biocatalytic cascade reaction systems. The link between all cascades was the use of carbon–carbon bond forming enzyme in one reaction step per cascade.

Cascade reaction that synthesises 3-hydroxyisobutyric acid, a methacrylic acid precursor used as important intermediate for the preparation of polymers, is a novel approach that consists of three enzymes. Proposed biocatalytic synthesis of 3-hydroxyisobutyric acid can be performed by aldolase-catalysed aldol addition of propanal to formaldehyde followed by an enzymatic oxidation catalysed by aldehyde dehydrogenase of the resulting 3-hydroxy-2-methylpropanal to 3-hydroxyisobutyric acid with coenzyme regeneration by NADH oxidase. Developed mathematical model for aldol addition was used for the reaction optimization. At the optimal process conditions, the aldol addition product concentration after 5.5 hours was 814 mM (72 g L^{-1}), product yield was 88.5% and volume productivity was 313.7 g L^{-1} d^{-1}. Since aldehyde dehydrogenase accepts propanal and formaldehyde as substrates, this cascade could not be performed in a one-pot synthesis, but consecutive, by starting oxidation after aldol addition was completed. Panel of 25 aldehyde dehydrogenases was tested as oxidation step catalyst. Mathematical model of oxidation with coenzyme regeneration by NADH oxidase was developed and validated. It was confirmed by NMR analysis that proposed enzymatic cascade scheme produced desired product, 3-hydroxyisobutyric acid. The yield on oxidation product of 66.5% was achieved with the final product concentration of 26.32 mM (2.7 g L^{-1}).

The second optimized cascade reaction in this work is the biocatalytic synthesis of amino acid L-homoserine in a cascade containing Class II pyruvate-dependent aldolase and transaminase as biocatalysts starting from formaldehyde and pyruvate, and L-alanine used in transamination reaction step. Reactions catalysed by separate enzymes (cell free extracts) and *E. coli* cells containing the same co-expressed enzymes were optimized based on developed mathematical model. Detailed kinetic parameters comparison is made between those two types of biocatalysts. Optimized reaction performed in the fed-batch reactor produced 672 mM (80.1 g L^{-1}) of L-homoserine after 25 hours of reaction with volume productivity of 76.23 g L^{-1} d^{-1} with cell free extract enzymes as catalysts, and 640.74 mM (76.3 g L^{-1}) of L-

homoserine with volume productivity of 62 g L^{-1} d^{-1} when whole cells containing both enzymes were used as catalysts.

The third cascade reaction was the synthesis of iminosugar precursor. Two strategies for biocatalytic production of iminosugar precursor were proposed and examined within this doctoral thesis. One approach suggested Cbz-*N*-3-amino-1,2-propanediol and second approach involved 3-chloro-1,2-propanediol as oxidation substrate. Only cascade system from the first approach produced the desired aldol adduct, an iminosugar precursor whose molecular mass was confirmed by LC-MS analysis. Research drawback was caused by incomplete kinetic measurements due to the fact that intermediates and final product molecules are not commercially available chemicals and therefore no comprehensive mathematical model could be developed. Nevertheless, with available kinetic measurements and parameters determined and experience gained during process investigation, some important conclusions regarding this biocatalytic synthesis were withdrawn and substrate conversion of 64% corresponding to product concentration of 13.32 mM (4.2 g L^{-1}) was achieved.

Key words: biocatalysis, enzyme, iminosugar, L-homoserine, methacrylic acid, process optimization, reaction engineering

SAŽETAK

Biokataliza je u središtu pozornosti zbog njezine upotrebe za sintezu lijekova čineći proizvodne procese održivijima. Posljednjih godina pokazalo se veliko zanimanje za korištenje višeenzimskih kaskada kao alata u organskoj sintezi. U ovom je radu korištena metodologija reakcijskog inženjerstva kako bi se opisala i optimizirala tri odvojena biokatalitička kaskadna reakcijska sustava. Veza između istraživanih sustava bila je upotreba enzima koji stvaraju vezu između ugljikovih atoma u jednom od reakcijskih koraka.

Kaskadna reakcija kojom se sintetizira 3-hidroksiizomaslačna kiselina, prekursor metakrilne kiseline koja se koristi kao važan međuprodukt za pripravu polimera, novi je pristup koji se sastoji od upotrebe triju enzima. Predložena biokatalitička sinteza 3-hidroksiizomaslačne kiseline može se provesti aldolnom adicijom propanala na formaldehid kataliziranom aldolazom, nakon čega slijedi enzimska oksidacija dobivenog 3-hidroksi-2-metilpropanala katalizirana aldehid dehidrogenazom u 3-hidroksiizomaslačnu kiselinu uz regeneraciju koenzima kataliziranu NADH-oksidazom. Razvijeni matematički model aldolne adicije korištenje za optimizaciju reakcijskih uvjeta. Pri optimalnim procesnim uvjetima, koncentracija produkta aldolne adicije nakon 5,5 sati iznosila je 814 mM (72 g L^{-1}), iskorištenje na produktu 88,5%, a volumna produktivnost 313,7 g L^{-1} d^{-1}. Budući da aldehid dehidrogenaza prihvaća propanal i formaldehid kao supstrate, ova se kaskada ne može provesti u reaktoru odjednom, već uzastopno pokretanjem oksidacije nakon što reakcija aldolne adicije završi. U svrhu pronalaska katalizatora za reakciju oksidacije ispitano je 25 različitih aldehid dehidrogenaza. Razvijen je i validiran matematički model oksidacije uz regeneraciju koenzima kataliziranu NADH-oksidazom. NMR analizom potvrđeno je da predložena enzimska kaskadna reakcija proizvodi željeni produkt, 3-hidroksiizomaslačnu kiselinu. Postignuto je iskorištenje na oksidacijskom produktu od 66,5% uz koncentraciju produkta od 26,32 mM (2,7 g L^{-1}).

Druga optimizirana kaskadna reakcija u ovom radu je biokatalitička sinteza aminokiseline L-homoserina u kaskadi kataliziranoj piruvat-ovisnom aldolazom klase II i transaminazom, gdje su početni supstrati formaldehid i piruvat te L-alanin koji se koristi u reakciji transaminacije. Na temelju razvijenog matematičkog modela optimizirane su reakcije katalizirane zasebnim enzimima (ekstrakt stanica bez stanične stijenke) i stanicama *E. coli* koje sadrže iste enzime dobivene ko-ekspresijom. Napravljena je detaljna usporedba kinetičkih parametara za navedena dva tipa biokatalizatora. Provođenjem optimizirane reakcije u šaržnom reaktoru proizvedeno je 672 mM (80,1 g L^{-1}) L-homoserina nakon 25 sati

reakcije s volumnom produktivnosti od 76,23 g L^{-1} d^{-1} koristeći ekstrakte enzima kao katalizatore te 640,74 mM (76,3 g L^{-1}) L-homoserina uz volumnu produktivnost od 62 g L^{-1} d^{-1} kada su kao katalizator korištene cijele stanice koje sadrže oba enzima.

Kao treća kaskadna reakcija, u ovoj su doktorskoj disertaciji predložene i ispitane dvije strategije za biokatalitičku proizvodnju prekursora iminošećera. Jedan pristup temelji se na Cbz-*N*-3-amino-1,2-propandiolu, a drugi na 3-kloro-1,2-propandiolu kao početnim supstratima. Kaskadni sustav prvog pristupa jedini je proizveo željeni aldolni produkt, prekursor iminošećera, čija je molekularna masa potvrđena LC-MS analizom. Nedostatak ovog istraživanja proizlazi iz nepotpunih kinetičkih mjerenja zbog činjenice da međuprodukti i produkti ovog reakcijskog sustava nisu komercijalno dostupne kemikalije. Iz tog razloga nije bilo moguće razviti sveobuhvatan matematički model. Ipak, s raspoloživim kinetičkim mjerenjima i procijenjenim parametrima te iskustvom stečenim tijekom istraživanja ove biokatalitičke sinteze, izvedeni su važni zaključci te je postignuta konverzija supstrata od 64% koja odgovara koncentraciji proizvoda od 13,32 mM (4,2 g L^{-1}).

Ključne riječi: biokataliza, enzim, iminošećer, L-homoserin, metakrilna kiselina, optimizacija procesa, reakcijsko inženjerstvo

TABLE OF CONTENTS

1 INTRODUCTION 1
2 BIOCATALYSIS 5
2.1 Biocatalytic cascade reactions 5
2.2 Enzymatic carbon–carbon bond formation 6
2.3 Protein engineering and overexpression 6
2.4 Coenzyme regeneration 8
3 THESIS FRAMEWORK: Biosynthesis of industrially valuable products 9
3.1 Methacrylic acid 9
3.2 L-homoserine 9
3.3 Iminosugars 11
4 MATHEMATICAL MODELLING AND PROCESS OPTIMIZATION 13
4.1 Kinetic models 14
4.2 Mass balance equations 17
4.2.1 Batch reactor 17
4.2.2 Fed-batch reactor 18
4.3 Kinetic modelling of cell free extract enzymes and enzymes contained in cells 18
5 SYNTHESIS OF METHACRYLIC ACID PRECURSOR 21
5.1 Introduction 21
5.2 Experimental part 22
5.2.1 Materials 22
5.2.2 Apparatus 23
5.2.3 Analytical methods 23
5.2.4 Experimental procedures 25
5.3 Results and discussion 36
5.3.1 FSA^{D6Q} overexpression in E. coli 36
5.3.2 Influence of pH on FSA^{D6Q} activity 36
5.3.3 Kinetics of aldol addition of 5B to 5A catalysed by FSA 37
5.3.4 Incubation of aldolase FSA^{D6Q} with substrates 41
5.3.5 Stability of reactants and products in the reaction solution 42
5.3.6 LC-MS analysis of aldol products 43
5.3.7 Mathematical model and optimization of aldol addition 43
5.3.8 Kinetic measurements of oxidation catalysed by aldehyde dehydrogenase 003 51
5.3.9 Mathematical model development for oxidation of 5C 59
5.3.10 Validation of the mathematical model for oxidation of 5C in the batch reactor 62
5.3.11 Screening for more suitable aldehyde dehydrogenase 64
5.3.12 Characterization of the oxidation product 5D 67
5.4 Conclusions 69
6 SYNTHESIS OF L-HOMOSERINE 71
6.1 Introduction 71
6.2 Experimental part 72
6.2.1 Materials 72
6.2.2 Apparatus 72
6.2.3 Analytical methods 73
6.2.4 Experimental procedures 74
6.3 Results and discussion: process optimization catalysed by CFE enzymes 80
6.3.1 Kinetics of transaminase-catalysed reaction 80
6.3.2 Kinetic parameters for different aldolases in the aldol addition of 6C and 6D 85
6.3.3 Instability of 4-hydroxy-2-oxobutanoate 95
6.3.4 Enzyme stability during incubation 96
6.3.5 Stability of reaction components during incubation with enzymes 97
6.3.6 Mathematical model development and validation 98
6.3.7 Cascade simulations 105
6.3.8 Optimized reaction – validation of model simulations 108
6.4 Results and discussion: process optimization catalysed by lyophilised whole cells containing YfaU 013 and TA 039 111
6.4.1 Kinetics of the reactions catalysed by whole cells 111
6.4.2 Stability of reaction components during incubation with cells 116
6.4.3 Optimized reaction 119

6.5 Conclusions 120
7 SYNTHESIS OF IMINOSUGAR PRECURSOR 121
7.1 Introduction 121
7.1.1 Approach I: Cbz-N-3-amino-1,2-propanediol as starting substrate 121
7.1.2 Approach II: 3-chloro-1,2-propanediol as starting substrate 123
7.2 Experimental part 124
7.2.1 Materials 124
7.2.2 Apparatus 125
7.2.3 Analytical methods 125
7.3 Experimental procedures – Approach I 127
7.3.1 Screening for the most suitable oxido-reductase 127
7.3.2 pH dependence of HLADH 127
7.3.3 Cbz protection group 127
7.3.4 HLADH kinetic measurements 128
7.3.5 NADH oxidase isolation from Lactococcus lactis 128
7.3.6 Chemical oxidation of alcohol 7A 129
7.3.7 Preliminary experiments conducted in the batch reactor 130
7.3.8 LC-MS analysis of the aldol product 130
7.3.9 The influence of NAD^+ concentration on the substrate conversion in the cascade 130
7.3.10 The influence of different initial substrate concentrations on the conversion in the cascade 130
7.3.11 The influence of HLADH/NOX activity ratio on the aldol adduct evolving 131
7.3.12 Operational stability of HLADH, NOX and FSA during the cascade reaction 131
7.3.13 Effect of aeration on enzymes' activity 132
7.3.14 Cascade reactions in batch reactor with multiple enzymes and substrates additions 132
7.4 Results and discussion – Approach I 134
7.4.1 Screening for the most suitable oxido-reductase 134
7.4.2 pH dependence of HLADH 135
7.4.3 Cbz protection group 136
7.4.4 HLADH kinetic measurements 137
7.4.5 Isolation of NADH oxidase from Lactococcus lactis 141
7.4.6 Chemical oxidation of alcohol 7A 142
7.4.7 Preliminary experiments conducted in batch reactor 142
7.4.8 LC-MS analysis of the aldol product 143
7.4.9 The influence of NAD^+ concentration on substrate conversion in the cascade 144
7.4.10 The influence of different initial substrate concentrations on the conversion in the cascade 145
7.4.11 The influence of HLADH/NOX activity ratio on the aldol adduct evolving 145
7.4.12 Operational stability of HLADH, NOX and FSA during the cascade reaction 146
7.4.13 Effect of aeration on enzymes' activity 147
7.4.14 Cascade reactions in the batch reactor 149
7.5 Experimental procedures – Approach II 151
7.5.1 Screening for the most suitable oxido-reductase 151
7.5.2 Kinetics of 7H oxidation catalysed by galactose oxidase 151
7.5.3 Enzymatic 3-chloro-1,2-propanediol oxidation and cascade reaction 152
7.5.4 3-Chloro-1,2-propanediol chemical oxidation and enzymatic aldol addition 153
7.6 Results and discussion – Approach II 155
7.6.1 Screening for the most suitable oxido-reductase 155
7.6.2 Kinetics of the oxidation of 7H catalysed by galactose oxidase 156
7.6.3 Enzymatic 3-chloro-1,2-propanediol oxidation and cascade reaction 157
7.6.4 3-Chloro-1,2-propanediol chemical oxidation and enzymatic aldol addition 159
7.7 Conclusions 160
8 THESIS CONCLUSIONS 163
9 REFERENCES 167
10 APPENDIX 179
SYMBOLS
BIOGRAPHY

1 INTRODUCTION

Biocatalysis can be broadly defined as the use of enzymes or whole cells as biocatalysts for industrial synthetic chemistry. Biocatalysts have been used for hundreds of years in the production of alcohol via fermentation, and cheese via enzymatic breakdown of milk proteins. Over the past few decades, major advances in our understanding of the protein structure–function relationship have increased the range of available biocatalytic applications (Johannes, Simurdiak & Zhao, 2005).

Biocatalysis is nowadays being more and more used for the synthesis of pharmaceuticals with an effort of making manufacturing processes more sustainable and more efficient (Sun et al., 2018; Wohlgemuth, 2007). It has long been recognized that the exquisite selectivity of enzymes can be used to great effect both in laboratory scale organic synthetic schemes and also at a larger scale, for industrial application. Today, several hundred biocatalytic processes operate at an industrial scale, which prove the interest and drive (both economic and environmental) for the implementation of such processes (Woodley, 2013; Pollard & Woodley, 2007; Zaks, 2001). Biocatalysis offers advantages over chemical synthesis as enzyme-catalysed reactions are often highly enantioselective and regioselective. They can be carried out at ambient temperature and atmospheric pressure, thus avoiding the use of more extreme conditions (Patel, 2008).

Many of the most interesting non-natural chemical reactions which could potentially be catalysed by enzymes are thermodynamically unfavourable and thus limited by the reaction equilibrium. As in nature, such reactions can be altered by coupling with other reactions (Abu & Woodley, 2015). In recent years, much interest has been shown in the use of multi-enzyme cascades as a tool in organic synthesis (Findrik & Vasić-Rački, 2009; Sudar et al., 2015; Hernández et al., 2017a). By coupling an energetically unfavourable reaction with a more favourable one, the multi-enzyme cascade mimics the approach taken in nature in metabolic pathways (Abu & Woodley, 2015; Findrik & Vasić-Rački, 2009).

It is known for a long time that reaction engineering is an efficient and effective methodology to design and size the reactors in the chemical industry (Ringborg & Woodley, 2016). Likewise, it can be used for describing and optimizing a biocatalytic reaction system (Zhong, Wei & Percival Zhang, 2017; Jia, Liu & Han, 2017; Molla et al., 2017; Scherkus et al., 2017). Reaction engineering application can positively affect the reaction time, by-product formation, enzyme stability, product concentration as well as other process metrics. To

achieve high product concentrations, substrate loadings can be arranged through different feeding strategies, or in a simple batch process (Findrik et al., 2005; Findrik & Vasić-Rački, 2009).

The aim of this doctoral thesis is the development and optimization of new biocatalytic synthetic routes for the production of three industrially valuable precursor molecules. The link between all three investigated reaction systems in this work is the use of C–C (carbon–carbon) bond forming aldolase in one reaction step per cascade system.

The first reaction system investigated in this doctoral thesis is aldol addition coupled with oxidation forming a methacrylic acid precursor, an important bulk chemical. Three types of enzymes are used in this biocatalytic pathway. The first step of this reaction system is C–C bond formation between propionaldehyde and formaldehyde by enzyme D-fructose-6-phosphate aldolase. The reaction product, 3-hydroxy-2-methylpropanal is oxidized in the second reaction step by aldehyde dehydrogenase with coenzyme NAD^+ regeneration by NADH oxidase. Cascade was studied in detail and most efficient biocatalysts in terms of activity, substrate affinity and operational stability are selected.

The second enzymatic cascade system studied in this thesis consists of aldol addition of formaldehyde and sodium pyruvate catalysed by a pyruvate aldolase, 2 keto 3 deoxy-L-rhamnonate aldolase (YfaU, EC 4.1.2.53), and transamination the produced aldol adduct and L-alanine catalysed by transaminase. L-Homoserine is targeted cascade product of interest, an important metabolic intermediate for the synthesis of essential amino acids and a valuable building block in the manufacture of industrial products (Hernández et al., 2017b).

The third investigated reaction system is the synthesis of iminosugar precursors. Two approaches are proposed within this thesis and investigated in detail. Approach I has Cbz protected amino alcohol (Cbz-*N*-3-amino-1,2-propanediol) and approach II 3-chloro-1,2-propanediol as a starting cascade substrate. After alcohol oxidation in the first step, obtained aldehyde is catalysed by D-fructose-6-phosphate aldolase variant FSA^{A129S} forming aldol adducts of interest, molecules that can be used as iminosugar building blocks.

The main focus of this study is put on the mathematical model development and process optimization for obtaining industrially significant values of process metrics such as maximum concentrations of products, product yields, substrate conversions and volume productivities in all studied biocatalytic reaction systems. Proposed reaction schemes have a potential industrial application. To be considered for scale-up, enzymatic cascades have to reach satisfactory process metrics at laboratory scale. Therefore, the aim of this research was

reaching them where possible by applying reaction engineering methodology and selected biocatalysts.

2 BIOCATALYSIS

2.1 Biocatalytic cascade reactions

Biocatalysts/enzymes are naturally present in all living cells; in microorganisms, plants, animals and humans. They are the catalysts of life forged by evolution with unequalled efficiency and selectivity (Li et al., 2012). Applying biocatalysts to chemical manufacturing industry can help develop greener, sustainable and cost-efficient processes that are more alike to the ones found in nature (Posorske, 1984; Sheldon & Woodley, 2018).

The biggest role of biocatalysis remains in the pharmaceutical sector, where its exquisite regio- and stereoselective properties enable difficult syntheses (Pollard & Woodley, 2007). Throughout the past 100 years, industrial biotechnology has grown into a multi-billion US dollar market, which has now even begun to take over a larger part of chemical production in a rapidly growing bio-economy (Wittmann & Liao, 2017). Both isolated enzymes and whole-cell biocatalysts are being increasingly used to assist in synthetic routes towards complex molecules of industrial interest (Ishii et al., 2007; Milker et al., 2017).

With the recent advances in synthetic biology, there is an increasing interest in the design of multi-step enzymatic conversions for the synthesis of speciality chemicals and pharmaceutical intermediates (McArthur & Fong, 2010). Some advantages of this type of biotransformations, compared to a traditional organic synthesis, are the productivity improvement and the absence of intermediate product recovery steps, which are money and time consuming (Bruggink, 2003). Enzymatic cascades can provide added value to a synthetic scheme by starting from cheaper raw materials or making more valuable products. Additionally, they can be used to help shift the equilibrium of otherwise thermodynamically unfavourable reactions to give a higher conversion of the target product (Abu, Gundersen & Woodley, 2015). Unfavorable equilibrium reactions benefit from the cascade concept since continuous removal of product in a subsequent reaction step can drive the reaction towards product formation.

Due to the stated benefits, biocatalytic cascade reactions are being more explored and applied today (Fessner, 2015). So far, a large number of biocatalytic cascade reactions has been developed; from simple oxido-reduction reaction coupled with cofactor regeneration, to highly complex multi-enzyme synthesis (Findrik & Vasić-Rački, 2007; Sudar et al., 2015).

Biocatalytic cascade reactions, studied in this doctoral thesis, occur in multiple enzyme-catalysed reaction steps. It is important to emphasize that it can be challenging to combine several enzymes *in vitro* for the conversion of non-natural substrates.

2.2 Enzymatic carbon–carbon bond formation

Carbon–carbon (C–C) bond forming reactions are of central importance in organic synthesis for creating new molecular frameworks, and in the production of pharmaceuticals, commodities and fine chemicals. Carbon–carbon bond formation is the corner stone reaction of organic synthesis which allows the creation of complex compounds from the simpler ones (Li, 2005).

Enzymatic C–C bond formation reactions, as opposed to non-enzymatic, are carried out under physiological conditions without the need for protecting group techniques. C–C bond forming enzymes replace traditional chemical synthesis with advantage of being enantio- and chemoselective. Enzymatic aldol addition reactions mediated by aldolases are one of the ways of C–C bond formation (Clapés, 2010; Clapés, 2016; Schmidt, Eger & Kroutil, 2016; Busto, 2016; Breuer, Bonnekessel & Schneider, 2012). Stereoselective C–C bond formation is particularly valuable in asymmetric synthesis because of its potential for stereodivergent product generation, by which multiple stereoisomeric products can be derived from common synthetic building blocks (Clapés, 2015). Therefore, it is not surprising that the number of enzymes catalyzing various C–C bond forming reactions is constantly increasing (Resch et al., 2011).

In this dissertation all investigated cascades for the synthesis of industrially valuable products employ different aldolases which form C–C bond. Hence, C–C bond forming enzymes are outlined in this thesis.

2.3 Protein engineering and overexpression

Since enzymes in nature, i.e. wild type enzymes, do not always meet the required demands for the industrial use, enzyme engineering can be used to develop a catalyst with properties matching the process requirements (Otte & Hauer, 2015; Illanes et al., 2012; Nestl, Nebel & Hauer, 2011). Scientific progress in the field of enzyme modification enables the opportunity to tune a given biocatalyst for a specific industrial application. Much work has

been focused on extending the substrate repertoire and altering enzyme selectivity (Woodley, 2013).

The combination of molecular biology techniques, such as directed evolution, along with new and efficient high-throughput screening methods, have fueled further advances of biocatalysis to the chemical and the pharmaceutical industries (Zaks, 2001; Adrio & Demain, 2010). Molecular biology engineering methods can be used to improve stability, substrate specificity and stereospecificity of an enzyme. They have advanced greatly in the recent years and they can be used to produce industrially suitable catalysts in less time and money consuming manner (Kapoor, Rafiq & Sharma, 2017; Windle et al., 2014). The gram-negative bacterium *Escherichia coli* offers the means for rapid, high yield, and economical production of recombinant proteins (Sivashanmugam et al., 2009). The advantages of fast growth in an inexpensive medium, the well-characterized genetics, and the availability of a large number of cloning vectors and mutant host strains make *E. coli* the first choice for production of recombinant proteins (Jana & Deb, 2005). Most of the enzymes used in this research are overexpressed in *E. coli* and provided such from project partners. Overexpression and purification of aldolase FSA D6Q is performed as a part of this research. Detailed protocol is presented in chapter 5.3.1.

Enzymes can be used within their natural source of origin (whole cell) or they can be isolated and used in a soluble or immobilised state (Wichmann & Vasić-Rački, 2005). Conventionally, the main disadvantage of using the whole cells is the unwanted side reactions that take place due to the presence of other enzymes (D'Souza, 2001). However, when using whole cells in which target protein overexpression was carried out, the activity of that protein usually overcomes metabolic side reactions (Rios-Solis et al., 2015). *E. coli* cells containing co-expressed transaminase and aldolase are used in this study for L-homoserine synthesis.

The development of more specific and stable biocatalysts, either isolated enzymes or whole cells, generated by the new methods of genetic engineering, together with improved reaction systems by reaction engineering have led to new industrial biotransformations (Liese & Filho, 1999). It is expected that both protein and process engineering work simultaneously towards future process implementation, as they offer complementary solutions to the process design problem (Woodley, 2018). Hence, protein engineering can significantly improve enzyme kinetic parameters, which basically determine the process outcome. Challenges in the cascade reaction development can be resolved through interdisciplinary approach linking

chemistry, biology and engineering which can surely pave the way for faster commercialization of biotechnological solutions (Heiden et al., 2014).

2.4 Coenzyme regeneration

Some enzymes such as aldehyde dehydrogenase used in chapter 5 and alcohol dehydrogenase used in chapter 7 require coenzyme for their catalytic function, in this case nicotinamide adenine dinucleotide. Various methods can be used for the regeneration of coenzymes; biological, enzymatic, electrochemical, chemical and photochemical (Chenault & Whitesides, 1987). An enzyme-coupled regeneration is a simple approach in which a second enzyme is added to the reaction system (Wichmann & Vasić-Rački, 2005). *In situ* regeneration systems were employed in this dissertation due to the high process price when coenzymes are being used in stoichiometric quantities (Weckbecker, Gröger & Hummel, 2010; Wichmann & Vasić-Rački 2005; Woodyer, Johannes & Zhao, 2006). An example of this method, for the regeneration of coenzyme NAD^+, is the use of NADH oxidase (Rocha-Martín et al., 2011). Two NADH oxidases are used in this work. Bacteria *Lactococcus lactis* was aerobically grown in a bioreactor to produce NADH oxidase which has been isolated and purified from the cells and used as a biocatalyst according to the procedure described in literature (Sudar et al., 2014) (chapter 7.3.5). Another purified and lyophilised NADH oxidase was provided from project partner Prozomix (UK) for the use in the second reaction step of methacrylic acid precursor synthesis (Chapter 5).

3 THESIS FRAMEWORK: Biosynthesis of industrially valuable products

3.1 Methacrylic acid

3-Hydroxyisobutyric acid is an important intermediate in the biosynthesis of methacrylic acid (MAA) and methyl methacrylate (MMA). MAA and MMA are important intermediates for the preparation of polymers, in particular poly(methyl methacrylate) with global annual production of 1.5 million tons and annual market of $2.1/$8.1 billion in the US/worldwide, respectively (Darabi Mahboub et al., 2016; Przybylski et al., 2018). MMA has been made almost exclusively by a three-step process from acetone and hydrogen cyanide, via acetone cyanohydrin. In this process, large proportions of sulfuric acid are used, and disposal of the acidic sludge by-product is expensive (Cavani et al., 2001; Pyo et al., 2012). New greener and simpler processes have been devised for the MAA and MMA production. One such approach produces MAA precursor 3-hydroxyisobutyric acid from simple-structured starting substrates, formaldehyde and propanal. Proposed enzymatic cascade studied in this work consists of aldolase-catalysed aldol addition followed by oxidation by aldehyde dehydrogenase as a useful green alternative to the traditional synthesis of the MAA.

3.2 L-Homoserine

Amino acids are widely industrially produced and utilized. They play an important role in the pharmaceutical, agrochemical and chemical industry. The discovery of the functions of amino acids has led to the expansion of their field of use. In addition to seasoning and other food use, amino acids are used in many fields such as animal nutrients, pharmaceuticals, and cosmetics (Wendisch et al., 2016; Yokota & Ikeda, 2017; Hermann, 2003). They are frequently used for the preparation of various pharmaceutically active substances and agrochemicals, or as resolving agents for chiral acids (Höhne et al., 2008). The worldwide amino acids market has amount of about 5 billion dollars. Monosodium glutamate and animal feed additives, methionine and lysine, account for about 75% of this sales value (Barnicki, Bommaraju & Kent, 2017).

Until about 20 years ago many smaller volume amino acids were still manufactured by the hydrolysis of animal protein products (gelatin, hair, feathers). As today pharmaceutical companies demand products certified as being of non-animal origin, amino acid manufacturers have developed biotechnological processes for almost all natural amino acids, and for some unnatural amino acids as well (Kragl, Vasić-Rački & Wandrey, 1996; Karau &

Grayson, 2003). Major amino acids for the food and animal feed industries are today produced on a very large scale using fermentation or synthetic processes. DL- Methionine is produced in annual volumes of more than 0.5 million tons by chemical synthesis (Grayson & Kessler, 2015).

L-Homoserine is not one of the common amino acids encoded by DNA. It differs from the amino acid serine by insertion of an additional -CH_2- unit into the backbone. Homoserine is an intermediate in the biosynthesis of three essential amino acids: methionine, threonine (an isomer of homoserine), and isoleucine and has a role as a human metabolite (Berg, Tymoczko & Stryer, 2002). L-homoserine is an amino acid that can be readily converted into a range of chiral amino-substituted heterocycles, which are valuable building blocks for the synthesis of new pharmaceuticals. Simple chiral derivatives derived from L-homoserine include lactones, tetrahydrofurans, tetrahydropyrroles and tetrahydrothiophenes (Kalyanam et al., 2008). L-Homoserine is a non-proteinogenic amino acid, which plays an important role in the biosynthesis of both L-threonine and L-methionine, and in the industrial fermentation process to manufacture L-threonine.

Methionine is one of two sulfur-containing amino acids along with cysteine. As an essential amino acid, intake of methionine from food is required for humans and animals. Methionine is used primarily as a building block of proteins in the body. Methionine is a highly important feed additive and can be added to poultry feed as the first limiting amino acid. To use methionine for food and pharmaceuticals, DL-methionine needs to be converted to L-methionine using acetylation and enzymatic process (Yokota & Ikeda, 2017; Hermann, 2003). Cascade system studied in this thesis produces L-homoserine that can be used as a precursor for L-methionine production. From all the published fermentation data it can be concluded that up to now no more than 5 g L^{-1} methionine are achievable without using genetically modified organisms (GMOs). The very highest L-methionine concentration from microorganisms reached so far amounts of 35 g L^{-1} and is published as a patent using a GMO of *Escherichia coli (E. coli)* (Willke, 2014; Hirasawa & Shimizu, 2016).

Proposed reaction scheme for L-homoserine synthesis applied in this work includes catalysis by two types of enzymes: Class II pyruvate-dependent aldolase and transaminase. Despite a big interest in transaminase catalysed reactions (Gundersen et al., 2016; Truppo, Turner & Rozzell, 2009; Hernández et al., 2017a; Koszelewski et al., 2009; Leuchs et al., 2013; Savile et al., 2010; Park, Dong & Shin, 2013; Park et al., 2003), they are often demanding to implement on an industrial scale due to frequent thermodynamic and kinetic

challenges (Gundersen et al., 2016). That is why enzymes can be coupled with other enzymes forming a cascade reaction systems (Findrik & Vasić-Rački, 2009; Santacoloma et al., 2011; Schrittwieser et al., 2018), which enables shifting of transaminase catalysed reaction equilibrium towards the wanted products (Hernández et al., 2017a; Koszelewski et al., 2009, Truppo, Turner & Rozzell, 2009) as in this research. The second enzyme, Class II pyruvate-dependent aldolase (YfaU) does not only serve solely as an equilibrium shifter, but also as a regenerating enzyme used to reduce the consumption of pyruvate as one of the substrates, similar to coenzyme regeneration systems (Hernández et al., 2017b). In the proposed cascade, YfaU was used for pyruvate recycling to reduce its quantities as a process feed, as well as to shift the equilibrium of this system towards L-homoserine synthesis. Reactions were catalysed by cell free extract (CFE) of two enzymes and by lyophilised *E. coli* cells containing these enzymes. Both biocatalysts were kinetically characterized in detail. Process optimization for both cases was performed based on developed mathematical model.

3.3 Iminosugars

An iminosugar, also known as an azasugar, is any analog of a sugar where a nitrogen atom has replaced the endocyclic oxygen atom of the structure. Iminosugars are common components of plants and may be responsible for some of their medical properties. Iminosugars have attracted a great interest among scientists due to their efficient inhibition of various glycosidases involved in the intestinal degradation of carbohydrates and are therefore used in the pharmaceutical industry for its properties connected to the application in diabetes treatment (Nash et al., 2011; Watson et al., 2001).

In terms of biochemical activity for medicinal applications, 1-deoxynojirimycin and 1,4-dideoxy-1,4-imino-D-arabinitol are alpha-glucosidase inhibitors that have anti-diabetic and anti-viral activity. Deoxynojirimycin was modified to produce two derivatives now used as medicines *N*-hydroxyethyl-1-deoxynojirimycin (commercially known as *Miglitol*) as coadyuvant for diabetes treatment and *N*-butyl-1-deoxynojirimycin (commercially known as *Miglustat*) for Gaucher's disease treatment. Some other iminosugars show anti-cancer activity (Jones et al., 1985; Scofield et al., 1995; Asano et al., 2000).

Aldol adducts containing amino groups are important building blocks of many naturally occurring molecules, including iminosugars (Gutierrez et al., 2011). Such aldol products can be synthesised through cascade reaction proposed in this thesis consisting of the amino alcohol Cbz-*N*-3-amino-1,2-propanediol oxidation with an ensuing aldol addition of

dihydroxyacetone, where both transformations are catalysed by enzymes. Alternatively, another approach for iminosugar building block synthesis is proposed and investigated in this work that uses 3-chloro-1,2-propanediol as starting material.

4 MATHEMATICAL MODELLING AND PROCESS OPTIMIZATION

To bridge the gap between the lab scale and industrial scale process, mathematical modelling can be very useful. Mathematical model of a process can be used to simulate different scenarios and conditions of a process to avoid extensive experimental work (Santacoloma et al., 2011). By using simulations, it is possible to gain better understanding of the interactions between reaction components, it helps focusing of experimental work, which saves time, efforts and reduces cost (Heitzig et al., 2014; Price et al., 2013). One of the largest fine chemical manufacturers in the world, Lonza, recognized the potential of using mathematical modelling (Brass, Hoeks & Rohner, 1997), i.e. reduction of cost and environmental impact by (i) shortening the time necessary to define optimal operating conditions and reactor type (Vasić-Rački, Findrik & Vrsalović Presečki, 2011; Ringborg & Woodley, 2016), (ii) decreasing the consumption of chemicals, energy and water and, in turn, (iii) production of waste.

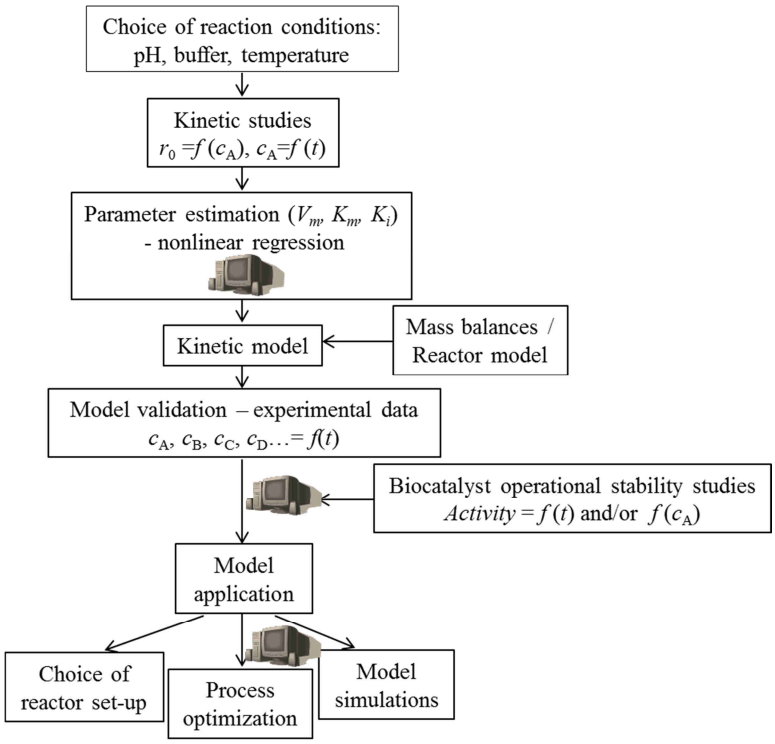

Figure 4.1 Simplified methodology towards a successful cascade set-up (Findrik Blažević et al., 2018).

Modelling increases our knowledge about the process since it enables the simulation of different reaction courses. This offers better understanding of the effect that different

variables have on the equilibrium, conversion etc. Mathematical modelling is useful in finding operational conditions for creating optimal microenvironment for the biocatalyst to obtain industrially significant values of process metrics. It is important for the model to be effective for a wide range of variations of the internal process variables (Vasić-Rački, Kragl & Liese, 2003). The model development of the reactor with the reaction catalysed by isolated soluble enzymes consists of enzyme kinetic modelling and reactor modelling (Vasić-Rački, Findrik & Vrsalović Presečki, 2011). Many methods for optimization towards maximum yield and productivity have been successfully applied on enzyme cascades (Agudo & Reetz, 2013; Kunjapur, Tarasova & Prather, 2014). A strategy employed to set-up and optimize multi-enzymatic cascade reactions in this doctoral work is based on a scheme presented in Figure 4.1.

The mathematical modelling and its use for process development and optimization are still not sufficiently used in industrial environment (Ringborg & Woodley, 2016). The modelling data found in the literature is scarce and with limited use due to lack of experimental data for model validation (Zhong, Wei & Zhang, 2016). Thus, most of the reported models do not describe the reaction systems in significant variable ranges. Also, they do not consider the influence of all compounds present in the system on the reaction rate (Vasić-Rački, Kragl & Liese, 2003) and process outcome, an important issue that was done in this work.

4.1 Kinetic models

To reach industrial application, each enzyme and reaction system has to be kinetically characterized, i.e. a kinetic model has to be developed. In other words, it is necessary to determine the kinetics of the reactions in the process to describe an enzymatic biotransformation with a mathematical model (Vasić-Rački, Findrik & Vrsalović Presečki, 2011; Vasić-Rački et al., 2003). Every compound in the reaction medium has an effect on the reaction rate and this effect should be defined with a proper mathematical description of the process (Vasić-Rački, Findrik & Vrsalović Presečki, 2011). Even though the method of collecting kinetic data in the batch mode is the slowest and most labor intensive, it is considered the most robust in terms of wide applicability (Ringborg & Woodley, 2016).

The enzyme also has to be studied in terms of stability because the reaction conditions in industrial processes are much harsher than in biological systems (Pollard & Woodley, 2007).

Mathematical model of a process consists of a kinetic model and mass balance equations for every reaction compound in a reactor. Fundamental expression of enzyme kinetics is the Michaelis-Menten equation (Bailey et al., 1977) presented by Equation 4.1, where r_S designates the reaction rate (mmol dm^{-3} mm^{-1}), c_S designates substrate concentration (mmol dm^{-3}), V_m stands for maximum reaction rate (mmol dm^{-3} min^{-1}) and K_m is the Michaelis constant (mmol dm^{-3}).

$$r_S = \frac{V_m \cdot c_S}{K_m^S + c_S} \tag{4.1}$$

This equation describes the dependence of the enzyme reaction rate on the concentration of one substrate. According to this equation, it is possible to distinguish three regions of reaction rate dependence on substrate concentration shown in Figure 4.2.

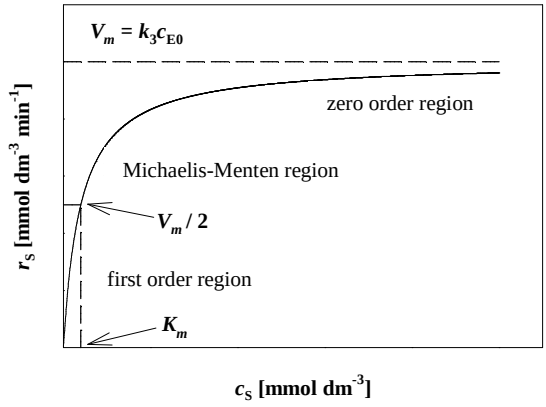

Figure 4.2 Dependence of the initial reaction rate on substrate concentration for Michaelis-Menten kinetics.

Michaelis constant (K_m) has a physicochemical meaning of ‘‘the substrate concentration that indicates one-half maximum velocity of an enzyme reaction” (Ishii et al., 2007). When substrate concentration is low ($c_S << K_m^S$) the dependence of the reaction rate on substrate concentration is linear. In this case, the reaction can be described with a first order kinetics. When substrate concentration is high ($c_S >> K_m^S$), reaction rate can be described with a zero order kinetics. This means that the reaction rate does not depend on the substrate concentration. In the intermediate substrate concentration range, the full Michaelis-Menten equation must be used (Dunn et al., 1992).

Apart from the simple Michaelis-Menten equation, double substrate Michaelis-Menten equation is also very frequently used (Equation 4.2) and can be further expanded to describe a reaction with three or more substrates.

$$r_S = \frac{V_m \cdot c_{S1} \cdot c_{S2}}{(K_m^{S1} + c_{S1}) \cdot (K_m^{S2} + c_{S2})} \tag{4.2}$$

Equation 4.1 can also be expanded to describe enzyme inhibition where K_i designates the inhibition constant (mmol dm^{-3}). Enzyme reaction is inhibited when a reaction component, an inhibitor, decreases reaction rate. There are three type of reverse enzyme inhibition; competitive (Equation 4.3), uncompetitive (Equation 4.4) and non-competitive (Equation 4.5).

$$r_S = \frac{V_m \cdot c_S}{K_m^S \cdot \left(1 + \frac{c_P}{K_i^P}\right) + c_S} \tag{4.3}$$

$$r_S = \frac{V_m \cdot c_S}{K_m^S + c_S \cdot \left(1 + \frac{c_P}{K_i^P}\right)} \tag{4.4}$$

$$r_S = \frac{V_m \cdot c_S}{(K_m^S + c_S) \cdot \left(1 + \frac{c_P}{K_i^P}\right)} \tag{4.5}$$

When competitive inhibition occurs, an inhibitor competes with a substrate for the active site of an enzyme. Noncompetitive inhibition occurs when inhibitor binds on the enzyme but not in the active site. Uncompetitive inhibition is the combination of previously mentioned inhibitions (Segel, 1975).

Decay of enzyme activity is the second reason for the decrease of the reaction rate. Enzyme activity decay is usually described by using a first (Equation 4.6) order kinetics (Laidler & Bunting 1973). It is an important aspect in bioprocess development since it affects process efficiency. For that purpose it is necessary to determine the enzyme activity at different conditions, especially during the reaction, which is known as operational stability of biocatalyst (Schoemaker, Mink & Wubbolts, 2003).

$$\frac{\mathrm{d}V_m}{\mathrm{d}t} = -k_d \cdot V_m \quad \Rightarrow \quad V_m = V_{m0} \cdot e^{-k_d \cdot t} \tag{4.6}$$

4.2 Mass balance equations

Mass balance of a reaction component is directly related to the used reactor type. In this thesis mathematical models were developed for the batch reactor and the fed-batch reactor and they will be described in the following chapters.

4.2.1 Batch reactor

Batch and semi-batch reactors are the main device of batch processes which are widely used to produce pharmaceuticals, polymers, biotechnologicals etc (Garcia et al., 1995). Three phases can be distinguished in a batch operation; filling phase, reaction phase and emptying phase (Donati & Paludetto 1999). Batch reactor (Figure 4.3) is a closed system which means there is no adding or removing of additional material from the reactor, except at the filling or emptying phase. Thus, concentrations of reactants and products in a batch reactor change with time and this type of reactor works in unsteady state (Gomzi, 1998). When density of the reaction mixture is constant, mass balance equation for reactant *A* in ideal batch reactor is presented by Equation 4.7, and mass balance for product *P* by Equation 4.8 where r stands for reaction rate (mmol dm^{-3} min^{-1}), whereas dc_A/dt and dc_P/dt stand for the change in reactant and product concentration in time, respectively.

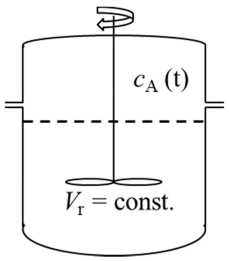

Figure 4.3 Batch reactor.

$$\frac{dc_A}{dt} = -r \tag{4.7}$$

$$\frac{dc_P}{dt} = r \tag{4.8}$$

4.2.2 Fed-batch reactor

Fed-batch reactor (Figure 4.4) is a type of a batch reactor with a feed of one or more reaction components. The volume of the reaction changes with time and its increase has to be included in the mathematical equations. Mass balance equations for reactant *A* and product *P* are presented by Equations 4.9 and 4.10 where $-c_{\mathrm{A/P}} \cdot \frac{\mathrm{d}V}{\mathrm{d}t} \cdot \frac{1}{V}$ designates the decrease in substrate or product concentration due to increased volume. Expression $c_{\mathrm{A},0} \cdot q_1$ stands for reactant concentration increase caused by reactant feed labeled as q_1, the volume flow rate ($\mathrm{cm}^3\ \mathrm{h}^{-1}$).

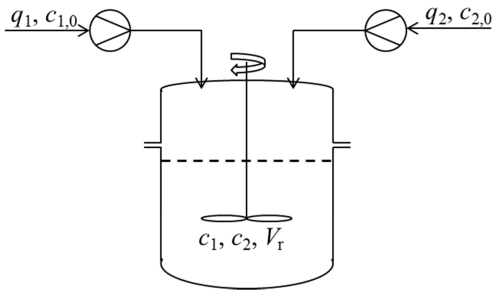

Figure 4.4 Fed-batch reactor.

$$\frac{\mathrm{d}c_{\mathrm{A}}}{\mathrm{d}t} = \frac{1}{V} \cdot \left(-c_{\mathrm{A}} \cdot \frac{\mathrm{d}V}{\mathrm{d}t} + c_{A,0} \cdot q_1 \right) - r_1 \tag{4.9}$$

$$\frac{\mathrm{d}c_{\mathrm{P}}}{\mathrm{d}t} = \frac{1}{V} \cdot \left(-c_{\mathrm{P}} \cdot \frac{\mathrm{d}V}{\mathrm{d}t} \right) + r_1 \tag{4.10}$$

4.3 Kinetic modelling of cell free extract enzymes and enzymes contained in cells

All three separate cascade systems that are a part of this research include different isolated enzymes as catalysts. Applied *in vitro* kinetic modelling results in model development based on measurements where single enzymes are used. During L-homoserine synthesis research, both isolated enzymes and whole cells containing the same overexpressed enzymes were used as biocatalysts.

Irrespective of whether multi-step enzymatic conversions pathways are ultimately applied *in vivo* (as a whole cell biocatalyst) or *in vitro* (as isolated or immobilised enzymes), there is a need to understand the mechanisms of the enzymes involved and to model reaction

kinetics in order to optimize the overall conversion yield (Rios-Solis et al., 2015; Meyer, Pellaux & Panke, 2007). *In vitro* kinetic model developed for cascade catalysed by enzymes can be adapted and used to describe the process within whole cells containing same types of overexpressed enzymes. This approach, used in this research, is a novelty and such efforts are so far scarce.

One work that published results obtained with this approach is a research from Milker et al (Milker et al., 2017). The group developed a kinetic model for the simulation and optimization of an *in vivo* redox cascade in *E. coli,* using a combination of an alcohol dehydrogenase, an enoate reductase, and a Baeyer-Villiger monooxygenase for the synthesis of lactones. The model was used to estimate the concentrations of active enzymes in the sequential biotransformations to identify bottlenecks together with their reasons and how to overcome them. They estimated adapted Michaelis-Menten parameters from *in vitro* experiments with isolated enzymes, and used these values to simulate the change in concentrations of intermediates and products during the *in vivo* cascade reactions. By using this approach the model identified bottlenecks and they could improve the process.

Another research (Rios-Solis et al., 2015) focused on determining the kinetics of separate steps in a multi-step enzymatic cascade and using that knowledge while fine tuning the protein expression system in a cell.

In this thesis L-homoserine synthesis kinetics was measured *in vitro* using isolated cell free extract (CFE) enzymes aldolase and transaminase and lyophilised *E. coli* cells containing the same overexpressed enzymes. Kinetic models were compared and were the basis for the understanding of the cascade system operating with both separate enzymes and lyophilised whole cells.

5 SYNTHESIS OF METHACRYLIC ACID PRECURSOR

5.1 Introduction

Biocatalytic cascade for the synthesis of MAA precursor was investigated in this section of the thesis. The two steps cascade consisted of aldol addition as the first step followed by oxidation in the second step. The first reaction step was the enzymatic carbon–carbon bond formation between formaldehyde (**5A**) and propionaldehyde (**5B**) via aldol addition (Scheme 5.1). The aldol adduct obtained is commonly known as Roche aldehyde, widely used as intermediate in synthetic chemistry in fine and large volume chemical manufacturing industry (Schmid, Baro & Laschat, 2017). The second step was the enzymatic oxidation of the aldol 3-hydroxy-2-methylpropanal (**5C**), generated in the first reaction.

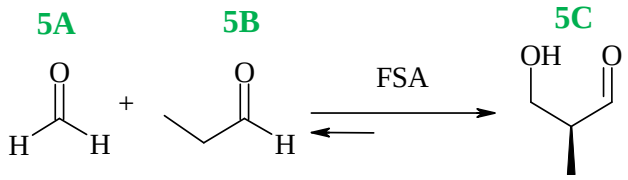

Scheme 5.1 Aldol addition of propionaldehyde (**5B**) to formaldehyde (**5A**) catalysed by FSA.

The oxidation reaction was catalysed by aldehyde dehydrogenase with coenzyme regeneration by NADH oxidase as presented in Scheme 5.2. The product of this reaction is 3-hydroxy-2-methylpropanoic acid (**5D**), a precursor for methacrylic acid (**5E**).

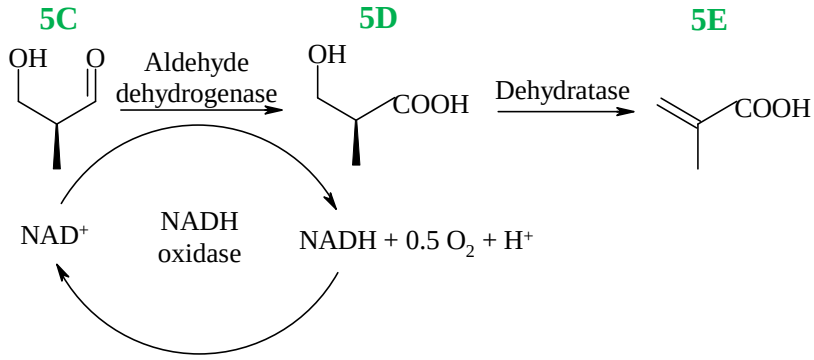

Scheme 5.2 Enzymatic synthesis of 3-hydroxy-2-methylpropanal (**5C**), the corresponding carboxylic acid (**5D**) and methacrylic acid (**5E**).

The aim of this research was maximizing process metrics (e.g. yield on product) by developing and validating a mathematical model for both reaction steps. The investigation

5A – Formaldehyde, **5B** – Propanal, **5C** – 3-Hydroxy-2-methylpropanal, **5D** – 3-Hydroxy-2-methylpropanoic acid, **5E** – Methacrylic acid, **5F** – 3-Hydroxy-2-methylpentanal

was divided in two parts; (1) optimization of aldol addition by the selected FSA variant and (2) screening for the most suitable biocatalyst for oxidation step and maximizing **5D** yield.

5.2 Experimental part

5.2.1 Materials

Reaction component labels are given according to Table 5.1.

Table 5.1 Labels given to each reaction component in this chapter.

Compound	Label
Formaldehyde	**5A**
Propionaldehyde (propanal)	**5B**
3-Hydroxy-2-methylpropanal	**5C**
3-Hydroxy-2-methylpropanoic acid (*β*-hydroxyisobutyric acid)	**5D**
Methacrylic acid	**5E**
3-Hydroxy-2-methylpentanal	**5F**
4-Bromophenacyl-*β*-hydroxyisobutyrate	**5G**

Chemicals and enzymes used in this chapter are the following. Propanal (97%) was purchased from Alfa Aesar (Germany). Formaldehyde (36%, p.a.) was purchased from T.T.T. Ltd. (Croatia). Triethanolamine (TEA), trifluoroacetic acid (TFA), formic acid, dimethylformamide (99.8%) (DMF), 2,4'-dibromo-acetophenone (>98%), Sodium (*R*)- and (*S*)-*β*-hydroxyisobutyrate and acetonitrile were purchased from Sigma Aldrich (Germany). *O*-Benzylhydroxylamine hydrochloride ($BnONH_2 \cdot HCl$) and pyridine were purchased from Acros Organics (Belgium). Celite 577 fine was purchased from Fluka (Germany). Methanol gradient grade (MeOH) was from J.T. Baker (USA). Hexane (97%) and ethyl-acetate (99.8%) were from BDH Prolabo Chemicals (United Kingdom). Competent cells M15 were from Life Science Market (Sweden). Isopropyl β-D-1-thiogalactopyranoside (IPTG), kanamycin sulphate and ampicilin sodium salt were from Fischer Scientific (USA). Yeast extract and bactotrypton were from Liofilchem (Italy). Agar was purchased from Biolife (Italy). Sodium chloride was from Lachner (Czech Republic).

D-Fructose-6-phosphate aldolase (FSA) D6Q variant from *E. coli* was expressed and purified in the labs of prof. Pere Clapés at IQAC-CSIC (Spain) and the Faculty of Chemical Engineering and Technology at the University of Zagreb (Croatia). FSA variants D6A and D6E were expressed and purified in the labs of prof. Wolf-Dieter Fessner at TU Darmstadt

5A – Formaldehyde, **5B** – Propanal, **5C** – 3-Hydroxy-2-methylpropanal, **5D** – 3-Hydroxy-2-methylpropanoic acid, **5E** – Methacrylic acid, **5F** – 3-Hydroxy-2-methylpentanal

(Germany). Cell free extracts (CFE) aldehyde dehydrogenase (AlDH 003), NADH oxidase (NOX 009) and panel of 24 additional aldehyde dehydrogenases (AlDH 24-47) were supplied by Prozomix Ltd (United Kingdom).

5.2.2 Apparatus

Apparatus used in Chapter 5 is listed in Appendix (Table 10.1).

5.2.3 Analytical methods

Reactions were monitored by HPLC with UV detection at 215 nm. Methods used are presented in Table 5.2. Methods A and B were used for monitoring the experiments regarding kinetics and reaction optimization. Both methods are appropriate for analysis of **5A**, **5B** and **5C**. During the research, method B was introduced with Phenomenex Kinetex column purchase for shortening the time of analysis. Method C was used for monitoring the chirality of the derivatized oxidation product, 4-bromophenacyl-β-hydroxyisobutyrate (**5G**).

Table 5.2 HPLC methods.

METHOD	COMPOUND	COLUMN	ELUENTS	CONDITIONS
A	**5A** *, **5B** *, **5C*** * derivatized	Phenomenex LiChrospher® C18 column (5 µm, 4 × 250 mm)	A: 0.095% v/v TFA in acetonitrile/water 80:20 B: (0.1% v/v) trifluoroacetic acid (TFA) in water	Gradient elution: 90 to 0% B 30 min, 0% B 5 min, 0 - 90% B 11 min, flow-rate 1 mL min^{-1}, 215 nm, column temperature 30 °C
B		Phenomenex Kinetex® C18 (5 µm, 4,6 × 250 mm)	A: 0.095% v/v TFA in acetonitrile/water 80:20 B: (0.1% v/v) trifluoroacetic acid (TFA) in water	Gradient elution: 90 to 0% B 10 min, 0% B 2 min, 0 - 90% B 3 min, 90% B 1 min, flow-rate 1.5 mL min^{-1}, 215 nm, column temperature 30 °C
C	**5G**	Chiral Lux Cellulose-1 column (250 x 4.6 mm, 5 µm)	A: *n*-hexane B: 2-propanol	Isocratic elution: 80% A and 20% of B, flow-rate 0.7 mL min^{-1}, 215 nm, column temperature 30°C, UV and RI detection employed

5.2.3.1 Derivatization of aldehydes and aldols

Derivatization with $BnONH_2 \cdot HCl$ (Garrabou et al., 2009) was required to enable aldehyde and aldol molecules (Scheme 5.3) visibility on HPLC at 215 nm (methods A and B from Table 5.2). Samples (5 µL) were mixed with derivatization solution (50 µL) containing

5A – Formaldehyde, **5B** – Propanal, **5C** – 3-Hydroxy-2-methylpropanal, **5D** – 3-Hydroxy-2-methylpropanoic acid, **5E** – Methacrylic acid, **5F** – 3-Hydroxy-2-methylpentanal

$BnONH_2 \cdot HCl$ (130 mM $BnONH_2 \cdot HCl$ in pyridine/methanol/water = 33:15:2 v/v) for 5 min at 25 °C and 1000 rpm. The capacity, i.e. concentration of the derivatization solution was taken into account while dealing with reaction mixture. Methanol (500 µL) was added in the sample followed by centrifugation at 5000 g and 4 °C for 5 min. The enzyme precipitated and the upper phase was used for the analysis. Chromatograms and calibration curves for **5A** and **5B** are presented in the Appendix (Figure 10.2). Retention times for **5A**, **5B** and **5C** when method A (Table 5.2) was used were 20.1 min, 24.6 min and 18.1 min, respectively in linearity range from 5 to 100 mM. Retention times for **5A**, **5B** and **5C** when method B (Table 5.2) was used were 8.7 min, 10.1 min and 7.8 min, respectively in linearity range from 5 to 50 mM.

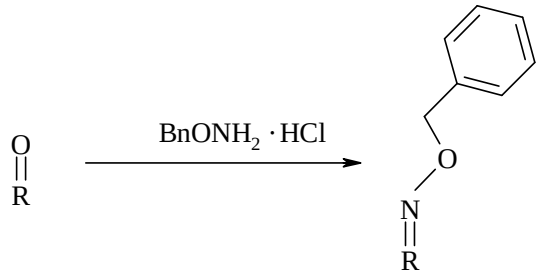

Scheme 5.3 Derivatization of aldehydes and aldols with $BnONH_2 \cdot HCl$.

5.2.3.2 Derivatization of acids

The 3-hydroxy-2-methylpropanal oxidation product (**5D**) needed to be derivatized with 2,4'-dibromo-acetophenone for enabling its visibility on HPLC at 215 nm (Scheme 5.4). This compound works for derivatization of acids (Mehta, Oeser & Carlson, 1998).

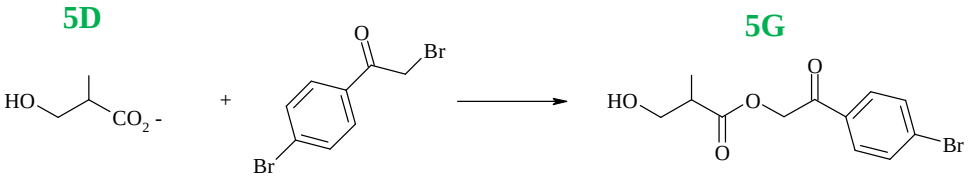

Scheme 5.4 *β*-hydroxyisobutyrate (**5D**) derivatization reaction.

Before analysis, a sample (20 µL) containing **5D** was mixed with 80 µL of derivatization solution of 2,4'-dibromo-acetophenone. It was incubated for 1 hour at 60°C. 400 µL of methanol was added in the sample, mixed and centrifuged (5 min, 5000 g, 4 °C). Derivatization solution was prepared in acetonitrile. 0.1 M concentration of 2,4'-dibromo-acetophenone was used in this case because the concentration of **5D** in the reaction was not

5A – Formaldehyde, **5B** – Propanal, **5C** – 3-Hydroxy-2-methylpropanal, **5D** – 3-Hydroxy-2-methylpropanoic acid, **5E** – Methacrylic acid, **5F** – 3-Hydroxy-2-methylpentanal

higher than 0.1 M. Linearity range for **5G** was from 1 to 90 mM when method A (Table 5.2) was used and its retention time was 19.1 min. When method B (Table 5.2) was used, retention time of **5G** was 8.4 min and linearity range was from 1 to 10 mM. Chromatogram and calibration curves for **5G** are presented in Figure 10.2.

5.2.4 Experimental procedures

5.2.4.1 FSA^{D6Q} overexpression in E. coli

Plasmid containing the gene for protein FSA variant D6Q synthesis was transformed in commercially available *E. coli* competent cells M15. The transformation was performed within the scope of this thesis during Short Term Scientific Mission at CSIC (Barcelona) in 2016. The protocol was later adjusted and used at the Department of Reaction Engineering and Catalysis, Faculty of Chemical Engineering and Technology (Zagreb) for producing additional amounts of enzyme FSA^{D6Q} used in this research.

The protocol started by placing plasmid PQT40-D6Q into *E. coli* M15 under sterile conditions (1 µL in 150 µL competent cells solution). The cells were heat shocked (5 minutes on ice, 30 seconds at 42 °C, 2 minutes on ice). 500 µL of liquid growth media (1% bactotrypton, 0.5% yeast extract, 1% NaCl) was added and incubated for 10 minutes at 37 °C and 200 rpm. The solution was poured on Petri dish containing agar (1% bactotrypton, 0.5% yeast extract, 1% NaCl, 1.5% agar). 100 µg/mL of antibiotic ampicillin (plasmid resistant) and 25 µg/mL of antibiotic kanamycin (*E. coli* M15 resistant) were previously added in the growth medium. The Petri dish containing the cells and growth medium was incubated overnight on 37 °C. Grown colonies were put into liquid growth media with previously added antibiotics and incubated for 24 hours at 37 °C and 200 rpm. 25 mL of grown culture was put in the 2 L Erlenmeyer flask containing 1 L of liquid growth media and antibiotics (50 µg/mL of ampicillin and 12.5 µg/mL of kanamycin) which was previously sterilized. Eight erlenmeyer flasks were incubated for 2 hours at 37 °C and 200 rpm. After 2 hours 500 µL of 1 M IPTG (expression triggering agent, Sivashanmugam et al., 2009) was added in each flask and stirred at 30 °C and 200 rpm overnight. The success of the expression process was examined by electrophoresis (Figure 5.1).

5A – Formaldehyde, **5B** – Propanal, **5C** – 3-Hydroxy-2-methylpropanal, **5D** – 3-Hydroxy-2-methylpropanoic acid, **5E** – Methacrylic acid, **5F** – 3-Hydroxy-2-methylpentanal

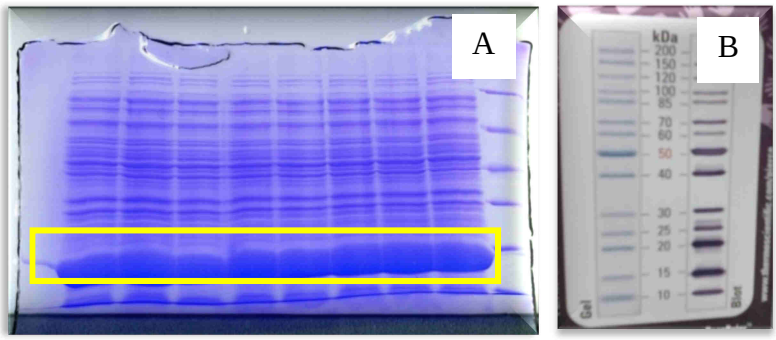

Figure 5.1 Electrophoresis gel A. samples developed from 8 flasks with highlighted overexpressed protein, B. reference table [kDa].

The cells were disrupted by French press at CSIC (Spain) or by ultrasound at the Department of Reaction Engineering and Catalysis (Croatia). Since the expressed enzyme is thermostable, other enzymes were denatured by incubation of the solution at 70 °C during 30 minutes. Next step was dialysis for separation of enzyme from buffer salts followed by lyophilisation. Protein content in lyophilised enzyme was determined by Bradford method (Bradford, 1976), shown in Figure 5.2.

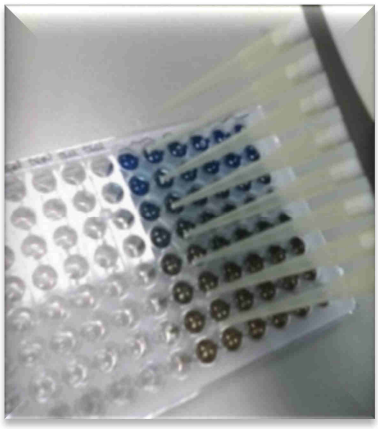

Figure 5.2 Bradford test for protein concentration determination.

5.2.4.2 Influence of pH on FSA^{D6Q} activity

The influence of pH on FSA^{D6Q} activity was tested in four different buffers (Tris HCl buffer, TEA HCl, borate buffer and glycine NaOH buffer) at pH 6.5, 7, 7.5, 8, 8.5 and 9. Reactions were conducted in 50 mM buffer, with 100 mM concentrations of **5A** and **5B** and concentration of FSA 0.5 mg mL^{-1}.

5A – Formaldehyde, **5B** – Propanal, **5C** – 3-Hydroxy-2-methylpropanal, **5D** – 3-Hydroxy-2-methylpropanoic acid, **5E** – Methacrylic acid, **5F** – 3-Hydroxy-2-methylpentanal

5.2.4.3 Aldolase kinetics measurements

Three variants of FSA: D6Q, D6A and D6E were tested for the aldol addition of **5B** to **5A**. The influence of concentration of substrates, **5A** and **5B**, on the initial reaction rate of each variant was measured. Based on these results, the best FSA variant was chosen for further studies of the aldol addition and process modelling and optimization of this reaction.

The influence of each reaction compound of aldol addition was monitored by keeping the concentrations of other compounds constant. Kinetic measurements were conducted as follows. A series of batch reactor experiments were carried out in which the change in **5C** concentration was monitored by HPLC. The influence of **5B** concentration on the specific enzyme activity was monitored up to concentrations of 2 M. In these measurements the concentration of **5A** was kept constant at 100 mM. The influence of **5A** concentration on the specific enzyme activity was monitored up to concentrations of 1.8 M. In these measurements the concentration of **5B** was kept constant at 100 mM.

Kinetic parameters were estimated from the dependence of the specific activity on the concentrations of each component of the reaction system using the initial reaction rate method (at substrate conversions less than 10%) presented in Equation 5.1 where *S.A.* designates the specific activity (U mg^{-1}). Change in product concentration in time is presented as $dc_{product}/dt$. V_r stands for reactor volume (cm^{-3}), V_{enzyme} for enzyme volume (cm^{-3}) and γ for enzyme concentration (mg cm^{-3}).

$$S.A. = \frac{dc_{product}}{dt} \cdot \frac{V_r}{V_{enzyme}} \cdot \frac{1}{\gamma_{enyzme}} \qquad \left[\frac{U}{mg}\right] \tag{5.1}$$

Generally, depending on available assays, kinetics can be measured spectrophotometrically or by following the kinetic tests by HPLC, GC, etc. FSA kinetic measurements were done by performing batch reactor experiments and following the concentration of product by HPLC. Kinetic parameters were estimated by using non-linear regression analysis available in the software SCIENTIST from the collected experimental data in the form of dependence of the specific activity on the concentration of substrate and product. Based on the estimated kinetic parameters and the reaction scheme, kinetic models were developed.

Once the best FSA variant was chosen for further research, additional kinetic measurements were performed with this enzyme. The influence of aldol addition product **5C** on the specific enzyme activity was monitored up to concentrations of 80 mM. In these

5A – Formaldehyde, **5B** – Propanal, **5C** – 3-Hydroxy-2-methylpropanal, **5D** – 3-Hydroxy-2-methylpropanoic acid, **5E** – Methacrylic acid, **5F** – 3-Hydroxy-2-methylpentanal

measurements the initial concentrations of **5A** and **5B** were kept constant at 100 mM. The influence of methanol concentration on specific enzyme activity, which was used as formaldehyde stabilizer in commercial stock solution, was also monitored up to 320 mM to estimate its inhibition potential. Apart from the kinetics of the main reaction, i.e. cross-aldol addition of **5A** and **5B**, the kinetics of self-addition of **5B** were also investigated. The influence of **5B** concentration on the specific enzyme activity in the self-aldol addition reaction of **5B** was monitored up to concentrations of 700 mM, whereas the influence of methanol concentration in this reaction was monitored up to 300 mM.

5.2.4.4 Aldolase incubation

It was found that FSA^{D6Q} shows no activity towards the aldol addition of dihydroxyacetone (DHA) to D-glyceraldehyde-3-phosphate (DG3P) to furnish D-fructose-6-phosphate used in the standard spectrophotometric assay for FSA activity. Therefore, FSA activity during the aldol addition between **5A** and **5B** was measured by using the alternative method to test the operational stability of enzyme during the aldol addition. The alternative activity assay was performing separate reactions (independent batch reactor experiments) with same initial conditions from which FSA activity can be calculated by using the initial reaction rate method. The initial concentrations of **5A** and **5B** in this assay were 100 mM, and the reaction volume was 500 µL. The reaction substrates for the activity assay were always freshly prepared by mixing **5A** solution (50 µL of 1 M stock solution prepared in buffer), **5B** solution (50 µL of 1 M stock solution prepared in buffer) dissolved in 100 µL of 50 mM TEA HCl buffer, pH 8.0. The activity test reaction was started by adding 300 µL of an enzyme solution prepared from the sample withdrawn from the reactor in which the main reaction takes place. The enzyme sample was prepared as follows: The amount of enzyme sample withdrawn from the main reaction to start the reaction in the assay always corresponded to 0.5 mg mL^{-1} protein concentration in the assay. So, the sample volume depended on the enzyme concentration in the main reaction. For example, in the case where FSA^{D6Q} concentration in the main aldol addition was 25 mg mL^{-1}, 10 µL were taken for the assay. Before starting the assay reaction, the enzyme sample from the reactor was filtrated with an *Amicon ® Ultra filter unit* (5 min, 5000 g) in order to separate the enzyme from reaction components (**5A**, **5B** and **5C**) which would influence the result, and was diluted (removed from the filter unit) in 300 µL of 50 mM TEA HCl buffer pH 8.0. In this form the enzyme was used to start the

5A – Formaldehyde, **5B** – Propanal, **5C** – 3-Hydroxy-2-methylpropanal, **5D** – 3-Hydroxy-2-methylpropanoic acid, **5E** – Methacrylic acid, **5F** – 3-Hydroxy-2-methylpentanal

reaction in the assay, and its volume was always 300 µL and the volume of the mixture in the assay was always 500 µL. The reaction was carried out in an *Eppendorf* tube at 25 °C and on a shaker at 1000 rpm in 50 mM TEA HCl buffer, pH 8.0. Six samples were taken during 45 minutes from the assay mixture, derivatized with $BnONH_2 \cdot HCl$ and analysed on HPLC.

From the change in product concentration *vs* time, initial reaction rate was calculated (Equation 5.1). From this value specific activity of enzyme was calculated by dividing the initial reaction rate with the enzyme concentration in the assay. FSA^{D6Q} activity was measured for 5-6 times during one experiment and the collected data were used to estimate the value of operational stability decay rate of the enzyme.

5.2.4.5 Stability of reactants and products in the reaction solution

Aldehydes are strong electrophilic compounds and may react with nucleophiles present on protein surfaces, with water generating hydrates or with other nucleophiles present in the reaction medium. Considering the reactivity of aldehydes, their stability was investigated at the reaction conditions without and with enzyme. **5A** (9 µL of 13.43 M solution) and **5B** (9 µL of 13.33 M solution) were incubated separately as well as together in 1.2 mL batch reactor on a shaker at 1000 rpm, in 50 mM TEA HCl buffer pH 8.0 and at 25 °C without the enzyme and with enzyme (3 mg mL^{-1}). Solutions were always freshly prepared and sampling was started immediately. The change in substrate concentration was monitored for 24 hours. The experiments with enzyme addition were carried out to evaluate the peaks that evolve in these reactions and draw proper conclusions about side-reactions in this reaction system. Stability of the main aldol product **5C** and aldol product of the self-addition reaction **5F** was also evaluated by following its concentration over 24 hours in experiments without and with enzyme (3 mg mL^{-1}).

5.2.4.6 LC-MS analysis of aldol products

LC-MS analysis was performed to confirm the aldol addition product (**5C**) and the product of **5B** self-addition (**5F**). The column and the conditions for LC-MS analysis were the same as for HPLC (Method A, Table 5.2), except the use of formic acid instead of TFA in the mobile phase. HPLC with DAD and MS detection was used. The selected ion monitoring method was used to confirm the molecular weight of the derivatized product peak. The mass spectrometer was equipped with electrospray ionization (ESI) source and operated in positive

5A – Formaldehyde, **5B** – Propanal, **5C** – 3-Hydroxy-2-methylpropanal, **5D** – 3-Hydroxy-2-methylpropanoic acid, **5E** – Methacrylic acid, **5F** – 3-Hydroxy-2-methylpentanal

polarity mode. ESI+ conditions: capillary voltage 1.10 kV, nebulizing gas flow 1.5 L·min^{-1}, drying gas flow 15 L·min^{-1}, 300 °C.

5.2.4.7 Aldol addition in the batch reactor

Experiments of aldol addition of **5B** to **5A** were carried out in 50 mM TEA HCl buffer pH 8.0 at 25 °C in different batch reactor volumes ranging from 0.5 to 15 mL on a shaker. Different initial equimolar concentrations of substrates were used ranging from 100 to 2000 mM. Selected **5A** and **5B** concentrations were freshly prepared from the stock solutions (13.43 M and 13.33 M were the stock solutions concentrations of **5A** and **5B**, respectively) and dissolved in buffer. Reactions were started immediately by adding the enzyme in concentration selected for each experiment, from a stock solution of an appropriate concentration. The first sample was taken immediately after enzyme addition, and reactions were usually monitored until maximum substrate conversion was achieved, i.e. from 6 to 48 hours.

5.2.4.8 Aldol addition in the fed-batch reactor

Fed-batch experiments were carried out in glass reactor (Figure 5.3) with double wall at 25 °C on a shaker at 250 rpm in 50 mM TEA HCl buffer pH 8.0. The first fed-batch reactor experiment was carried out at 5 mL starting working volume, with a final volume of 5.35 mL. Its purpose was to validate developed mathematical model. The initial concentrations of **5A** and **5B** in the reactor were 122.0 and 100.0 mM, respectively. The enzyme concentration was 20.62 mg mL^{-1}. The initial reaction mixture was freshly prepared from the concentrated solution solutions of **5A** (39 µL of 12.95 M solution) and **5B** (37 µL of 13.53 M solution) in buffer (4924 µL), and the reaction was started by adding 103.1 mg of enzyme to the reactor to reach the concentration of 20.62 mg mL^{-1}. The first sample was taken before enzyme addition and starting the pumps. The feeding of substrates to the reactor was started immediately upon preparation of the initial reaction mixture and starting the reaction. Two syringe pumps (PHD 4400 Syringe Pump Series, Harvard Apparatus, USA) with high-pressure stainless steel pistons (8 mL, Harvard Apparatus) were used to supply the solution to the reactor. One piston (feed 1) contained a solution of **5A** (12.95 M), and the other piston (feed 2) contained a solution of **5B** (13.53 M). The flow rates of feed 1 and 2 were 0.26 and 0.27 µL·min^{-1},

5A – Formaldehyde, **5B** – Propanal, **5C** – 3-Hydroxy-2-methylpropanal, **5D** – 3-Hydroxy-2-methylpropanoic acid, **5E** – Methacrylic acid, **5F** – 3-Hydroxy-2-methylpentanal

respectively. The experiment was carried out for almost 30 hours. Sampling was done at regular time intervals.

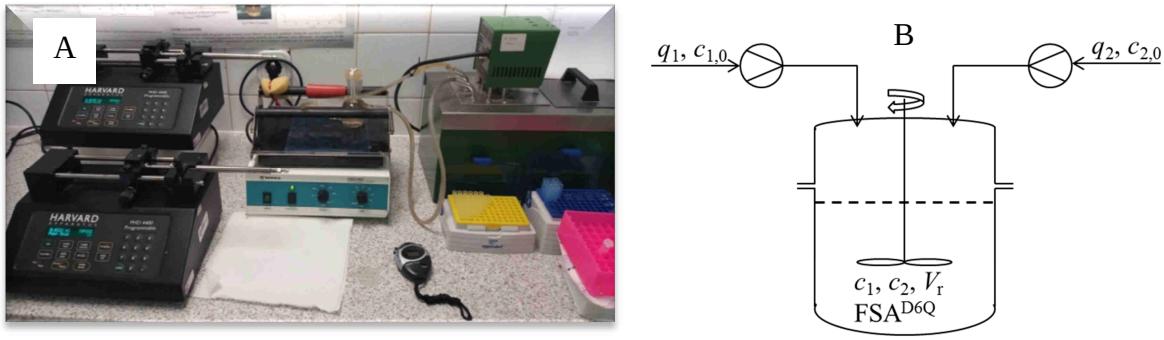

Figure 5.3 Experimental set-up (A) and scheme of reactor (B) used for the fed-batch experiments.

After process optimization with the use of the mathematical model, another experiment in the fed-batch reactor was carried at the flow-rates in feeds 1 and 2 of 1.4 and 1.26 μL·min^{-1}, respectively. The concentrations of **5A** and **5B** in the pump pistons (feed 1 and 2), as well as the initial volume, were the same as in the first experiment. The final volume was 5.80 mL. The initial enzyme concentration in the reactor was 60.32 mg mL^{-1}, and the initial concentrations of **5A** and **5B** in the reactor were 150 mM. The solution was freshly prepared from the concentrated solutions of **5A** (58 μL of 12.95 M solution) and **5B** (55.5 μL of 13.53 M solution) in buffer (4887 μL) and reaction was started by adding 301.6 mg of enzyme to the reactor. Everything else was the same as in the first experiment.

5.2.4.9 One-pot aldol addition and oxidation versus consecutive reactions

Initial idea was to perform one-pot aldol addition of **5B** to **5A** catalysed by FSA^{D6Q} and oxidation of **5C** catalysed by aldehyde dehydrogenase (Scheme 5.5). Since **5A** and **5B** have carbonyl group, it was assumed that they both can act as substrates for aldehyde dehydrogenase. This was tested experimentally by measuring the kinetics of oxidation of **5A** and **5B** catalysed by aldehyde dehydrogenase.

5A – Formaldehyde, **5B** – Propanal, **5C** – 3-Hydroxy-2-methylpropanal, **5D** – 3-Hydroxy-2-methylpropanoic acid, **5E** – Methacrylic acid, **5F** – 3-Hydroxy-2-methylpentanal

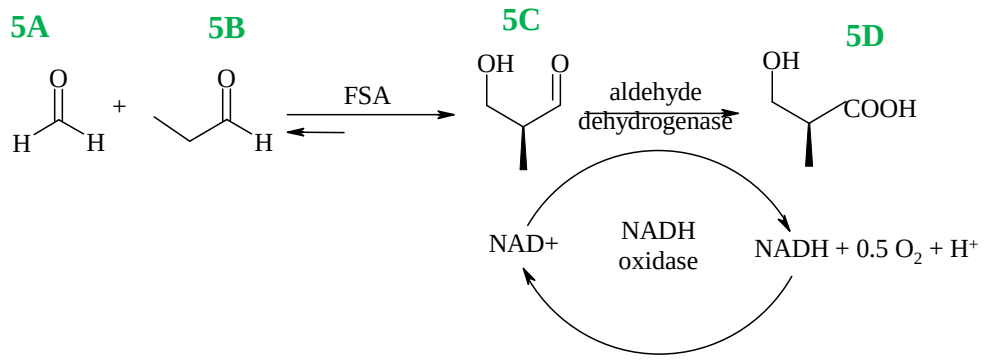

Scheme 5.5 Enzymatic cascade: aldol addition of **5B** to **5A** and oxidation of **5C** towards **5D**. the arrows of NAD regeneration must be connected with the main arrow

The influence of concentrations of **5A** and **5B** on the activity of aldehyde dehydrogenase was determined up to concentrations of 250 mM. The influence of NAD^+ concentration on aldehyde dehydrogenase activity was evaluated up to 8 mM at fixed concentrations of aldehydes **5A** and **5B** of 200 mM. Experiments were conducted in 50 mM TEA HCl buffer pH 8.0 at 25 °C at 1000 rpm.

5.2.4.10 Kinetics of 5C oxidation catalysed by lyophilised aldehyde dehydrogenase 003, CFE

Since product of aldol addition, **5C** is not commercially available due to complex isolation and purification as well as poor stability, for each measurement, it was freshly produced by aldol addition of **5B** (100 mM) to **5A** (100 mM) catalysed by FSA^{D6Q} (3 mg mL^{-1}) during 20 hours. Reaction was stopped when both substrates were converted to product **5C** (more than 90%). The enzyme was removed by *Amicon ® Ultra filter unit* (cut off 10 kDa) and the solution of **5C** in buffer was used for spectrophotometric kinetic measurements oxidation and as substrate for all oxidation batch experiments. Buffer used in these experiments was 0.5 M TEA HCl pH 8.0.

Kinetic measurements for oxidation of **5C** catalysed by crude AlDH 003 were conducted at 25 °C and 1000 rpm in 50 mM TEA HCl buffer pH 8.0. The influence of **5C**, **5A**, **5D**, NAD^+ and NADH concentrations on AlDH 003 specific activity was measured in 1.01 mL reactions. The concentration of AlDH 003 in each measurement was 0.05 mg mL^{-1}.

5.2.4.11 Kinetics of 5C oxidation catalysed by purified aldehyde dehydrogenase 003

Kinetic measurements for oxidation of **5C** catalysed by purified suspension of AlDH 003 were conducted at 25 °C and 1000 rpm in 50 mM TEA HCl buffer pH 8.0. The influence

5A – Formaldehyde, **5B** – Propanal, **5C** – 3-Hydroxy-2-methylpropanal, **5D** – 3-Hydroxy-2-methylpropanoic acid, **5E** – Methacrylic acid, **5F** – 3-Hydroxy-2-methylpentanal

of **5C**, **5A**, NAD^+ and NADH concentrations on specific activity of AlDH 003 in purified suspension was measured in 1.01 mL reactions. The concentration of AlDH 003 in each measurement was 0.05 mg mL^{-1}.

5.2.4.12 Kinetics of coenzyme NAD^+ regeneration catalysed by NOX 009

The kinetics of NAD^+ regeneration catalysed by NOX 009 was investigated at 25 °C and 1000 rpm in 50 mM TEA HCl buffer pH 8.0. The dependence of NOX specific activity on the concentration of NADH, O_2, NAD^+, **5A** and **5B** was determined.

5.2.4.13 Oxidation of 5C in the batch reactor catalysed by lyophilised aldehyde dehydrogenase 003, CFE

A mathematical model was developed based on kinetic measurements and validated in batch reactor. The aldol adduct **5C** was converted to the corresponding carboxylate **5D** by enzymatic oxidation using aldehyde dehydrogenase (AlDH 003). Regeneration of NAD^+ was accomplished by NADH oxidase (NOX 009) as shown in Scheme 5.5. A series of batch experiments was performed with experimental details given in Figure 5.21 legend. Since it is not commercially available, **5C** was always freshly produced in a way described in Chapter 5.2.4.10 for being used as a starting oxidation substrate. Reaction volume was 3.5 mL and the reactions were conducted in 500 mM TEA HCl buffer pH 8.0, at 25 °C and 1000 rpm.

5.2.4.14 Screening for a more suitable aldehyde dehydrogenase biocatalyst

Since it was proved that the suggested multi-enzymatic reaction scheme (Scheme 5.5) works in practice and produces desired compound **5D** but not efficient enough, a panel of 24 additional aldehyde dehydrogenases were tested for oxidation of **5C** with coenzyme regeneration by NOX. Screening purpose was discovering AlDH that gives the highest **5D** yield.

Twenty five batch experiments with same initial conditions but different aldehyde dehydrogenase were performed (twenty four new enzymes from AlDH panel and previously used and investigated AlDH 003 for comparison). Initial concentration of substrate **5C** was 35.39 mM. Concentrations of NAD^+, NOX and AlDH were 1 mM, 10 mg mL^{-1} and 10 mg mL^{-1}, respectively. Total reaction volume was 1.5 mL. Reactions were performed in 0.5 M

5A – Formaldehyde, **5B** – Propanal, **5C** – 3-Hydroxy-2-methylpropanal, **5D** – 3-Hydroxy-2-methylpropanoic acid, **5E** – Methacrylic acid, **5F** – 3-Hydroxy-2-methylpentanal

TEA HCl buffer pH 8 at 1000 rpm and 25°C and monitored for 24 hours. Higher concentration buffer was used due to the formation of acidic product.

5.2.4.15 Characterization of the oxidation product 5D

To evaluate the chirality of the obtained product **5C**, it was oxidized to **5D**. The procedure was as follows. The synthesis of **5C** was conducted in a 50 mL Falcon tube with 12 mL of reaction volume. The reaction was carried out in 50 mM TEA HCl buffer pH 8, and at 25 °C on a shaker at 1000 rpm for 19 h. Initial concentrations of **5A** and **5B** were 100 mM, whereas FSA^{D6Q} concentration was 3 mg mL^{-1}. Aldehyde dehydrogenase (AlDH 003) was used for the oxidation of **5C** to **5D**. The reaction mixture contained 1 mM NAD^{+}, 80 mM of **5C**, 10 mg mL^{-1} of NADH oxidase (NOX 009) and 10 mg mL^{-1} of AlDH 003. The reaction was started when AlDH was introduced into reaction mixture and was finished after 3 hours. Total reaction volume was 15 mL and the reaction was carried out in 50 mL Falcon tube at 25 °C on a shaker at 1000 rpm.

Obtained product derivatized with 2,4'-dibromo-acetophenone was detected by HPLC and then isolated and purified for NMR analysis and analysis on chiral HPLC column.

As it was not possible to isolate it directly, the product **5D** was identified by the derivatization reaction with 2,4'-dibromo-acetophenone yielding **5G**. The procedure of product identification was as follows. After the oxidation reaction was finished, 150 mL of methanol was added to the reaction mixture and the precipitated enzymes were filtered off using Celite. Methanol was then evaporated and the residue was lyophilised. The solid obtained was dissolved in 10 mL of DMF and 1.5 mmol of 2,4'-dibromo-acetophenone was added. After 7 hours of reaction, the mixture was diluted with 50 mL of ethyl acetate. 50 g of silica gel was then added and solvent was evaporated to dryness. Product purification was carried by column chromatography (47x4.5 cm) on silica gel (100 g) with a gradient elution using a hexane/ethyl acetate mixture of 100:0 (200 mL), 90:10 (200 mL); 80:20 (200 mL), 70:30 (200 mL) 60:40 (200 mL) and 50:50 (1 L). The product eluted at 50:50 mixture. Fractions containing pure product were pooled and the solvent evaporated obtaining 102.3 mg of **5G**.

Product was characterized by NMR at IQAC-CSIC (Spain). Enantiomeric excesses were determined by chiral HPLC column Lux Cellulose-1 by applying method C from Table 5.2. Purified samples of isolated reaction product **5G** were dissolved in the mobile phase and

5A – Formaldehyde, **5B** – Propanal, **5C** – 3-Hydroxy-2-methylpropanal, **5D** – 3-Hydroxy-2-methylpropanoic acid, **5E** – Methacrylic acid, **5F** – 3-Hydroxy-2-methylpentanal

analysed by HPLC. Commercially available **5D** *R*- and *S*- enantiomers derivatized with 2,4'-dibromo-acetophenone were used as analytical standards for chiral column analysis.

5A – Formaldehyde, **5B** – Propanal, **5C** – 3-Hydroxy-2-methylpropanal, **5D** – 3-Hydroxy-2-methylpropanoic acid, **5E** – Methacrylic acid, **5F** – 3-Hydroxy-2-methylpentanal

5.3 Results and discussion

In the first part of this chapter the results of the aldol addition catalysed by FSA are presented. These results include detailed kinetic measurements, model development and optimization which led to process optimization in fed-batch reactor.

The second part of this chapter describes the research of aldol adduct **5C** oxidation by aldehyde dehydrogenase. Developed model for oxidation catalysed by AlDH 003 is presented and is based on investigated kinetic measurements. Finally, alternative aldehyde dehydrogenases were screened and used as biocatalyst for this reaction step.

5.3.1 FSA^{D6Q} overexpression in E. coli

FSA^{D6Q} was overexpressed in *E. coli* and produced for the synthetic purposes. Bradford protein assay had shown 100% protein content in produced lyophilised powder. Produced FSA^{D6Q} (Figure 5.4) was used as biocatalyst in the reaction of aldol addition of **5B** to **5A**.

Figure 5.4 FSA^{D6Q} purified after overexpression in *E. coli*.

5.3.2 Influence of pH on FSA^{D6Q} activity

The influence of pH on FSA^{D6Q} activity was measured and results are presented in Figure 5.5. The measurements showed that FSA^{D6Q} activity increases with the pH. However, at basic pHs the rates of spontaneous non-enzymatic aldol reactions and degradations also increase (Pyo et al., 2011). Therefore, 50 mM TEA HCl pH 8.0 was used as a working buffer for further experiments.

5A – Formaldehyde, **5B** – Propanal, **5C** – 3-Hydroxy-2-methylpropanal, **5D** – 3-Hydroxy-2-methylpropanoic acid, **5E** – Methacrylic acid, **5F** – 3-Hydroxy-2-methylpentanal

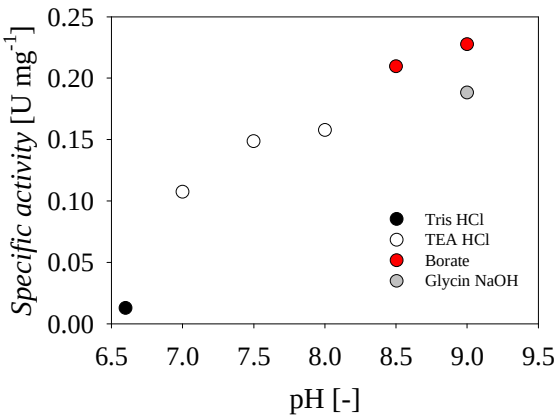

Figure 5.5 The influence of pH on FSA^{D6Q} activity (50 mM buffer, c_{5A} = 100 mM, c_{5B} = 100 mM, 25 °C, $\gamma_{FSA\ D6Q}$ = 0.5 mg mL^{-1}).

5.3.3 Kinetics of aldol addition of 5B to 5A catalysed by FSA

Three variants of FSA: D6Q, D6A and D6E were evaluated for the aldol addition of **5B** to **5A**. The influence of **5B** and **5A** concentrations on the initial reaction rate showed the typical shape of Michaelis-Menten kinetics which included substrate inhibition for all three enzyme variants (Figure 5.6).

Estimated kinetic parameter values for all three variants are presented in Table 5.3, and the dependencies of specific activities of enzyme on substrate concentrations are presented in Figure 5.6.

Table 5.3 Kinetic parameters for aldol addition of **5A** and **5B**.

Parameter	**Unit**	**FSA^{D6Q}**	**FSA^{D6A}**	**FSA^{D6E}**
V_m	U mg^{-1}	3.42 ± 0.05	1.74 ± 0.11	0.74 ± 0.03
K_m^{5A}	mM	102.24 ± 4.01	67.52 ± 7.22	36.33 ± 8.82
K_m^{5B}	mM	668.96 ± 14.17	82.85 ± 7.74	220.71 ± 25.89
K_i^{5A}	mM	679.94 ± 38.81	183.19 ± 29.25	377.28 ± 68.70
K_i^{5B}	mM	230.56 ± 10.86	873.39 ± 138.18	298.99 ± 41.57

5A – Formaldehyde, **5B** – Propanal, **5C** – 3-Hydroxy-2-methylpropanal, **5D** – 3-Hydroxy-2-methylpropanoic acid, **5E** – Methacrylic acid, **5F** – 3-Hydroxy-2-methylpentanal

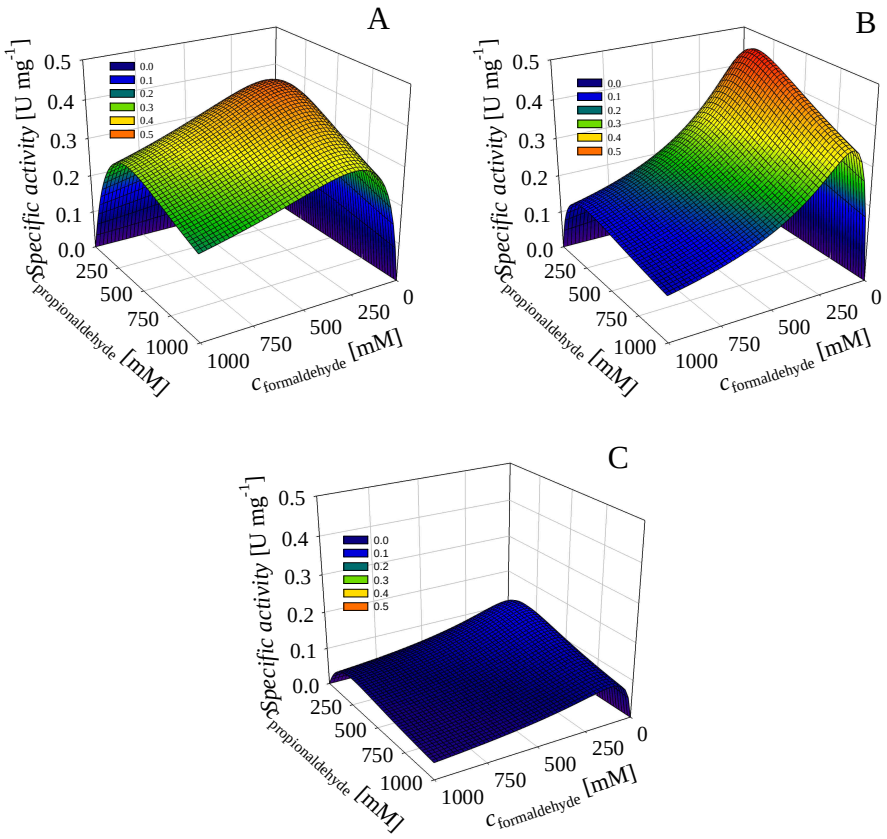

Figure 5.6 Dependence of specific activity of FSA A. D6Q, B. D6A and C. D6E on the concentration of substrates **5A** and **5B** (50 mM TEA HCl buffer pH 8.0, γ_{FSA} = 0.5 mg mL^{-1}, 1000 rpm, 25 °C).

FSA variant D6Q was chosen as the most suitable enzyme to continue with the optimization of the aldol addition since it has high activity towards both substrates in broad concentration range (V_m). Also, inhibition effect of **5A** on variants D6A and D6E is stronger. Hence, it would be more difficult to obtain optimal reaction conditions.

Kinetics of FSA^{D6Q} variant were investigated in more detail and these results are shown in Figure 5.7. The values of apparent kinetic parameters are estimated; maximum reaction rate, V_{m1}, Michaelis and inhibition constants for **5B** and **5A**, i.e. K_{m1}^{5B}, K_{m1}^{5A}, K_{i1}^{5B} and K_{i1}^{5A}, respectively (Table 5.4). As K_{m1}^{5A} is about six-fold lower than K_{m1}^{5B} the enzyme has higher affinity towards **5A**. Product **5C** did not inhibit the FSA^{D6Q} (Fig. 2C). Since methanol is present as stabilizer in the commercial aqueous preparation of **5A**, its effect on the aldol addition reaction was studied. Methanol slightly inhibited the FSA^{D6Q} (Figure 5.7D, Table 5.4).

5A – Formaldehyde, **5B** – Propanal, **5C** – 3-Hydroxy-2-methylpropanal, **5D** – 3-Hydroxy-2-methylpropanoic acid, **5E** – Methacrylic acid, **5F** – 3-Hydroxy-2-methylpentanal

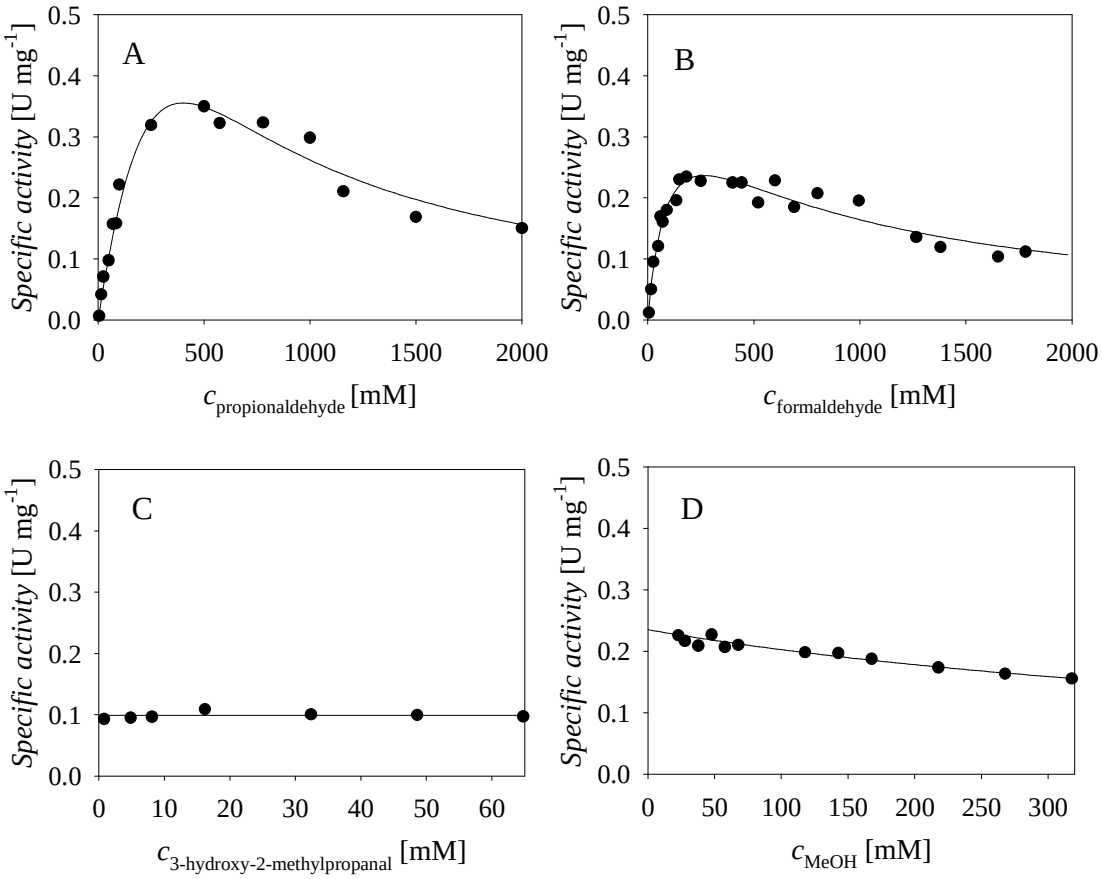

Figure 5.7 The kinetics of FSA^{D6Q} catalysed aldol addition of **5B** to **5A** (50 mM TEA HCl buffer pH 8.0, 25 °C, 1000 rpm, V_r = 0.5 mL, $\gamma_{FSA\ D6Q}$ = 0.5 mg mL^{-1}). The dependence of FSA^{D6Q} specific activity on A. **5B** concentration (c_{5A} = 100 mM), B. **5A** concentration (c_{5B} = 100 mM), C. **5C** concentration (c_{5A} = c_{5B} = 100 mM) and D. MeOH (c_{5A} = c_{5B} = 100 mM). Legend: black circles – experimental data, line – model.

Table 5.4 Estimated kinetic parameters in the aldol addition of **5B** to **5A** and self-addition of **5B** catalysed by FSA^{D6Q}.

Aldol addition of **5B** to **5A** catalysed by FSA^{D6Q}		
Parameter	Unit	Value
V_{m1}	U mg^{-1}	3.42 ± 0.05
K_{m1}^{5A}	mM	102.24 ± 4.01
K_{m1}^{5B}	mM	668.96 ± 14.17
K_{i1}^{5B}	mM	230.56 ± 10.86
K_{i1}^{5A}	mM	679.94 ± 38.81
K_{i1}^{MeOH}	mM	626.35 ± 18.35
Self-addition of **5B** catalysed by FSA^{D6Q}		
Parameter	Unit	Value
V_{m2}	U mg^{-1}	1.80 ± 0.17
K_{m2}^{5B}	mM	403.06 ± 77.82
K_{i2}^{5A}	mM	74.09 ± 15.36

5A – Formaldehyde, **5B** – Propanal, **5C** – 3-Hydroxy-2-methylpropanal, **5D** – 3-Hydroxy-2-methylpropanoic acid, **5E** – Methacrylic acid, **5F** – 3-Hydroxy-2-methylpentanal

It was observed during reactions that self-addition of **5B** occurs (Scheme 5.6). Therefore, kinetics of this reaction was also investigated. The influence of **5B** concentration on the FSA^{D6Q} specific activity can also be described by Michaelis-Menten kinetics (Figure 5.8A). The apparent maximum reaction rate of self-addition, V_{m2}, was about two-fold lower than V_{m1} and K_{m2}^{5B} was similar to K_{m1}^{5B} for the cross-aldol addition reaction (Table 5.4). Thus, the influence of the rate of the self-addition reaction on the formation of aldol of interest could not be neglected and it was included in the model. It was also found that methanol did not act as inhibitor for this reaction up to 300 mM (Figure 5.8B). The inhibition of FSA^{D6Q} activity by **5A** in the self-aldol addition (K_{i2}^{5A} = 74.1 ± 15.4 mM) was stronger than that in the cross-aldol reaction (K_{i1}^{5A} = 679.9 ± 38.8 mM) (Figure 5.8C, Table 5.4).

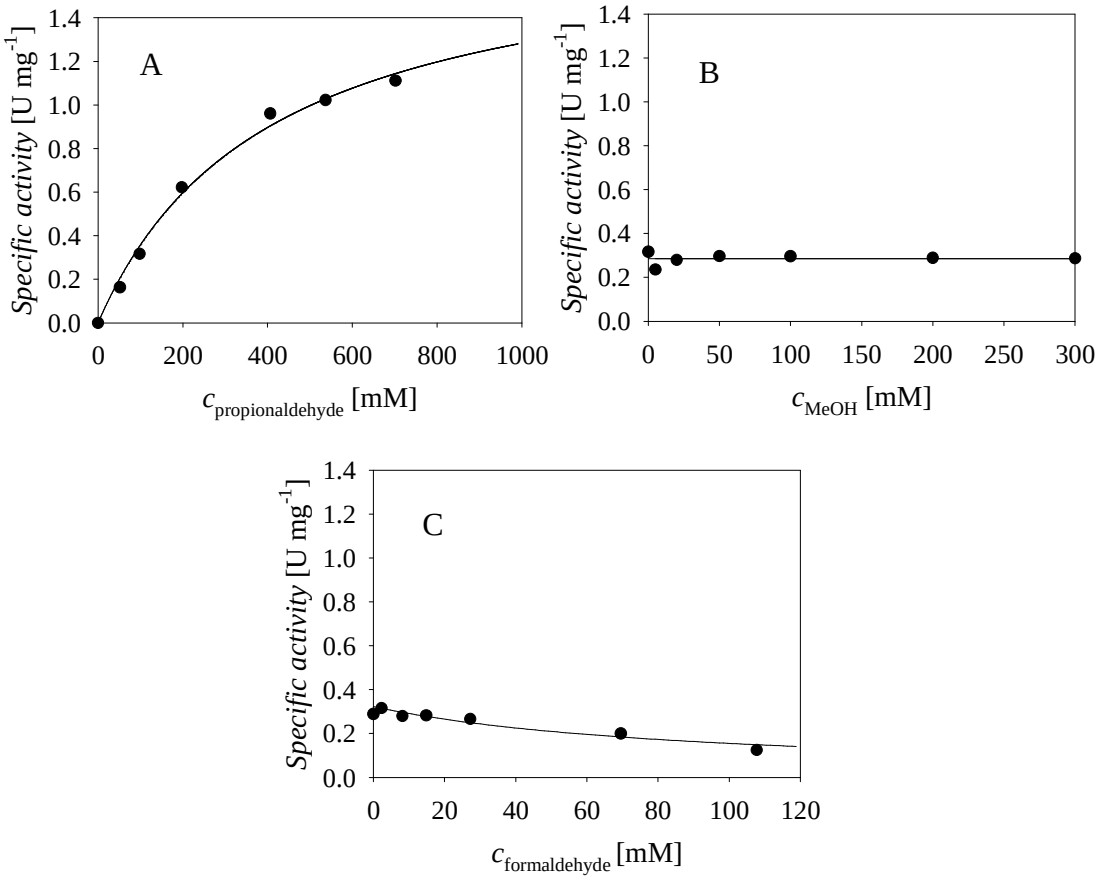

Figure 5.8 The kinetics of FSA^{D6Q} catalysed self-addition of **5B** (50 mM TEA HCl buffer pH 8.0, 25 °C, 1000 rpm, V_r = 0.5 mL, $\gamma_{FSA\ D6Q}$ = 0.5 mg mL^{-1}). The dependence of FSA^{D6Q} specific activity on A. **5B** concentration, B. MeOH (c_{5B} = 100 mM), C. **5A** concentration (c_{5B} = 100 mM). Legend: black circles – experimental data, line – model.

5A – Formaldehyde, **5B** – Propanal, **5C** – 3-Hydroxy-2-methylpropanal, **5D** – 3-Hydroxy-2-methylpropanoic acid, **5E** – Methacrylic acid, **5F** – 3-Hydroxy-2-methylpentanal

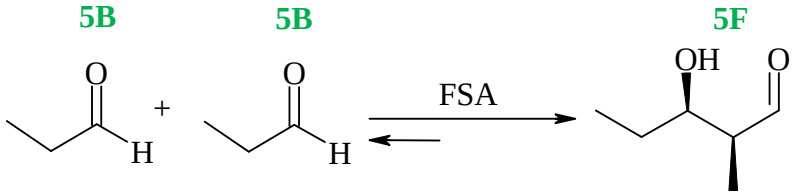

Scheme 5.6 Self-addition of propionaldehyde (**5B**) catalysed by FSA forming **5F** (Junker et al., 2018).

5.3.4 Incubation of aldolase FSA^{D6Q} with substrates

FSA^{D6Q} was independently incubated with different concentrations of **5A** and **5B**. Enzyme was not severely inactivated by **5B** and only up to 10% of activity is lost in 24 hours, regardless of the concentration used (Figure 5.9A).

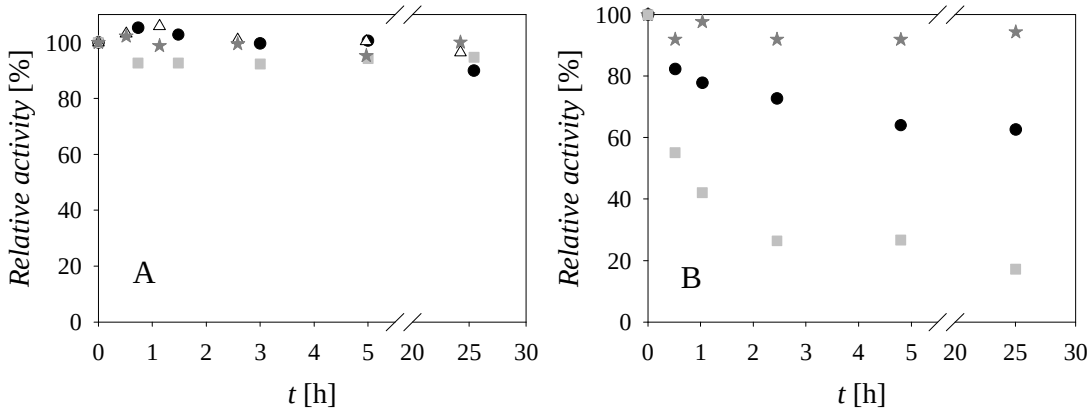

Figure 5.9 The influence of A. **5B** and B. **5A** concentration on FSA^{D6Q} activity during incubation (50 mM TEA HCl buffer pH 8.0, 25 °C, 1000 rpm, V_r = 0.5 mL, $\gamma_{FSA\ D6Q}$ = 0.5 mg mL^{-1}). Legend: white triangles – 50 mM, dark grey stars – 100 mM, black circles – 200 mM, grey squares – 500 mM.

On the other hand, as expected, **5A** significantly inactivated FSA^{D6Q} (Figure 5.9B) owing to its strong electrophilic character. Nearly 80% of the initial enzyme activity is lost after 5 hours of incubation with 500 mM, but the activity remains nearly constant after that up to 25 hours. Increasing the initial concentration of **5A** causes faster enzyme inactivation (Figure 5.9B) than that of **5B**. It is thus expected that **5A** will have a crucial influence on both enzyme activity and its operational stability.

5A – Formaldehyde, **5B** – Propanal, **5C** – 3-Hydroxy-2-methylpropanal, **5D** – 3-Hydroxy-2-methylpropanoic acid, **5E** – Methacrylic acid, **5F** – 3-Hydroxy-2-methylpentanal

5.3.5 Stability of reactants and products in the reaction solution

It was found that **5A** is stable for 24 hours in presence and absence of the enzyme. On the other hand, **5B** underwent spontaneous self-aldol addition (i.e., 10% conversion after 23 hours) and biocatalysed self-aldol addition (i.e., 55% conversion after 3.8 hours) where **5F** is produced. Also, non-biocatalytic aldol addition of **5B** to **5A** was detected (i.e., 17% **5A** conversion after 24 hours). Considering that the enzymatic aldol addition of **5B** to **5A** and the self-aldol addition of **5B** are the fastest reactions, it can safely be assumed that the non-biocatalytic reactions did not have a significant influence on the outcome of the process, and, therefore they can be neglected.

Aldol products **5C** and **5F** are aldehydes as well, and under the reaction conditions they underwent spontaneous non-enzymatic side reactions that were not investigated in detail (Figure 5.10). The rate of the unspecific transformation of **5C** and **5F** was described by the first order kinetics (Table 5.6, Equations 5.3 and 5.4) and the data (Figure 5.10) were used to estimate the reaction rate constants k_1 and k_2 (Table 5.5).

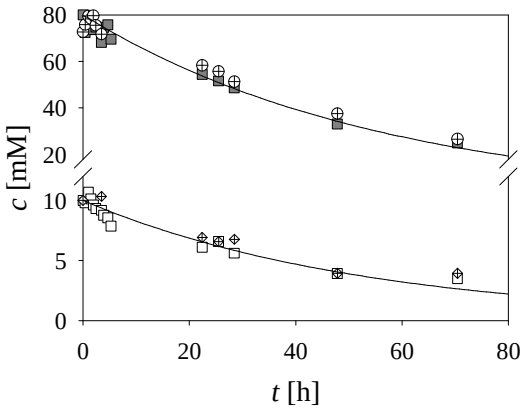

Figure 5.10 Unspecific transformation of **5C** and **5F** in the batch reactor (50 mM TEA HCl buffer pH 8.0, 25 °C, 1000 rpm, V_r = 1.2 mL) with ($\gamma_{\text{FSA D6Q}}$ = 3.0 mg mL^{-1}) and without the presence of enzyme. Legend: grey squares – **5C** in experiment without enzyme, white squares – **5F** in experiment without enzyme, crossed circle – **5C** in experiment with enzyme, crossed diamonds – **5F** in experiment with enzyme, line – model.

Table 5.5 Estimated rate constants for the unspecific transformation of aldol products **5C** and **5F**.

Reaction rate constants for the unspecific transformation of aldol products **5C** and **5F**		
k_1	min^{-1}	$2.95 \cdot 10^{-4} \pm 1.2 \cdot 10^{-5}$
k_2	min^{-1}	$3.93 \cdot 10^{-4} \pm 1.3 \cdot 10^{-5}$

5A – Formaldehyde, **5B** – Propanal, **5C** – 3-Hydroxy-2-methylpropanal, **5D** – 3-Hydroxy-2-methylpropanoic acid, **5E** – Methacrylic acid, **5F** – 3-Hydroxy-2-methylpentanal

5.3.6 LC-MS analysis of aldol products

The analysis on LC-MS was performed to confirm the aldol addition product **5C** (Scheme 5.1) and propionaldehyde self-addition product **5F** (Scheme 5.6). It was shown that 3-hydroxy-2-methylpropanal and 3-hydroxy-2-methylbutanal are indeed the products designated on the reaction scheme as they were identified by HPLC-MS spectra as shown in Appendix (Figure 10.3).

5.3.7 Mathematical model and optimization of aldol addition

Model developed for each individual reaction system was validated by independent experiments carried out in different reactors. After successful validation, mathematical model was used for choosing the best reactor mode and process optimization.

The mathematical model of the aldol addition of **5B** to **5A** catalysed by FSA^{D6Q} consists of kinetic and reactor's mass balance equations (Table 5.6). The reaction kinetics was described by the double substrate Michaelis-Menten equation including substrate inhibitions by **5B** and **5A**, as well as with non-competitive inhibition by MeOH (Equation 5.2), which is used commercially to stabilize **5A**. Its content in **5A** solution is 4.8 mol%. Self-aldol addition of **5B** was described by double substrate Michaelis-Menten kinetics including competitive inhibition by **5A** (Equation 5.3). All kinetic constants were estimated from the experimental data, as described earlier, by using the initial reaction rate vs substrate concentration data acquired by using the initial reaction rate method. Equations 5.4 and 5.5 represent the rates of unspecific transformation of aldol products **5C** and **5F**, respectively. The kinetic constants of the first order were estimated from the experimental data **5C** and **5F** concentration vs time in the independent experiments (Figure 5.10).

Mass balance equations for **5A**, **5B**, **5C** and **5F** in the batch reactor are represented by Equations 5.6-5.9. The mass balance for **5B** includes its consumption in the cross-aldol (r_1) and self-addition (r_2). It was necessary to add coefficient 2 for r_2 because 2 molecules of **5B** react to form 1 molecule of **5C**. Mass balance equations for **5A**, **5B**, **5C**, **5F**, FSA^{D6Q} and MeOH in the fed-batch reactor are represented by Equations 5.10-5.15. Equation 5.16 represents the change in reactor volume during the experiment defined by the sum of flow rates of the two feeds.

The enzyme operational stability decay was described by the first order kinetics (Equation 5.17A). Enzyme operational stability decay rate constants (k_d) were estimated

5A – Formaldehyde, **5B** – Propanal, **5C** – 3-Hydroxy-2-methylpropanal, **5D** – 3-Hydroxy-2-methylpropanoic acid, **5E** – Methacrylic acid, **5F** – 3-Hydroxy-2-methylpentanal

directly from the batch reactor experiments by using the concentration vs time curve or by using the enzyme activity vs time data that was collected in part of the experiments. Based on these results the dependence of the operational stability decay rate constant on the initial concentration of **5A** was described by Equation 5.17B.

Table 5.6 Mathematical model for the aldol addition of **5B** to **5A** in the batch and fed-batch reactor.

KINETIC EQUATIONS	
$r_1 = \frac{V_{m1} \cdot \gamma_{\mathrm{FSA}} \cdot c_{5\mathrm{A}} \cdot c_{5\mathrm{B}}}{\left[\left(K_{m1}^{\ 5\mathrm{A}} + c_{5\mathrm{A}} + \frac{c^2_{\ 5\mathrm{A}}}{K_{i1}^{\ 5\mathrm{A}}}\right) \cdot \left(K_{m1}^{\ 5\mathrm{B}} + c_{5\mathrm{B}} + \frac{c^2_{\ 5\mathrm{B}}}{K_{i1}^{\ 5\mathrm{B}}}\right)\right]} \cdot \frac{1}{1 + \frac{c_{\mathrm{MeOH}}}{K_{i1}^{\mathrm{MeOH}}}}$ (5.2)	
$r_2 = \frac{V_{m2} \cdot \gamma_{\mathrm{FSA}} \cdot c^2_{5\mathrm{B}}}{\left(K_{m2}^{\ 5\mathrm{B}} \cdot \left(1 + \frac{c_{5\mathrm{A}}}{K_{i2}^{\ 5\mathrm{A}}}\right) + c_{5\mathrm{B}}\right)^2}$ (5.3)	
$r_3 = k_1 \cdot c_{5C}$ (5.4)	$r_4 = k_2 \cdot c_{5F}$ (5.5)
MASS BALANCES IN THE BATCH REACTOR	
$\frac{\mathrm{d}c_{5\mathrm{A}}}{\mathrm{d}t} = -r_1$ (5.6)	$\frac{\mathrm{d}c_{5\mathrm{B}}}{\mathrm{d}t} = -r_1 - 2 \cdot r_2$ (5.7)
$\frac{\mathrm{d}c_{5\mathrm{C}}}{\mathrm{d}t} = r_1 - r_3$ (5.8)	$\frac{\mathrm{d}c_{5\mathrm{F}}}{\mathrm{d}t} = r_2 - r_4$ (5.9)
MASS BALANCES IN THE FED-BATCH REACTOR	
$\frac{\mathrm{d}c_{5\mathrm{A}}}{\mathrm{d}t} = \frac{1}{V} \cdot \left(-c_{5\mathrm{A}} \cdot \frac{\mathrm{d}V}{\mathrm{d}t} + c_{5A,0} \cdot q_1\right) - r_1$ (5.10)	$\frac{\mathrm{d}c_{5\mathrm{B}}}{\mathrm{d}t} = \frac{1}{V} \cdot \left(-c_{5\mathrm{B}} \cdot \frac{\mathrm{d}V}{\mathrm{d}t} + c_{5\mathrm{B},0} \cdot q_2\right) - r_1 - 2 \cdot r_2$ (5.11)
$\frac{\mathrm{d}c_{5\mathrm{C}}}{\mathrm{d}t} = \frac{1}{V} \cdot \left(-c_{5\mathrm{C}} \cdot \frac{\mathrm{d}V}{\mathrm{d}t}\right) + r_1$ (5.12)	$\frac{\mathrm{d}c_{5\mathrm{F}}}{\mathrm{d}t} = \frac{1}{V} \cdot \left(-c_{5\mathrm{F}} \cdot \frac{\mathrm{d}V}{\mathrm{d}t}\right) + r_2$ (5.13)
$\frac{\mathrm{d}\gamma_{\mathrm{FSA}}}{\mathrm{d}t} = \frac{1}{V} \cdot \left(-\gamma_{\mathrm{FSA}} \cdot \frac{\mathrm{d}V}{\mathrm{d}t}\right)$ (5.14)	$\frac{\mathrm{d}c_{\mathrm{MeOH}}}{\mathrm{d}t} = \frac{1}{V} \cdot \left(-c_{\mathrm{MeOH}} \cdot \frac{\mathrm{d}V}{\mathrm{d}t} + c_{\mathrm{MeOH},0} \cdot q_1\right)$ (5.15)
$\frac{\mathrm{d}V}{\mathrm{d}t} = q_1 + q_2$ (5.16)	
ENZYME OPERATIONAL STABILITY DECAY	
$\frac{\mathrm{d}\gamma_{\mathrm{FSA}}}{\mathrm{d}t} = -k_d \cdot \gamma_{\mathrm{FSA}}$ (5.17A)	$k_d = \frac{a \cdot c_{5\mathrm{A},0}}{b + c_{5\mathrm{A},0}}$ (5.17B)

5A – Formaldehyde, **5B** – Propanal, **5C** – 3-Hydroxy-2-methylpropanal, **5D** – 3-Hydroxy-2-methylpropanoic acid, **5E** – Methacrylic acid, **5F** – 3-Hydroxy-2-methylpentanal

5.3.7.1 Model validation of aldol addition in batch reactor

To validate and confirm the applicability of the mathematical model for the batch reactor (Table 5.6, Equations 5.2-5.9, 5.17A), experiments were conducted at different concentrations of substrates up to 2 M and FSA^{D6Q} up to 26 mg mL^{-1}.

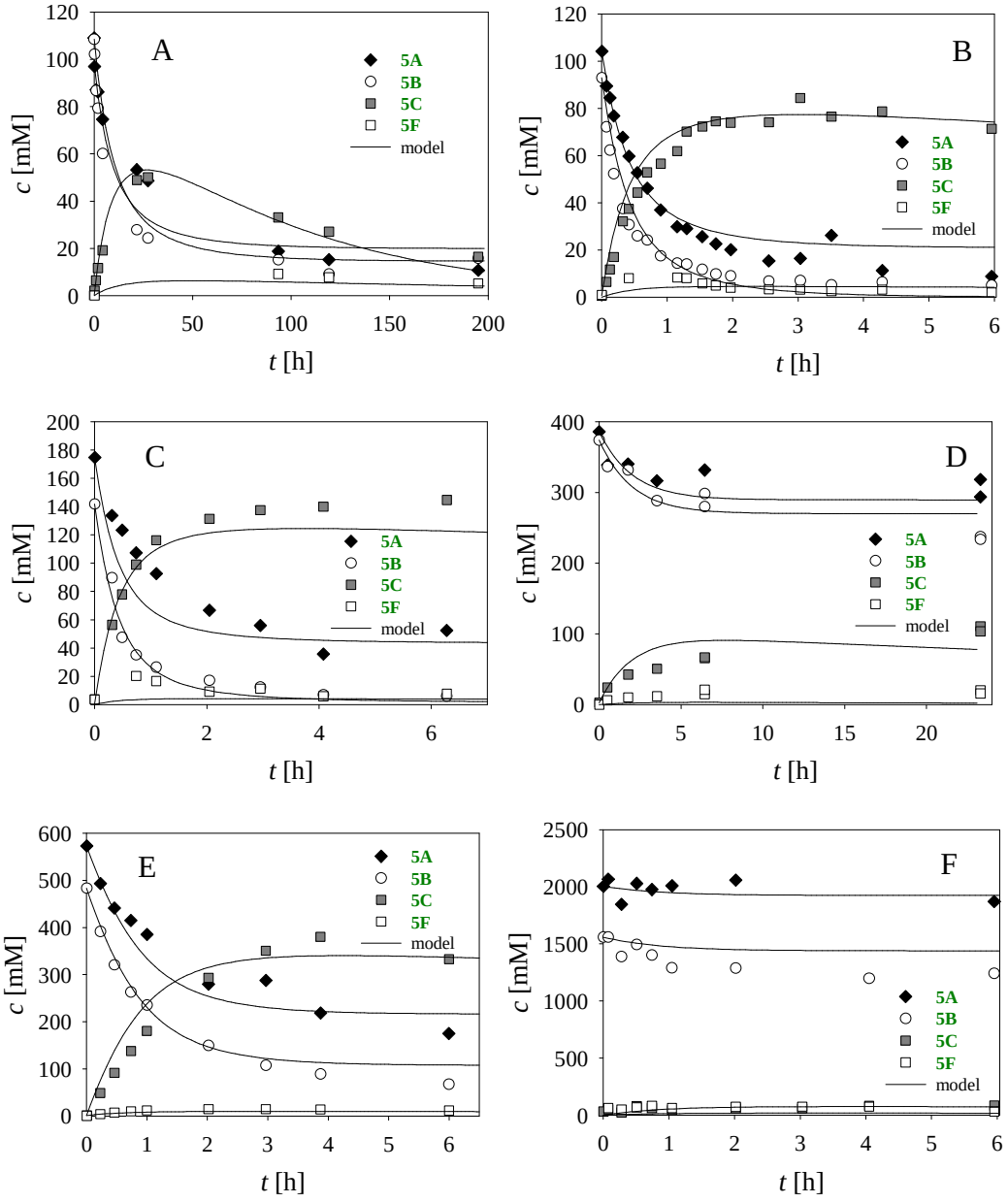

Figure 5.11 Mathematical model validation in batch reactor experiments carried out at different experimental conditions (50 mM TEA HCl buffer pH 8.0, 25 °C, 1000 rpm). A. c_{5A} = 109.0 mM, c_{5B} = 108.5 mM, V_r = 1.0 mL, $\gamma_{FSA\ D6Q}$ = 1.0 mg mL^{-1}, B. c_{5A} = 104.3 mM, c_{5B} = 93.0 mM, V_r = 1.8 mL, $\gamma_{FSA\ D6Q}$ = 26.3 mg mL^{-1}, C. c_{5A} = 174.7 mM, c_{5B} = 141.8 mM, V_r = 0.9 mL, $\gamma_{FSA\ D6Q}$ = 25.0 mg mL^{-1}, D. c_{5A} = 386,1 mM, c_{5B} = 374.1 mM, V_r = 0.5 mL, $\gamma_{FSA\ D6Q}$ = 3.0 mg mL^{-1}, E. c_{5A} = 573.2 mM, c_{5B} = 483.5 mM, V_r = 0.9 mL, $\gamma_{FSA\ D6Q}$ = 25.0 mg mL^{-1}, F. c_{5A} = 2003.3 mM, c_{5B} = 1559.0 mM, V_r = 0.9 mL, $\gamma_{FSA\ D6Q}$ = 25.2 mg mL^{-1}.

5A – Formaldehyde, **5B** – Propanal, **5C** – 3-Hydroxy-2-methylpropanal, **5D** – 3-Hydroxy-2-methylpropanoic acid, **5E** – Methacrylic acid, **5F** – 3-Hydroxy-2-methylpentanal

The model enabled a good fit for a broad experimental range (Figure 5.11). Degradation of **5C** and **5F** is more visible when lower enzyme concentrations are used (Figure 5.11A) and the rate of enzymatic reaction is slower than the rate of product unspecific transformation.

The lower the FSA^{D6Q} concentration the higher extend of aldol adducts non-enzymatic side reactions (Figure 5.11A) occurred. This is consistent with the fact that under these conditions the rates of biocatalytic aldol addition and the non-catalytic side reactions were similar.

Table 5.7 Operational stability decay rate constants of the first order estimated from the data activity vs time measured by the enzyme assay during batch reactor experiments carried out at different initial equimolar concentrations of **5B** and **5A**.

Concentration of substrates	**k_d [min^{-1}]**	**$t_{1/2}$ [min]**
100 mM	0.0021 ± 0.0002	328.77
200 mM	0.0056 ± 0.0006	123.56
300 mM	0.0105 ± 0.0009	65.78
500 mM	0.0139 ± 0.0009	49.84
1000 mM	0.0159 ± 0.0013	43.51
2000 mM	0.0226 ± 0.0017	30.65

Table 5.8 Dependence of operational stability decay rate constant on the initial concentration of **5A**.

Dependence of operational stability decay rate constant on the initial concentration of **5A** – model parameters		
a	min^{-1}	0.0334 ± 0.0042
b	mM	929.96 ± 223.65

The operational stability decay rate constants of FSA^{D6Q} were estimated by monitoring its activity during batch experiments (Table 5.7) or by estimating it directly from the batch reactor experiment by using the mathematical model (Table 5.6, Equations 5.2-5.9, 5.17A). In the latter case, the experimental data of concentration vs time were used and all the other kinetic parameters (Table 5.4) were kept constant. Results for the estimated constants (k_d) by using both methods are presented in Figure 5.12. The k_d of FSA^{D6Q} strongly depends on the initial concentration of **5A**, as it was expected from the enzyme incubation experiments (Figure 5.9B). While increasing the concentration of **5A**, k_d increased and, consequently, the enzyme half-life time dropped dramatically (Figure 5.12). The dependence of k_d on the initial concentration of **5A** can be described by a hyperbolic equation as presented before in the literature for aldehydes (Vasić-Rački et al., 2003). The kinetic equation and the estimated

5A – Formaldehyde, **5B** – Propanal, **5C** – 3-Hydroxy-2-methylpropanal, **5D** – 3-Hydroxy-2-methylpropanoic acid, **5E** – Methacrylic acid, **5F** – 3-Hydroxy-2-methylpentanal

kinetic parameters are presented in Table 5.6, Equation 5.18 and Table 5.8, respectively. It can be concluded that the implementation of this reaction in a synthetic process requires an initial concentration of **5A** below 200 mM (Figure 5.12). These results also explain why substrate conversion in some experiments presented in Figure 5.11 (i.e. D and F) is low. The deactivating effect of **5A** can be diminished by increasing the concentration of enzyme. Depending on enzyme and substrate concentration, the yield of aldol adduct can vary significantly (Figure 5.13). Thus, **5C** yield (i.e. calculated as the ratio of **5C** to the limiting reactant **5B**) increased with FSA^{D6Q} concentration, whereas it dropped on increasing the substrate concentration (Figure 5.13B). Apart from experimental results, model simulations showed how the non-enzymatic side reactions of **5C** influences the aldol yield and the importance to monitor the reaction to prevent product loss (Figure 5.13C). It also reveals that while increasing the FSA^{D6Q} concentration, the rate of unspecific transformation of **5C** can be neglected up to ca. 5 hours (Figure 5.13C and 5.13D). However, owing to this unspecific side reaction, repetitive batch reactor cannot be used to increase the production, because it would imply long incubation times compromising the product stability. Thus, fed-batch reactor could be the reactor of choice for obtaining optimal results in terms of **5C** productivity.

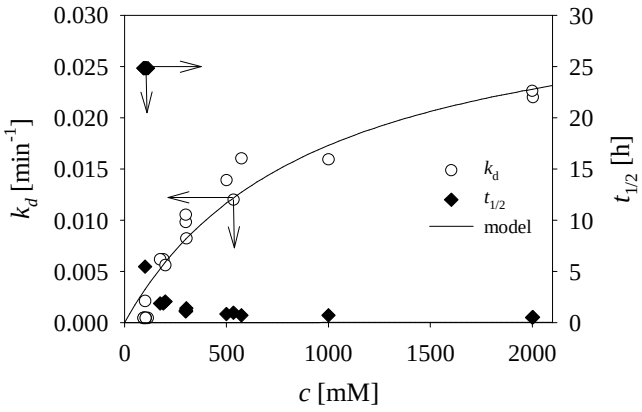

Figure 5.12 Change in FSA^{D6Q} operational stability decay constant and half-life time in batch reactor experiments carried out at different initial concentrations of **5B** and **5A** (50 mM TEA HCl buffer, pH 8.0, 25 °C, 1000 rpm, concentrations of substrates in Table 5.6).

5A – Formaldehyde, **5B** – Propanal, **5C** – 3-Hydroxy-2-methylpropanal, **5D** – 3-Hydroxy-2-methylpropanoic acid, **5E** – Methacrylic acid, **5F** – 3-Hydroxy-2-methylpentanal

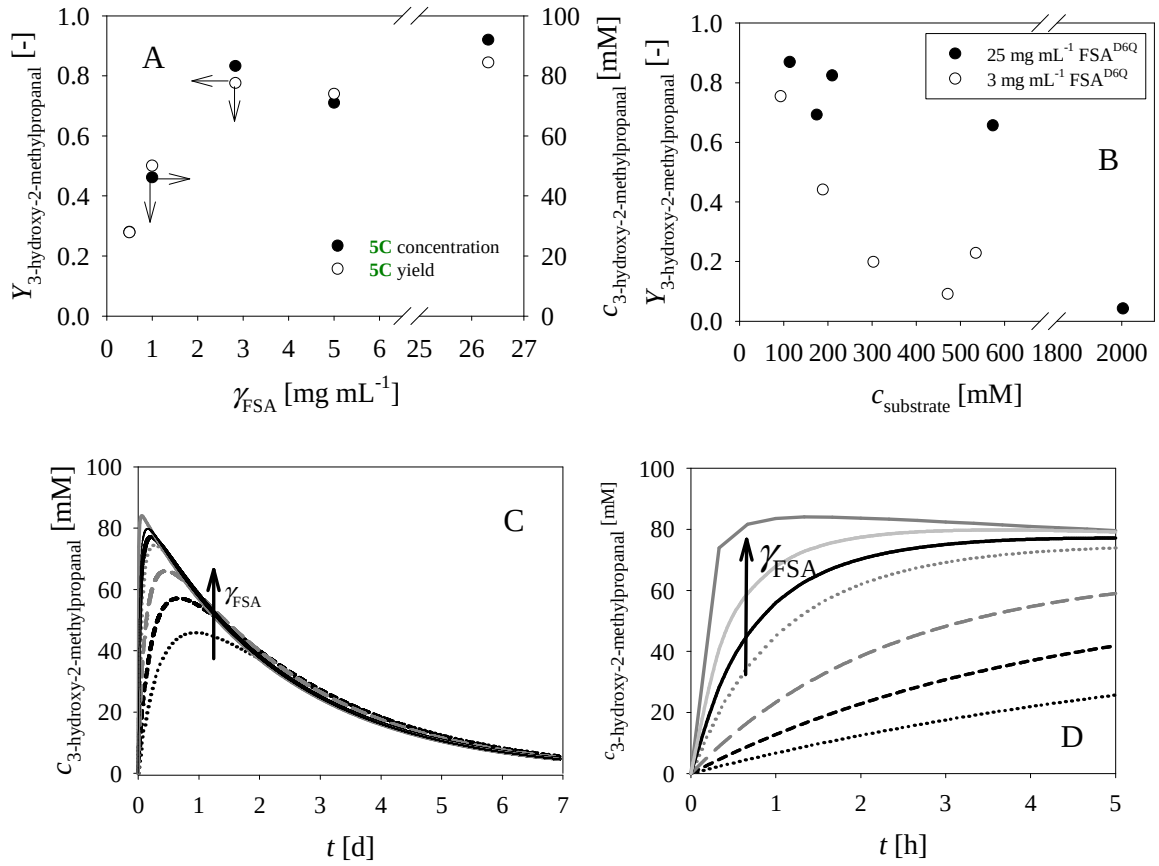

Figure 5.13 A. The influence of FSA^{D6Q} concentration on the reaction yield and maximum product concentration – based on experimental results in the batch reactor (50 mM TEA HCl buffer pH 8.0, 25 °C, 1000 rpm, $c_{5A} \approx c_{25A} \approx 100$ mM). B. Influence of substrate **5A** and **5B** concentrations on yield of **5C** (50 mM TEA HCl buffer pH 8.0, 25 °C, 1000 rpm). Simulation – the influence of enzyme concentration on the reaction outcome (Legend: black dotted line – 1 mg mL^{-1}, black short dash line – 2 mg mL^{-1}, dark grey long dash line – 4 mg mL^{-1}, dark grey dotted line – 10 mg mL^{-1}, black line – 15 mg mL^{-1}, dark grey line – 100 mg mL^{-1}) presented during 7 days (C) and 5 hours (D).

5.3.7.2 Model validation and process optimization of aldol addition in fed-batch reactor

Previously presented data showed that **5A** will significantly influence FSA^{D6Q} activity and stability while **5B** caused by-product formation in self-addition reaction. Thus, a fed-batch reactor was the candidate of choice to carry out the reaction. By slow addition of **5B** and **5A**, their concentrations can be kept at low level during the entire process and enzyme operational stability and product yield can be maximized.

5A – Formaldehyde, **5B** – Propanal, **5C** – 3-Hydroxy-2-methylpropanal, **5D** – 3-Hydroxy-2-methylpropanoic acid, **5E** – Methacrylic acid, **5F** – 3-Hydroxy-2-methylpentanal

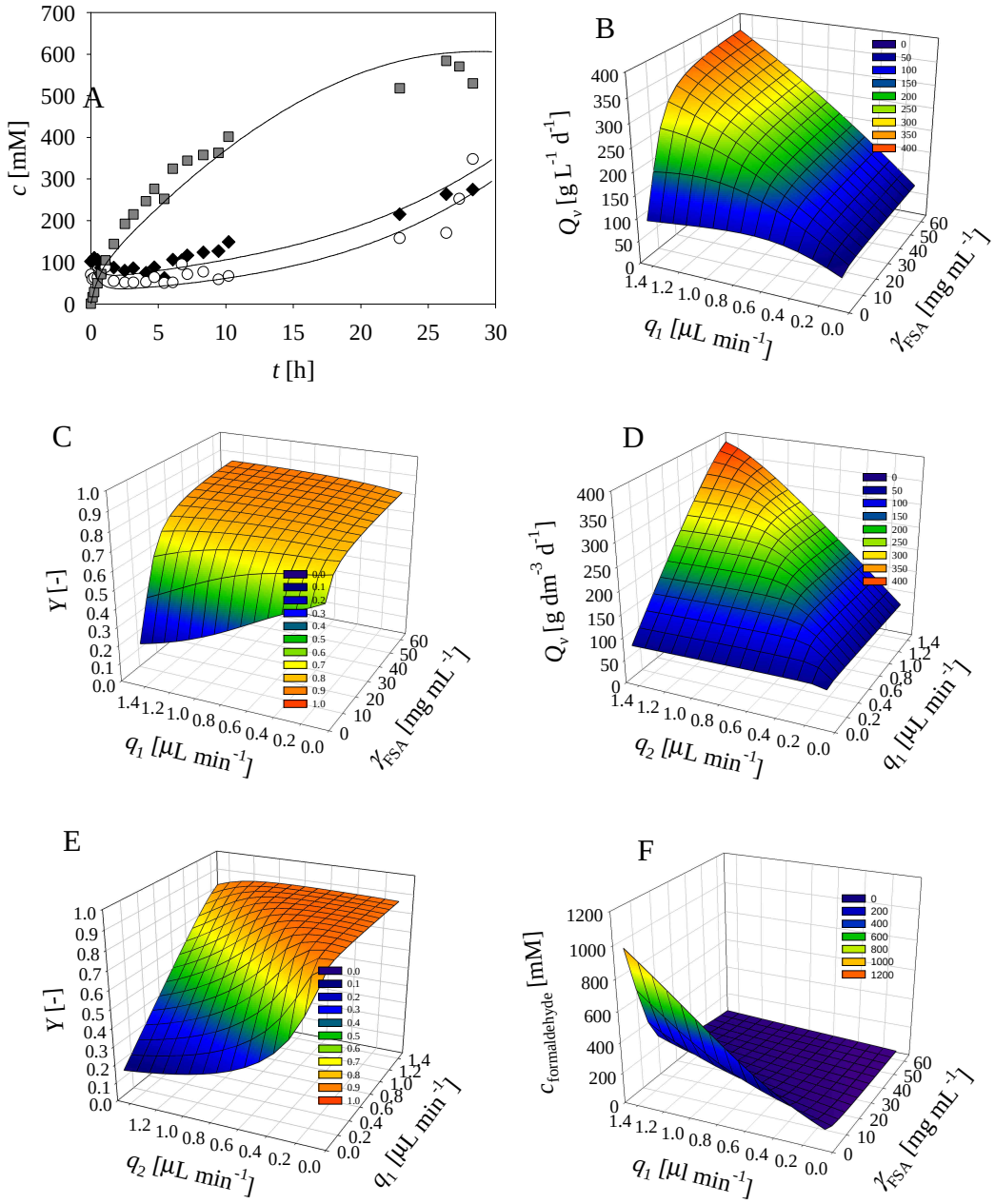

Figure 5.14 Aldol addition of **5B** to **5A** in fed-batch reactor (50 mM TEA HCl buffer pH 8.0, 25 °C, 250 rpm, V_0 = 5 mL). A. $c_{5A,0} \approx c_{5B,0} \approx 100$ mM, $\gamma_{FSA\ D6Q,0}$ = 20.62 mg mL^{-1}, q_1 = 0.26 µL min^{-1}, q_2 = 0.27 µL min^{-1}. Legend: grey squares – **5C** concentration, black diamonds – **5A** concentration, white circles – **5B** concentration, line – model. Model simulations ($c_{5A,0} \approx c_{5B,0} \approx 150$ mM, $c_{5A,\ feed\ 1}$ = 13.43 M, $c_{5B,\ feed\ 2}$ = 13.33 M, t = 6 h) to evaluate: B. and C. the influence of feed flow-rates and FSA^{D6Q} concentration on volume productivity and product yield (q_2 = 0.9 q_1), respectively; D. and E. the influence of individual feed flow-rates on volume productivity and product yield ($\gamma_{FSA\ D6Q,0}$ = 60 mg mL^{-1}), respectively. F. The influence of feed flow-rates and FSA^{D6Q} concentration on the final concentration of **5A** in the reactor (q_2 = 0.9 q_1).

5A – Formaldehyde, **5B** – Propanal, **5C** – 3-Hydroxy-2-methylpropanal, **5D** – 3-Hydroxy-2-methylpropanoic acid, **5E** – Methacrylic acid, **5F** – 3-Hydroxy-2-methylpentanal

Figure 5.14A shows the results of the first fed-batch experiment, which were used to validate the proposed mathematical model (Table 5.6, Equations 5.2-5.5, 5.10-5.18). Since model simulations fit the data well, it was used to evaluate the influence of feed flow-rates and FSA^{D6Q} concentration on the volume productivity and yield of product (Figures 5.14B and 5.14C, respectively), and to find out the experimental conditions at which optimal process metrics, i.e. volume productivity, product concentration and product yield can be obtained.

Feed 2 (**5B**)/feed 1 (**5A**) ratio was kept constant in these simulations at 0.9. The results of the model simulations showed that high flow-rates, as well as FSA^{D6Q} concentrations, on the limits of the investigated variable range, enable obtaining volume productivities of ca 350 g L^{-1} d^{-1} and 85% **5C** yield (Figures 5.14B and 5.14C). A significant influence of the feed flow-rates on the volume productivity was found (Figure 5.14D). Additionally, these flow-rates have to be well balanced to obtain high product yield, minimizing the effect of self-aldol addition of **5B** (Figure 5.14E). Maximum flow-rate of feed 1 within the investigated range, and lower flow-rates of feed 2 are necessary to obtain maximum product yield. In both cases concentrated commercially available solutions of substrates are supplied to the reactor.

Owing to that high flow-rates mean high substrate concentrations in the reactor, simulations were performed to evaluate the effect of flow-rates, as well as enzyme concentration on the final **5A** concentration in the reactor after 6 hours (Figure 5.14F). Flow-rate ratio of feed 2 and 1 was kept constant at 0.9. The simulation shows that flow-rates have to be chosen carefully, because the excess of **5A** in the reactor will cause rapid FSA^{D6Q} inactivation. In addition, the surplus of **5B** will increase the rate of the by-product **5F** formation and lower the product yield.

The next fed-batch experiment was carried out at 60 mg mL^{-1} of FSA^{D6Q}. The flow-rates of feed 1 and 2 were set to 1.4 and 1.26 µL min^{-1}, respectively. Under these conditions the simulations showed that the concentrations of **5A** and **5B** in the reactor during 6 hours of the experiment will be below 200 mM, which will ensure slow FSA^{D6Q} operational stability decay, and higher product yield. The experimental results (Figure 5.15) showed a good agreement with the mathematical model (Table 5.6, Equations 5.2-5.5, 5.10-5.18). The final concentration of **5C** after 5.5 hours was 814 mM (72 g L^{-1}), volume productivity was 313.7 g L^{-1} d^{-1} and yield of **5C** was 88.5%. Figure 5.15 also presents the change in product yield and volume productivity during the experiment calculated from the experimental data in comparison to model simulation.

5A – Formaldehyde, **5B** – Propanal, **5C** – 3-Hydroxy-2-methylpropanal, **5D** – 3-Hydroxy-2-methylpropanoic acid, **5E** – Methacrylic acid, **5F** – 3-Hydroxy-2-methylpentanal

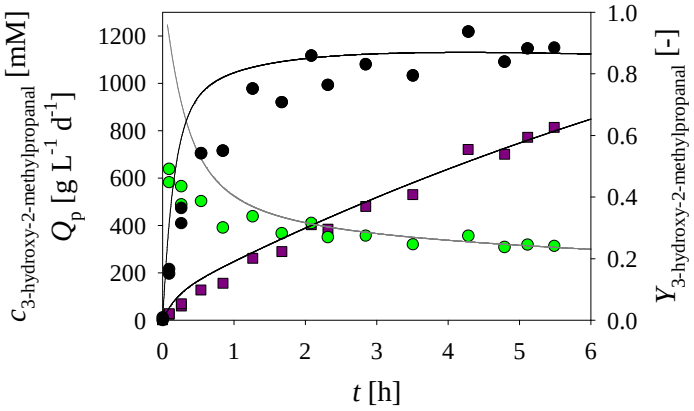

Figure 5.15 Aldol addition of **5B** to **5A** in fed-batch reactor (50 mM TEA HCl buffer pH 8.0, 25 °C, 250 rpm, V_0 = 5 mL) at the selected conditions according to the model simulations ($c_{\mathbf{5A},\text{ feed 1}}$ = 13.43 M, $c_{\mathbf{5B},\text{ feed 2}}$ = 13.33 M, $c_{\mathbf{5A}} \approx c_{\mathbf{5B}} \approx$ 150 mM, $\gamma_{\text{FSA D6Q,0}}$ = 60 mg mL^{-1}, q_1 = 1.4 µL min^{-1}, q_2 = 1.26 µL min^{-1}). Legend: dark purple squares – **5C** concentration, black circles – product yield, green circles – volume productivity, line – model.

5.3.8 Kinetic measurements of oxidation catalysed by aldehyde dehydrogenase 003

The second step of the cascade reaction towards MAA precursor (Scheme 5.2) is the oxidation of aldehyde **5C** to the corresponding carboxylate **5D** by enzymatic oxidation using aldehyde dehydrogenase (AlDH 003) from Prozomix Ltd (United Kingdom). Regeneration of NAD^+ was accomplished by NADH oxidase (NOX 009) from Prozomix as well (Scheme 5.5).

Kinetic measurements are divided in four sections. First, the influence of concentrations of aldol addition substrates **5A** and **5B** on the activity of aldehyde dehydrogenase was determined to prove the assumption that this cascade cannot be performed in a one-pot synthesis. Also, reactions in the batch reactor were performed with each substrate and presented in the same chapter. Next, crude lyophilised non-purified enzyme (CFE) AlDH 003 kinetics was investigated in the oxidation of **5C**. It was found that CFE contains some NADH oxidase activity. Therefore, the kinetics of NADH oxidation catalysed by AlDH 003 were determined as well. Afterwards, purified suspension of AlDH 003 was investigated and the results of the kinetic measurements are shown. At last, the kinetics of NADH oxidation catalysed by NADH oxidase CFE 009 was investigated in detail and its kinetic parameters are estimated and included in the model as well.

5A – Formaldehyde, **5B** – Propanal, **5C** – 3-Hydroxy-2-methylpropanal, **5D** – 3-Hydroxy-2-methylpropanoic acid, **5E** – Methacrylic acid, **5F** – 3-Hydroxy-2-methylpentanal

5.3.8.1 5A and 5B oxidation kinetics and reactions in the batch reactor catalysed by lyophilised aldehyde dehydrogenase 003, CFE

We envisaged that methacrylic acid synthesis could be performed in a one-pot synthesis. Detailed kinetic analysis showed that one-pot reaction setting will not have a desired outcome. Namely, the results of measuring the influence of concentration of **5A** and **5B** on AlDH activity showed that aldol addition and oxidation steps of the proposed enzymatic cascade system cannot be carried out in a one-pot synthesis since both **5A** and **5B** also act as AlDH substrates (Figures 5.16A and 5.16D). Thus, two reactions were carried out and optimized separately and performed in consecutive order (i.e., one-pot two steps). Information gained by conducting this set of experiments is also important because **5A** and **5B** are to some extent present in the oxidation reaction solution as unconverted substrates from aldol addition, and can cause the formation of by-products. The estimated kinetic parameters are presented in Tables 5.9 and 5.10. It can be seen that the maximum rate of oxidation of **5B** (Table 5.10) is much higher than the rate of oxidation of **5C** (Table 5.13, Chapter 5.3.8.3). Therefore, the concentration of **5B** after the aldol addition step should be minimal. AlDH has high activity towards **5A** as well, but it is also inhibited by this compound. The affinity of enzyme towards **5A** is low, whereas this is not the case for affinity towards **5B**. In this case, the problem with **5A** is in the fact that it will not degrade in the reactor and, therefore, it will negatively affect the enzymes.

Table 5.9 Kinetic parameters of oxidation of **5A** catalysed by AlDH 003 CFE.

Parameter	Unit	Value
V_{m4}	U mg^{-1}	0.190 ± 0.010
$K_{m4}^{\mathbf{5A}}$	mM	2.136 ± 0.234
$K_{i4}^{\mathbf{5A}}$	mM	381.517 ± 65.204
K_{m4}^{NAD+}	mM	0.174 ± 0.043
K_{i4}^{NADH}	mM	0.009 ± 0.002

Table 5.10 Kinetic parameters of oxidation of **5B** catalysed by AlDH 003 CFE.

Parameter	Unit	Value
V_{m5}	U mg^{-1}	4.835 ± 0.140
$K_{m5}^{\mathbf{5B}}$	mM	2.513 ± 0.409
K_{m5}^{NAD+}	mM	0.299 ± 0.034
K_{i5}^{NADH}	mM	0.032 ± 0.003

5A – Formaldehyde, **5B** – Propanal, **5C** – 3-Hydroxy-2-methylpropanal, **5D** – 3-Hydroxy-2-methylpropanoic acid, **5E** – Methacrylic acid, **5F** – 3-Hydroxy-2-methylpentanal

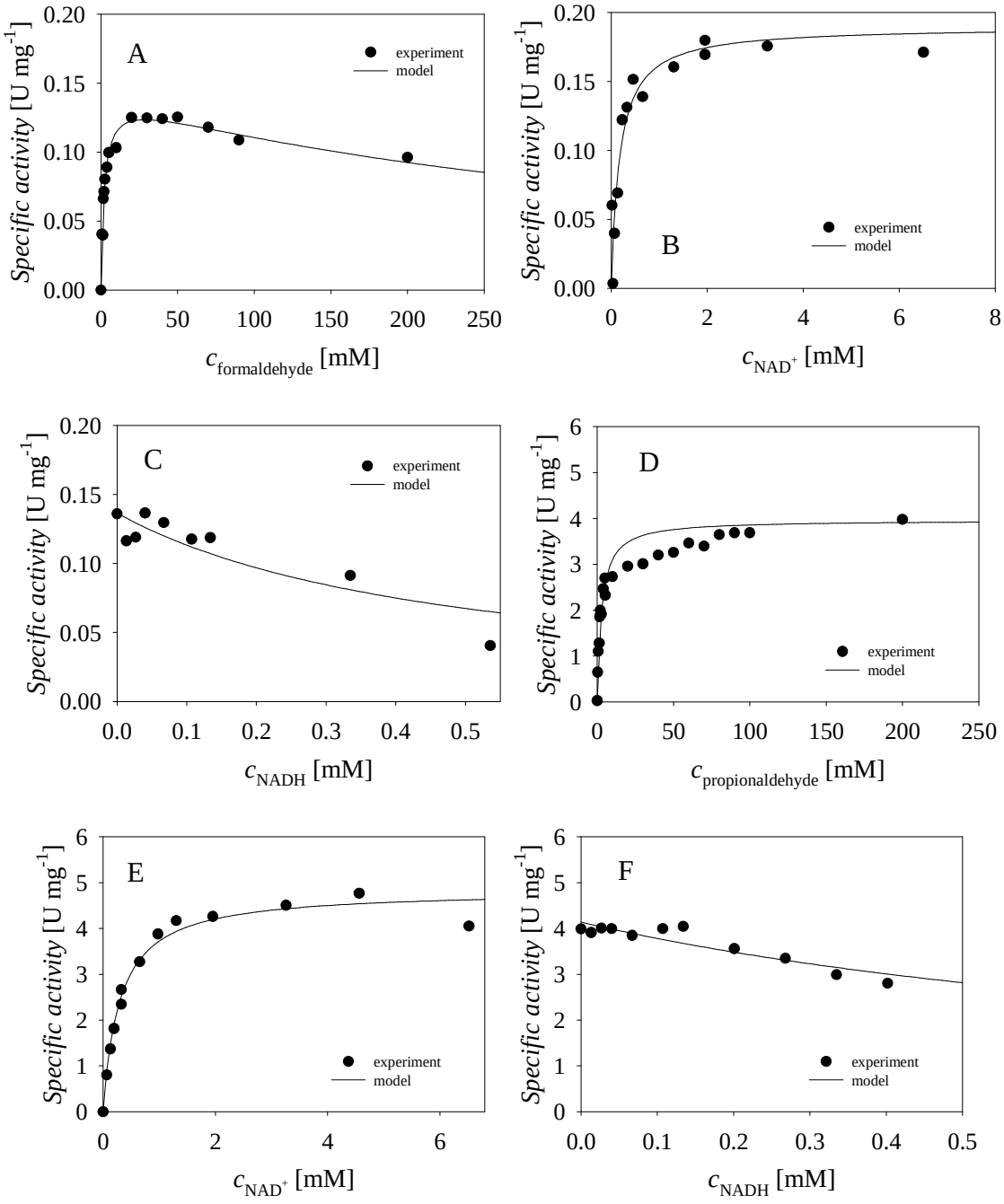

Figure 5.16 The dependence of AlDH 003 CFE specific activity on the concentration of A. **5A** (c_{NAD+} = 9.78 mM), B. NAD^+ (c_{5A} = 30.0 mM), C. NADH (c_{5A} = 30.0 mM, c_{NAD+} = 9.75 mM), D. **5B** (c_{NAD+} = 9.78 mM), E. NAD^+ (c_{5B} = 299.87 mM), F. NADH (c_{5B} = 299.87 mM, c_{NAD+} = 9.78 mM), 50 mM TEA HCl buffer pH 8.0, 340 nm, 25 °C, V_r = 1 mL, γ_{AlDH} = 0.05 mg mL^{-1}.

Batch experiments were performed were **5A** and **5B** were oxidised by AlDH 003 CFE separately with coenzyme NAD^+ regeneration by NOX 009. The results are shown in Figure 5.17 and correspond to the data presented in Tables 5.10 and 5.11. The reaction where **5B** is catalysed by AlDH is fast due to high V_m value and absence of substrate inhibition effect. On

5A – Formaldehyde, **5B** – Propanal, **5C** – 3-Hydroxy-2-methylpropanal, **5D** – 3-Hydroxy-2-methylpropanoic acid, **5E** – Methacrylic acid, **5F** – 3-Hydroxy-2-methylpentanal

the other hand, reaction where **5A** is oxidised by AlDH didn't result in substrate conversion due to inhibition by substrate (K_i^{5A}) and significantly lower V_m value compared to **5B**.

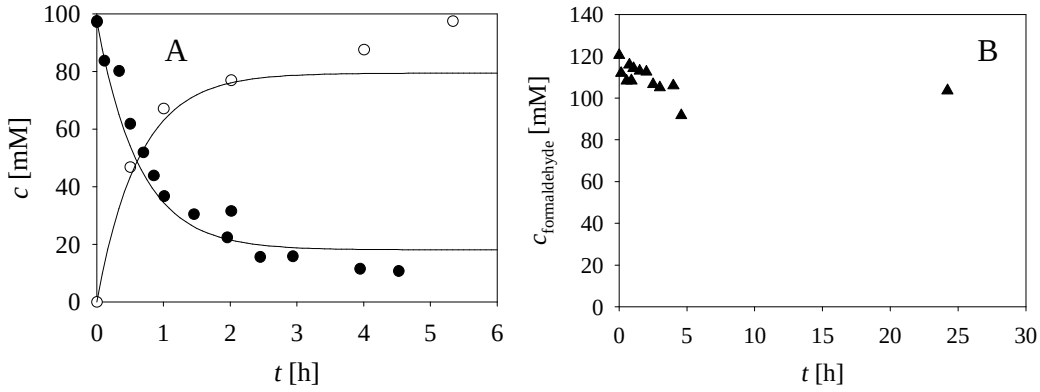

Figure 5.17 Batch reactor experiments A. **5B** catalysed by AlDH 003 CFE, B. **5A** catalysed by AlDH 003 CFE ($c_{substrate}$ = 100 mM, c_{NAD+} = 1 mM, γ_{AlDH} = 10 mg mL^{-1}, γ_{NOX} = 5 mg mL^{-1}, 50 mM TEA HCl buffer pH 8.0). Legend: black circles – **5B**, white circles – propionic acid, black triangles – **5A**.

5.3.8.2 Kinetics of 5C oxidation catalysed by lyophilised aldehyde dehydrogenase 003, CFE

To investigate the oxidation kinetics the same methodology was used as in the first reactions step of aldol addition. Figure 5.18 presents the results of the influences of each reaction compound on the specific activity of crude AlDH 003. The estimated kinetic parameters are shown in Table 5.11. It can be seen that the influence of substrates can be described by Michaelis-Menten equation (Figures 5.18A and 5.18B), and that NADH and **5A** inhibit the reaction (Figures 5.18C and 5.18D). Thus, the concentration of **5A** should be kept low after the first step to improve the oxidation reaction (K_i^{5A}, Table 5.11). Compound **5D** does not inhibit the reaction (Figure 5.18E).

Table 5.11 Estimated kinetic parameters in the oxidation of **5C** catalysed by crude AlDH 003.

Parameter	Unit	Value
V_m	U mg^{-1}	0.391 ± 0.011
K_m^{5C}	mM	0.342 ± 0.041
K_m^{NAD+}	mM	0.033 ± 0.003
K_i^{NADH}	mM	0.019 ± 0.005
K_i^{5A}	mM	10.768 ± 0.441

5A – Formaldehyde, **5B** – Propanal, **5C** – 3-Hydroxy-2-methylpropanal, **5D** – 3-Hydroxy-2-methylpropanoic acid, **5E** – Methacrylic acid, **5F** – 3-Hydroxy-2-methylpentanal

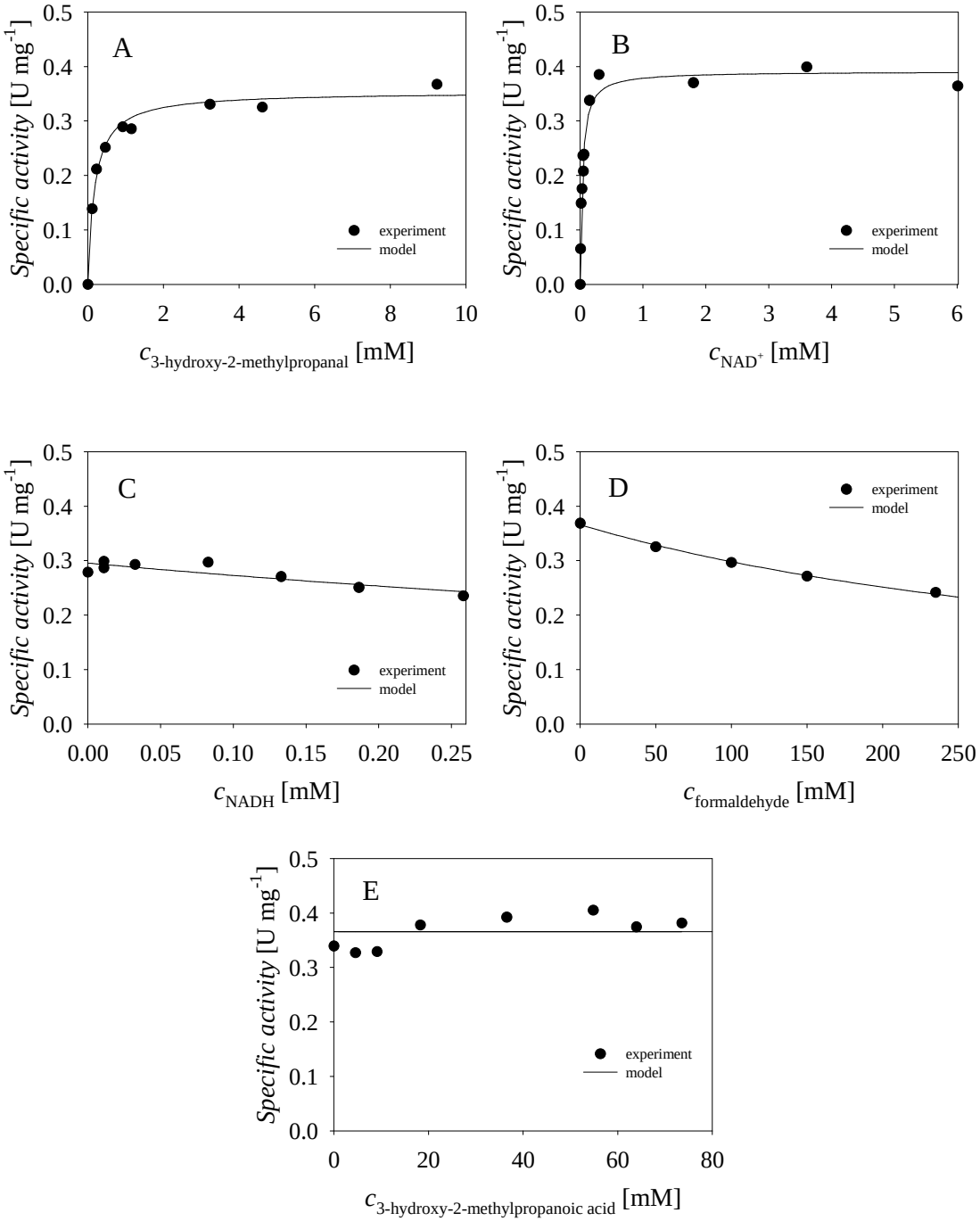

Figure 5.18 The kinetics of oxidation of **5C** catalysed by crude AlDH 003 (50 mM TEA HCl buffer pH 8.0, 25 °C, V_r = 1.01 mL, γ_{AlDH} = 0.05 mg mL^{-1}). The dependence of AlDH specific activity on the concentration of A. **5C** (c_{NAD+} = 2.1 mM), B. NAD$^+$ (c_{5C} = 81.6 mM), C. NADH (c_{5C} = 13.6 mM, c_{NAD+} = 2.1 mM) and D. **5A** (c_{5C} = 13.6 mM, c_{NAD+} = 2.1 mM), E. **5D** (c_{5C} = 9.7 mM, c_{NAD+} = 2.2 mM).

Estimated kinetic parameters (Table 5.11) show high inhibition of enzyme by NADH. The apparent affinity of AlDH 003 toward **5C** is high (K_m^{5C}).

5A – Formaldehyde, **5B** – Propanal, **5C** – 3-Hydroxy-2-methylpropanal, **5D** – 3-Hydroxy-2-methylpropanoic acid, **5E** – Methacrylic acid, **5F** – 3-Hydroxy-2-methylpentanal

As mentioned previously, CFE AlDH 003 contains NOX impurities and its effect on the reaction was considered. Table 5.12 presents the estimated kinetic parameters for the activity of NOX in aldehyde dehydrogenase that were estimated from the experimental data (not shown); i.e. the influence of NADH and NAD^+ on the oxidation of NADH catalysed by AlDH 003 CFE. From the maximum reaction rate it can be seen that it is not very high enzyme activity (V_m, Table 5.12), but cannot be neglected.

Table 5.12 Estimated kinetic parameters for the coenzyme NAD^+ regeneration catalysed by AlDH 003 (NOX activity within AlDH 003).

Parameter	Unit	Value
V_m	U mg^{-1}	0.026 ± 0.001
K_{mi}^{NADH}	mM	0.028 ± 0.002
K_i^{NAD+}	mM	0.019 ± 0.004

5.3.8.3 Kinetics of 5C oxidation catalysed by purified aldehyde dehydrogenase 003

The results of the kinetic investigations of purified AlDH 003 are presented in Figure 5.19A and 5.19B. It can be seen that the influence of concentrations of **5C** and NAD^+ on the specific activity of AlDH can be described by Michaelis-Menten kinetics. The enzyme is inhibited by NADH (Figure 5.19C) and **5A** (Figure 5.19D). The influence of **5A** concentration on the activity of aldehyde dehydrogenase was tested because there is always some **5A** left after the first reaction step of aldol addition. Estimated kinetic parameters are presented in Table 5.13.

Table 5.13 Estimated kinetic parameters in the oxidation of **5C** catalysed by AlDH 003 CFE.

Parameter	Unit	Value
V_{m1}	U mg^{-1}	0.062 ± 0.001
K_{m1}^{5C}	mM	0.362 ± 0.041
K_{m1}^{NAD+}	mM	0.465 ± 0.039
K_{i1}^{NADH}	mM	0.086 ± 0.008
K_{i1}^{5A}	mM	1.225 ± 0.112

They indicate good affinity of aldehyde dehydrogenase towards **5C** (K_{m1}^{5C}). Also, there is strong inhibition of the enzyme by NADH (K_{i1}^{NADH}), but this can be resolved by an efficient coenzyme regeneration catalysed by NOX and in this case concentration of NADH in the system is negligible. The purpose of the coenzyme regeneration was therefore not only the minimization of consumption of NAD^+, but also minimizing the inhibiting effect of

5A – Formaldehyde, **5B** – Propanal, **5C** – 3-Hydroxy-2-methylpropanal, **5D** – 3-Hydroxy-2-methylpropanoic acid, **5E** – Methacrylic acid, **5F** – 3-Hydroxy-2-methylpentanal

NADH. The inhibition by **5A** is not significant either, since its final concentration in the solution after the first reaction step, i.e. aldol addition, was usually below 10 mM. Reverse reaction was evaluated but not detected.

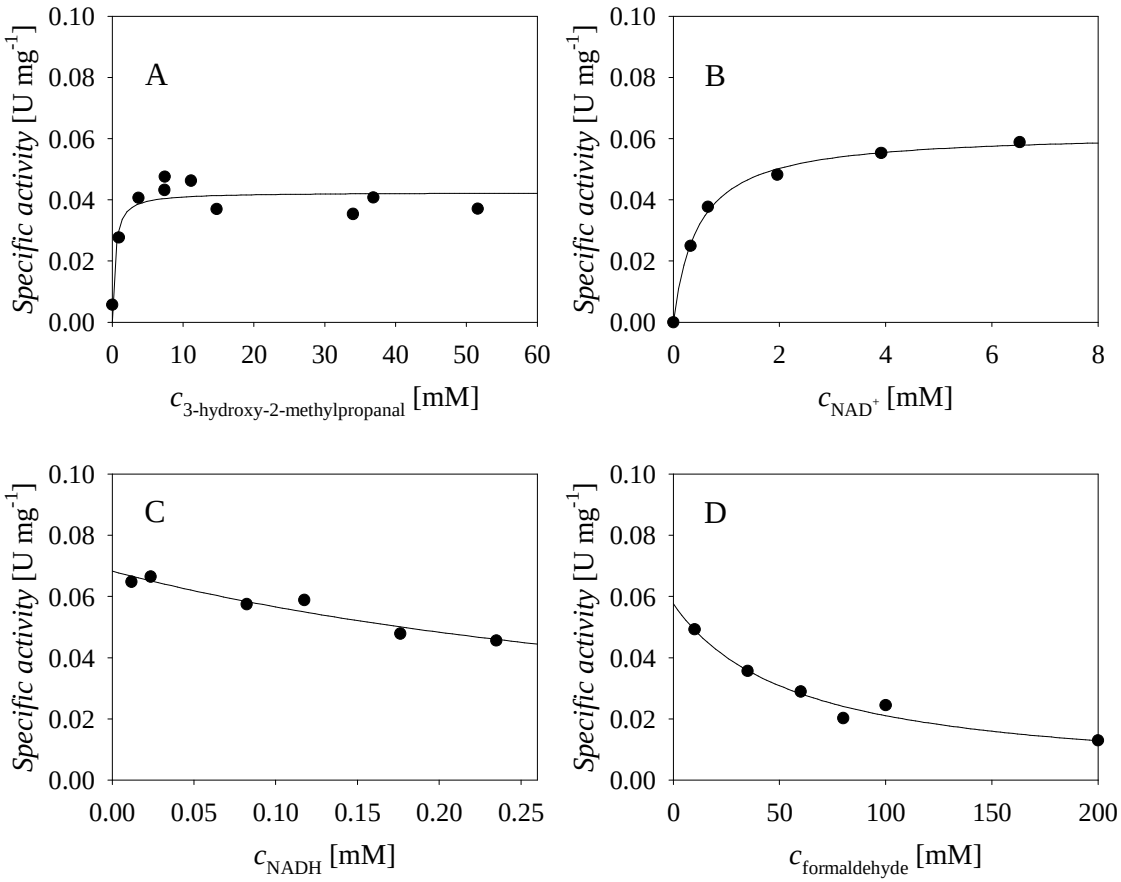

Figure 5.19 The kinetics of oxidation of **5C** catalysed by purified suspension of AlDH 003 (50 mM TEA HCl buffer pH 8.0, 25 °C, V_r = 1.01 mL, γ_{AlDH} = 0.05 mg mL^{-1}). The dependence of AlDH specific activity on the concentration of **A**. **5C** (c_{NAD+} = 2.2 mM), **B**. NAD$^+$ (c_{5C} = 16.7 mM), **C**. NADH (c_{5C} = 16.7 mM, c_{NAD+} = 2.2 mM) and **D**. **5A** (c_{5C} = 16.7 mM, c_{NAD+} = 2.2 mM). Legend: black circles – experimental data, line – model.

5.3.8.4 Kinetics of coenzyme NAD$^+$ regeneration reaction catalysed by NOX 009

The kinetics of NAD$^+$ regeneration reaction catalysed by NOX 009 was investigated and results are presented in Figure 5.20. The enzyme showed good affinity towards NADH and excellent towards O_2 which can be seen from low K_m values estimated from the experimental data (Table 5.14). This is the most important property of this oxidase and means that oxygen should not be the limiting factor in this reaction system while maximum NOX activity can be obtained at O_2 concentration close to zero.

5A – Formaldehyde, **5B** – Propanal, **5C** – 3-Hydroxy-2-methylpropanal, **5D** – 3-Hydroxy-2-methylpropanoic acid, **5E** – Methacrylic acid, **5F** – 3-Hydroxy-2-methylpentanal

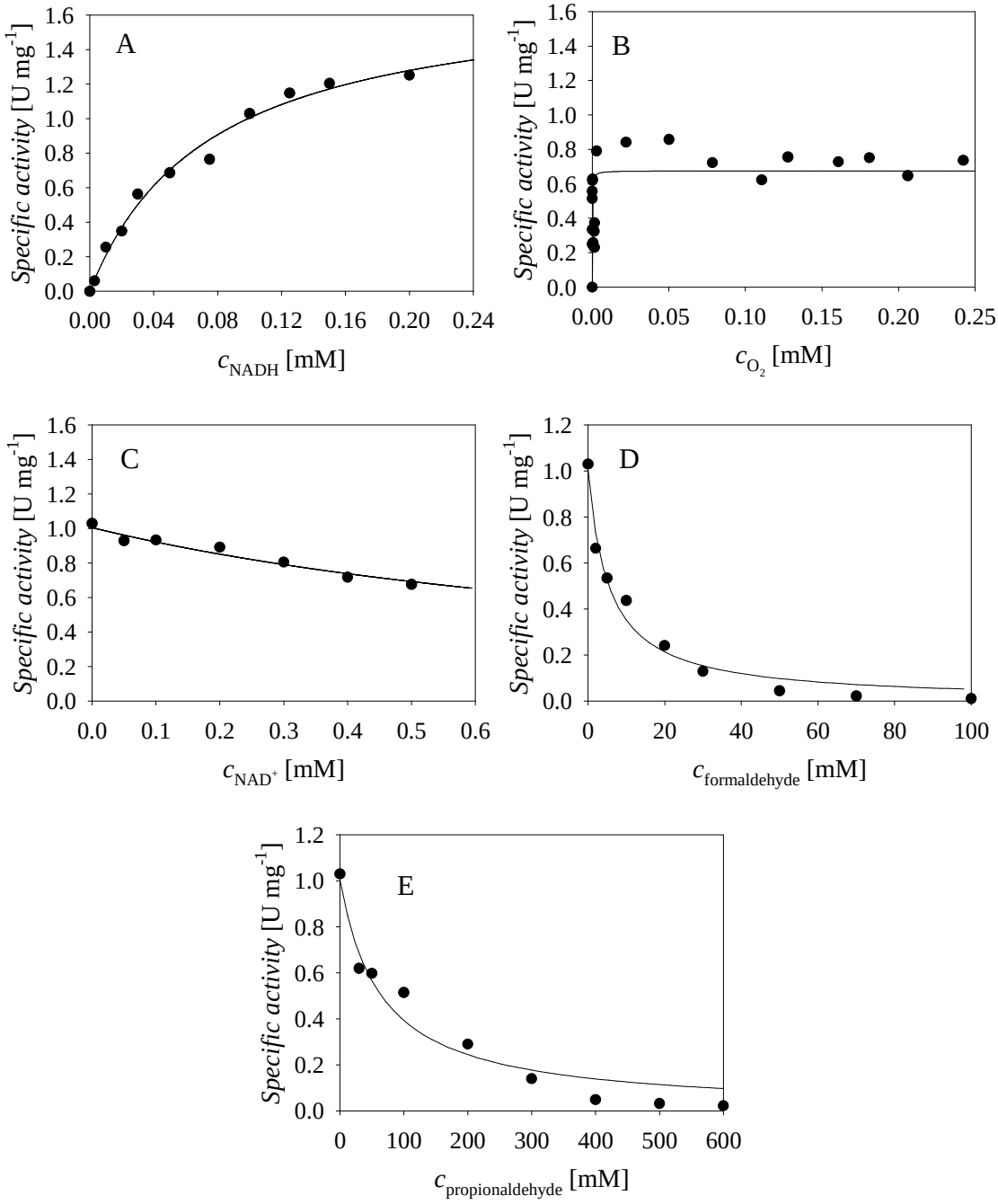

Figure 5.20 The kinetics of NOX catalysed oxidation of NADH (50 mM TEA HCl buffer pH 8.0, 25 °C, V_r = 1.01 mL, γ_{NOX} = 0.1 mg mL^{-1}). The dependence of NOX specific activity on the concentration of A. NADH, B. O_2 (c_{NADH} = 0.1 mM), C. NAD^+ (c_{NADH} = 0.1 mM), D. **5A** (c_{NADH} = 0.1 mM) and E. **5B** (c_{NADH} = 0.1 mM). Legend: black circles – experimental data, line – model.

The enzyme is inhibited by the presence of low concentrations of **5A** (K_{i2}^{5A}) and slightly inhibited by **5B** (K_{i2}^{5B}). Inhibition by NAD^+ is the most severe (K_{i2}^{NAD+}). Estimated kinetic parameters are presented in Table 5.14.

5A – Formaldehyde, **5B** – Propanal, **5C** – 3-Hydroxy-2-methylpropanal, **5D** – 3-Hydroxy-2-methylpropanoic acid, **5E** – Methacrylic acid, **5F** – 3-Hydroxy-2-methylpentanal

Comparison of the kinetic parameters estimated from the measurements with NOX present in crude AlDH (Table 5.12) and CFE NOX 009 used in oxidation reactions (Table 5.14) shows that NOX activity in crude is significantly lower since V_m value is ca. 70 times larger for CFE NOX. It can be concluded that pure CFE NOX is needed for fast and successful coenzyme regeneration. Nevertheless, the activity of NOX from AlDH is included in the model since it takes part in coenzyme regeneration reaction during **5C** oxidation.

Table 5.14 Estimated kinetic parameters in the coenzyme regeneration reaction catalysed by NOX.

Parameter	Unit	Value
V_{m2}	U mg^{-1}	1.761 ± 0.115
K_{m2}^{NADH}	mM	0.075 ± 0.011
$K_{m2}^{O_2}$	µM	0.091 ± 0.032
K_{i2}^{NAD+}	mM	0.476 ± 0.034
K_{i2}^{5A}	mM	4.835 ± 0.936
K_{i2}^{5B}	mM	51.059 ± 10.059

5.3.9 Development of mathematical model for oxidation of 5C

Based on the obtained data and reaction scheme (Scheme 5.2) the mathematical model for the **5C** oxidation step was developed and is presented in Table 5.15. From all data presented in previous section, kinetic parameters estimated from the kinetic measurements with purified AlDH 003 are used in the model. Coenzyme regeneration catalysed by CFE NOX 009 as well as with NOX present in AlDH 003 were used in the model while the reactor experiments were carried out with AlDH 003 CFE since the purified enzyme was available in limited quantities, and was found to be very unstable.

The model consists of kinetic and mass balance equations. The reaction rate of **5C** oxidation was described by the double substrate Michaelis-Menten equation with included competitive product inhibition by **5A** and NADH (Equation 5.18). The reaction rate of coenzyme regeneration was described by the double substrate Michaelis-Menten equation with included non-competitive inhibition by NADH and non-competitive inhibitions by **5A** and **5B**. Since Michaelis constant for O_2 is really low for this enzyme, it was assumed that oxygen concentration will not have influence on the reaction. Thus, the equation was simplified to single substrate Michaelis-Menten kinetics including non-competitive inhibition by NADH and non-competitive inhibitions by **5A** and **5B** (Equation 5.19). AlDH contains

5A – Formaldehyde, **5B** – Propanal, **5C** – 3-Hydroxy-2-methylpropanal, **5D** – 3-Hydroxy-2-methylpropanoic acid, **5E** – Methacrylic acid, **5F** – 3-Hydroxy-2-methylpentanal

NOX impurities, so there is an additional NOX in the solution. The reaction rate of NADH oxidation by NOX was described by Equation 5.20, analogous to the previous equation. It was assumed that chemical transformation of **5C** follows the kinetic model of the first order. The kinetic constant was estimated from experimental data using Equation 5.23 and included in the model. The same equation was used in modelling of aldol addition (k_1 = 0.00029 ± 0.00001 min^{-1} (Table 5.5) = k_{5C} (Equation 5.4, Table 5.6)). It was also assumed that **5C** transforms into alternative product in the reaction catalysed by AlDH 003. The kinetic constant was estimated from experimental data (k_{5c1} = 0.00109 ± 0.00008 min^{-1}, Equation 5.24).

All kinetic constants were estimated from the experimental data presented before, i.e. initial reaction rate vs substrate concentration acquired by using the initial reaction rate method. Mass balance equations for **5C**, **5D**, NAD^+ and NADH in the batch reactor are represented by Equations 5.25-5.30, respectively. The ezyme operational stability decay of AlDH and NOX was described by the first order kinetics (Equations 5.31-5.33). Enzyme operational stability decay rate constants were estimated from the batch reactor experiments carried out at different initial conditions.

The **5A** oxidation catalysed by AlDH (Equation 5.21) is very slow as can be seen from previously presented kinetic parameters and performed in batch reactor experiments. The reaction rate of **5B** oxidation catalysed by AlDH (Equation 5.22) depends on **5B** concentration. Since **5B** concentration is very low at the start of the oxidation step after the aldol addition, it can be neglected.

5A – Formaldehyde, **5B** – Propanal, **5C** – 3-Hydroxy-2-methylpropanal, **5D** – 3-Hydroxy-2-methylpropanoic acid, **5E** – Methacrylic acid, **5F** – 3-Hydroxy-2-methylpentanal

Table 5.15 Mathematical model for the oxidation of **5C** with coenzyme regeneration in the batch reactor.

KINETIC EQUATIONS

Oxidation of **5C** by AlDH 003

$$r_1 = \frac{V_{m1} \cdot \gamma_{\text{ADH}} \cdot c_{\text{5C}} \cdot c_{\text{NAD}^+}}{\left[\left(K_{m1}^{\text{5C}} \cdot \left(1 + \frac{c_{\text{5A}}}{K_{i1}^{\text{5A}}}\right) + c_{\text{5C}}\right) \cdot \left(K_{m1}^{\text{NAD}^+} \cdot \left(1 + \frac{c_{\text{NADH}}}{K_{i1}^{\text{NADH}}}\right) + c_{\text{NAD}^+}\right)\right]} \quad (5.18)$$

Coenzyme NAD^+ regeneration by CFE NOX

$$r_2 = \frac{V_{m2} \cdot \gamma_{\text{NOX}} \cdot c_{\text{NADH}}}{\left(K_{m2}^{\text{NADH}} + c_{\text{NADH}} \cdot \left(1 + \frac{c_{\text{NADH}}}{K_i^{\text{NADH}}}\right)\right) \cdot \left(1 + \frac{c_{\text{5A}}}{K_{i2}^{\text{5A}}} + \frac{c_{\text{5B}}}{K_{i2}^{\text{5B}}}\right)} \quad (5.19)$$

Coenzyme NAD^+ regeneration by NOX contained in AlDH 003

$$r_3 = \frac{V_{m3} \cdot \gamma_{\text{NOX(AlDH)}} \cdot c_{\text{NADH}}}{\left(K_{m3}^{\text{NADH}} + c_{\text{NADH}} \cdot \left(1 + \frac{c_{\text{NADH}}}{K_{i3}^{\text{NADH}}}\right)\right) \cdot \left(1 + \frac{c_{\text{5A}}}{K_{i2}^{\text{5A}}} + \frac{c_{\text{5B}}}{K_{i2}^{\text{5B}}}\right)} \quad (5.20)$$

5A and **5B** oxidation by AlDH

$$r_6 = \frac{V_{m4} \cdot \gamma_{\text{ADH}} \cdot c_{\text{5A}} \cdot c_{\text{NAD}^+}}{\left[\left(K_{m4}^{\text{5A}} + c_{\text{5A}} + \frac{c_{\text{5A}}^2}{K_{i4}^{\text{5A}}}\right) \cdot \left(K_{m4}^{\text{NAD}^+} \cdot \left(1 + \frac{c_{\text{NADH}}}{K_{i1}^{\text{NADH}}}\right) + c_{\text{NAD}^+}\right)\right]} \quad (5.21)$$

$$r_7 = \frac{V_{m5} \cdot \gamma_{\text{ADH}} \cdot c_{\text{5B}} \cdot c_{\text{NAD}^+}}{\left[\left(K_{m5}^{\text{5B}} + c_{\text{5A}}\right) \cdot \left(K_{m5}^{\text{NAD}^+} \cdot \left(1 + \frac{c_{\text{NADH}}}{K_{i1}^{\text{NADH}}}\right) + c_{\text{NAD}^+}\right)\right]} \quad (5.22)$$

5C decay

$$r_4 = k_{\text{5C}} \cdot c_{\text{5C}} \quad (5.23) \qquad r_5 = k_{\text{5C1}} \cdot c_{\text{5C}} \quad (5.24)$$

MASS BALANCES IN THE BATCH REACTOR

$$\frac{\mathrm{d}c_{\text{5C}}}{\mathrm{d}t} = -r_1 - r_4 - r_5 \quad (5.25) \qquad \frac{\mathrm{d}c_{\text{5D}}}{\mathrm{d}t} = r_1 \quad (5.26)$$

$$\frac{\mathrm{d}c_{\text{NAD}^+}}{\mathrm{d}t} = -r_1 + r_2 + r_3 \quad (5.27) \qquad \frac{\mathrm{d}c_{\text{NADH}}}{\mathrm{d}t} = r_1 - r_2 - r_3 \quad (5.28)$$

$$\frac{\mathrm{d}c_{\text{5A}}}{\mathrm{d}t} = -r_6 \quad (5.29) \qquad \frac{\mathrm{d}c_{\text{5B}}}{\mathrm{d}t} = -r_7 \quad (5.30)$$

ENZYME OPERATIONAL STABILITY DECAY

$$\frac{\mathrm{d}\gamma_{\text{AlDH}}}{\mathrm{d}t} = -k_{d1} \cdot \gamma_{\text{AlDH}} \quad (5.31) \qquad \frac{\mathrm{d}\gamma_{\text{NOX(AlDH)}}}{\mathrm{d}t} = -k_{d2} \cdot \gamma_{\text{NOX(AlDH)}} \quad (5.32) \qquad \frac{\mathrm{d}\gamma_{\text{NOX}}}{\mathrm{d}t} = -k_{d3} \cdot \gamma_{\text{NOX}} \quad (5.33)$$

5A – Formaldehyde, **5B** – Propanal, **5C** – 3-Hydroxy-2-methylpropanal, **5D** – 3-Hydroxy-2-methylpropanoic acid, **5E** – Methacrylic acid, **5F** – 3-Hydroxy-2-methylpentanal

5.3.10 Validation of the mathematical model for oxidation of 5C in the batch reactor

A series of batch reactor experiments (Figure 5.21) was carried out to validate the mathematical model for the oxidation of **5C**.

The operational stability decay rate constants of enzymes were estimated directly from these experiments (Figure 5.21). At the end of aldol addition there is always some **5A** and **5B** left, and they affect stability of both enzymes. The composition of the reaction solution used for the experiments presented in Figure 5.21C is presented in Table 5.16 together with the estimated values of operational stability decay rate constants and yield on **5D**. The presented results indicate that the presence of **5A** negatively affects the operational stability of NOX present in crude AlDH (k_{d2}), as well as NOX 009 (k_{d3}) added individually in the solution. As the concentration of **5A** increases, k_{d2} and k_{d3} increase as well. This was not found to be the case for AlDH. Estimated half-life time of aldehyde dehydrogenase is 141 min, NOX (aldehyde dehydrogenase) 3 min and NOX (009) 22 min (Experiments 3 – red and 4 – green, Table 5.16, Figure 5.21). The same constants were used for the simulation of experiments presented in Figure 5.21A and 5.21B. Thus, **5A** should be degraded before starting the oxidation to achieve better enzyme stability and consequently yield on **5D**. Both **5A** and **5B** are monitored during oxidation, and it was found that **5B** was not problematic, since its initial concentration was not high and it was converted fast to the corresponding acid. This was not the case for **5A** because its oxidation by aldehyde dehydrogenase was inhibited by substrate, and the enzyme has low affinity towards it (Table 5.9). **5A** does not significantly degrade during the oxidation of **5C**. Developed mathematical model (Table 5.15, Equations 5.18-5.33) described the data well (Figure 5.21).

AlDH catalyses unspecific transformation of **5C** as explained in the previous chapter. Therefore, by increasing the enzyme concentration it was not possible to produce higher concentration of product **5C**, which would in other case be the best solution for overcoming the spontaneous chemical degradation of **5C**. Because of this drawback, other aldehyde dehydrogenases were tested as alternatives for **5C** oxidation.

5A – Formaldehyde, **5B** – Propanal, **5C** – 3-Hydroxy-2-methylpropanal, **5D** – 3-Hydroxy-2-methylpropanoic acid, **5E** – Methacrylic acid, **5F** – 3-Hydroxy-2-methylpentanal

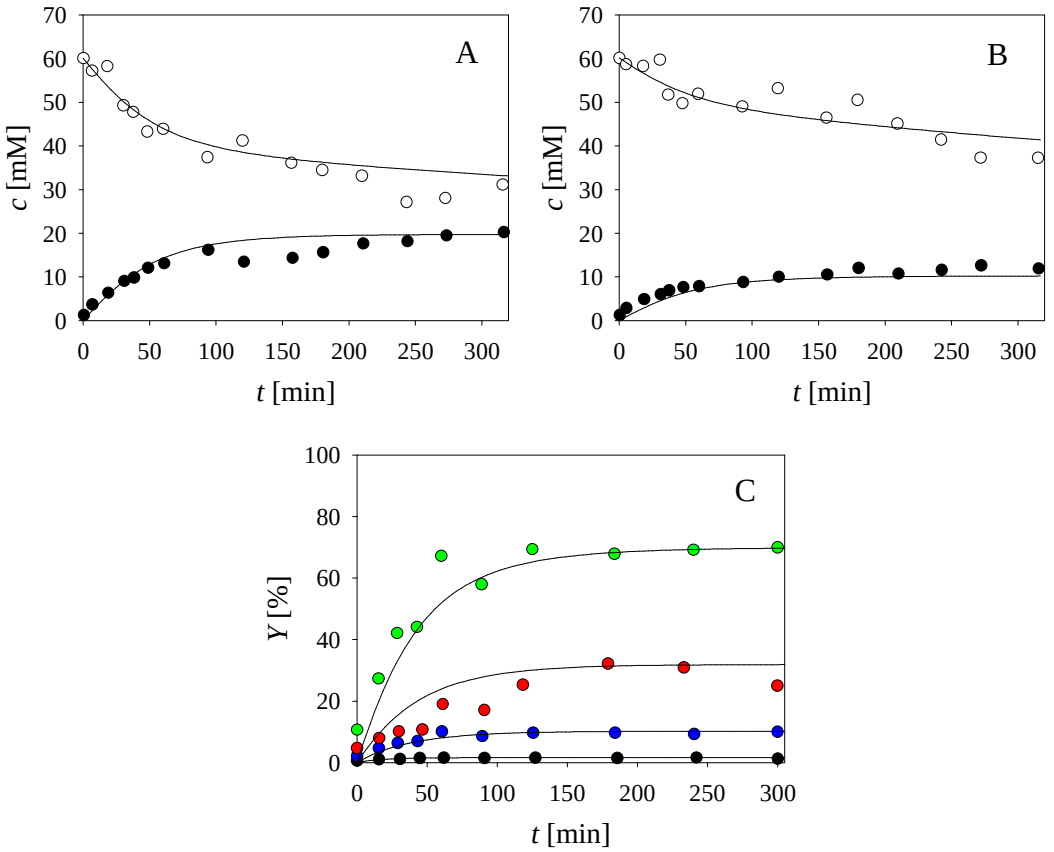

Figure 5.21 Oxidation of **5C** to **5D** in the batch reactor (500 mM TEA HCl buffer pH 8.0, 25 °C, 1000 rpm). **A**. c_{5C} = 60.1 mM, c_{NAD+} = 1.0 mM, V_r = 3.5 mL, γ_{AlDH} = 10.0 mg mL^{-1}, γ_{NOX} = 10.0 mg mL^{-1} (white circles – **5C**, black circles – **5D**), **B**. c_{5C} = 60.1 mM, c_{NAD+} = 1.0 mM, V_r = 3.5 mL, γ_{AlDH} = 10.0 mg mL^{-1}, γ_{NOX} = 5.0 mg mL^{-1} (white circles – **5C**, black circles – **5D**), **C**. c_{NAD+} = 1.0 mM, γ_{AlDH} = 10.0 mg mL^{-1}, γ_{NOX} = 5.0 mg mL^{-1} V_r = 2.0 mL; black circles – c_{5C} = 252.5 mM, blue circles – c_{5C} = 89.8 mM, red circles – c_{5C} = 43.8 mM, green circles – c_{5C} = 17.6 mM. Legend: black circles – experimental data, line – model.

Table 5.16 The effect of composition of reaction solution on yield of **5C** and estimated values of operational stability decay rate constants (Experiments from Figure 5.21C).

Legend (Fig. 5.21C)	c_{5C} [mM]	c_{5A} [mM]	c_{5B} [mM]	Y_{5D} [%]	k_{d1} [min^{-1}] AlDH	k_{d2} [min^{-1}] AlDH (NOX)	k_{d3} [min^{-1}] NOX 009
black circles	252.5	66.1	15.3	1.3	0.0049	0.0764	0.4163
blue circles	89.8	49.1	11.4	7.2	0.0049	0.0352	0.4312
red circles	43.8	26.3	6.2	32.7	0.0049	0.0321	0.2315
green circles	17.6	12.9	3.8	70.0	0.0049	0.0321	0.2315

In the published fermentative process for **5D** production, 6 mg L^{-1} (0.058 mM) of **5D** after 27 hours was obtained (Marx et al., 2010), whereas 2.3 g L^{-1} (22 mM) was obtained in another multistep microbial process (Lang et al., 2015). In another patent (Haas et al., 2015)

5A – Formaldehyde, **5B** – Propanal, **5C** – 3-Hydroxy-2-methylpropanal, **5D** – 3-Hydroxy-2-methylpropanoic acid, **5E** – Methacrylic acid, **5F** – 3-Hydroxy-2-methylpentanal

413 mg L^{-1} (3.97 mM) of **5D** was reported. In this thesis, when AlDH 003 was used as biocatalyst for **5C** oxidation, the best result was obtained 2.5 g L^{-1} (24 mM) of **5D**. Since **5D** is an important intermediate molecule with market potential and its production with AlDH 003 could not be further improved, other biocatalysts were screened to find the ones with better applicability in this reaction system.

5.3.11 Screening for more suitable aldehyde dehydrogenase

Considering the poor yield on **5D** by using AlDH 003, alternative AlDHs from Prozomix Ltd were evaluated. Twenty five batch experiments with same initial conditions (described in Chapter 5.2.4.12) were performed and monitored for 24 hours. Comparison included 24 new enzymes from AlDH panel and previously used and investigated AlDH 003 (Table 5.17). Results suggested that five catalysts from the tested panel (bold in Table 5.17 and Figure 5.23) showed better performance than AlDH 003 in the oxidation reaction of **5C**. The highest yield of **5D** was achieved in the reaction catalysed by AlDH 41 (Figure 5.22 and 5.23D). This is why it was suggested that further research on this topic should be done with this enzyme.

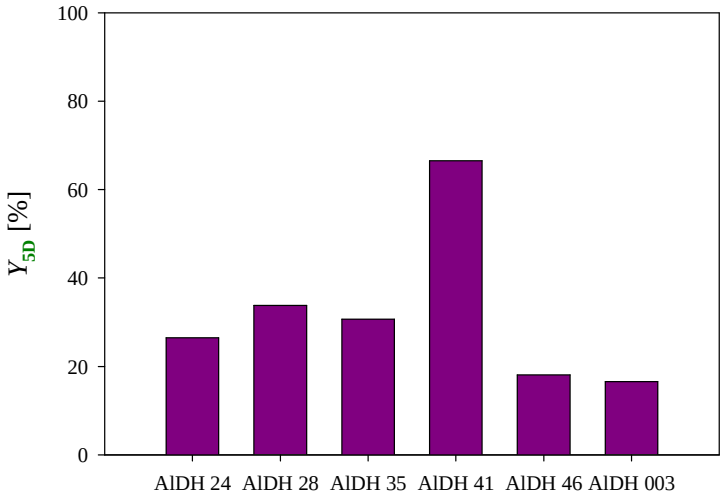

Figure 5.22 Highest yields of **5D** after 24 hours in oxidation reactions catalysed by enzymes of the AlDH panel.

5A – Formaldehyde, **5B** – Propanal, **5C** – 3-Hydroxy-2-methylpropanal, **5D** – 3-Hydroxy-2-methylpropanoic acid, **5E** – Methacrylic acid, **5F** – 3-Hydroxy-2-methylpentanal

Table 5.17 Oxidation of **5C** by 25 different AlDHs with shown concentrations of product **5D** after 24 hours (0.5 M TEA HCl buffer pH 8.0, 25 °C, 1000 rpm, γ_{AlDH} = 10.0 mg mL^{-1}, $\gamma_{NOX\ 009}$ = 10.0 mg mL^{-1}, γ_{AlDH} = 10.0 mg mL^{-1}, c_{NAD+} = 1 mM, c_{5C} = 70 mM).

AlDH	c_{5D} [mM]	AlDH	c_{5D} [mM]
24	**11.89**	37	0.98
25	0.49	38	3.80
26	1.19	39	2.14
27	0.60	40	1.06
28	**14.98**	**41**	**26.32**
29	0.34	42	0.71
30	1.64	43	0.72
31	0.56	44	2.22
32	1.46	45	3.55
33	1.80	**46**	**6.39**
34	0.53	47	0.98
35	**13.83**	**3**	**6.26**
36	0.61		

5A – Formaldehyde, **5B** – Propanal, **5C** – 3-Hydroxy-2-methylpropanal, **5D** – 3-Hydroxy-2-methylpropanoic acid, **5E** – Methacrylic acid, **5F** – 3-Hydroxy-2-methylpentanal

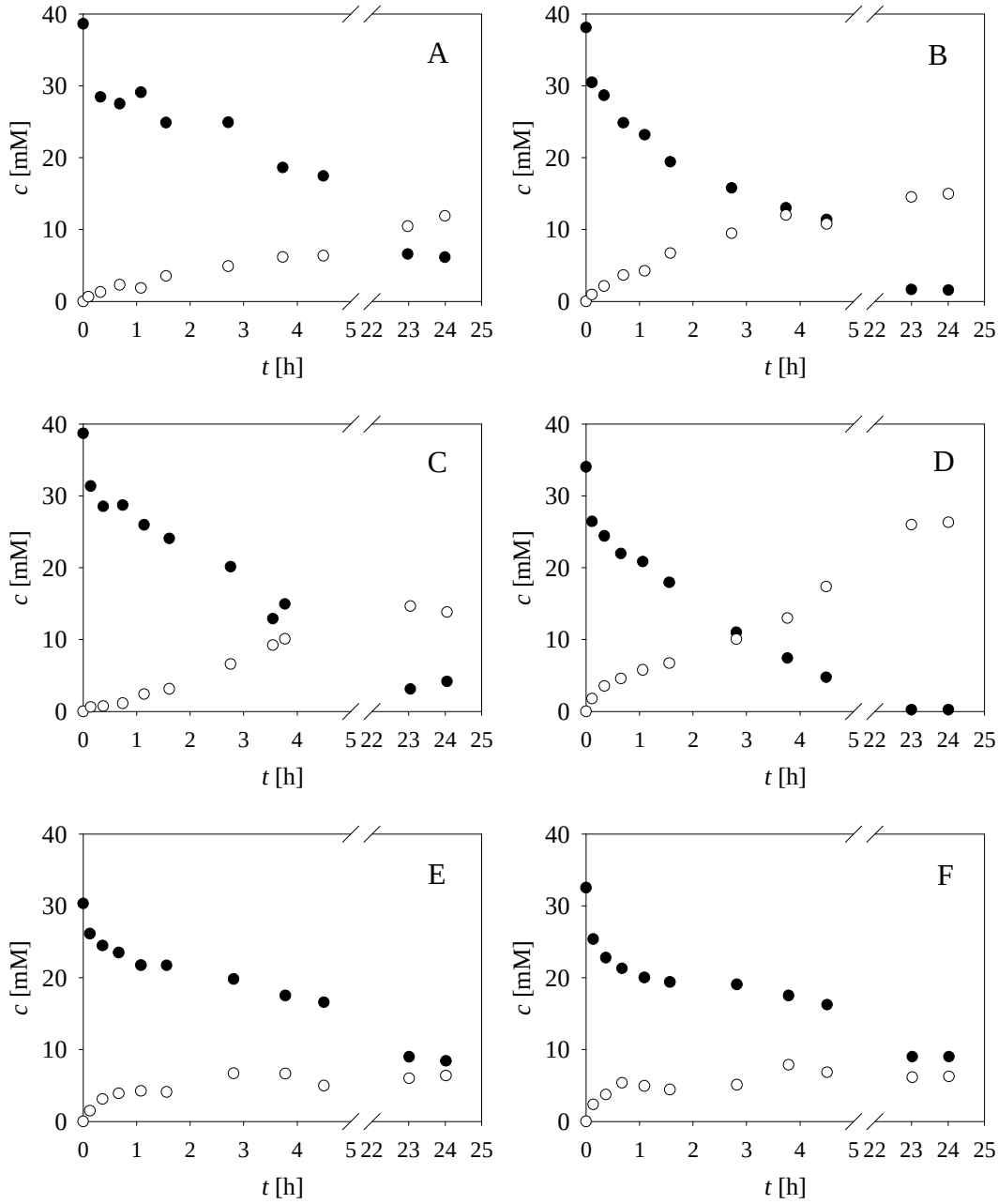

Figure 5.23 AlDH panel screening – selection of the best enzymes. A. AlDH 24, B. AlDH 28, C. AlDH 35, D. AlDH 41, E. AlDH 46, F. AlDH 3 (c_{5C} = 35.39 mM, c_{NAD+} = 1 mM, $c_{NOX\ 009}$ = 10 mg mL^{-1}, c_{AlDH} = 10 mg mL^{-1}, V_r = 1.5 mL, 0.5 M TEA HCl buffer pH 8, 1000 rpm, 25 °C). Black circles – **5C**, white cicrcles – **5D**.

5A – Formaldehyde, **5B** – Propanal, **5C** – 3-Hydroxy-2-methylpropanal, **5D** – 3-Hydroxy-2-methylpropanoic acid, **5E** – Methacrylic acid, **5F** – 3-Hydroxy-2-methylpentanal

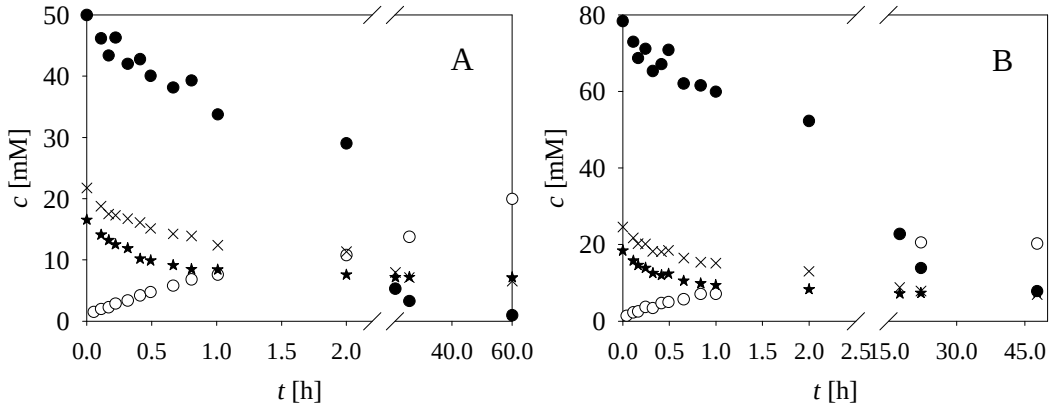

Figure 5.24 Oxidation with AlDH 41 – additional experiments (c_{NAD+} = 1 mM, V_r = 1.3 mL, 0.5 M TEA HCl buffer pH 8, 1000 rpm, 25 °C). A. c_{5C} = 46.17 mM, $c_{NOX\ 009}$ = 10.46 mg mL^{-1}, c_{AlDH} = 5 mg mL^{-1}, B. c_{5C} = 78.36 mM, $c_{NOX\ 009}$ = 10.77 mg mL^{-1}, c_{AlDH} = 10 mg mL^{-1}. Black circles – **5C**, white cicrcles – **5D**, crosses – **5A**, stars – **5B**.

Additional experiments performed with AlDH 41 resulted in 43.18% yield on **5D** where initial **5C** concentration was 46.17 mM (Figure 5.24A) and 25.83 % yield on **5D** where initial **5C** concentration was 78.36 mM (Figure 5.24B). The reason for lower yield in these ractions as compared with the oxidation catalysed by AlDH 41 in panel screening reactions (Figure 5.23D) is most likely high dilution of **5C** solution in the oxidation due to specific way of obtaining **5C** for oxidation step by previously performing aldol addition. Because of this, initial concentrations of **5A** and **5B** in oxidation were also lower than in experiments presented in Figure 5.24. Data show that AlDH 41 catalyses the oxidation of **5A** and **5B** and probably causes inactivation. Furthermore, there is a disproportion between consumed substrate **5C** and produced product **5D** which suggests that unspecific transformation of **5C** into another unwanted and unidentified product also occurs, as in the case of AlDH 003. Further work outside the frame of this thesis should focus on performing the reaction at minimized initial concentrations of **5A** and **5B**.

5.3.12 Characterization of the oxidation product 5D

Analysis by NMR confirmed that **5D** is the oxidation product. As it was not possible to isolate it directly it was derivatized before the NMR analysis and transformed to 4-bromophenacyl-*β*-hydroxyisobutyrate (**5G**) according to procedure described in Chapter 5.2.4.15. 10 mg of product was dissolved in 1 mL of chloroform for the NMR analysis (99.80% $CDCl_3$) (Appendix, Figure 10.5). ^{1}H NMR (Figure 10.5A), ^{13}C (Figure 10.5B), 2D

5A – Formaldehyde, **5B** – Propanal, **5C** – 3-Hydroxy-2-methylpropanal, **5D** – 3-Hydroxy-2-methylpropanoic acid, **5E** – Methacrylic acid, **5F** – 3-Hydroxy-2-methylpentanal

COSY (Figure 10.5C) and 2D HSQC (Figure 10.5D) analyses were carried out. The results of NMR analysis were as follows: ^{1}H NMR (400 MHz, $CDCl_3$) δ 7.77 (d, *J* = 8.6 Hz, 2H), 7.64 (d, *J* = 8.6 Hz, 2H), 5.46 (d, *J* = 16.5 Hz, 1H), 5.30 (d, *J* = 16.5 Hz, 1H), 3.85 (m, 1H), 3.77 (t, *J* = 9.9 Hz, 1H), 2.86 (m, 1H), 1.23 (d, *J* = 7.1 Hz, 3H). ^{13}C NMR (101 MHz, $CDCl_3$) δ 192.1, 174.6, 132.4, 132.3, 129.6, 129.3, 65.7, 65.3, 42.3, 13.0.

Enantiomeric excesses of the synthesised product **5G** were determined by chiral HPLC column by diluting the purified product **5G** in the mobile phase. The retention times of (*S*)- and (*R*)-4-bromophenacyl-*β*-hydroxyisobutyrate were 18.04 and 20.10 min, respectively. Chromatograms are presented in Appendix (Figure 10.4). After derivatization with 2,4'-dibromo-acetophenone and analysis by chiral HPLC, **5D** turned out to be racemic mixture with *ee* 51% of (*S*)-enantiomer (Appendix, Figure 10.4). This loss of enantiomeric purity of **5D** could have occurred during enzymatic aldol reaction, the enzymatic oxidation reaction, during the derivatization with 2,4'-dibromo-acetophenone or as a consequence of the aqueous reaction medium at pH>7. The assumption is that the aqueous media at pH ≥ 7 (**5C** is especially prone to racemization under aqueous conditions) and the enzymatic oxidation step were the most plausible factors responsible for the loss of chiral integrity. Nevertheless, for the synthesis of MAA precursor chiral integrity of the product is irrelevant.

5A – Formaldehyde, **5B** – Propanal, **5C** – 3-Hydroxy-2-methylpropanal, **5D** – 3-Hydroxy-2-methylpropanoic acid, **5E** – Methacrylic acid, **5F** – 3-Hydroxy-2-methylpentanal

5.4 Conclusions

The results of the enzymatic carbon-carbon bond formation between propanal and formaldehyde catalysed by aldolase FSA^{D6Q} and enzymatic oxidation of obtained aldol product 3-hydroxy-2-methylpropanal by aldehyde dehydrogenase to synthesize 3-hydroxy-2-methylpropanoic acid, a precursor for methacrylic acid were presented in this dissertation section. This study proposes a process set-up, based on developed mathematical model, as well as reaction conditions for the cascade that can be used for further process development and scaling-up the system.

The reaction system was found to be complex due to the enzyme operational stability decay in the presence of formaldehyde, unspecific transformation of main reaction product 3-hydroxy-2-methylpropanal at the reaction conditions, self-aldol addition of propanal catalysed by FSA^{D6Q} and formation of by-product 3-hydroxy-2-methylpentanal. Increasing formaldehyde and propanal concentrations causes the increase of the enzyme operational stability decay rate, and as a consequence a dramatic decrease of product yield. Thus, it can be concluded that this reaction cannot be done successfully, i.e. with satisfactory process metrics, in the batch reactor. The applicability of the fed-batch reactor was evaluated and the mathematical model was used to optimize the concentrations of reactants and enzyme, i.e. the reaction conditions, to achieve the maximum product yield, product concentration and volume productivity. Experimental results have confirmed the simulations and after 5.5 hours volume productivity of 313.7 g L^{-1} d^{-1}, product concentration of 814 mM (72 g L^{-1}), and product yield of 88.5% were obtained. Considering reactive substrates used in this enzymatic reaction and the fact that no results from enzymatic transformation with these substrates are published according to our best knowledge, these numbers present an excellent result, as they correspond to the industrially applicable process metrics.

The aldehyde 3-hydroxy-2-methylpropanal was submitted to one-pot consecutive enzymatic oxidation catalysed by AlDH 003 where complete consumption of 3-hydroxy-2-methylpropanal with final concentration of 3-hydroxy-2-methylpropanoic acid being 24 mM was obtained, which is significantly better than obtained in a fermentative process. However, the additional enzymatic transformation of 3-hydroxy-2-methylpropanal, and the formation of the by-product has to be stressed out.

In a search for more suitable biocatalyst for oxidation, a panel of 24 different aldehyde dehydrogenases was tested and it was found that five of them gave higher product yield than AlDH 003. Biocatalyst selected as the enzyme with the highest potential for oxidation of 3-

5A – Formaldehyde, **5B** – Propanal, **5C** – 3-Hydroxy-2-methylpropanal, **5D** – 3-Hydroxy-2-methylpropanoic acid, **5E** – Methacrylic acid, **5F** – 3-Hydroxy-2-methylpentanal

hydroxy-2-methylpropanal was AlDH 41. The yield on 3-hydroxy-2-methylpropanoic acid of 66.5% was achieved with the final 3-hydroxy-2-methylpropanoic acid concentration of 26.32 mM (2.7 g L^{-1}). It was concluded that minimizing initial formaldehyde and propanal concentration would lead to more successful oxidation and AlDH 41 is selected as the most promising biocatalyst for further investigation and optimization outside the frame of this thesis.

5A – Formaldehyde, **5B** – Propanal, **5C** – 3-Hydroxy-2-methylpropanal, **5D** – 3-Hydroxy-2-methylpropanoic acid, **5E** – Methacrylic acid, **5F** – 3-Hydroxy-2-methylpentanal

6 SYNTHESIS OF L-HOMOSERINE

6.1 Introduction

The second cascade reaction system which was investigated in this work is the synthesis of L-homoserine. The cascade comprises a Class II metal cofactor dependent pyruvate aldolase and a transaminase as biocatalysts. Both separate enzymes and cells containing overexpressed enzymes were available for this research. Therefore, process employing cell free extract (CFE) enzymes and process where lyophilised whole cells containing these enzymes were kinetically characterized in detail and process optimization was performed based on developed mathematical models.

The synthesis of L-homoserine (6B) in the reaction system consisting of transaminase and aldolase starting from pyruvate (6C), formaldehyde (6D) and L-alanine (6A) (Scheme 6.1) was studied by Hernández and co-authors (Hernández et al., 2017a). It was shown that the concept works, however, the reaction was not studied from an enzyme reaction engineering point of view. It was the purpose of this work to evaluate the kinetics of both reactions and find the dependencies between different variables in the form of mathematical model which will enable descriptions of phenomena in the reaction and more important their explanations. The final goal of this work was to find the reaction set-up and the conditions at which volume productivity of L-homoserine above 2 g^{-1} L^{-1} h^{-1} and its concentration above 50 g L^{-1} can be achieved. These are relevant process numbers for industrial application of the process.

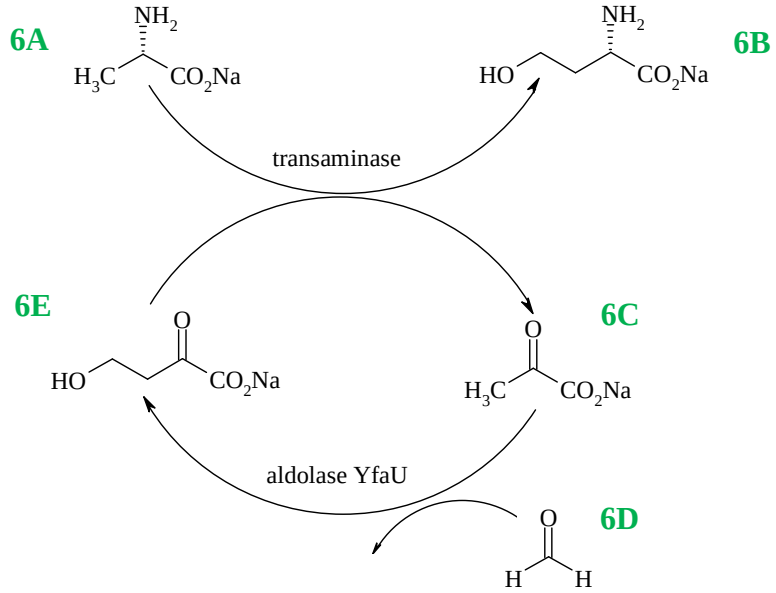

Scheme 6.1 The reaction scheme of the synthesis of L-homoserine.

6A – L-Alanine, **6B** – L-Homoserine, **6C** – Sodium pyruvate, **6D** – Formaldehyde, **6E** – 4-Hydroxy-2-oxobutanoate

Kinetic measurements were performed to quantify the influence of all reaction compounds on the activity of both enzymes alone and enzyme co-expressed in lyophilised cells. Complex interrelationships between process variables were discovered and kinetic model was developed. The results will be described in the following sections. Model was used for process optimization and achieving satisfactory process metrics during L-homoserine synthesis.

6.2 Experimental part

6.2.1 Materials

Chemicals and enzymes used in this chapter are the following. Formaldehyde (36%, p.a.) was purchased from T.T.T. Ltd. (Croatia). Triethanolamine (TEA), *N*-(benzyloxycarbonyloxy)succinimide (Cbz-OSu), trifluoroacetic acid (TFA), L-homoserine, L-alanine, pyruvate, and acetonitrile were purchased from Sigma Aldrich (Germany). *O*-Benzylhydroxylamine hydrochloride ($BnONH_2 \cdot HCl$) and pyridine were purchased from Acros Organics (Belgium). Pyridoxal 5'-phosphate monohydrate (PLP) was from Alfa Aesar (USA). Methanol gradient grade (MeOH) was from J.T. Baker (USA). 4-Hydroxy-2-oxobutanoate was synthesised and purified in the labs of IQAC-CSIC (Spain) and the Faculty of Chemical Engineering and Technology at the University of Zagreb (Croatia).

Transaminase 039 and all 2-keto-3-deoxy- L-rhamnonate aldolases (YfaUs) were from Prozomix Ltd (United Kingdom) as well as lyophilised cells YfaU(013)/PRO TRANS(039).

Reaction component labels are given according to Table 6.1.

Table 6.1 Labels given to each reaction component in this chapter.

Compound	Label
L-Alanine	**6A**
L-Homoserine	**6B**
Sodium pyruvate	**6C**
Formaldehyde	**6D**
4-Hydroxy-2-oxobutanoate	**6E**

6.2.2 Apparatus

Apparatus used in Chapter 6 is listed in Appendix (Table 10.1).

6A – L-Alanine, **6B** – L-Homoserine, **6C** – Sodium pyruvate, **6D** – Formaldehyde, **6E** – 4-Hydroxy-2-oxobutanoate

6.2.3 Analytical methods

Reactions were monitored by HPLC (Prominence, Shimadzu, Japan) with UV detection at 215 nm. Methods used are presented in Table 6.2. Chromatographs and calibration surves for **6A**, **6B**, **6C**, **6D** and **6E** are presented in Appendix (Figure 10.6).

Table 6.2 HPLC methods.

METHOD	COMPOUND	COLUMN	ELUENTS	CONDITIONS
A	**6A**, **6B**, **6C**, **6D**, **6E**	Phenomenex LiChrospher® C18 column (5 µm, 4 × 250 mm)	A: 0.095% v/v TFA in acetonitrile/water 80:20 B: (0.1% v/v) trifluoroacetic acid (TFA) in water	Gradient elution: 90 to 0% B 30 min, 0% B 5 min, 0 - 90% B 11 min, flow-rate 1 mL min^{-1}, 215 nm, column temperature 30 °C
B		Phenomenex Kinetex® C18 (5 µm, 4,6 × 250 mm)	A: 0.095% v/v TFA in acetonitrile/water 80:20 B: (0.1% v/v) trifluoroacetic acid (TFA) in water	Gradient elution: 90 to 0% B 10 min, 0% B 2 min, 0 - 90% B 3 min, 90% B 1 min, flow-rate 1.5 mL min^{-1}, 215 nm, column temperature 30 °C

Derivatization of the samples for HPLC analyses includes two derivatization reagents. Derivatization done by $BnONH_2 \cdot HCl$ was used for **6C**, **6D** and **6E** analysis, and derivatization by *N*-(benzyloxycarbonyloxy)succinimide (Cbz-OSu) was used for **6A** and **6B** analysis. Derivatization done by $BnONH_2$ is described in Chapter 5.2.3.1. Retention times for **6C**, **6D** and **6E** were 7.8 min, 8.5 min and 6.2 min, respectively, and their linearity range is from 1 to 10 mM.

6.2.3.1 Derivatization of amino acids

N-(Benzyloxycarbonyloxy)succinimide (Cbz-OSu) is a common reagent (Scheme 6.2) for the carboxybenzyl protection of amines (Hattori, Sajiki & Hirota, 2000). Procedure for sample derivatization with Cbz-OSu is as follows. 10 µL of sample was added to 50 µL of derivatization agent and mixed on Vortex mixer. It was incubated for 60 min at 60 °C. 440 µL of methanol was added in this mixture. The solution was mixed on Vortex, centrifuged for 5 min at 14 000 rpm. 350 µL was taken from the top of the vial and analysed by HPLC. 150 mM solution of Cbz-OSu reagent is prepared in acetonitrile. Retention times for **6A** and **6B** were 6.6 min and 5.6 min, respectively, and linearity range is from 2 to 20 mM.

6A – L-Alanine, **6B** – L-Homoserine, **6C** – Sodium pyruvate, **6D** – Formaldehyde, **6E** – 4-Hydroxy-2-oxobutanoate

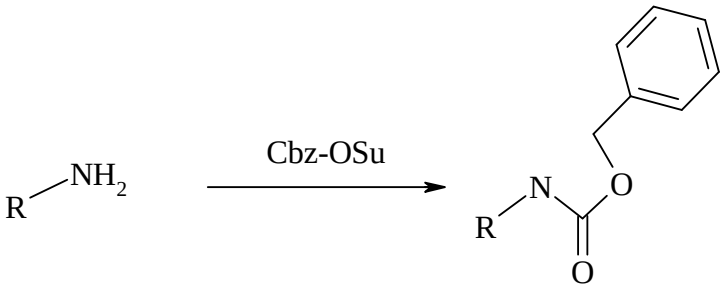

Scheme 6.2 Derivatization of amino acids with Cbz-OSu.

6.2.4 Experimental procedures

Experimental part is divided on: (i) measurements and research of both reaction steps catalysed by enzymes transaminase TA 039 and aldolases YfaUs, and (ii) kinetics and experiments where lyophilised whole cells YfaU(013)/PRO TRANS(039) were used.

6.2.4.1 Enzyme activity assay and enzyme kinetics

Transaminase and aldolase activities were measured in the studied reactions by using the initial reaction rate method in 0.5-mL batch reactor with 1 and 5 mg mL^{-1} of transaminase and aldolase, respectively, in 50 mM phosphate buffer pH 7.0 and at 25 °C. The linear slope, estimated from the change in product concentration at the beginning of the reaction when substrate conversion was <10%, was used to calculate specific enzyme activity (*S.A.*) presented in Equation 6.1 where *S.A.* designates the specific activity (U mg^{-1}). Change in product concentration in time is presented as $dc_{product}/dt$. V_r stands for reactor volume (cm^{-3}), V_{enzyme} stands for enzyme volume (cm^{-3}) and γstands for enzyme concentration (mg cm^{-3}).

$$S.A. = \frac{dc_{product}}{dt} \cdot \frac{V_r}{V_{enzyme}} \cdot \frac{1}{\gamma_{enyzme}} \quad \left[\frac{U}{mg}\right] \tag{6.1}$$

Kinetics of the reactions in the cascade system (Scheme 6.1) was determined for each enzymatic reaction separately, as well as considering the influence of the rest of the reaction compounds not directly present in the single reactions on the reaction outcome. This means that even though for example formaldehyde **6D** is not involved in the transaminase-catalysed reaction, its influence on transaminase activity was evaluated, and the corresponding kinetic constant was estimated from the experimental data. Thus, the influence of each reaction

6A – L-Alanine, **6B** – L-Homoserine, **6C** – Sodium pyruvate, **6D** – Formaldehyde, **6E** – 4-Hydroxy-2-oxobutanoate

compound on the initial reaction rate, i.e. enzyme specific activity, was examined by keeping the concentrations of other compounds constant. A series of batch reactor experiments were carried out for that purpose, in which the change in product concentration was monitored in each reaction by HPLC.

The influence of **6A** concentration on the TA 039 specific enzyme activity was monitored up to concentrations of 350 mM. In these measurements the concentration of **6E** was kept constant at 100 mM. The influence of **6E** concentration on the specific enzyme activity was monitored up to concentrations of 350 mM. In these measurements the concentration of **6A** was kept constant at 100 mM. The influence of **6B**, **6C** and **6D** was monitored up to concentrations of 400 mM. In these tests the concentration of **6A**, **6E** and PLP (pyridoxal 5'-phosphate monohydrate, coenzyme for transaminase activity) were 300 mM, 70 mM and 1 mM respectively. Also, the influence of PLP concentration up to 1.5 mM and MeOH concentration up to 500 mM were measured for this reaction.

Considering that transaminase catalyses a reversible reaction, reaction's kinetics was investigated in the reverse reaction as well. The influence of **6B** concentration on the TA 039 activity in reverse reaction was monitored up to concentrations of 400 mM. In these measurements the concentration of **6C** was kept constant at 100 mM. The influence of **6C** concentration on the TA 039 activity in reverse reaction was monitored up to concentrations of 400 mM. In these measurements the concentration of **6B** was kept constant at 100 mM. The influence of **6D**, was monitored up to concentrations of 300 mM, whereas the influence of **6A** and **6D** up to 400 mM. In these tests the concentration of **6B**, **6C** and PLP were 300 mM, 100 mM and 1 mM respectively. Also, the influence of PLP concentration up to 1.5 mM and MeOH concentration up to 400 mM were measured for the reverse reaction.

Kinetic of the reaction catalysed by YfaU was determined for concentrations of **6D** up to 850 mM and **6C** up to 800 mM, where the concentration of other substrate was kept constant (in most cases 100 mM, details can be found below figures in Chapter 6.3). Once YfaU 013 was chosen for further process investigation, additional kinetic measurements were performed. The influence of **6B** concentration on the YfaU 013 activity was monitored up to concentrations of 400 mM, concentration of **6A** up to 600 mM, concentration of **6E** up to 200 mM, concentration of PLP up to 1.5 mM and concentration of MeOH up to 200 mM. In these experiments concentrations of **6C** and **6D** were always 100 mM. The influence of methanol as **6D** stabilizer on enzyme activity was also measured to estimate its inhibition potential in all reactions. Such compounds can occasionally have detrimental effect on the reaction outcome

6A – L-Alanine, **6B** – L-Homoserine, **6C** – Sodium pyruvate, **6D** – Formaldehyde, **6E** – 4-Hydroxy-2-oxobutanoate

(Sudar et al., 2018). Despite the reverse reaction catalysed by YfaU 013 aldolase appeared not to be significant at first, it was not neglected and the influence of **6E**, **6C**, **6A** and **6B** up to concentration of 500 mM on enzyme activity in the retro-aldol reaction was determined.

During investigation of the aldolase panel, the catalytic constants k_{cat} were also calculated for all enzymes (Equation 6.2). The value is a result of dividing V_m value by enzyme concentration (molecular weight of enzyme estimated to be 31000 g mol^{-1} (31 kDa) was taken into account).

$$V_m\left[\frac{\text{mmol}}{\text{dm}^3\,\text{min}^{-1}}\right] = k_3\left[\frac{1}{\text{min}}\right]\cdot c_{E0}\left[\frac{\text{mmol}}{\text{dm}^3}\right] \qquad (6.2)$$

Kinetics of the reaction catalysed by the lyophilised whole cell biocatalyst (YfaU(013)/PRO TRANS(039)) was determined as well. Measurements were performed in the same way as for separate enzymes, by carrying out short reactions where initial reaction rate was followed and only one enzyme tested. Even though lyophilised cells contain both enzymes (i.e., aldolase and transaminase) measurements were carried out in such way to prevent the interference of the other enzyme. These measurements include kinetics of (i) aldol addition catalysed by YfaU 013 in the cells, (ii) reverse retro-aldol reaction catalysed by YfaU 013 in the cells, (iii) transamination catalysed by TA 039 in the cells and (iv) reverse transamination catalysed by TA 039 in the cells. Details of experimental conditions in kinetic tests are presented in Chapter 6.3 as described in the figure captions. As cells naturally contain sufficient amount of PLP, it was not necessary to add extra PLP in kinetic measurements or in cascade reactions catalysed by lyophilised cells.

6.2.4.2 Enzyme stability during incubation

As **6D** is a strong electrophile and therefore a reactive compound, it was expected that its presence will significantly affect stability of both enzymes since in cascade system transaminase is in contact with **6D**.

To evaluate the **6D** effect on transaminase, 25 mg mL^{-1} of transaminase was incubated with 0, 26.2, 47.7, 94.7, 189.9 and 458.8 mM of **6D**. Enzyme activity was followed during incubation for 24 h by using the following assay: The reaction mixture of 300 µL volume contained 300 mM **6B**, 300 mM **6C** and 1 mM of PLP. The reaction was started by adding the sample from the incubation solution, which was prepared as follows: 20 µL of solution was filtered through *Amicon ® Ultra filter unit* (0.5 mL vial, ultrafiltration unit with cut off 10 000

6A – L-Alanine, **6B** – L-Homoserine, **6C** – Sodium pyruvate, **6D** – Formaldehyde, **6E** – 4-Hydroxy-2-oxobutanoate

Da). Thus, enzyme concentration in the assay was 1 mg mL^{-1}. Enzyme was re-suspended in 175 µL of buffer and this solution was added to start the reaction. The reaction was followed by taking samples for 15 minutes and the initial reaction rate was calculated from the linear increase of **6E**, and used to calculate specific enzyme activity.

To evaluate the effect of **6D** on YfaU 013, 15 mg mL^{-1} of YfaU 013 was incubated with 0, 11.4, 63.2 and 116.7 mM of **6D**. Enzyme activity was followed during incubation for 24 h by using the following assay: The reaction mixture of 500 µL volume contained 50 mM **6D** and 50 mM **6C** and was started by adding the sample from the incubation solution which was prepared as follows: 10 µL of solution was filtered through *Amicon ® Ultra filter unit* (0.5 mL vial, ultrafiltration unit with cut off 10 000 Da). Thus, enzyme concentration in the assay was 0.3 mg mL^{-1}. Enzyme was re-suspended in 200 µL of buffer and this solution was added to start the reaction. The reaction was followed by taking samples for 15 minutes and the initial reaction rate was calculated from the linear increase of **6E**, and used to calculate specific enzyme activity.

6.2.4.3 Batch reactor experiments

A series of batch reactor experiments were carried out to validate the mathematical model for each reaction step separately. Transaminations of **6A** with **6E** catalysed by TA 039 and aldol additions catalysed by YfaU 013 were carried out in 50 mM phosphate buffer pH 7.0 and at 25 °C in 1-mL reactor volume on a shaker at 1000 rpm. Different initial concentrations of substrates for TA 039 and YfaU 013–catalysed reactions were designated in the legend of Figures 6.16 and 6.18. Reaction solutions were always freshly prepared and the reaction was started by the addition of enzyme. Reactions were usually monitored until maximum substrate conversion was achieved, i.e up to 6 hours.

Enzyme operational stability in the reactor was evaluated during the batch reactor experiments. Experiments carried out at different initial conditions were used for the estimation of operational stability decay rate constants. Enzyme operational stability decay was described in the model for both enzymes, i.e. YfaU 013 and TA 039.

6.2.4.4 Fed-batch experiments with cell free extract enzymes

Two fed-batch experiments were conducted and presented in Chapter 6.3.8. The reaction took place in the glass reactor with double wall which enabled thermosetting at 25 °C

6A – L-Alanine, **6B** – L-Homoserine, **6C** – Sodium pyruvate, **6D** – Formaldehyde, **6E** – 4-Hydroxy-2-oxobutanoate

on a shaker at 450 rpm. Initial reaction volume was 7.8 mL, and a final volume was 10.5 mL. **6D** was added slowly ($c_{\mathbf{6D},\text{feed}}$ = 3110 mM, $q_{\mathbf{6D}}$ = 3 µL min^{-1}) to the reactor by maintaining its concentration below 10 mM. Initial concentrations of **6A** and **6C** were set to ca. 600 and 250 mM, respectively, while PLP concentration was set to 0.26 mM. Concentrations of TA 039 and YfaU 013 differed in both reactions and they are presented in the legend below Figure 6.25. **6D** feed (3.11 M) at flow-rate of 3 µL min^{-1} was started immediately after the addition of enzymes. A syringe pump (PHD 4400 Syringe Pump Series, Harvard Apparatus) with high-pressure stainless steel pistons (8 mL, Harvard Apparatus) was used to supply the solution to the reactor. The feeding was carried out for 15 hours, and the experiment was left to run for 24 hours. Fed-batch reaction set-up is shown on Figure 6.1.

Figure 6.1 Experimental set-up for performing reaction in fed-batch mode.

6.2.4.5 Kinetics of the aldol addition and transamination catalysed by lyophilised whole cells containing YfaU 013 and TA 039

Kinetics of both reaction steps of the cascade reaction catalysed by lyophilised whole cell biocatalyst YfaU(013)/PRO TRANS(039) was measured using the same method as for separate enzyme kinetic measurements. Activity of the cells was measured in the studied reactions by using the initial reaction rate method in 1-mL batch reactor in 50 mM phosphate buffer pH 7.0 and at 25 °C. The linear slope, estimated from the change in product concentration at the beginning of the reaction when substrate conversion was <10%, was used to calculate specific activity of certain enzyme within the cells. Kinetics of the aldol addition, retro-aldol reaction, transamination and reverse transamination catalysed by cells were successfully measured by performing short reactions, regardless the fact that cells contain both aldolase and transaminase. Details of all kinetic measurements (cells concentration, substrates concentration, etc.) are presented below figures in Chapter 6.4.1.

6A – L-Alanine, **6B** – L-Homoserine, **6C** – Sodium pyruvate, **6D** – Formaldehyde, **6E** – 4-Hydroxy-2-oxobutanoate

6.2.4.6 Fed-batch experiments catalysed by lyophilised whole cells

Several different cell catalysed fed-batch experiments were performed. Initial volume was always 7.8 mL. **6D** feed was 3 μL min^{-1} of 3.1 M **6D** solution during 15 hours. A syringe pump (PHD 4400 Syringe Pump Series, Harvard Apparatus) with high-pressure stainless steel pistons (8 mL, Harvard Apparatus) was used to supply the **6D** solution to the reactor. Cells contain sufficient amount of coenzyme PLP for transaminase activity, so no PLP was added. Initial **6C** and **6A** concentrations were always 269 mM and 538 mM, respectively. Different cells concentrations in reaction are tested (51 mg mL^{-1} and 76 mg mL^{-1}). The reactions were carried out in a glass reactor with double wall to enable thermosetting at 25 °C on a shaker at 450 rpm in 50 mM phosphate buffer pH 7.0. In some reactions concentrations of **6C** and **6A** were increased after 6.5 hours by adding fresh chemicals up to their initial concentration. In the most successful cell catalysed fed-batch reaction **6C** and **6A** were re-added two times; after 6.5 hours and 13.2 hours. Considering the sensitivity of reaction equilibrium due to complex interdependence of each reaction step discovered by detailed kinetics analysis, and by using insights based on model simulations, the latter approach turned out to give the best results and is presented in Chapter 6.4.3.

6A – L-Alanine, **6B** – L-Homoserine, **6C** – Sodium pyruvate, **6D** – Formaldehyde, **6E** – 4-Hydroxy-2-oxobutanoate

6.3 Results and discussion: process optimization catalysed by cell free extract enzymes

6.3.1 Kinetics of transaminase-catalysed reaction

Transaminase catalyses an equilibrium reaction in which L-homoserine is synthesised by reductive transamination of **6A** to **6E**. The influence of the concentration of these substrates on the specific activity of TA 039 is presented in Figures 6.2A and 6.2B, respectively. They show typical Michaelis-Menten dependence for **6A**, and mild substrate inhibition by **6E**. The influence of coenzyme PLP on the specific transaminase activity is presented in Figure 6.2C and also shows Michaelis-Menten dependence, and reveals that concentrations of PLP above ca 1 mM should be used to obtain maximum enzyme activity of TA 039 during the reaction. Reaction products, i.e. **6B** and **6C** both inhibit the forward reaction (Figures 6.2D and 6.2E), which is also the case for **6D**, an inevitable reactant for aldolase in the cascade system (Figure 6.2F). As this inhibition is severe, this implies that only very low concentrations of **6D** should be present in the reactor if **6B** is to be synthesised. The effect of methanol, stabilizer of **6D**, was also evaluated and it was found that it slightly inhibits the reaction. The presented data (Figures 6.2A-G) were used to estimate the apparent kinetic parameters in the forward reaction that are presented in Table 6.3.

Table 6.3 Kinetic parameters of transaminase TA 039 in the forward reaction.

Parameter	Unit	Value
V_{m1}	U mg^{-1}	0.726 ± 0.037
$K_{m1,\ \mathbf{6A}}$	mM	75.186 ± 4.896
$K_{m1,\ \mathbf{6E}}$	mM	11.703 ± 1.865
$K_{m1,\mathrm{PLP}}$	mM	0.141 ± 0.013
$K_{i1,\ \mathbf{6E}}$	mM	237.269 ± 35.297
$K_{i1,\ \mathbf{6B}}$	mM	90.942 ± 10.310
$K_{i1,\ \mathbf{6C}}$	mM	30.177 ± 2.934
$K_{i1,\ \mathbf{6D}}$	mM	0.156 ± 0.015
$K_{i1,\mathrm{MeOH}}$	mM	1021.619 ± 162.433

6A – L-Alanine, **6B** – L-Homoserine, **6C** – Sodium pyruvate, **6D** – Formaldehyde, **6E** – 4-Hydroxy-2-oxobutanoate

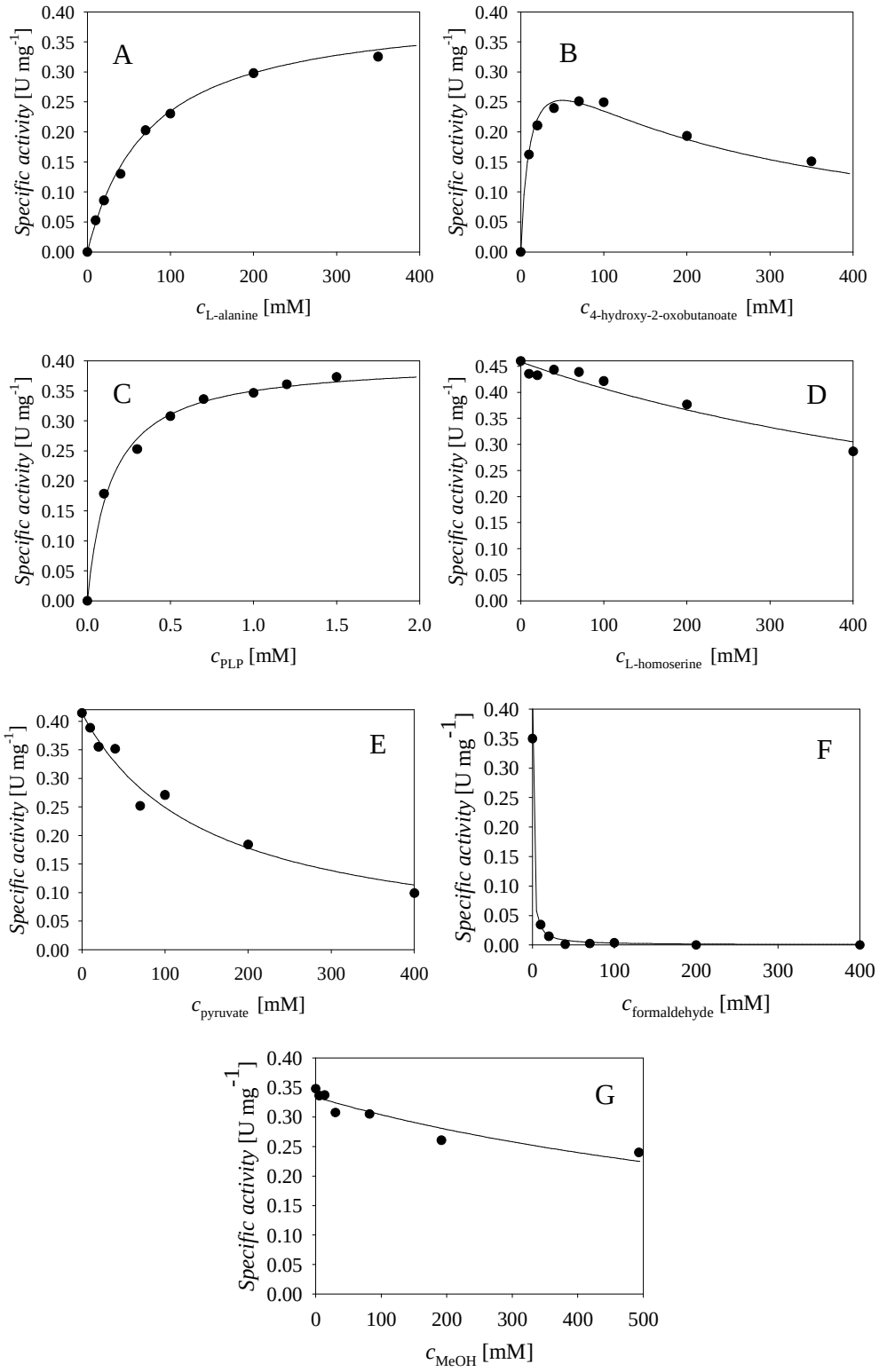

Figure 6.2 Dependence of transaminase specific activity (50 mM sodium phosphate buffer pH 7.0, 25 °C, γ_{TA39} = 1 mg mL^{-1}, $V_{reactor}$ = 0.5 mL) in the forward reaction on the concentration of A. **6A** (c_{6E} = 100 mM, c_{PLP} = 1 mM), B. **6E** (c_{6A} = 100 mM, c_{PLP} = 1 mM), C. PLP (c_{6A} = 300 mM, c_{6E} = 40 mM), D. **6B** (c_{6A} = 300 mM, c_{6E} = 70 mM, c_{PLP} = 1 mM), E. **6C** (c_{6A} = 300 mM, c_{6E} = 70 mM, c_{PLP} = 1 mM), F. **6D** (c_{6A}=300 mM, c_{6E}=70 mM, c_{PLP} = 1 mM), G. MeOH (c_{6A} = 300 mM, c_{6E} = 70 mM, c_{PLP} = 1 mM). Legend: black circles – experimental data, line – model.

6A – L-Alanine, **6B** – L-Homoserine, **6C** – Sodium pyruvate, **6D** – Formaldehyde, **6E** – 4-Hydroxy-2-oxobutanoate

The kinetics of the reverse reaction catalysed by TA 039 is presented in Figures 6.3A-G. The influence of **6B**, **6C** and PLP on the specific enzyme activity is presented in Figures 6.3A-C showing typical Michaelis-Menten dependencies. The influence of concentrations of **6D**, **6A**, **6E** and MeOH, are presented in Figures 6.3D-F, respectively, and they all inhibit enzyme in the reverse reaction.

Estimated kinetic parameters for TA 039-catalysed reaction system (Tables 6.3 and 6.4) show 2.9 fold higher maximum reaction rate for the, unwanted, reverse reaction (V_{m2}), than for the forward reaction (V_{m1}) which imply directly to the position of the reaction equilibrium.

High apparent values of Michaelis constant for **6A** ($K_{m1,\ 6A}$, Table 6.3) and **6B** ($K_{m2,\ 6B}$, Table 6.4), and lower for **6E** ($K_{m1,\ 6E}$, Table 6.3) and **6C** ($K_{m2,\ 6C}$, Table 6.4) were estimated which may imply to the affinity of enzyme towards the substrate. Substrate inhibition constant value for **6E** ($K_{i1,\ 6E}$, Table 6.3) implies mild inhibition. Even though transamination products **6C** and **6B** inhibit the enzyme in the forward reaction, their values imply mild product inhibition ($K_{i1,\ 6C}$ and $K_{i1,\ 6B}$, Table 6.3). The same can be stated for the inhibition by MeOH ($K_{i1,\ MeOH}$, Table 6.3), whereas this is not the case for **6D** ($K_{i1,\ 6D}$, Table 6.3). Compound **6D** seriously inhibits transamination reaction, and experimental data show that even at concentrations of **6D** that are ca 10 mM, a significant activity drop in the range of 90 % can be expected (Figure 6.2F).

Compounds **6A**, **6E** and MeOH mildly inhibit the reverse reaction ($K_{i2,\ 6A}$, $K_{i2,\ 6E}$ and $K_{i2,\ MeOH}$, Table 6.4), whereas **6D** acts as a more serious inhibitor ($K_{i2,\ 6D}$, Table 6.4), while the value of the estimated constant is quite low. Thus, from the presented data and the estimated kinetic parameters it can be assumed that the equilibrium of the reaction is shifted toward reactants. That is why and efficient pyruvate recycling system is necessary for the reaction to work towards the synthesis of **6B**. These data and the estimated kinetic parameters together with the reaction scheme were used to develop the kinetic model for the transaminase-catalysed reaction.

6A – L-Alanine, **6B** – L-Homoserine, **6C** – Sodium pyruvate, **6D** – Formaldehyde, **6E** – 4-Hydroxy-2-oxobutanoate

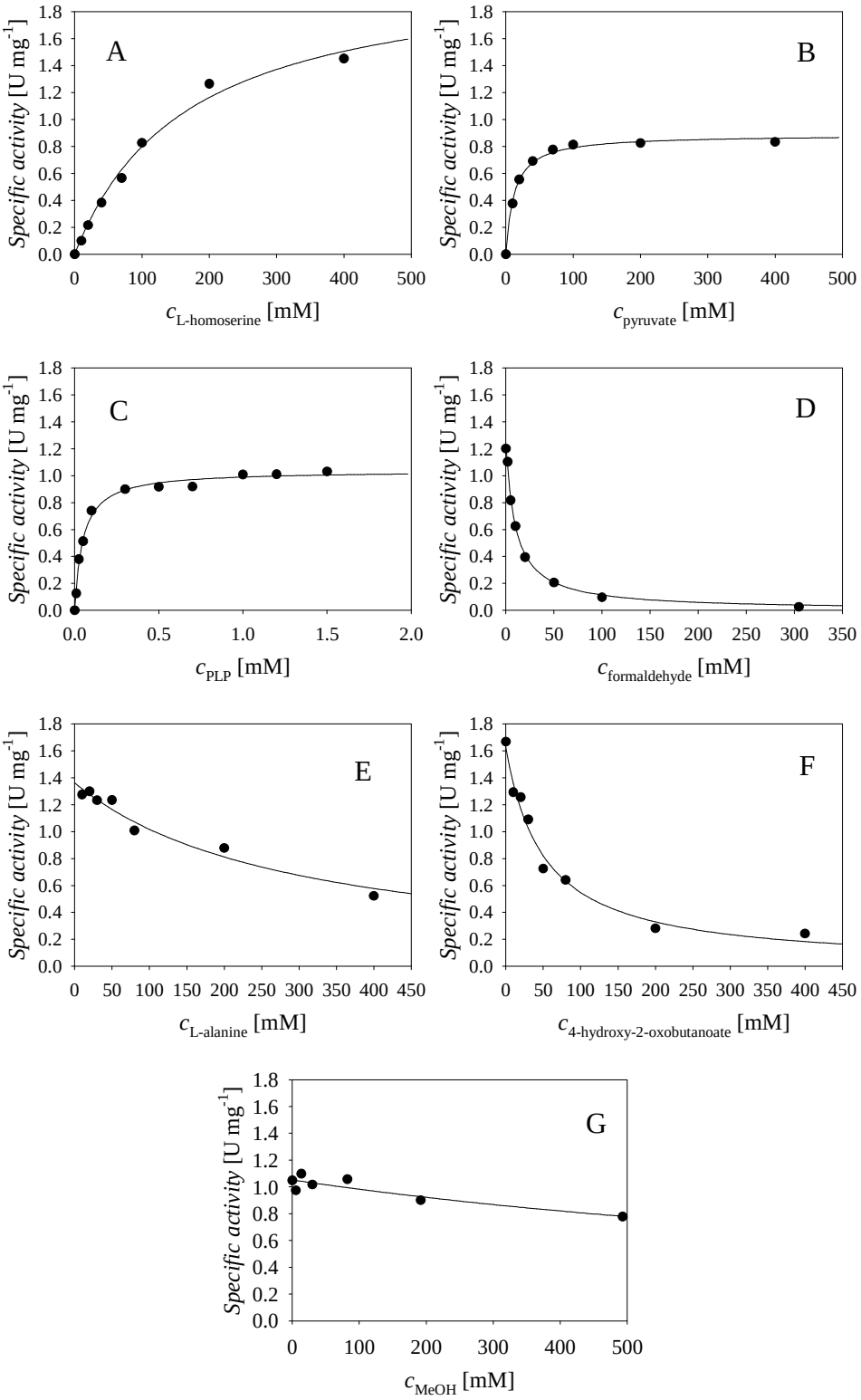

Figure 6.3 Dependence of transaminase specific activity (50 mM sodium phosphate buffer pH 7.0, 25 °C, γ_{TA39} = 1 mg mL^{-1}, $V_{reactor}$ = 0.5 mL) in the reverse reaction on the concentration of A. **6B** (c_{6C} = 100 mM, c_{PLP} = 1 mM), B. **6C** (c_{6B} = 100 mM, c_{PLP} = 1 mM), C. PLP (c_{6B} = 100 mM, c_{6C} = 100 mM), D. **6D** (c_{6B} = 300 mM, c_{6C} = 100 mM, c_{PLP}= 1 mM), E. **6A** (c_{6B} = 300 mM, c_{6C} = 100 mM, c_{PLP}=1 mM), F. **6D** (c_{6B} = 300 mM, c_{6C} = 100 mM, c_{PLP} = 1 mM), G. MeOH (c_{6B} = 300 mM, c_{6C} = 100 mM, c_{PLP} = 1 mM).

6A – L-Alanine, **6B** – L-Homoserine, **6C** – Sodium pyruvate, **6D** – Formaldehyde, **6E** – 4-Hydroxy-2-oxobutanoate

Table 6.4 Kinetic parameters of transaminase TA 039 in the reverse reaction.

Parameter	**Unit**	**Value**
V_{m2}	U mg^{-1}	2.137 ± 0.157
$K_{m2,\ \mathbf{6B}}$	mM	167.460 ± 26.085
$K_{m2,\ \mathbf{6C}}$	mM	12.145 ± 0.982
$K_{m2,\mathrm{PLP}}$	mM	0.048 ± 0.004
$K_{i2,\ \mathbf{6D}}$	mM	1.093 ± 0.091
$K_{i2,\ \mathbf{6A}}$	mM	31.899 ± 3.152
$K_{i2,\ \mathbf{6E}}$	mM	31.843 ± 2.738
$K_{i2,\ \mathrm{MeOH}}$	mM	1416.164 ± 281.911

6A – L-Alanine, **6B** – L-Homoserine, **6C** – Sodium pyruvate, **6D** – Formaldehyde, **6E** – 4-Hydroxy-2-oxobutanoate

6.3.2 Kinetic parameters for different aldolases in the aldol addition of 6C and 6D

Aldolase YfaU catalyses the reaction between **6C** and **6D** forming **6E** necessary for the main transamination reaction. Different YfaUs were tested for this reaction by determining its basic kinetics: the influence of **6C** and **6D** on initial reaction rate. The folding interference principle enables an activity-independent method for the selection of thermostable mutants of any protein (Chautarf et al., 2007). Mutations into the gene *yfaU* were carried out and two mutants (YfaU 013 and YfaU 014) showed higher melting temperature and half-life compared with YfaU WT (wild type) and higher or similar specific activity. These mutants were therefore, together with wild type enzyme, further analysed in terms of kinetics.

Potential biocatalysts tested for this reaction were: YfaU 013, YfaU 014, YfaU WT, MBP YfaU WT, YfaU 3, MBP YfaU 3, YfaU 5 and MBP YfaU 5. Proteins that are mainly expressed as inclusion bodies can be fused to another selected protein in order to solubilise the target protein expression (Raran-Kurussi & Waugh, 2012). In this regard, Maltose Binding Protein (MBP) from *E. coli* was selected, in this case, to improve the protein solubility in the active form and expression yields.

The influence of **6C** and **6D** concentration on the specific activity of YfaU 013 is presented in Figures 6.4A and 6.4B. Estimated values of kinetic constants are presented in Table 6.5.

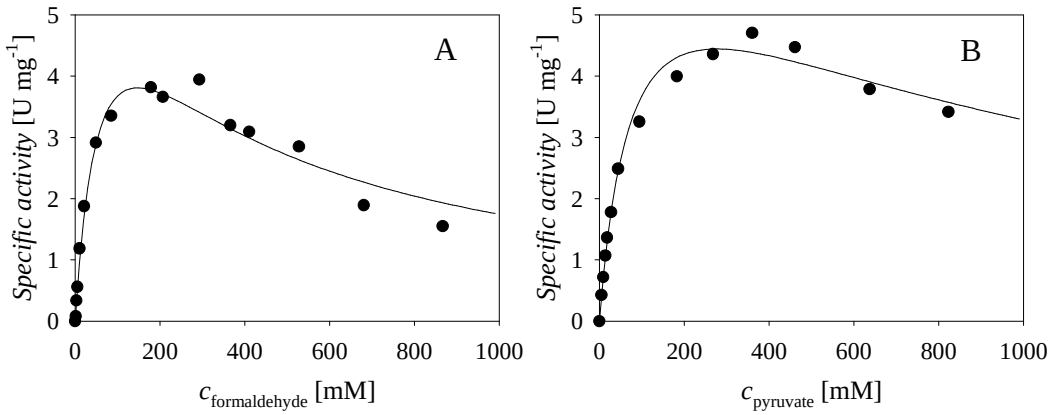

Figure 6.4 Kinetics of aldol addition of A. **6D** and B. **6C** catalysed by YfaU 013 (50 mM sodium phosphate buffer pH 7.0, 25 °C, $\gamma_{\text{YfaU 013}}$ = 0.25 mg mL^{-1}, V_{reactor} = 0.5 mL, A. $c_{\mathbf{6C}}$ = 142.93 mM, B. $c_{\mathbf{6D}}$ = 83.6 mM). Legend: black circles – experimental data, line – model.

6A – L-Alanine, **6B** – L-Homoserine, **6C** – Sodium pyruvate, **6D** – Formaldehyde, **6E** – 4-Hydroxy-2-oxobutanoate

Table 6.5 Estimated kinetic parameters for the aldol addition of **6C** and **6D** catalysed by YfaU 013.

Parameter	Unit	Value
V_m	U mg^{-1}	14.158 ± 2.435
k_{cat}	min^{-1}	439.71 ± 75.51
K_m^{6D}	mM	68.599 ± 17.956
K_i^{6D}	mM	318.278 ± 76.662
K_m^{6C}	mM	82.035 ± 16.444
K_i^{6C}	mM	933.246 ± 264.612

The influence of **6C** and **6D** concentration on the specific activity of YfaU 014 is presented in Figures 6.5A and 6.5B. Estimated values of kinetic constants are presented in Table 6.6.

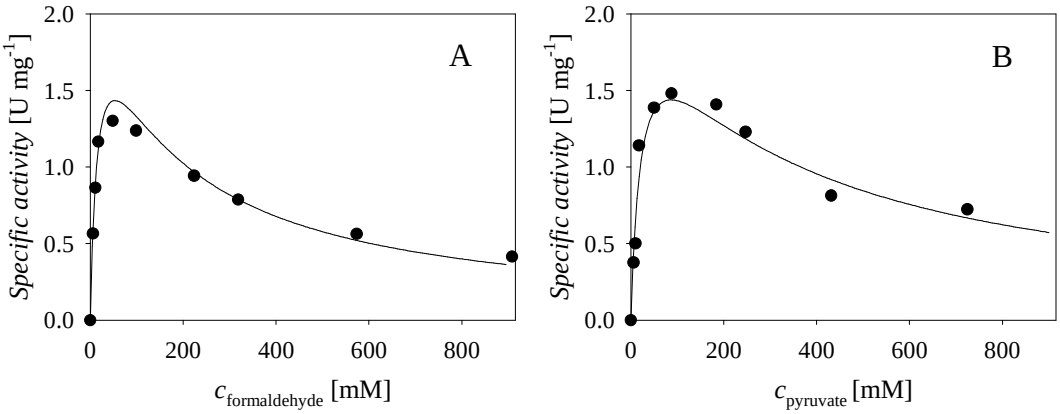

Figure 6.5 Kinetics of aldol addition of A. **6D** and B. **6C** catalysed by YfaU 014 (50 mM sodium phosphate buffer pH 7.0, 25 °C, $\gamma_{YfaU\ 014}$ = 0.2 mg mL^{-1}, $V_{reactor}$ = 1 mL, A. c_{6D} = 142.93 mM, B. c_{6C} = 83.6 mM). Legend: black circles – experimental data, line – model.

Table 6.6 Estimated kinetic parameters for the aldol addition of **6C** and **6D** catalysed by YfaU 014.

Parameter	Unit	Value
V_m	U mg^{-1}	3.71 ± 0.62
k_{cat}	min^{-1}	115.28 ± 19.26
K_m^{6D}	mM	17.59 ± 4.51
K_i^{6D}	mM	162.16 ± 38.17
K_m^{6C}	mM	23.86 ± 5.73
K_i^{6C}	mM	313.56 ± 80.01

6A – L-Alanine, **6B** – L-Homoserine, **6C** – Sodium pyruvate, **6D** – Formaldehyde, **6E** – 4-Hydroxy-2-oxobutanoate

The influence of **6C** and **6D** concentration on the specific activity of YfaU WT and MBP YfaU WT is presented in Figures 6.6A and 6.6B. Estimated values of kinetic constants are presented in Table 6.7.

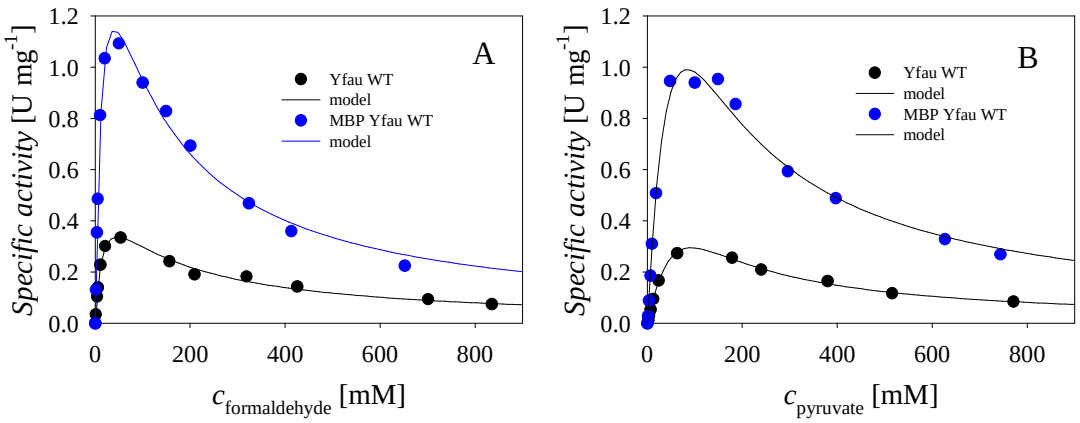

Figure 6.6 Kinetics of aldol addition of A. **6D** and B. **6C** catalysed by YfaU WT and MBP YfaU WT (50 mM phosphate buffer pH 7.0, $V_{reactor}$ = 0.5 mL, $\gamma_{Yfau\ WT}$ = 1 mg mL^{-1}, $\gamma_{MBP\ Yfau\ WT}$ = 0.5 mg mL^{-1}, A. c_{6C} = 100 mM, B. c_{6D} = 100 mM).

Table 6.7 Estimated kinetic parameters for the aldol addition of **6C** and **6D** catalysed by Yfau WT and MBP Yfau WT.

Parameter	**Unit**	**YfaU WT**	**MBP YfaU WT**
V_m	U mg^{-1}	3.65 ± 1.29	7.33 ± 1.36
k_{cat}	min^{-1}	113.42 ± 40.09	227.78 ± 42.26
K_m^{6D}	mM	24.09 ± 3.58	18.99 ± 2.51
K_i^{6D}	mM	94.53 ± 13.57	90.51 ± 11.64
K_m^{6C}	mM	209.18 ± 82.68	93.31 ± 21.04
K_i^{6C}	mM	46.61 ± 17.89	75.50 ± 16.63

6A – L-Alanine, **6B** – L-Homoserine, **6C** – Sodium pyruvate, **6D** – Formaldehyde, **6E** – 4-Hydroxy-2-oxobutanoate

The influence of **6C** and **6D** concentration on the specific activity of YfaU 3 and MBP YfaU 3 is presented in Figures 6.7A and 6.7B. Estimated values of kinetic constants are presented in Table 6.8.

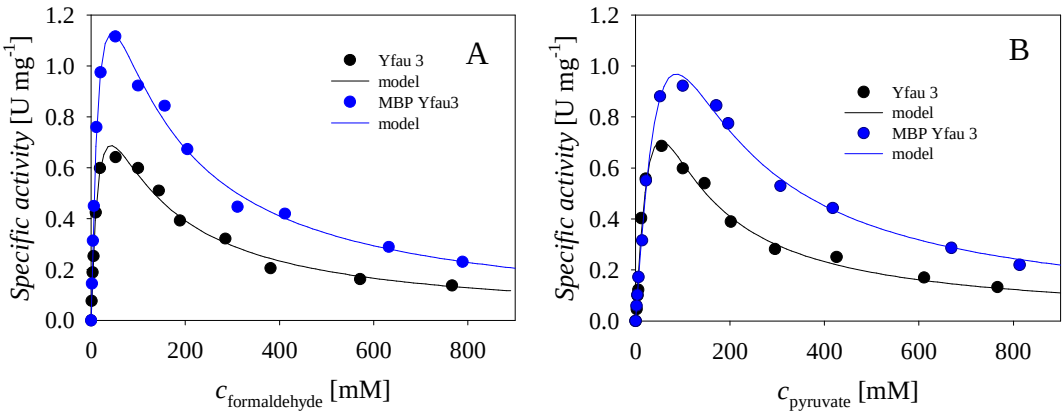

Figure 6.7 Kinetics of aldol addition of A. **6D** and B. **6C** catalysed by YfaU 3 and MBP YfaU 3 (50 mM phosphate buffer pH 7.0, $V_{reactor}$ = 0.5 mL, $\gamma_{Yfau\ 3}$ = 1 mg mL^{-1}, $\gamma_{MBP\ Yfau\ 3}$ = 1 mg mL^{-1}, A. c_{6C} = 100 mM, B. c_{6D} = 100 mM).

Table 6.8 Estimated kinetic parameters for the aldol addition of **6C** and **6D** catalysed by YfaU 3 and MBP YfaU 3.

Parameter	**Unit**	**YfaU 3**	**MBP YfaU 3**
V_m	U mg^{-1}	5.80 ± 1.70	8.94 ± 3.22
k_{cat}	min^{-1}	180.24 ± 52.83	277.81 ± 100.06
K_m^{6D}	mM	25.45 ± 5.55	20.06 ± 3.55
K_i^{6D}	mM	74.62 ± 16.29	104.64 ± 18.30
K_m^{6C}	mM	60.69 ± 19.88	169.27 ± 72.00
K_i^{6C}	mM	46.30 ± 15.35	58.34 ± 23.95

6A – L-Alanine, **6B** – L-Homoserine, **6C** – Sodium pyruvate, **6D** – Formaldehyde, **6E** – 4-Hydroxy-2-oxobutanoate

The influence of **6C** and **6D** concentration on the specific activity of YfaU 5 and MBP YfaU 5 is presented in Figures 6.8A and 6.8B. Estimated values of kinetic constants are presented in Table 6.9.

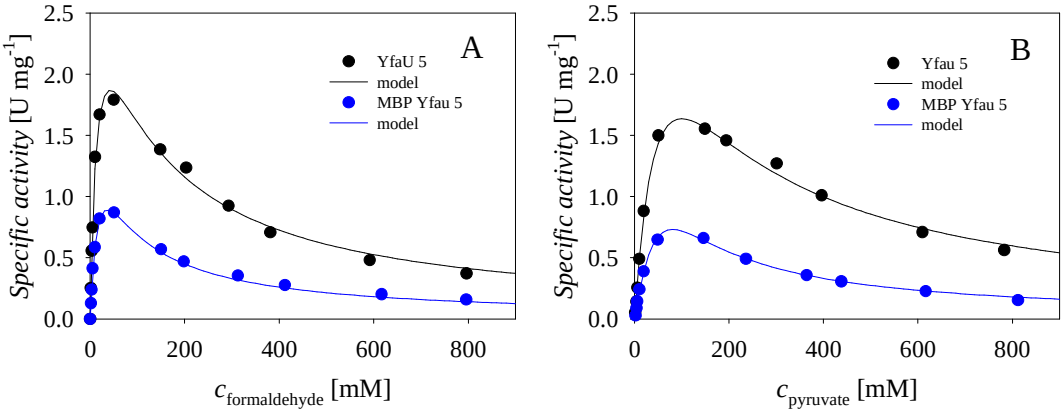

Figure 6.8 Kinetics of aldol addition of A. **6D** and B. **6C** catalysed by YfaU 5 and MBP YfaU 5 (50 mM phosphate buffer pH 7.0, $V_{reactor}$ = 0.5 mL, $\gamma_{Yfau\ 5}$ = 0.3 mg mL^{-1}, $\gamma_{MBP\ Yfau\ 5}$ = 0.5 mg mL^{-1}, A. $c_{\mathbf{6C}}$ = 100 mM, B. $c_{\mathbf{6D}}$ = 100 mM).

Table 6.9 Estimated kinetic parameters for the aldol addition of **6C** and **6D** catalysed by YfaU 5 and MBP YfaU 5.

Parameter	**Unit**	**YfaU 5**	**MBP YfaU 5**
V_m	U mg^{-1}	7.78 ± 0.90	6.40 ± 1.98
k_{cat}	min^{-1}	241.77 ± 27.97	198.88 ± 61.53
$K_m^{\mathbf{6D}}$	mM	16.52 ± 1.81	21.36 ± 4.28
$K_i^{\mathbf{6D}}$	mM	113.13 ± 11.82	84.07 ± 15.99
$K_m^{\mathbf{6C}}$	mM	65.94 ± 9.99	115.82 ± 42.67
$K_i^{\mathbf{6C}}$	mM	151.43 ± 21.89	70.06 ± 25.10

6A – L-Alanine, **6B** – L-Homoserine, **6C** – Sodium pyruvate, **6D** – Formaldehyde, **6E** – 4-Hydroxy-2-oxobutanoate

The results of kinetic measurements for the aldolase panel show that aldolase YfaU 013 has a highest maximum reaction rate and catalytic constant from all tested aldolases (Figure 6.9). It can be seen from estimated kinetic parameters that each enzyme is to some extent inhibited by substrates **6D** and **6C** (Tables 6.5 – 6.9) but YfaU 013's inhibition by both substrates is quite mild. YfaU 013 tolerates high concentrations of **6D** well over 1M, even though it exhibits lower activity at these concentrations. Since YfaU 013 affinity toward **6D** and **6C** is satisfactory and considering previously mentioned advantages over other tested enzymes, YfaU 013 was chosen as the most suitable aldolase for further use and research in this cascade system.

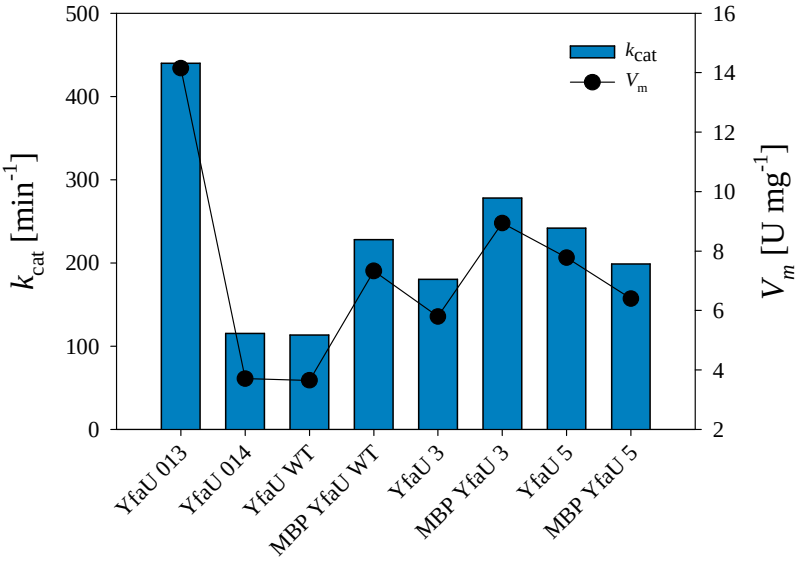

Figure 6.9 Catalytic constant and V_m values for each aldolase from the panel.

6A – L-Alanine, **6B** – L-Homoserine, **6C** – Sodium pyruvate, **6D** – Formaldehyde, **6E** – 4-Hydroxy-2-oxobutanoate

Once YfaU 013 was chosen for further process investigation, additional kinetic measurements were performed. In these experiments the influence of all compounds present in the cascade reaction were tested on aldolase activity during the reaction. These compounds are **6B**, **6A**, **6E**, methanol and PLP (Figure 6.10). Estimated kinetic parameters are shown in Table 6.10 and were included during model development.

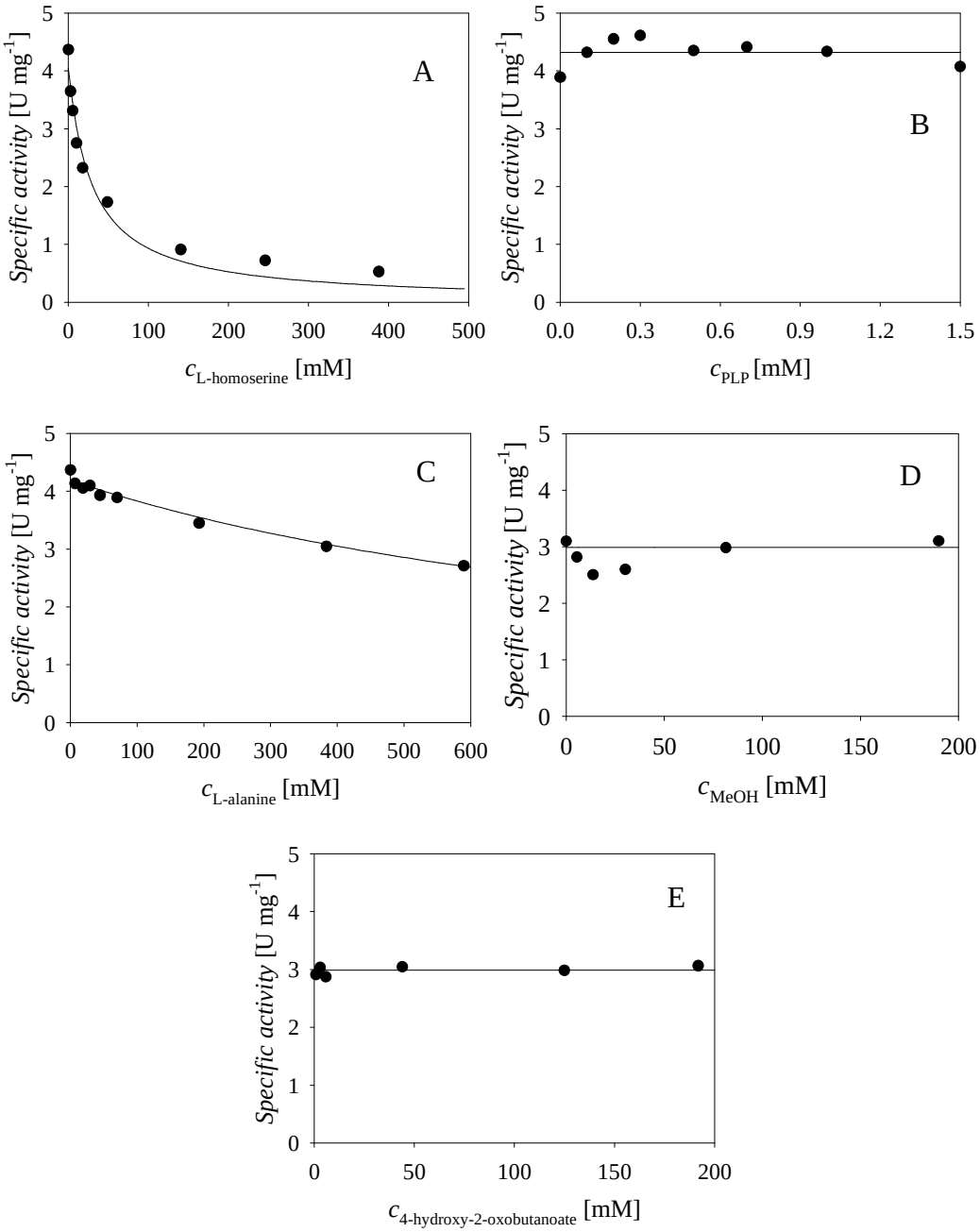

Figure 6.10 Dependence of aldolase YfaU 013 specific activity (50 mM sodium phosphate buffer pH 7.0, 25 °C, γ_{YfaU} = 0.25 mg mL^{-1}, $V_{reactor}$ = 0.5 mL, c_{6C} = 100 mM, c_{6D} = 100 mM) on the concentration of A. **6B**, B. PLP, C. **6A**, D. MeOH and E. **6E** in the aldol addition. Legend: black circles – experimental data, line – model.

6A – L-Alanine, **6B** – L-Homoserine, **6C** – Sodium pyruvate, **6D** – Formaldehyde, **6E** – 4-Hydroxy-2-oxobutanoate

It can be seen that **6B** and **6A** inhibit the aldol addition (Figures 6.10A and 6.10C), whereas PLP, MeOH and **6E** do not exhibit negative influence on the specific enzyme activity (Figures 6.10B, 6.10D and 6.10E).

Table 6.10 Kinetic parameters of YfaU 013-catalysed aldol addition of **6D** to **6C**.

Parameter	Unit	Value
V_{m3}	U mg^{-1}	14.158 ± 2.435
$K_{m3,\ \mathbf{6D}}$	mM	68.599 ± 17.956
$K_{m3,\ \mathbf{6C}}$	mM	82.035 ± 16.444
$K_{i3,\ \mathbf{6D}}$	mM	318.278 ± 76.662
$K_{i3,\ \mathbf{6C}}$	mM	933.246 ± 264.612
$K_{i3,\ \mathbf{6A}}$	mM	426.055 ± 32.269
$K_{i3,\ \mathbf{6B}}$	mM	12.720 ± 2.430

Retro-aldol reaction kinetics was also investigated to evaluate its effect on the reaction outcome. The results presented in Figures 6.11A-D and Table 6.11 show that the retro-aldol reaction exists, but the estimated maximum reaction rate (V_{m4}) is rather low in comparison to the maximum reaction rate of the aldol addition (V_{m3}); i.e. 117-fold lower. Additionally, the apparent Michaelis constant for **6E** is high ($K_{m4,\ \mathbf{6E}}$), and the retro-aldol reaction is inhibited by **6C** (Figure 6.11B).

Table 6.11 Kinetic parameters of YfaU 013-catalysed retro-aldol reaction of **6D** to **6C**.

Parameter	Unit	Value
V_{m4}	U mg^{-1}	0.121 ± 0.008
$K_{m4,\ \mathbf{6E}}$	mM	528.191 ± 56.354
$K_{i4,\ \mathbf{6C}}$	mM	26.783 ± 3.346

6A – L-Alanine, **6B** – L-Homoserine, **6C** – Sodium pyruvate, **6D** – Formaldehyde, **6E** – 4-Hydroxy-2-oxobutanoate

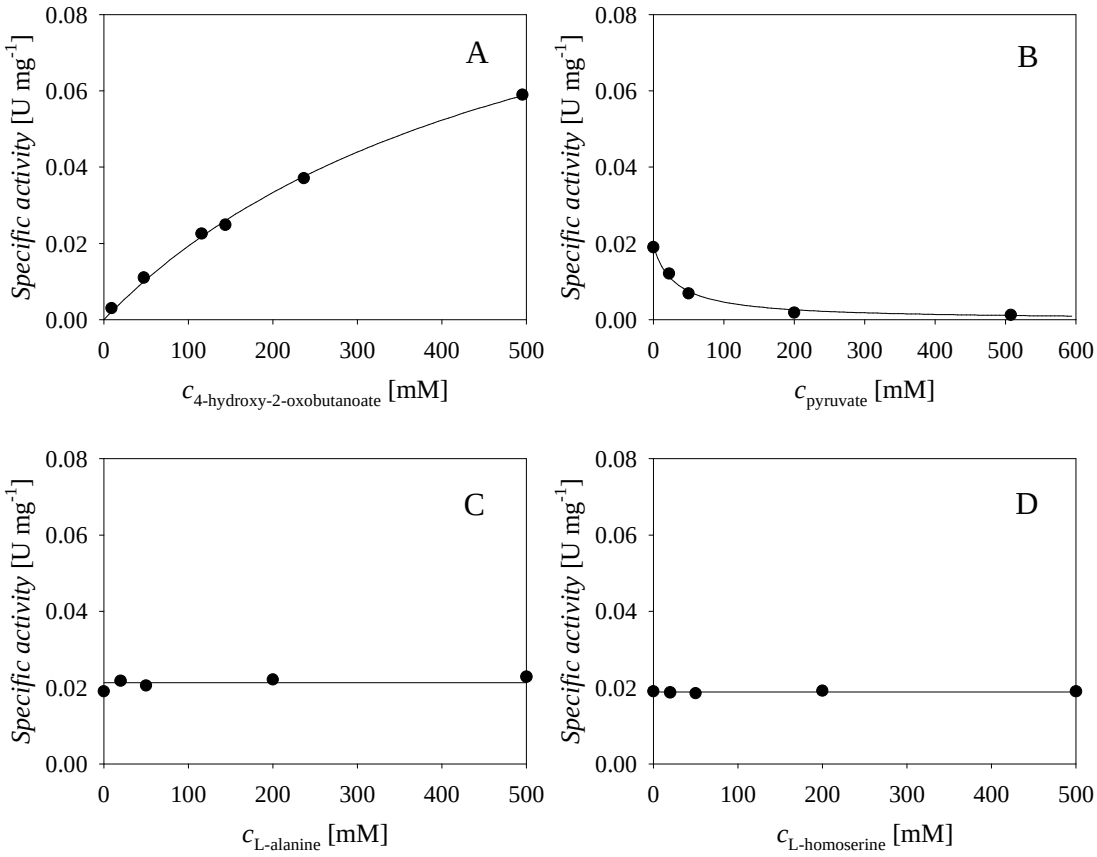

Figure 6.11 Dependence of YfaU 013 specific activity (50 mM sodium phosphate buffer pH 7.0, 25 °C, γ_{YfaU} = 5 mg mL^{-1}, $V_{reactor}$ = 0.5 mL) in the retro-aldol reaction on the concentration of A. **6E**, B. **6C** (c_{6E} = 100 mM), C. **6A** (c_{6E} = 100 mM), D. **6B** (c_{6E} = 100 mM). Legend: black circles – experimental data, line – model.

It is known that YfaU 013 can also catalyse the second aldol addition between **6E** and **6D**. That is why this reaction was also investigated in detail. The results presented in Figure 6.12A show that **6D** inhibits the enzyme as substrate in this reaction. They also show that YfaU 013 activity linearly depends on the concentration of **6E** in the reaction, which implies that this reaction can be kept 'under control' by consumption of **6E** in the TA 039-catalysed reaction at appropriate rate (Figure 6.12B). The reaction is also slightly inhibited by **6B**, **6A** and **6C** (Figures 6.12C-E). Estimated kinetic constants are presented in Table 6.12.

6A – L-Alanine, **6B** – L-Homoserine, **6C** – Sodium pyruvate, **6D** – Formaldehyde, **6E** – 4-Hydroxy-2-oxobutanoate

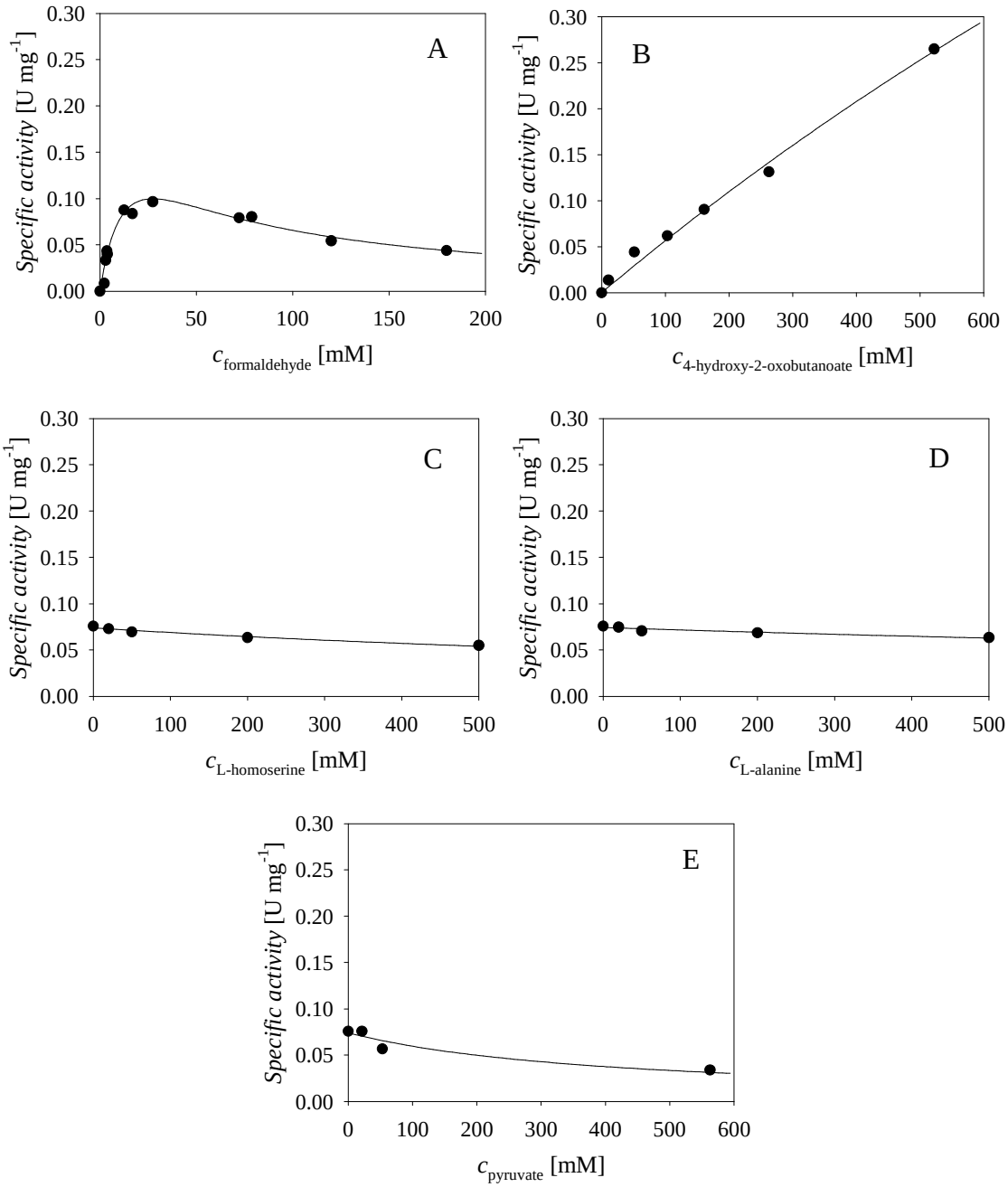

Figure 6.12 Kinetics of the 2nd aldol addition of **6D** to **6E** (50 mM sodium phosphate buffer pH 7.0, 25 °C, γ_{YfaU} = 10 mg mL^{-1}, $V_{reactor}$ = 0.3 mL). Dependence of aldolase specific activity in the aldol addition on the concentration of A. **6D** (c_{6E} = 100 mM), B. **6E** (c_{6D} = 100 mM), C. **6B** (c_{6E} = 100 mM, c_{6D} = 50 mM), D. **6A** (c_{6E} = 100 mM, c_{6D} = 50 mM), E. **6C** (c_{6E} = 100 mM, c_{6D} = 50 mM). Legend: black circles – experimental data, line – model.

6A – L-Alanine, **6B** – L-Homoserine, **6C** – Sodium pyruvate, **6D** – Formaldehyde, **6E** – 4-Hydroxy-2-oxobutanoate

Table 6.12 Kinetic parameters of YfaU 013 catalysed aldol addition of **6D** to **6E** – 2nd addition.

Parameter	Unit	Value
k_5	U mg^{-1} mM^{-1}	0.000515 ± 0.000133
$K_{m5,\ \mathbf{6D}}$	mM	16.116 ± 4.003
$K_{i5,\ \mathbf{6D}}$	mM	46.666 ± 11.111
$K_{i5,\ \mathbf{6B}}$	mM	1363.229 ± 117.026
$K_{i5,\ \mathbf{6A}}$	mM	2751.870 ± 380.778
$K_{i5,\ \mathbf{6C}}$	mM	411.716 ± 130.031

From all the obtained kinetic data in Chapters 6.3.1 and 6.3.2 it is clear that it is a very complex cascade system in which tuning of substrates/products concentration is necessary for a successful outcome. That is why a kinetic model is of paramount importance for minimization of lab effort to achieve this goal.

6.3.3 Stability of 4-hydroxy-2-oxobutanoate without the presence of enzyme

The stability of aldol **6E** was evaluated and it was found that it slowly degrades as shown in Figure 6.13. Reaction rate of this unspecific, non-catalysed transformation (r_6) was described by the kinetics of the first order, and this was included in the mathematical model as stability of **6E**. The kinetic constant of the first order was estimated to be $9.43 \cdot 10^{-5} \pm 1.15 \cdot 10^{-5}$ min^{-1}.

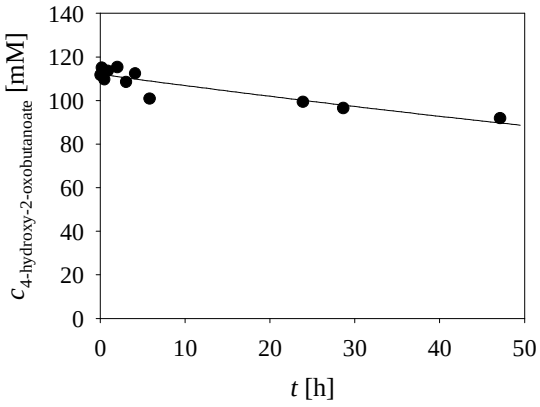

Figure 6.13 Evaluation of stability of aldol **6E** (50 mM sodium phosphate buffer pH 7.0, 25 °C) without the presence of enzyme. Legend: black circles – experimental data, line – model.

6A – L-Alanine, **6B** – L-Homoserine, **6C** – Sodium pyruvate, **6D** – Formaldehyde, **6E** – 4-Hydroxy-2-oxobutanoate

6.3.4 Enzyme stability during incubation

Figure 6.14 presents the results of TA 039 and YfaU 013 specific activity drop during incubation at different concentration of **6D**. It is evident that even after a very short contact with **6D** both enzymes lose their initial activity, and as the concentration of **6D** increases, the activity drop is faster. The same can be expected in the reactor. Thus, besides being an inhibiting substrate for both enzymes, **6D** also causes damage to the enzyme. When **6D** is absent from the solution, TA 039 showed better stability than YfaU 013. Namely, YfaU 013 loses nearly 25 % of its initial activity after 24 hours, whereas TA 039 loses up to 3-5 %. If the effect of **6D** is compared at similar conditions, at concentration of **6D** corresponding to ca. 100 mM, both enzymes lose 79 % of their initial activity after 24 hours. Similarity in the effect of **6D** on enzyme activity can be observed at other concentrations when calculating the percentage of the activity loss. It can be concluded that both enzymes are seriously affected by the presence of **6D** in the system, and it was expected that this would be so in the reactor. That is why its concentration had to be minimized and well-adjusted during the reaction.

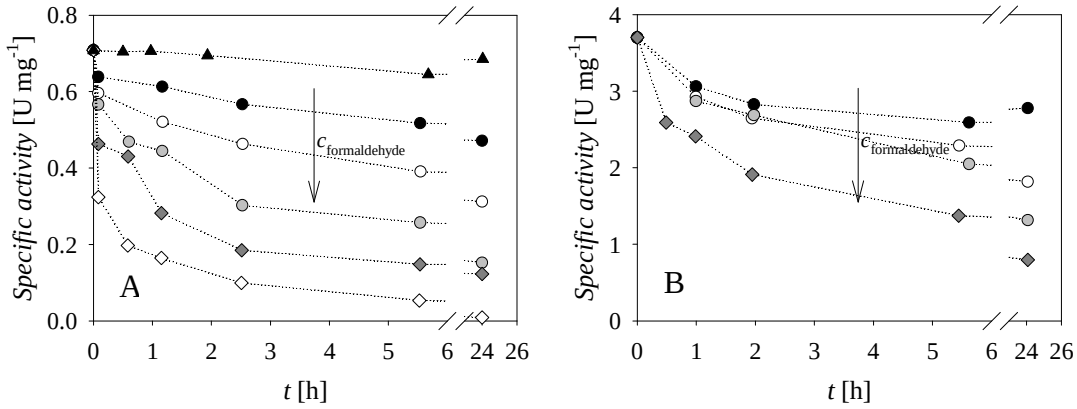

Figure 6.14 The influence of concentration of **6D** on the specific activity of A. TA 039 ($\gamma_{TA\ 039}$ = 25 mg mL^{-1}) and B. YfaU 013 ($\gamma_{YfaU\ 013}$ = 15 mg mL^{-1}) during incubation (50 mM sodium phosphate buffer pH 7.0, 25 °C). Legend: A. black triangles – c_{6D} = 0 mM; black circles – c_{6D} = 26.2 mM; white circles – c_{6D} = 47.7 mM; grey circles – c_{6D} = 94.7 mM; grey diamonds – c_{6D} = 189.9 mM; white diamonds – c_{6D} = 458.8 mM. B. black circles – c_{6D} = 0 mM; white circles – c_{6D} = 11.3 mM; grey circles – c_{6D} = 63.2 mM; grey diamonds – c_{6D} = 113.6 mM.

It can be expected that **6D** will have deactivating effect on both enzymes and therefore operational stability decay was included in the model for the cascade reaction.

6.3.5 Stability of reaction components during incubation with enzymes

Enzymes YfaU 013 and TA 039 (50 mg mL^{-1}) were incubated for 24 hours in the presence of reaction compounds, separately and combined as presented in Table 6.13. Stabilities are tested without enzymes as well.

Table 6.13 Cascade components consumption during incubation with and without enzymes ($c_{\text{each compound}}$ = 100 mM, V = 0.7 mL, 50 mM sodium phosphate buffer pH 7.0, 1000 rpm, 25 °C, 24 hours).

Experiment	Test content	Enzymes	Change in concentrations
1	**6C** and **6A**	$\gamma_{\text{YfaU 013}}$ = 5 mg mL^{-1}, $\gamma_{\text{TA 039}}$ = 5 mg mL^{-1}	YES
2	**6C** and **6A**	Without enzymes	NO
3	**6A**	$\gamma_{\text{YfaU 013}}$ = 5 mg mL^{-1}, $\gamma_{\text{TA 039}}$ = 5 mg mL^{-1}	NO
4	**6C**	$\gamma_{\text{YfaU 013}}$ = 5 mg mL^{-1}, $\gamma_{\text{TA 039}}$ = 5 mg mL^{-1}	YES
5	**6E** and **6A**	Without enzymes	NO
6	**6D** and **6C**	Without enzymes	NO
7	**6B**	$\gamma_{\text{YfaU 013}}$ = 5 mg mL^{-1}, $\gamma_{\text{TA 039}}$ = 5 mg mL^{-1}	NO
8	**6B**	Without enzymes	NO
9	**6E**	$\gamma_{\text{YfaU 013}}$ = 5 mg mL^{-1}, $\gamma_{\text{TA 039}}$ = 5 mg mL^{-1}	YES
10	**6E**	Without enzymes	SLOW DEGRADATION
11	**6B** and **6C**	$\gamma_{\text{YfaU 013}}$ = 5 mg mL^{-1}, $\gamma_{\text{TA 039}}$ = 5 mg mL^{-1}	YES
12	**6B** and **6C**	Without enzymes	NO
13	**6D** and **6E**	$\gamma_{\text{YfaU 013}}$ = 5 mg mL^{-1}, $\gamma_{\text{TA 039}}$ = 5 mg mL^{-1}	YES
14	**6D** and **6E**	Without enzymes	NO
15	**6E** and **6A**	Without enzymes	NO

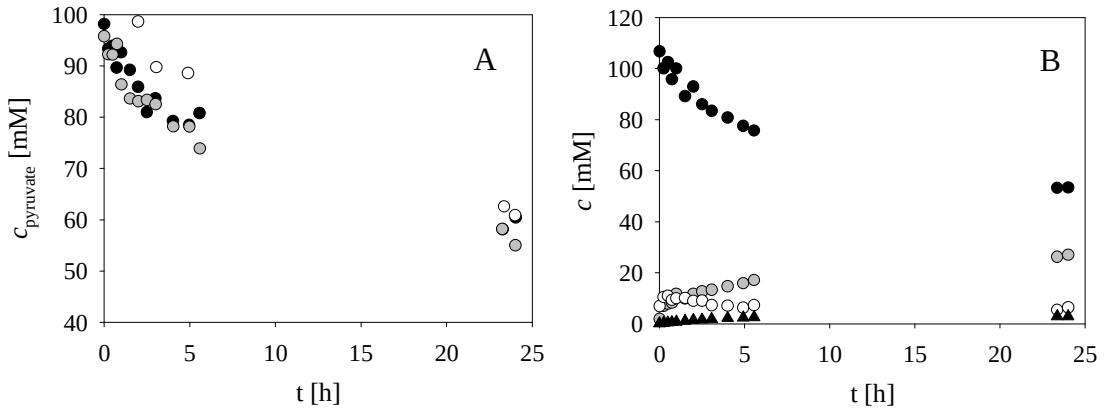

Figure 6.15 Incubation with 5 mg mL^{-1} of YfaU 013 and 5 mg mL^{-1} of TA 039 (50 mM sodium phosphate buffer pH 7.0, 25 °C) of A. black circles – **6C** (experiment 4 – Table 6.13); grey circles – **6C** and **6A** (experiment 1 – Table 6.13); white circles – **6C** and **6B** (experiment 11 – Table 6.13), B. **6E** (experiment 9 – Table 6.13).

6A – L-Alanine, **6B** – L-Homoserine, **6C** – Sodium pyruvate, **6D** – Formaldehyde, **6E** – 4-Hydroxy-2-oxobutanoate

It can be observed from Figure 6.15 and Table 6.13 that in experiment 1, 4 and 11 **6C** concentration changes were similar regardless of the presence of the second compound. Thus, **6C** is degraded or transformed under these conditions and this feature cannot be neglected in the model. Experiment 13 presents the second aldol addition which was kinetically characterized, whereas experiment 9 depicts the retro-aldol reaction of **6E**.

6.3.6 Development of mathematical model and its validation

Kinetic parameters were estimated from the experimental data. The data were collected by using the initial reaction rate method. It was assumed that during the prolonged use, enzyme operational stability decay will occur. It was assumed that it happens according to the kinetics of the first order. Enzyme operational stability decay rate constants were estimated directly form the batch reactor experiments. Non-linear regression methods (simplex and least squares fit) implemented in SCIENTIST software were used for parameter estimation. The same software was used for model simulations. Based on the data presented in Chapters 6.3.1 – 6.3.5 and the reaction scheme (Scheme 6.1) kinetic model for the cascade system was developed (Table 6.14). It consists of the kinetic and mass balance equations.

The reaction rate of the transaminase-catalysed reaction between **6A** and **6E** (r_1) was described by the two-substrate Michaelis-Menten equation including competitive inhibitions by **6B**, **6C** and **6D**, as well as non-competitive inhibition by MeOH (Equation 6.3). The influence of coenzyme PLP is described and included in the model by introducing factor *f*. It is not spent in the reaction but its concentration affects enzyme activity. Commercial **6D** contains up to 4.8 mol% of MeOH for its stabilization, which can act as a non-competitive inhibitor for enzymes. Reaction rate of the reverse transaminase-catalysed reaction between **6C** and **6B** (r_2) was described by two-substrate Michaelis-Menten equation including competitive inhibitions by **6E**, **6D** and **6A**, as well as non-competitive inhibition by MeOH (Equation 6.4).

The reaction rate of YfaU 013-catalysed aldol addition of **6C** and **6D** (r_3) was described by double substrate Michaelis-Menten equation including substrate inhibition by **6D** and **6C**, as well as competitive inhibition by **6A** and **6B** (Equation 6.5). The reaction rate of the retro-aldol reaction (r_4) was described by the Michaelis-Menten kinetics including competitive inhibition by **6C** (Equation 6.6). The reaction rate of the second aldol addition catalysed by YfaU 013 (r_5) between **6E** and **6D** was described with simplified expression (Equation 6.7) of two-substrate Michaelis-Menten kinetics with substrate **6D** inhibition,

6A – L-Alanine, **6B** – L-Homoserine, **6C** – Sodium pyruvate, **6D** – Formaldehyde, **6E** – 4-Hydroxy-2-oxobutanoate

whereas reaction rate depends linearly on the concentration of **6E**. Instead of maximum reaction rate for this reaction, there is k_5 in the equation, which corresponds to the quotient of V_{m5} and $K_{m5,6E}$. It was not possible to determine the value of V_{m5} due to the linearity of experimental data. Unspecific transformations of **6C** (enzymatic transformation) and **6E** (non-enzymatic transformation) were estimated from experiments and inserted in the model. Its reaction rates (r_6 and r_7) were described by the first order kinetics (Equations 6.8 and 6.9).

Mass balance equations for **6A**, **6E**, **6B**, **6C** and **6D** for the cascade reaction in the batch reactor are represented by Equations 6.10-6.14. Even though these balances are presented for the cascade reaction, kinetic models for the separate reaction steps were evaluated and in those cases all reaction rates are not relevant. The same is valid for the kinetic equations. For example, in the aldol addition reaction (r_3, Equation 6.5) **6A** and **6B** are not present. That is why these concentrations are considered to be zero and inhibition members of the equation for these compounds can be neglected.

Mass balance equations for **6A**, **6E**, **6B**, **6C**, **6D**, PLP, YfaU 013 and TA 039 in the fed-batch reactor are represented by Equations 6.15-6.22, respectively. Equation 6.23 represents the change in reactor volume during the experiment defined by the flow-rate of solution of **6D**.

Enzyme operational stability decay for TA 039 and YfaU 013 was described by the first order kinetics, i.e. Equations 6.24 and 6.25, respectively.

The validity of the kinetic model was evaluated for both reactions of the cascade separately. This was necessary at this point as in the cascade reactions many new interdependencies between the variables occur, and model complexity increases.

6A – L-Alanine, **6B** – L-Homoserine, **6C** – Sodium pyruvate, **6D** – Formaldehyde, **6E** – 4-Hydroxy-2-oxobutanoate

Table 6.14 Mathematical model for the cascade reaction system.

KINETIC EQUATIONS

Transaminase catalysed reaction

$$r_1 = \frac{V_{m2} \cdot \gamma_{TA} \cdot c_{6A} \cdot c_{6E} \cdot f}{\left(K_{m1,6A} \cdot \left(1 + \frac{c_{6C}}{K_{i1,6C}} + \frac{c_{6D}}{K_{i1,6D}}\right) + c_{6A}\right) \cdot \left(K_{m1,6E} \cdot \left(1 + \frac{c_{6B}}{K_{i1,6B}}\right) + c_{6E} + \frac{c_{6E}^2}{K_{i1,6E}}\right) \cdot \left(1 + \frac{c_{MeOH}}{K_{i,MeOH}}\right)} \quad (6.3)$$

$$f = \frac{c_{PLP}}{K_{m,PLP} + c_{PLP}}$$

Reverse transamination reaction

$$r_2 = \frac{V_{m2} \cdot \gamma_{TA} \cdot c_{6B} \cdot c_{6C} \cdot f}{\left(K_{m2,6B} \cdot \left(1 + \frac{c_{6E}}{K_{i2,6E}}\right) + c_{6B}\right) \cdot \left(K_{m2,6C} \cdot \left(1 + \frac{c_{6D}}{K_{i2,6D}} + \frac{c_{6A}}{K_{i2,6A}}\right) + c_{6C}\right) \cdot \left(1 + \frac{c_{MeOH}}{K_{i,MeOH}}\right)} \quad (6.4)$$

Aldol addition

$$r_3 = \frac{V_{m3} \cdot \gamma_{YfaU} \cdot c_{6C} \cdot c_{6D}}{\left(K_{m3,6C} \cdot \left(1 + \frac{c_{6B}}{K_{i3,6B}} + \frac{c_{6A}}{K_{i3,6A}}\right) + c_{6C} + \frac{c_{6C}^2}{K_{i3,6C}}\right) \cdot \left(K_{m3,6D} + c_{6D} + \frac{c_{6D}^2}{K_{i3,6D}}\right)} \quad (6.5)$$

Retro-aldol reaction

$$r_4 = \frac{V_{m4} \cdot \gamma_{YfaU} \cdot c_{6E}}{K_{m4,6E} \cdot \left(1 + \frac{c_{6C}}{K_{i4,6C}}\right) + c_{6E}} \quad (6.6)$$

2nd aldol addition

$$r_5 = \frac{k_5 \cdot \gamma_{YfaU} \cdot c_{6D} \cdot c_{6E}}{K_{m5,6D} + c_{6D} + \frac{c_{6D}^2}{K_{i5,6D}}} \quad (6.7)$$

Unspecific transformation of **6E**

$$r_6 = k_6 \cdot c_{6E} \quad (6.8)$$

$$r_7 = k_7 \cdot \gamma_{YfaU} \cdot c_{6C} \quad (6.9)$$

MASS BALANCES IN THE BATCH REACTOR

$$\frac{dc_{6A}}{dt} = -r_1 + r_2 \quad (6.10)$$

$$\frac{dc_{6E}}{dt} = -r_1 + r_2 + r_3 - r_4 - r_5 - r_6 \quad (6.11)$$

$$\frac{dc_{6B}}{dt} = r_1 - r_2 \quad (6.12)$$

$$\frac{dc_{6C}}{dt} = r_1 - r_2 - r_3 + r_4 - r_7 \quad (6.13)$$

$$\frac{dc_{6D}}{dt} = -r_3 - r_5 + r_4 \quad (6.14)$$

MASS BALANCES IN THE FED-BATCH REACTOR

$$\frac{dc_{6A}}{dt} = \frac{1}{V} \cdot \left(-c_{6A} \cdot \frac{dV}{dt}\right) - r_1 + r_2 \quad (6.15)$$

$$\frac{dc_{6E}}{dt} = \frac{1}{V} \cdot \left(-c_{6E} \cdot \frac{dV}{dt}\right) - r_1 + r_2 + r_3 - r_4 - r_5 - r_6 \quad (6.16)$$

$$\frac{dc_{6B}}{dt} = \frac{1}{V} \cdot \left(-c_{6B} \cdot \frac{dV}{dt}\right) + r_1 - r_2 \quad (6.17)$$

$$\frac{dc_{6C}}{dt} = \frac{1}{V} \cdot \left(-c_{6C} \cdot \frac{dV}{dt}\right) + r_1 - r_2 - r_3 + r_4 - r_7 \quad (6.18)$$

$$\frac{dc_{6D}}{dt} = \frac{1}{V} \cdot \left(-c_{6D} \cdot \frac{dV}{dt} + c_{6D,0} \cdot q\right) - r_3 - r_5 + r_4 \quad (6.19)$$

$$\frac{dc_{MeOH}}{dt} = \frac{1}{V} \cdot \left(-c_{MeOH} \cdot \frac{dV}{dt} + c_{MeOH} \cdot q\right) \quad (6.20)$$

$$\frac{d\gamma_{YfaU}}{dt} = \frac{1}{V} \cdot \left(-\gamma_{YfaU} \cdot \frac{dV}{dt} + \gamma_{YfaU,0} \cdot q\right) \quad (6.21)$$

$$\frac{d\gamma_{TA}}{dt} = \frac{1}{V} \cdot \left(-\gamma_{TA} \cdot \frac{dV}{dt} + \gamma_{TA.0} \cdot q\right) \quad (6.22)$$

$$\frac{dV}{dt} = q \quad (6.23)$$

ENZYME OPERATIONAL STABILITY DECAY

$$\frac{d\gamma_{TA}}{dt} = -k_{d,1} \cdot \gamma_{TA} \quad (6.24)$$

$$\frac{d\gamma_{YfaU}}{dt} = -k_{d,2} \cdot \gamma_{YfaU} \quad (6.25)$$

6A – L-Alanine, **6B** – L-Homoserine, **6C** – Sodium pyruvate, **6D** – Formaldehyde, **6E** – 4-Hydroxy-2-oxobutanoate

6.3.6.1 Model validation of transaminase-catalysed reaction

Mathematical model for the transaminase-catalysed reaction in the batch reactor (Table 6.14, Equations 6.3, 6.4, 6.10-6.13) was validated on several experiments carried out at different experimental conditions of substrate and enzyme concentrations (Figure 6.16). As shown in Figure 6.16, good agreement of model with experimental data in the wide range of experimental conditions was obtained. Since these reactions were fast, it was not necessary to include enzyme deactivation in the model.

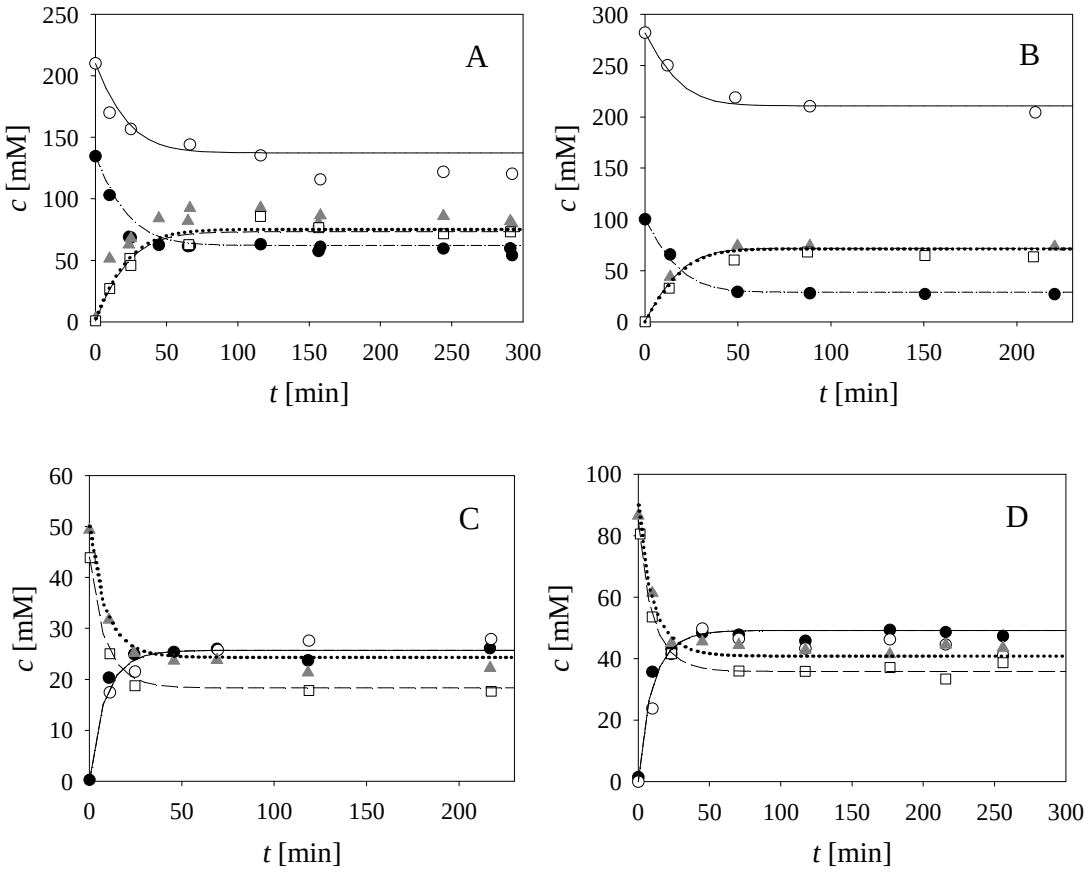

Figure 6.16 Validation of the mathematical model for TA 039-catalysed reactions in the batch reactor (50 mM sodium phosphate buffer pH 7.0, 25 °C, $V_{reactor}$ = 1 mL). Forward reactions: A. and B. (c_{6E} = 100 mM, c_{6A} = 100 mM, c_{PLP} = 2 mM, γ_{TA} = 10 mg mL^{-1}). Reverse reactions C. and D (c_{6C} = 100 mM, c_{6B} = 100 mM, c_{PLP} = 1 mM, γ_{TA} = 10 mg mL^{-1}). Legend: black circles – **6E**; white circles – **6A**; grey triangles – **6C**; white squares – **6B**; dash-dotted line – **6E** model; full line – **6A** model; dotted line – **6C** model; long dash line – **6B** model.

An unfavourable position of thermodynamic equilibrium for the transamination of **6A** can be seen in all presented batch reactions (Figure 6.16). Since it was crucial for the success of this cascade, reaction equilibrium was studied more detailed.

6A – L-Alanine, **6B** – L-Homoserine, **6C** – Sodium pyruvate, **6D** – Formaldehyde, **6E** – 4-Hydroxy-2-oxobutanoate

In chemistry, Le Châtelier's principle is used to manipulate the outcomes of reversible reactions, often to increase the yield of reactions (Campbell, 1985). Equation 6.26 where [C] and [D] are concentrations of reaction products and [A] and [B] those of reactants, shows that by removing product from the reaction, the equilibrium is shifted towards product formation. Likewise, when product is being recycled in the system, the same effect is achieved.

$$K = \frac{[C][D]}{[A][B]} \tag{6.26}$$

Equilibrium constants were determined according to Tufvesson et al. (2012). Constants were determined using developed mathematical model by observing the change in the reaction quotient Q (Equation 6.27) over 24 hours.

$$Q = \frac{[C][D]}{[A][B]} \xrightarrow{t=\infty} K \tag{6.27}$$

The reaction quotients (Q_{0h} and Q_{24h}) were calculated at time 0 and 24h (Table 6.15). The equilibrium constants were estimated in Excel (Microsoft, USA) from a power based curve fit presented in Figure 6.17 A between the ratio Q_{24h}/Q_{0h} and Q_{0h}, by calculating the value of Q_{0h}, corresponding to $Q_{24h}/Q_{0h}=1$. Data were fitted to a hyperbolic equation $Q_{24h}/Q_{0h} = 0.6619 \cdot Q_{0h}^{-0.992}$, $R^2 = 0.9858$. Estimated equilibrium constant value was found to be 0.6669. Figure 6.17 B shows good fitting of experimental data and Q_t values based on simulation. Low equilibrium constant value confirms the fact that this reaction equilibrium does not encourage product formation. These findings are in agreement with previous work with a different transaminase in Hernández et al. (2017a). The investigated cascade has the advantage that pyruvate (**6C**) is the product of transamination catalysed by TA 039 and a substrate for aldol addition catalysed by YfaU 013. Therefore, **6C** is shifting the transamination equilibrium toward L-homoserine (**6B**) formation by constant decrease of **6C** concentration, while it is being recycled by aldol addition reaction.

6A – L-Alanine, **6B** – L-Homoserine, **6C** – Sodium pyruvate, **6D** – Formaldehyde, **6E** – 4-Hydroxy-2-oxobutanoate

Table 6.15 Q_{24h}/Q_{0h} ratio calculation from model simulations.

$c_{6E,\ 0h}$ [mM]	$c_{6A,\ 0h}$ [mM]	$c_{6B,\ 0h}$ [mM]	$c_{6C,\ 0h}$ [mM]	Q_0	$c_{6E,\ 24h}$ [mM]	$c_{6A,\ 24h}$ [mM]	$c_{6B,\ 24h}$ [mM]	$c_{6C,\ 24h}$ [mM]	Q_{24h}	Q_{24h}/Q_0
250	600	220	20	0.0293	152.28	502.28	317.72	117.72	0.4890	16.6709
70	300	492.2	2	0.0469	51.45	281.45	510.75	20.55	0.7250	15.4658
60	250	351.6	4	0.0938	43.76	233.76	367.84	20.24	0.7276	7.7605
50	200	234.4	8	0.1875	37.35	187.35	247.05	20.65	0.7290	3.8873
40	150	140.6	16	0.3749	32.88	142.88	147.72	23.12	0.7269	1.9388
30	100	70.3	32	0.7499	30.35	100.35	69.95	31.65	0.7269	0.9694
100	600	100	600	1.0000	128.67	628.67	71.33	571.33	0.5038	0.5038
20	50	23.4	64	1.4976	25.01	55.01	18.39	58.99	0.7887	0.5266
35	27	56	31	1.8370	45.22	37.22	45.78	20.78	0.5652	0.3077
15	30	20	48	2.1333	20.92	35.92	14.08	42.08	0.7885	0.3696
100	600	300	500	2.5000	228.91	728.91	171.09	371.09	0.3805	0.1522
10	25	5.9	128	3.0208	12.92	27.92	2.98	125.08	1.0313	0.3414

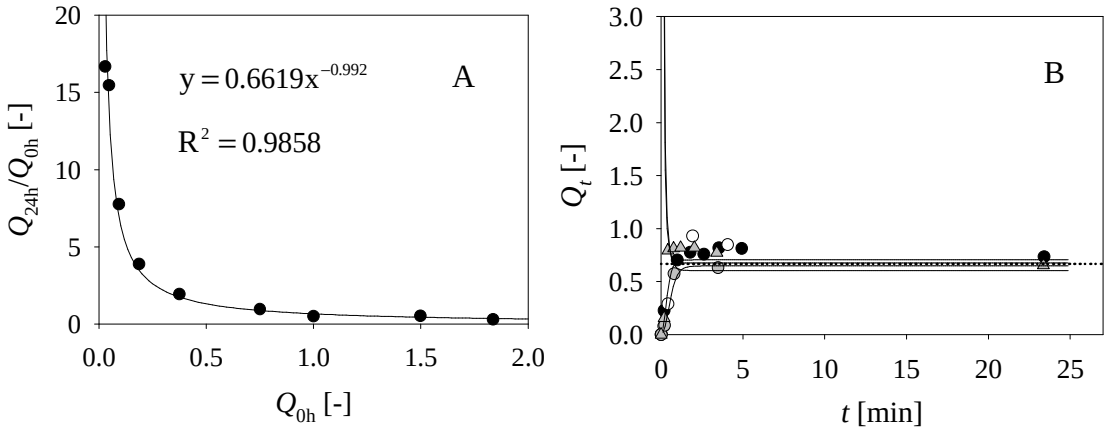

Figure 6.17 A. Model-based determination of K_{eq} for transamination of **6E** with **6A** to yield **6B** (values presented in Table 6.15). The simulations were done at different initial concentrations of reactants and products and set for 24 hours. Quotients Q_{24h}/Q_{0h} were plotted against Q_{0h}. B. Q_t during four different reaction – comparison of simulation Q_t calculation (lines) and experimental data (dots).

6.3.6.2 Model validation of YfaU 013-catalysed reaction

Mathematical model for the reaction catalysed by aldolase YfaU 013 in the batch reactor (Table 6.14, Equations 6.5-6.9, 6.11, 6.13, 6.14) was validated in the batch reactor with several experiments carried out at different experimental conditions of substrate and enzyme concentrations that are presented in Figure 6.18. The good agreement between experimental data and the model data in the wide range of experimental conditions was shown. The reaction catalysed by YfaU 013 is fast and therefore, concentration of **6D** quickly

6A – L-Alanine, **6B** – L-Homoserine, **6C** – Sodium pyruvate, **6D** – Formaldehyde, **6E** – 4-Hydroxy-2-oxobutanoate

drops down under 10 mM even in reactions where YfaU 013 concentration was 1 mg mL^{-1} (Figures 6.18A-D). Consequently, the concentration of by-product, i.e. product of the second aldol addition increases faster in batch with higher YfaU 013 concentration (Figure 6.18E) compared to experiments with lower YfaU 013 concentration (Figures 6.18A-D). Since these reactions were fast, it was not necessary to include enzyme deactivation in the model.

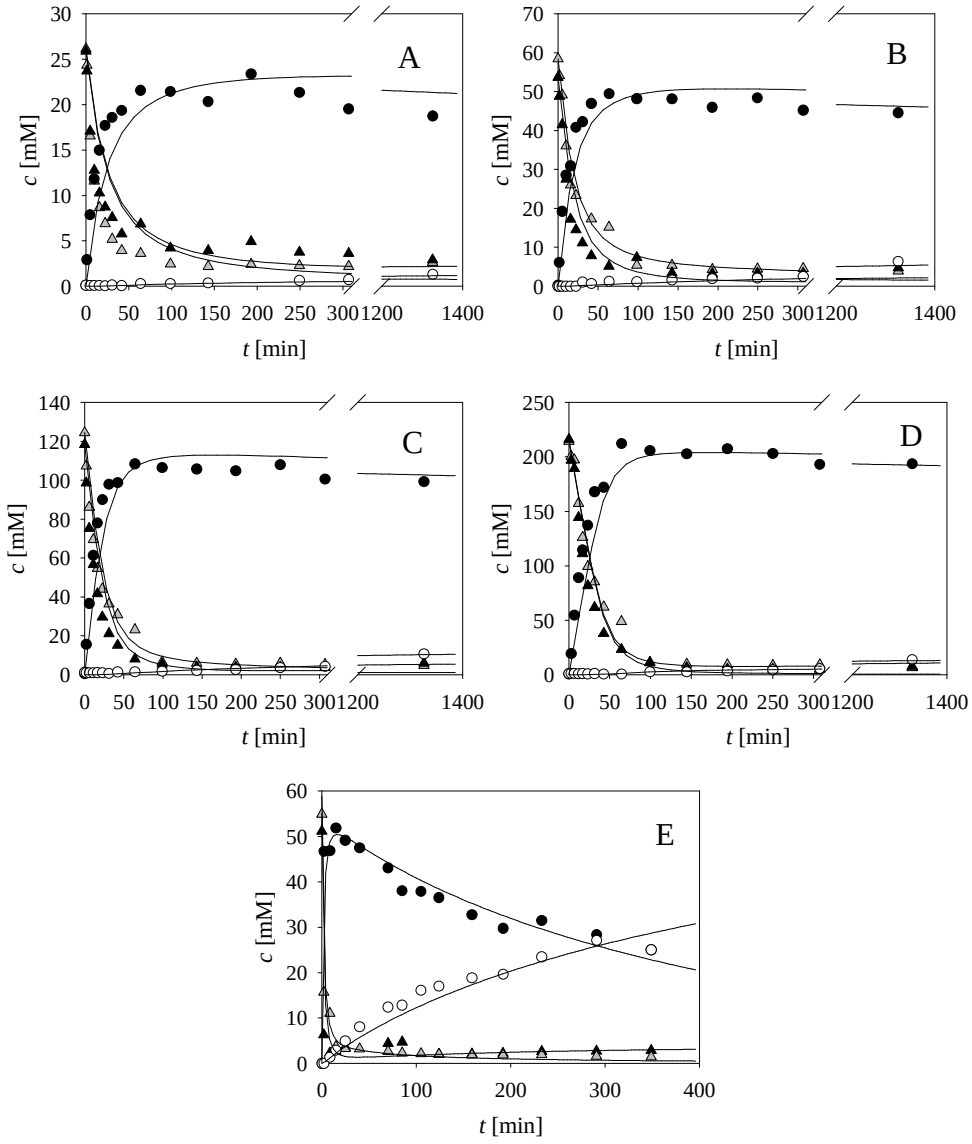

Figure 6.18 Validation of the mathematical model for YfaU 013-catalysed aldol addition in the batch reactor (50 mM sodium phosphate buffer pH 7.0, 25 °C). A. c_{6C} = 26.1 mM, c_{6D} = 25.9 mM, $\gamma_{YfaU\ 013}$ = 1 mg mL^{-1}, B. c_{6C} = 53.7 mM, c_{6D} = 58.5 mM, $\gamma_{YfaU\ 013}$ = 1 mg mL^{-1}, C. c_{6C} = 118.4 mM, c_{6D} = 124.5 mM, $\gamma_{YfaU\ 013}$ = 1 mg mL^{-1}, D. c_{6C} = 216.0 mM, c_{6D} = 214.4 mM, $\gamma_{YfaU\ 013}$ = 1 mg mL^{-1}, E. c_{6C} = 51.1 mM, c_{6D} = 54.9 mM, $\gamma_{YfaU\ 013}$ = 10 mg mL^{-1}. Legend: grey triangles – **6C**, black circles – **6E**, black triangles – **6D**, white circles – by-product, second aldol addition product, line – model.

6A – L-Alanine, **6B** – L-Homoserine, **6C** – Sodium pyruvate, **6D** – Formaldehyde, **6E** – 4-Hydroxy-2-oxobutanoate

6.3.7 Cascade simulations

Mathematical model was used for performing simulations of process outcomes for different initial conditions. The aim of all simulations was to get an insight of how different process set-ups determine the process outcomes.

The effect of variables on the reaction outcome carried out in the fed-batch reactor were simulated and presented in Figure 6.19. Simulations show how different concentrations of **6A** and **6C** influence the concentration of evolving product **6B**. This simulation shows that with higher initial **6A** and **6C** concentration in the system product **6B** concentration increases. In simulations presented in Figure 6.19 different enzyme concentrations ratios were used and it can be seen that better results can be obtained when transaminase concentration is higher in comparison to aldolase.

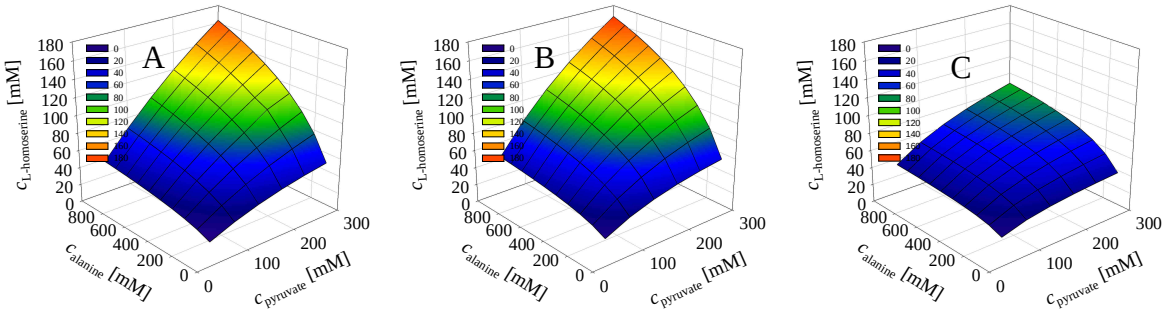

Figure 6.19 Cascade simulations of influence of **6A** and **6C** concentrations on product **6B** formation (V_0 = 7.8 mL, $c_{\mathbf{6D},\ feed}$ = 3110 mM, $q_{\mathbf{6D}}$ = 0.8 µL min^{-1}, $\gamma_{TA\ 039}$ = 100 mg mL^{-1}, $\gamma_{YfaU\ 013}$ = 400 mg mL^{-1}, $c_{\mathbf{6A}}$ = 100 – 1000 mM, $c_{\mathbf{6C}}$ = 50 – 300 mM, c_{PLP} = 1 mM). A. $\gamma_{TA\ 039}$ = 40 mg mL^{-1}, $\gamma_{YfaU\ 013}$ = 15 mg mL^{-1}, B. $\gamma_{TA\ 039}$ = 40 mg mL^{-1}, $\gamma_{YfaU\ 013}$ = 40 mg mL^{-1}, C. $\gamma_{TA\ 039}$ = 40 mg mL^{-1}, $\gamma_{YfaU\ 013}$ = 400 mg mL^{-1}.

Figure 6.19C simulates the reaction with the concentration of YfaU 013 10 times higher than TA 039. Concentration of desired product is lower compared to simulations where YfaU 013 concentration was lower or equal to TA 039 concentration (Figures 6.19A and 6.19B). The same trend can be seen in Figure 6.20 where simulations were done to test the influence of aldolase YfaU 013 and TA 039 concentrations on formation of product **6B**. This implies that for the success of the process the choice of enzyme concentrations should be made carefully. This was also discussed in Hernández et al., 2017a.

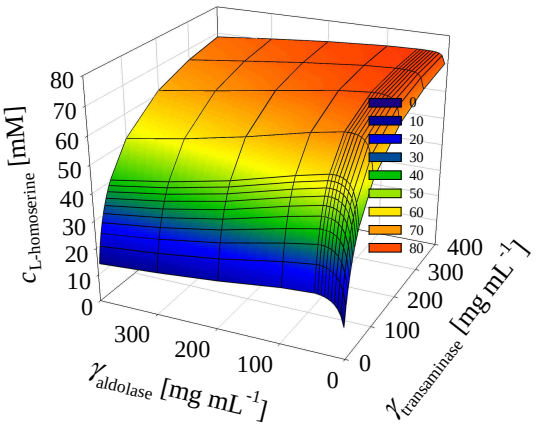

Figure 6.20 Influence of aldolase YfaU 013 and TA 039 concentrations on formation of product **6B** (V_0 = 7.8 mL, $c_{6D,\ feed}$ = 3110 mM, q_{6D} = 3 µL min^{-1}, c_{6A} = 100 mM, c_{6C} = 300 mM).

Simulation presented in Figure 6.21 shows the effect of different feed flow-rates of **6D** and **6C** on the concentration of produced **6B**. It is clear that **6D** feed has a strong impact on the process outcome, which was stressed in the process optimization. It can also be seen that **6C** feeding strategy would not help in increasing the process metrics outcome. Thus, it was neglected as a strategy.

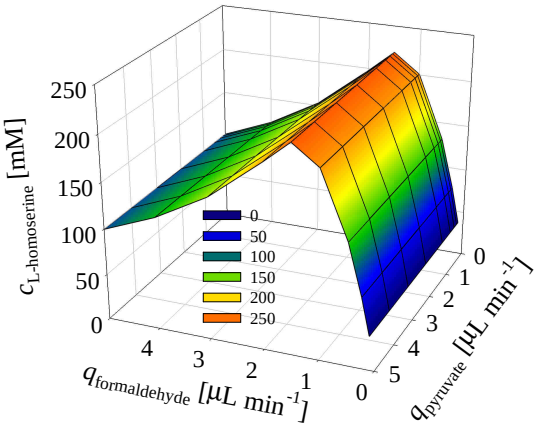

Figure 6.21 Cascade simulations of influence of **6D** and **6C** feed on product **6B** formation (V_0 = 7.8 mL, $c_{6C,\ feed}$ = 900 mM, q_{6C} = 0 – 5 µL min^{-1}, $c_{6D,\ feed}$ = 3110 mM, q_{6D} = 0.1 – 5 µL min^{-1}, $\gamma_{TA\ 039}$ = 100 mg mL^{-1}, $\gamma_{YfaU\ 013}$ = 400 mg mL^{-1}, c_{6A} = 600 mM, c_{6C} = 300 mM, c_{PLP} = 1 mM).

Ideal maximum concentration of **6C** in the cascade is between 200 and 250 mM since it shifts the equilibrium toward **6B** formation and its negative effect on TA 039 activity is acceptable at that concentration (Figure 6.4B). Also, its concentration reduces with **6B** formation and therefore its inhibiting effect decreases over time.

6A – L-Alanine, **6B** – L-Homoserine, **6C** – Sodium pyruvate, **6D** – Formaldehyde, **6E** – 4-Hydroxy-2-oxobutanoate

Process simulation also shows that initial **6A** concentrations of ca. 650 mM are optimal to start the reaction with.

Figure 6.22 shows how **6B** production can be improved by adding fresh amounts of **6A** and **6C** in certain reaction times. Figure 6.22A shows concentration of substrates, and Figure 6.22B shows concentrations of **6E** and **6B**. This simulation was the basis for performing successful optimized cascade reaction that gave the highest concentration of product **6B** presented in next chapter. Compared to other performed simulation, this process set-up of re-adding **6A** and **6C** with continuous flow of **6D** gave the highest product **6B** concentration at the end of the reaction.

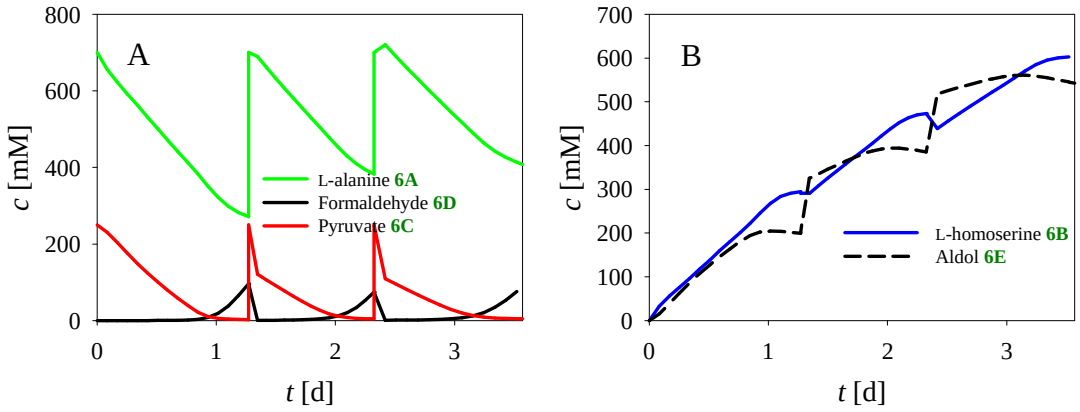

Figure 6.22 Cascade simulation with re-adding **6A** and **6C** with continuous flow of **6D** (V_0 = 7.8 mL, $c_{\mathbf{6D},\text{feed}}$ = 3110 mM, $q_{\mathbf{6D}}$ = 1 µL min^{-1}, $c_{\mathbf{6C},0}$ = 250 mM, $c_{\mathbf{6A},0}$ = 700 mM, $\gamma_{\text{TA 039}}$ = 100 mg mL^{-1}, $\gamma_{\text{YfaU 013}}$ = 400 mg mL^{-1}, c_{PLP} = 1 mM). **6A** and **6C** were re-added after 1.27 days and 2.32 days up to their initial concentrations of 700 mM and 250 mM, respectively.

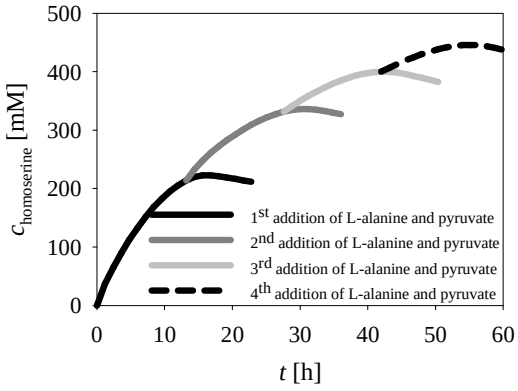

Figure 6.23 Cascade simulation with 4 additions of **6A** and **6C** with continuous flow of **6D** (V_0 = 7.8 mL, $c_{\mathbf{6D},\text{feed}}$ = 3110 mM, $q_{\mathbf{6D}}$ = 1.5 µL min^{-1}, $c_{\mathbf{6C},0}$ = 300 mM, $c_{\mathbf{6A},0}$ = 600 mM, $\gamma_{\text{TA 039}}$ = 50 mg mL^{-1}, $\gamma_{\text{YfaU 013}}$ = 25 mg mL^{-1}, c_{PLP} = 1 mM).

6A – L-Alanine, **6B** – L-Homoserine, **6C** – Sodium pyruvate, **6D** – Formaldehyde, **6E** – 4-Hydroxy-2-oxobutanoate

The strategy was also applied at other initial enzyme concentrations to confirm the results at lower enzyme YfaU 013 and TA 039 concentrations (Figure 6.23). It was shown that the lower the enzyme concentration, the more **6B** is formed.

Simulation presented in Figure 6.24 shows how a different new aldolase or YfaU improved by genetic engineering techniques could improve this process. K_m value for **6C** of YfaU 013 is 82.035 mM. If this value were somehow decreased, the affinity of enzyme toward substrate **6C** would increase. This would have a positive effect on the cascade since lower concentrations of **6C** in the system would be sufficient for **6E** formation. In that case, **6C** concentration could be kept minimal during cascade and its inhibiting effect on transaminase (Figure 6.2E, Table 6.3) would be significantly lower. On the other side, when K_i value for **6B** of aldolase would be higher (K_i for **6B** of YfaU 013 is 12.720, Table 6.10), its inhibiting effect on aldolase would decrease and high amounts of product **6B** that accumulate during reaction wouldn't cause high inhibition of aldolase. Therefore, high K_i value for **6B** would positively effect on the process outcome.

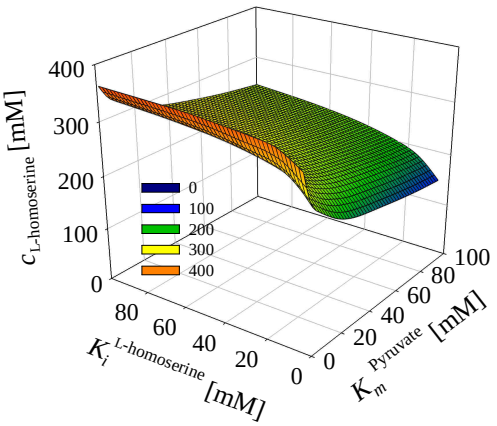

Figure 6.24 Cascade simulation with improved enzymes in terms of K_m for **6C** and K_i for **6B**.

6.3.8 Optimized reaction – validation of model simulations

Even though model simulations presented in the previous chapter were only qualitative, they were used to increase the knowledge of the process and improve the process metrics. Two fed-batch experiments catalysed by YfaU 013 and TA 039 in which **6D** was slowly added to the reactor were carried out and the results are presented in Figure 6.25. Substrate **6D** was added slowly to the reactor by maintaining its concentration below 10 mM in order to diminish its negative effect on activity and stability of both enzymes.

6A – L-Alanine, **6B** – L-Homoserine, **6C** – Sodium pyruvate, **6D** – Formaldehyde, **6E** – 4-Hydroxy-2-oxobutanoate

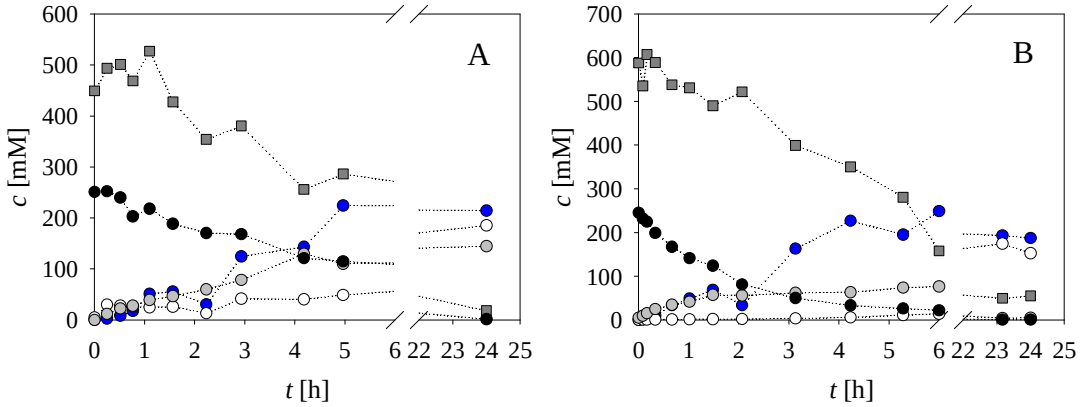

Figure 6.25 Fed-batch experiments (50 mM sodium phosphate buffer pH 7.0, 25 °C, 450 rpm, V_0 = 7.8 mL, $c_{\mathbf{6D},feed}$ = 3110 mM, $q_{\mathbf{6D}\ (15h)}$ = 3 µL min^{-1}, c_{PLP} = 0.26 mM) A. $c_{\mathbf{6C}}$ = 251 mM, $c_{\mathbf{6A}}$ = 449 mM, $\gamma_{TA\ 039}$ = 20 mg mL^{-1}, $\gamma_{YfaU\ 013}$ = 3.8 mg mL^{-1}. B. $c_{\mathbf{6C}}$ = 245 mM, $c_{\mathbf{6A}}$ = 587 mM, $c_{\mathbf{6D},0}$ = 10 mM, $\gamma_{TA\ 039}$ = 29.7 mg mL^{-1}, $\gamma_{YfaU\ 013}$ = 37.2 mg mL^{-1}. Legend: Grey squares – **6A**, blue circles – **6B**, black circles – **6C**, white circles – **6D**, grey circles – **6E**.

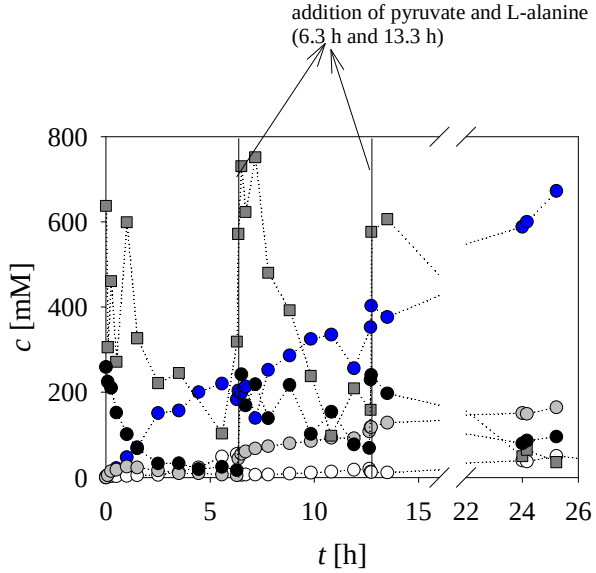

Figure 6.26 Optimized fed-batch experiment (50 mM sodium phosphate buffer pH 7.0, 25 °C, 450 rpm, V_0 = 7.8 mL, $c_{\mathbf{6D},feed}$ = 3110 mM, $q_{\mathbf{6D}\ (15h)}$ = 3 µL min^{-1}, c_{PLP} = 0.27 mM, $c_{\mathbf{6C}}$ = 259 mM, $c_{\mathbf{6A}}$ = 637 mM, $\gamma_{TA\ 039}$ = 40.1 mg mL^{-1}, $\gamma_{YfaU\ 013}$ = 50.1 mg mL^{-1}. Legend: Grey squares – **6A**, blue circles – **6B**, black circles – **6C**, white circles – **6D**, grey circles – **6E**.

The maximum concentration of **6B** obtained in these experiments was in the range of 200 mM, which was not sufficient for industrial exploitation.

The third experiment presented in Figure 6.26 was carried out according to the optimization strategy. It was carried out as fed-batch considering the continuous addition of **6D**. Two extra additions of substrates **6A** and **6C** was performed after 6.3 and 13.3 h. This resulted in increase of **6B** concentration of 672 mM (80.1 g L^{-1}), volume productivity of 3.2 g

6A – L-Alanine, **6B** – L-Homoserine, **6C** – Sodium pyruvate, **6D** – Formaldehyde, **6E** – 4-Hydroxy-2-oxobutanoate

L^{-1} h^{-1} and yield of 60%. Even though the yield was not higher than 85%, other process metrics were enough for industrial exploitation.

6A – L-Alanine, **6B** – L-Homoserine, **6C** – Sodium pyruvate, **6D** – Formaldehyde, **6E** – 4-Hydroxy-2-oxobutanoate

6.4 Results and discussion: process optimization catalysed by lyophilised whole cells containing YfaU 013 and TA 039

6.4.1 Kinetics of the reactions catalysed by whole cells

Kinetics of whole cell biocatalyst YfaU(013)/PRO TRANS(039) was determined. Kinetic measurements were made for each reaction step, i.e. aldol addition catalysed by YfaU 013 and transamination catalysed by TA 039 as well as their reverse reactions. Based on kinetic measurements conducted with separate CFE enzymes, some kinetic measurements where excluded in cells kinetic research such as influence of PLP concentration (cells contain PLP) and kinetic measurements where no influence of specific compound concentration on enzyme activity was detected. Since the same enzymes were used in both cases (CFE enzymes and co-expressed enzymes in the cells), analogous results were expected and their comparison is presented in this chapter.

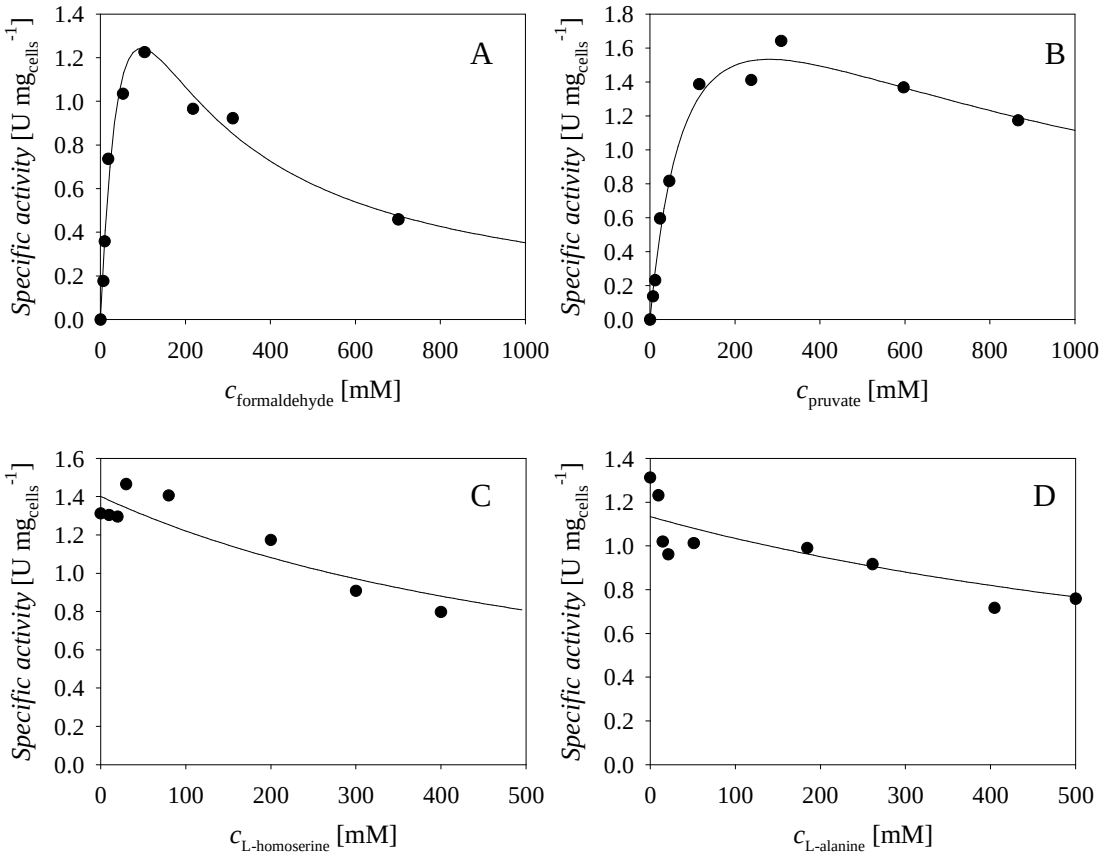

Figure 6.27 Kinetics of aldol addition catalysed by YfaU 013 in cells (50 mM sodium phosphate buffer pH 7.0, 25 °C, γ_{cells} = 0.2 mg mL^{-1}, $V_{reactor}$ = 1 mL) on the concentration of A. **6D** (c_{6C} = 100 mM), B. **6C** (c_{6D} = 100 mM), C. **6B** (c_{6C} = 200 mM, c_{6D} = 100 mM), D. **6A** (c_{6C} = 200 mM, c_{6D} = 100 mM). Legend: black circles – experimental data, line – model.

6A – L-Alanine, **6B** – L-Homoserine, **6C** – Sodium pyruvate, **6D** – Formaldehyde, **6E** – 4-Hydroxy-2-oxobutanoate

Table 6.16 Kinetic parameters for aldol addition of **6D** and **6C** catalysed by YfaU 013 cells.

Parameter	Unit	Value
V_{m3}	U mg_{cells}^{-1}	6.379 ± 1.514
$K_{m3,\ 6D}$	mM	70.963 ± 23.183
$K_{m3,\ 6C}$	mM	95.751 ± 22.823
$K_{i3,\ 6D}$	mM	131.186 ± 41.999
$K_{i3,\ 6C}$	mM	818.800 ± 251.327
$K_{i3,\ 6B}$	mM	83.444 ± 3.825
$K_{i3,\ 6A}$	mM	289.440 ± 77.841

Kinetics of aldol addition of **6D** and **6C** catalysed by YfaU 013 in cells is presented in Figure 6.27 and estimated parameters are shown in Table 6.16. When these results are compared to kinetic measurement results of aldol addition catalysed by CFE YfaU 013 presented in Figure 6.4 and Table 6.5, it can be seen that Michaelis-Menten curve has the same shape for both measurements. The obvious difference is higher V_m value for CFE enzymes. The reason for V_m values difference between CFE enzymes and whole cells biocatalyst is the difference in enzyme content in gram of CFE lyophilisate and enzyme content in gram of lyophilised whole cells. Moreover, the affinity of enzymes towards **6D** and **6C** in both cases is the same, which can be seen from the same K_m values for **6D** and **6C**. K_i values comparison for **6B** shows that there is a stronger inhibiting effect of **6B** on YfaU 013 in reaction catalysed by CFE enzyme.

Kinetics of retro-aldol reaction of **6D** and **6C** catalysed by YfaU 013 in cells is presented in Figure 6.28 and estimated parameters are shown in Table 6.17. Results are comparable to CFE enzyme kinetics (Figure 6.11, Table 6.11) since V_m value is the same for both cases and **6C** acts as inhibitor in this reaction.

Table 6.17 Kinetic parameters for reverse aldol addition catalysed by YfaU 013 cells.

Parameter	Unit	Value
V_{m4}	U mg_{cells}^{-1}	0.100 ± 0.010
$K_{m4,\ 6E}$	mM	196.062 ±
$K_{i4,\ 6C}$	mM	49.386 ±

6A – L-Alanine, **6B** – L-Homoserine, **6C** – Sodium pyruvate, **6D** – Formaldehyde, **6E** – 4-Hydroxy-2-oxobutanoate

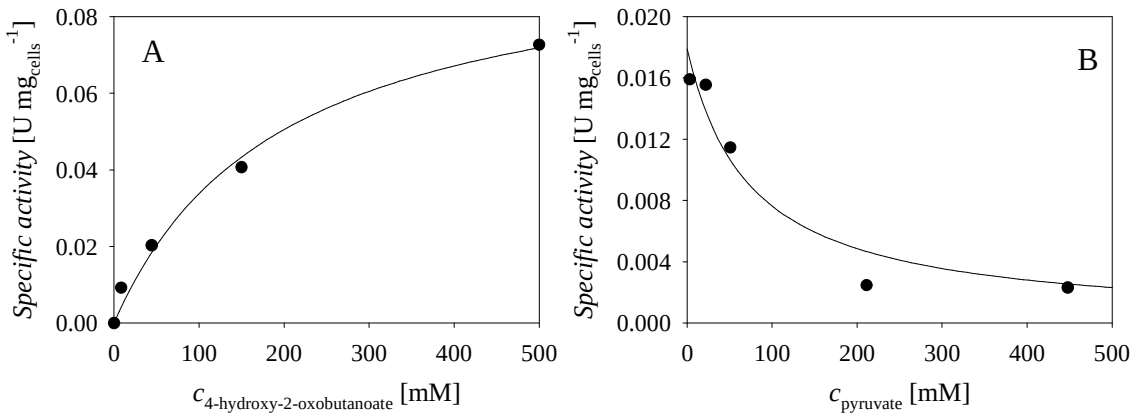

Figure 6.28 Kinetics of reverse aldol addition catalysed by YfaU 013 in cells (50 mM sodium phosphate buffer pH 7.0, 25 °C, γ_{cells} = 10 mg mL^{-1}, $V_{reactor}$ = 1 mL) on the concentration of A. **6E**, B. **6C** (c_{6E} = 100 mM). Legend: black circles – experimental data, line – model.

Kinetics of transamination of **6E** and **6A** catalysed by TA 039 in cells is presented in Figure 6.29 and estimated parameters are shown in Table 6.18. The results of kinetic measurements for transamination catalysed by CFE TA 039 (Figure 6.2, Table 6.3) and TA 039 in the cells differ. As in the comparison of aldol addition kinetic measurement result, V_m value is higher for CFE TA 039 catalysed reaction. In the case for YfaU 013, V_m value is 2.2-fold higher and in the case for TA 039 it is 7-fold higher. Cells show higher affinity towards substrate **6A** and lower towards substrate **6E**. Still, there is an inhibiting effect of substrate **6E** in reaction catalysed by CFE TA 039, and there is none in the reaction with cells. Inhibiting effects of **6C** and **6D** are comparable in both cases, **6D** strongly inhibits transamination catalysed by both biocatalyst types (K_i values in Table 6.3 and Table 6.18).

Table 6.18 Kinetic parameters for transamination of **6A** and **6C** catalysed by TA 039 in cells.

Parameter	Unit	Value
V_{m1}	U mg$_{cells}^{-1}$	0.104 ± 0.003
$K_{m1,\ 6E}$	mM	36.119 ± 3.901
$K_{m1,\ 6A}$	mM	14.656 ± 2.130
$K_{i1,\ 6D}$	mM	0.018 ± 0.001
$K_{i1,\ 6C}$	mM	45.775 ± 9.503

6A – L-Alanine, **6B** – L-Homoserine, **6C** – Sodium pyruvate, **6D** – Formaldehyde, **6E** – 4-Hydroxy-2-oxobutanoate

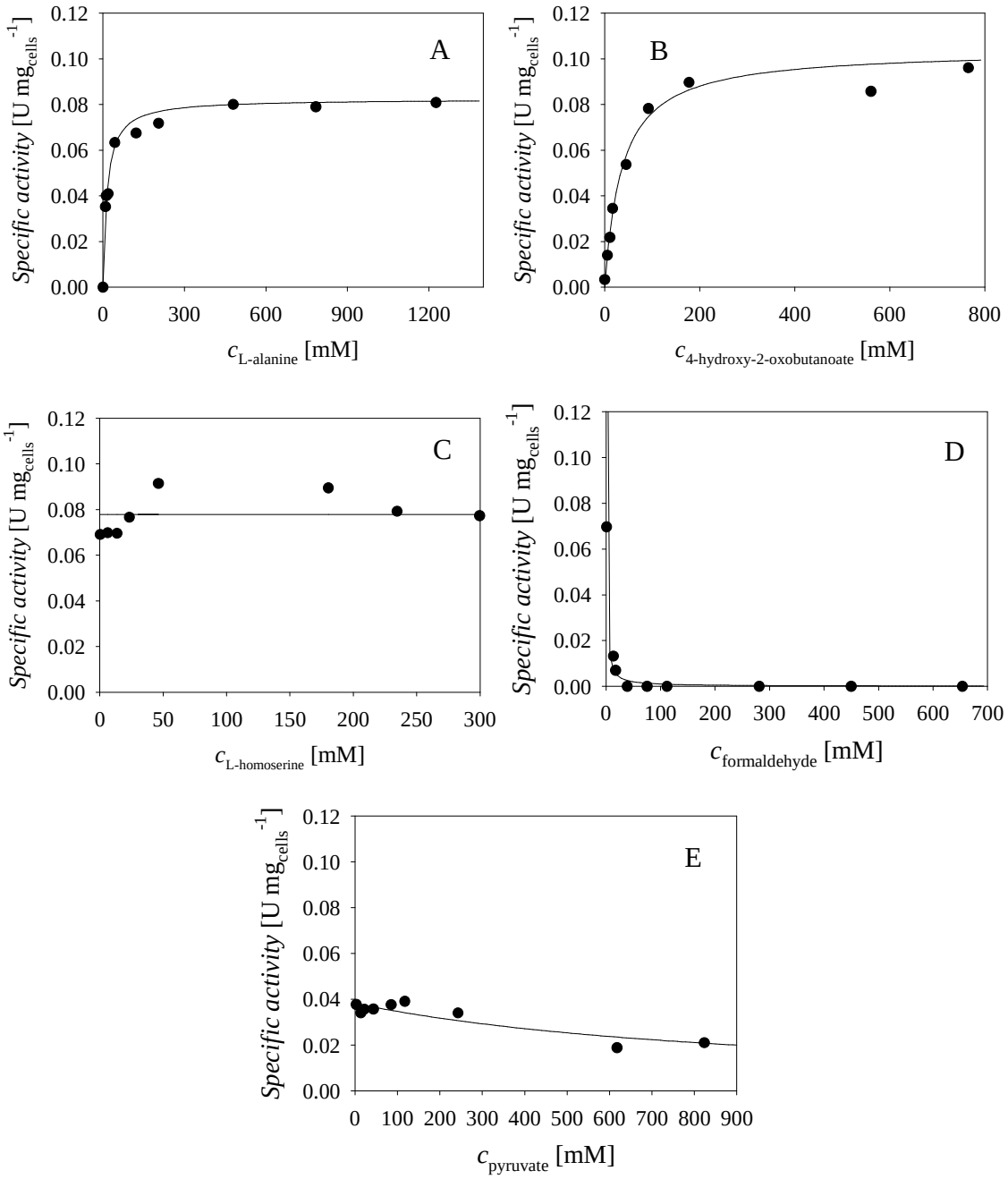

Figure 6.29 Kinetics of transamination catalysed by TA 039 in cells (50 mM sodium phosphate buffer pH 7.0, 25 °C, γ_{cells} = 5 mg mL^{-1}, $V_{reactor}$ = 1 mL) on the concentration of A. **6A** (c_{6E} = 100 mM), B. **6E** (c_{6A} = 100 mM), C. **6B** (c_{6A} = 300 mM, c_{6E} = 100 mM), D. **6D** (c_{6A} = 300 mM, c_{6E} = 100 mM), E. **6C** (c_{6A} = 300 mM, c_{6E} = 100 mM). Legend: black circles – experimental data, line – model.

Kinetics of reverse transamination of **6E** and **6A** catalysed by TA 039 in cells is presented in Figure 6.30 and estimated parameters are shown in Table 6.18. All measurements are similar to the results of kinetics of the reverse transamination catalysed by CFE TA 039 (Figure 6.3, Table 6.4) with the difference in V_m value. Also, **6A** is stronger inibitor in CFE

6A – L-Alanine, **6B** – L-Homoserine, **6C** – Sodium pyruvate, **6D** – Formaldehyde, **6E** – 4-Hydroxy-2-oxobutanoate

TA 039 catalysed reaction compared to cells, whereas **6E** inhibits more the reaction catalysed by cells (Table 6.4, Table 6.19).

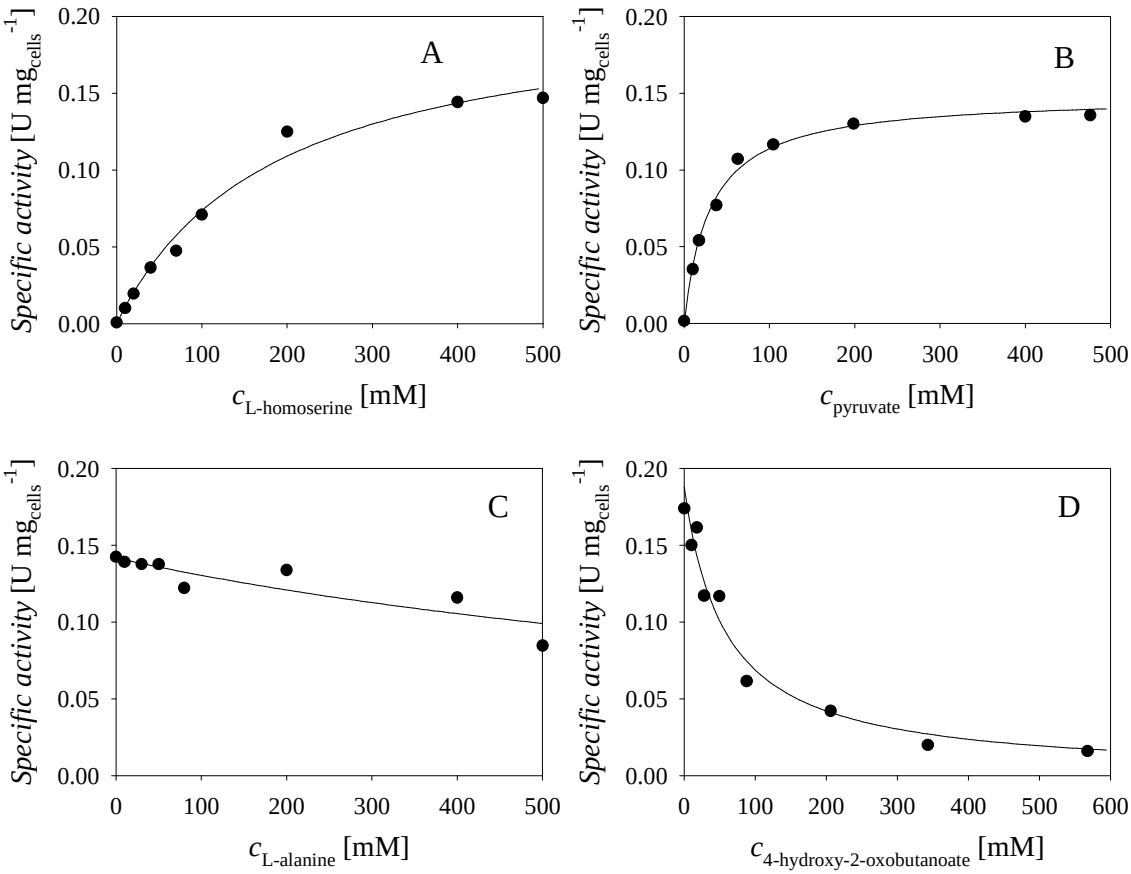

Figure 6.30 Kinetics of reverse transamination catalysed by TA 039 in cells (50 mM sodium phosphate buffer pH 7.0, 25 °C, γ_{cells} = 5 mg mL^{-1}, $V_{reactor}$ = 1 mL) on the concentration of A. **6B** (c_{6C} = 200 mM), B. **6C** (c_{6B} = 200 mM), C. **6A** (c_{6B} = 200 mM, c_{6C} = 200 mM), D. **6E** (c_{6B} = 200 mM, c_{6C} = 200 mM). Legend: black circles – experimental data, line – model.

Kinetic measurement where the influence of **6D** concentration on reverse transamination catalysed by TA 039 in the cells was carried out but this measurement was not successful since aldol addition catalysed by YfaU 013 in the cells overcame reverse transamination reaction (Scheme 6.1). This result and unability to perform this measurements using cells as biocatalyst is in line with estimated kinetic parameters since V_m of aldol addition catalysed by YfaU 013 in the cells (Table 6.16) is significantly higher than the V_m of reverse transamination catalysed by TA 039 in the cells (Table 6.19).

6A – L-Alanine, **6B** – L-Homoserine, **6C** – Sodium pyruvate, **6D** – Formaldehyde, **6E** – 4-Hydroxy-2-oxobutanoate

Table 6.19 Kinetic parameters for reverse transamination catalysed by TA 039 in cells.

Parameter	Unit	Value
V_{m2}	U mg_{cells}^{-1}	0.211 ± 0.017
$K_{m2,\ 6B}$	mM	185.968 ± 34.574
$K_{m2,\ 6C}$	mM	30.279 ± 2.850
$K_{i2,\ 6A}$	mM	561.628 ± 15.427
$K_{i2,\ 6E}$	mM	7.595 ± 0.935

6.4.2 Stability of reaction components during incubation with cells

Competent cells YfaU(013)/PRO TRANS(039) (50 mg mL^{-1}) were incubated for three days in the presence of different concentrations of **6B**, **6A** and **6C** separately. Results show that cells consume **6B** at rate, which depends on **6B** concentration. Figure 6.31A shows dependence of **6B** concentration with the time. The data were simulated by the kinetics of the 2nd order which was found to describe the data well. From the rate constants presented in Figure 6.31B it can be seen that the rate of **6B** consumption depends on **6B** concentration. Similar trend was obtained for **6A** (Figure 6.32), but with much lower rates of consumption (Figure 6.32B). Results for **6C** presented in Figure 6.33 show that it is very quickly consumed by the cells.

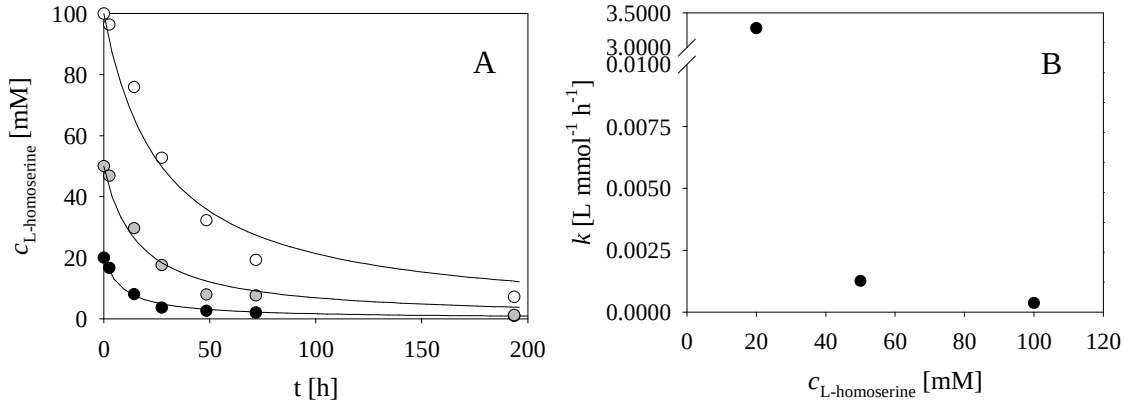

Figure 6.31 **6B** consumption during incubation with competent cells (V = 1 mL, 1000 rpm, 25 °C, buffer, 50 mg mL^{-1} of cells). A. Time dependence of **6B** concentration. B. The dependence of reaction rate constant on **6B** concentration. Legend:

6A – L-Alanine, **6B** – L-Homoserine, **6C** – Sodium pyruvate, **6D** – Formaldehyde, **6E** – 4-Hydroxy-2-oxobutanoate

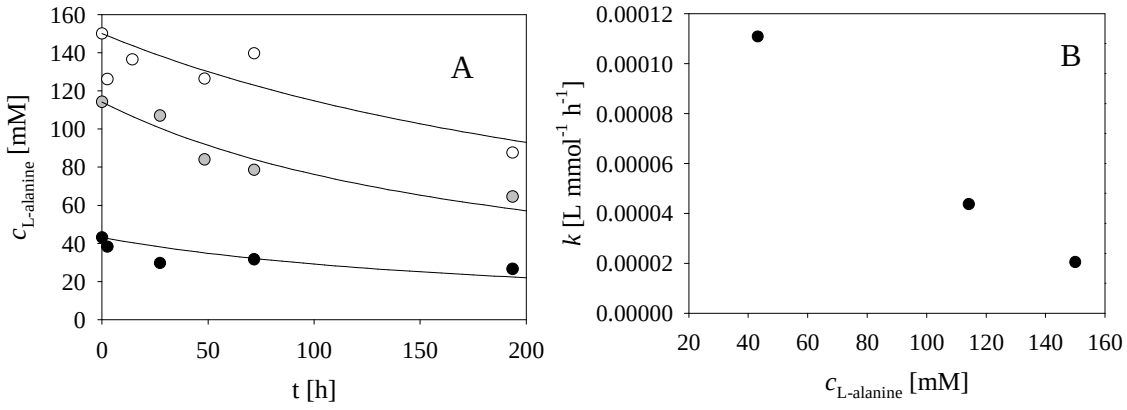

Figure 6.32 **6A** consumption during incubation with competent cells (V = 1 mL, 1000 rpm, 25 °C, buffer, 50 mg mL^{-1} of cells). A. Time dependence of **6A** concentration. B. The dependence of reaction rate constant on **6A** concentration.

It was found that **6C** transforms to **6A** which means that lyophilised cells have an active **6C** metabolism and the presence of alanine dehydrogenase.

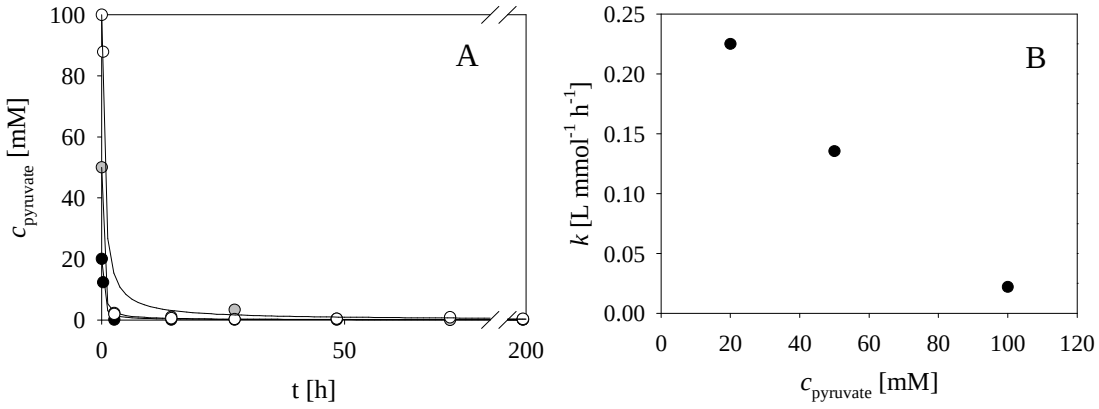

Figure 6.33 **6C** consumption during incubation with competent cells (V = 1 mL, 1000 rpm, 25 °C, buffer, 50 mg mL^{-1} of cells). A. Time dependence of **6C** concentration. B. The dependence of reaction rate constant on **6C** concentration.

As in the experiment in Figure 6.33 dilution of samples was too high for detection of **6A**, incubation experiments were carried out with **6C** without **6A**, and **6C** with **6A** (Figure 6.34). The results show that **6C** concentration decreases, while **6A** concentration increases. The experiment showed in Figure 6.34A shows that **6A** is probably formed from **6C**, as there was no **6A** in the beginning of this experiment. Figure 6.34B also shows an increase of **6A** concentration and degradation of **6C**.

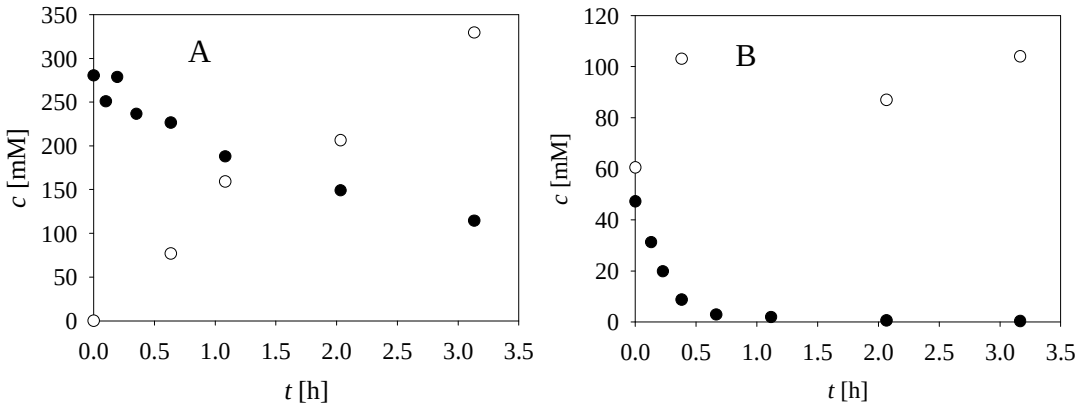

Figure 6.34 Incubation of **6C** A. in the absence and B. together with **6A** (V = 1 mL, 1000 rpm, 25 °C, buffer, 50 mg mL^{-1} of cells). Legend: white circles – **6A**, black circles – **6C**.

6A – L-Alanine, **6B** – L-Homoserine, **6C** – Sodium pyruvate, **6D** – Formaldehyde, **6E** – 4-Hydroxy-2-oxobutanoate

6.4.3 Optimized reaction

The fed-batch reactor experiment catalysed by lyophilised whole cells containing YfaU 013 and TA 039 that gave the highest concentration of desired product **6B** is here presented. In this experiment ca. 7.69 mmol of **6B** was obtained with the consumption of 5.74 mmol of **6C**, which shows **6C** regeneration in the system. Calculated volume productivity after 29.25 hours was 2.6 g L^{-1} h^{-1}, at **6B** concentration of 640.74 mM (76.3 g L^{-1}). The product yield calculated according to the added **6A** was 65%. These are very similar results to those obtained with CFE of both enzymes and confirm the same system behaviour. They also show that by determining enzyme kinetics of CFEs conclusions can be drawn for the whole-cell system.

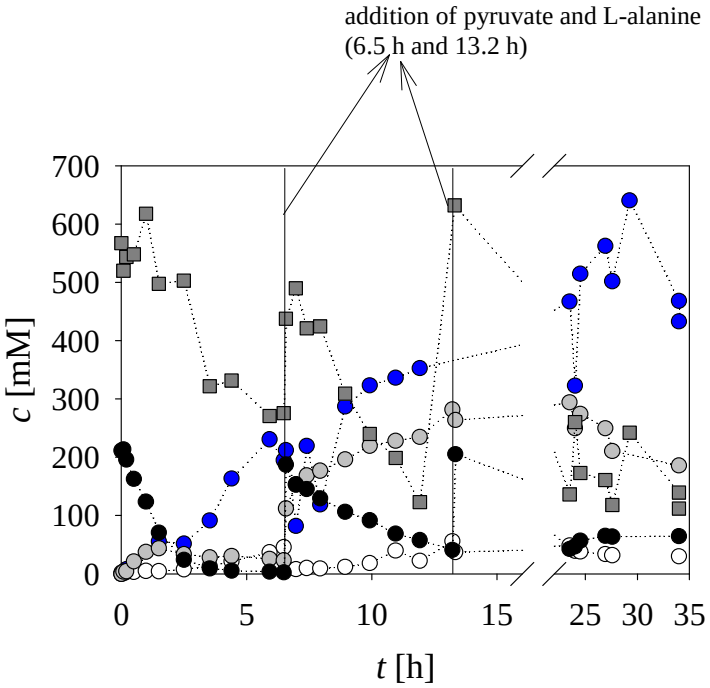

Figure 6.35 Optimized fed-batch experiment with whole cells biocatalyst (50 mM sodium phosphate buffer pH 7.0, 25 °C, 450 rpm, V_0 = 7.8 mL, $c_{6D,feed}$ = 3110 mM, q_{6D} = 3 µL min^{-1}, c_{6C} = 211 mM, c_{6A} = 576 mM, γ_{cells} = 76.29 mg mL^{-1}. Legend: Grey squares – **6A**, blue circles – **6B**, black circles – **6C**, white circles – **6D**, grey circles – **6E**.

6A – L-Alanine, **6B** – L-Homoserine, **6C** – Sodium pyruvate, **6D** – Formaldehyde, **6E** – 4-Hydroxy-2-oxobutanoate

6.5 Conclusions

The synthesis of L-homoserine in the reaction system consisting of transaminase and aldolase starting from pyruvate, formaldehyde and L-alanine was studied. Detailed kinetic measurements and parameters estimation was done for reactions catalysed by separate CFE enzymes and for reactions catalysed by *E. coli* cells that contain both enzymes. Since the same enzymes (aldolase YfaU 013 and transaminase TA 039) were used as biocatalysts in both cases, Michaelis-Menten kinetic curves have the same trend in most cases and kinetic parameters are comparable with some exceptions. Maximum reaction rates differ due to the difference in enzyme content in two types of biocatalyst.

Reactions catalysed by separate enzymes (cell free extracts) and *E. coli* cells containing the same co-expressed enzymes were optimized based on developed mathematical model. Optimized reaction in fed-batch reactor with continuous formaldehyde feed and two additions of L-alanine and pyruvate up to their initial concentrations produced 672 mM (76.23 g L^{-1} d^{-1}) of L-homoserine after 25 hours of reaction when cell free extract enzymes were used and 640.74 mM (62 g L^{-1} d^{-1}) of L-homoserine when whole cell biocatalyst was used. Obtained process metrics presented a good result with potential for industrial use. Industrial project partners confirmed that optimized process set-up and approach presented within this research produces expected results on a larger scale as well. Therefore, the results were not only reproducible in our lab but also in partner's lab, and up-scaled experiments confirmed the applicability and potential of developed mathematical model for L-homoserine synthesis.

6A – L-Alanine, **6B** – L-Homoserine, **6C** – Sodium pyruvate, **6D** – Formaldehyde, **6E** – 4-Hydroxy-2-oxobutanoate

7 SYNTHESIS OF IMINOSUGAR PRECURSOR

7.1 Introduction

Iminosugars have attracted a great interest among scientists due to their efficient inhibition of various glycosidases involved in the intestinal degradation of carbohydrates (Nash et al., 2011). Carbohydrates are crucially important to the function of the human body and aberrations in sugar metabolism occur in most diseases. Iminosugars can correct many of these faults. In their simplest form, they resemble furanose and pyranose monosaccharides with nitrogen replacing the endocyclic oxygen atom (Asano et al., 2000; Watson et al., 2001).

The aim of this research was to explore new biocatalytic pathways for iminosugar precursor synthesis. Depending on the starting substrate molecule, typically an alcohol, the first reaction step in the cascade reaction was catalysed by a suitable oxidoreductase. The following aldol addition was catalysed by an aldolase to form the iminosugar precursor.

Two strategies for biocatalytic production of the precursor of the iminosugars *Miglustat* (*N*-butyl-deoxynojirimycin) and *Miglitol* (*N*-hydroxyethyl-deoxynojirimycin) were examined within this doctoral thesis. Since aldol adducts containing amino groups are important building blocks of iminosugars, one approach suggested the use of the Cbz-*N*-3-amino-1,2-propanediol as a starting substrate. Second approach involved 3-chloro-1,2-propanediol as starting substrate. An attempt was made to convert both *in situ* generated aldehydes by D-fructose-6-phosphate aldolase variant, FSA^{A129S}, into the corresponding aldol adduct product.

7.1.1 Approach I: Cbz-N-3-amino-1,2-propanediol as starting substrate

The proposed cascade reaction consists of oxidation step and aldol addition step planned to be performed in a one-pot synthesis due to instability of the aldehyde Cbz-*N*-3-amino-2-hydroxypropanal (**7F**) intermediate. The proposed reaction scheme is presented in Scheme 7.1. The first reaction step is alcohol oxidation catalysed by horse liver alcohol dehydrogenase (HLADH) with coenzyme regeneration by NADH oxidase (NOX 009) from Prozomix or own produced (Chapters 7.3.5 and 7.4.5). The second reaction step in a cascade is aldol addition of dihydroxyacetone to intermediate aldehyde **7F** catalysed by D-fructose-6-phosphate aldolase (FSA^{A129S}) producing aldol adduct **7G**, precursor of the iminosugars.

7A – Cbz-*N*-3-amino-1,2-propanediol (racemic mixture), **7B** – (*S*)-3-Amino-1,2-propanediol,
7C – (*R*)-3-Amino-1,2-propanediol, **7D** – (*S*)-Cbz-*N*-3-amino-1,2-propanediol, **7E** – (*R*)-Cbz-*N*-3-amino-1,2-propanediol,
7F – Cbz-*N*-3-amino-2-hydroxypropanal, **7G** – Cbz-*N*-6-amino-1,3,4,5-tetrahydroxy-hexan-2-one
7H – 3-Chloro-1,2-propanediol (racemic mixture), **7I** – (*S*)-3-Chloro-1,2-propanediol, **7J** – (*R*)-3-Chloro-1,2-propanediol

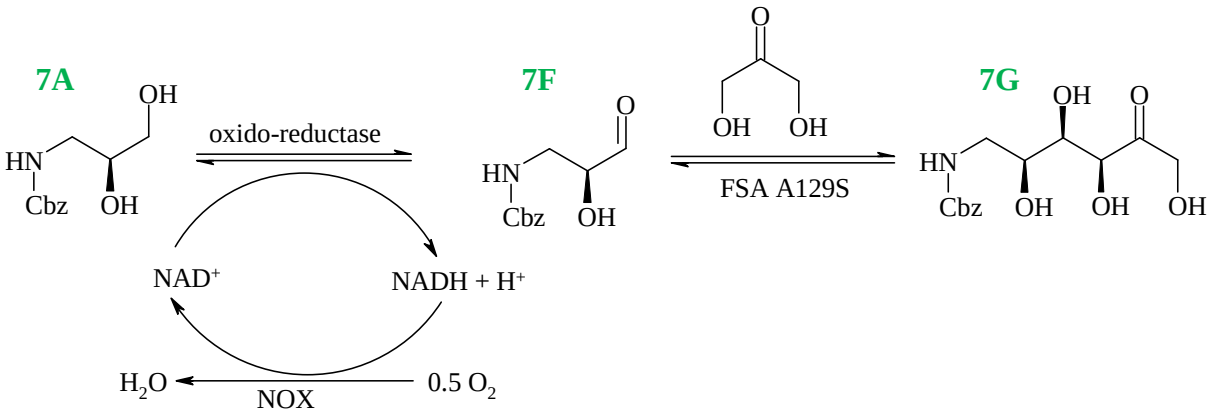

Scheme 7.1 Iminosugar precursor synthesis with Cbz-*N*-3-amino-1,2-propanediol as starting substrate (Approach I).

Proposed synthetic route is based on a similar previously investigated cascade (Sudar et al., 2015) where Cbz-*N*-3-aminopropan**ol** was a starting substrate and horse liver alcohol dehydrogenase (HLADH) was used as a catalyst for the oxidation step. Similar to this substrate, Cbz-*N*-3-aminopropane**diol** was used in this research of this thesis.

Carboxybenzyl group (Cbz) is commonly used in organic synthesis as a protecting group for amines. It is known that the affinity of HLADH towards Cbz-protected alcohol is higher than towards unprotected molecules due to the size of a substrate molecule. Hence, the research of the cascade with aminopropanediol began with investigating the kinetics with the Cbz-protected substrate. Several enzymes with known potential for alcohol oxidation were evaluated as biocatalysts for the **7A** oxidation:

- Horse liver alcohol dehydrogenase (HLADH) from Sigma Aldrich (Germany)
- Horse liver alcohol dehydrogenase (HLADH) from Forschungszentrum (FZ) Jülich (Germany)
- Yeast alcohol dehydrogenase (YADH) from Sigma Aldrich (Germany)
- Panels with 192 oxido-reductases (KREDs) from Prozomix Ltd (United Kingdom)

7A – Cbz-*N*-3-amino-1,2-propanediol (racemic mixture), **7B** – (*S*)-3-Amino-1,2-propanediol,
7C – (*R*)-3-Amino-1,2-propanediol, **7D** – (*S*)-Cbz-*N*-3-amino-1,2-propanediol, **7E** – (*R*)-Cbz-*N*-3-amino-1,2-propanediol,
7F – Cbz-*N*-3-amino-2-hydroxypropanal, **7G** – Cbz-*N*-6-amino-1,3,4,5-tetrahydroxy-hexan-2-one
7H – 3-Chloro-1,2-propanediol (racemic mixture), **7I** – (*S*)-3-Chloro-1,2-propanediol, **7J** – (*R*)-3-Chloro-1,2-propanediol

7.1.2 Approach II: 3-chloro-1,2-propanediol as starting substrate

Second approach for the iminosugar precursor synthesis was based on 3-chloro-1,2-propanediol (**7H**) as a starting substrate. Proposed cascade concept is shown in Scheme 7.2.

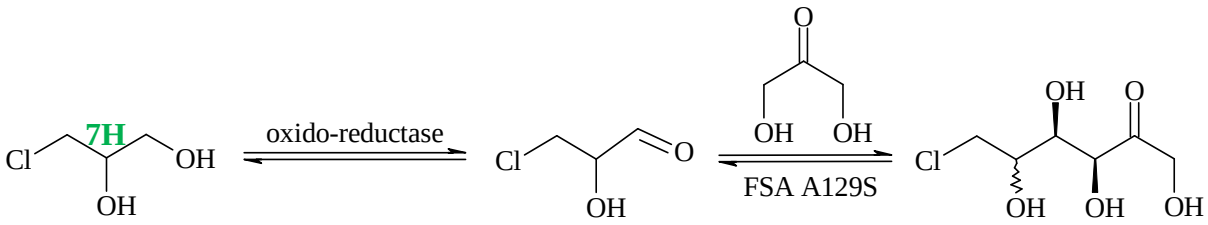

Scheme 7.2 Iminosugar precursor synthesis with 3-chloro-1,2-propanediol as starting substrate (Approach II).

Several enzymes with known potential for alcohol oxidation are tested as biocatalysts for the **7H** oxidation both on racemic and enantiomerically pure substrate:

- Horse liver alcohol dehydrogenase (HLADH) from Sigma Aldrich (Germany)
- Yeast alcohol dehydrogenase (YADH) from Sigma Aldrich (Germany)
- Panels with 192 oxido-reductases (KREDs) from Prozomix Ltd (United Kingdom)
- Galactose oxidase (GOD) from *Dactylium dendroides* from Sigma Aldrich (Germany)

7A – Cbz-*N*-3-amino-1,2-propanediol (racemic mixture), **7B** – (*S*)-3-Amino-1,2-propanediol,
7C – (*R*)-3-Amino-1,2-propanediol, **7D** – (*S*)-Cbz-*N*-3-amino-1,2-propanediol, **7E** – (*R*)-Cbz-*N*-3-amino-1,2-propanediol,
7F – Cbz-*N*-3-amino-2-hydroxypropanal, **7G** – Cbz-*N*-6-amino-1,3,4,5-tetrahydroxy-hexan-2-one
7H – 3-Chloro-1,2-propanediol (racemic mixture), **7I** – (*S*)-3-Chloro-1,2-propanediol, **7J** – (*R*)-3-Chloro-1,2-propanediol

7.2 Experimental part

7.2.1 Materials

Chemicals and enzymes used in this chapter are the following. *N*-(Benzyloxycarbonyl)-3-amino-1,2-propanediol, (*S*)-3-amino-1,2-propanediol, (*R*)-3-amino-1,2-propanediol, (±)-3-chloro-1,2-propanediol, (*R*)-(-)-3-chloro-1,2-propanediol, (*S*)-(+)-3-chloro-1,2-propanediol, dihydroxyacetone (DHA), *β*-Nicotinamide adenine dinucleotide hydrate (NAD^+), *β*-nicotinamide adenine dinucleotide (NADH), 2-iodoxybenzoic acid (IBX), triethanolamine (TEA), trifluoroacetic acid (TFA), formic acid, iodonitrotetrazolium chloride (INT) and acetonitrile were purchased from Sigma Aldrich (Germany). (±)-3-Chloro-1,2-propanediol and *O*-dianisidine were purchased from Alfa Aesar (USA). 2,2′-Azino-bis(3-ethylbenzothiazoline-6-sulfonic acid (ABTS) was purchased from AppliChem GmbH (Germany).

Horse liver alcohol dehydrogenase, yeast alcohol dehydrogenase, galactose oxidase and peroxidase from horseradish were purchased from Sigma Aldrich (Germany). D-fructose-6-phosphate aldolase (FSA^{A129S}) was expressed and purified in the labs of IQAC-CSIC (Spain). NADH oxidase (NOX 009) and oxido-reductases (KREDS panels) were from Prozomix Ltd (United Kingdom). Horse liver alcohol dehydrogenase was from Forschungszentrum (FZ) Jülich (Germany). NOX suspension was isolated and purified from cultivated *Lactococcus lactis* in the labs of Department of Reaction Engineering and Catalysis, Faculty of Chemical Engineering and Technology (Croatia).

Reaction component labels are given according to Table 7.1.

Table 7.1 Labels given to each reaction component in this chapter.

Compound	Label
Cbz-*N*-3-amino-1,2-propanediol (racemic mixture)	**7A**
(*S*)-3-Amino-1,2-propanediol	**7B**
(*R*)-3-Amino-1,2-propanediol	**7C**
(*S*)-Cbz-*N*-3-amino-1,2-propanediol	**7D**
(*R*)-Cbz-*N*-3-amino-1,2-propanediol	**7E**
Cbz-*N*-3-amino-2-hydroxypropanal	**7F**
Cbz-*N*-6-amino-1,3,4,5-tetrahydroxy-hexan-2-one	**7G**
3-Chloro-1,2-propanediol (racemic mixture)	**7H**
(*S*)-3-Chloro-1,2-propanediol	**7I**
(*R*)-3-Chloro-1,2-propanediol	**7J**

7A – Cbz-*N*-3-amino-1,2-propanediol (racemic mixture), **7B** – (*S*)-3-Amino-1,2-propanediol,
7C – (*R*)-3-Amino-1,2-propanediol, **7D** – (*S*)-Cbz-*N*-3-amino-1,2-propanediol, **7E** – (*R*)-Cbz-*N*-3-amino-1,2-propanediol,
7F – Cbz-*N*-3-amino-2-hydroxypropanal, **7G** – Cbz-*N*-6-amino-1,3,4,5-tetrahydroxy-hexan-2-one
7H – 3-Chloro-1,2-propanediol (racemic mixture), **7I** – (*S*)-3-Chloro-1,2-propanediol, **7J** – (*R*)-3-Chloro-1,2-propanediol

7.2.2 Apparatus

Apparatus used in Chapter 7 is listed in Appendix (Table 10.1).

7.2.3 Analytical methods

7.2.3.1 Approach I

7A, **7D**, **7E** and **7G** concentrations were followed by HPLC on a LiChrospher (Phenomenex) C18, 250x4 (5 μm) column. The method was described in the literature (Concia et al., 2009). Two mobile phases were employed. The mobile phase A consisted of ultrapure water with the addition of trifluoroacetic acid (TFA) (0.1% v/v), and the mobile phase B consisted of acetonitrile, water and TFA (80% acetonitrile, 20% water, 0.095% TFA). Gradient elution from 10 to 70% B during 30 minutes at total flow rate of 1.0 cm^3 min^{-1} was used. UV detection at 215 nm at 30 °C was used. Linearity range for **7A** was from 0.07 to 1.47 mM and its retention time was 12.2 min (Appendix, Figure 10.8). Retention times of two **7G** peaks were 10.5 and 11.2 min.

Chiral HPLC column was used for the analysis of **7A**. Both UV and RI detection were employed. Racemic substrate was followed by HPLC on a chiral Lux Cellulose-1 (250 x 4.6 mm, 5 μm). The mobile phase used was 80% v/v of *n*-hexane and 20% *v*/*v* of 2-propanol at the flow rate of 0.7 mL min^{-1}. Standard commercial samples of racemic **7A** were dissolved in the mobile phase. The analyses were done at 215 nm and 30 °C. Chromatographs of **7A**, **7D** and **7E** are presented in Appendix (Figure 10.7). Retention times for **7E** and **7D** were 14.89 and 15.98 min with UV detection, and 15.25 and 16.34 min with RID, respectively. Their linearity range is from 0.05 to 0.7 mM.

7.2.3.2 Approach II

Analyses of **7H** were performed on Shimadzu gas chromatograph equipped with a hydrogen flame-ionization detector on ZB-WAX column (30 m x 0.53 mm i.d. x 1 μm). Quantitative analysis was performed from peak areas by the external standard method. Samples were diluted in ethyl acetate. **7H** calibration curve was in range between 1 and 4 mM. Developed method used helium as a carrier gas at the flow-rate 17.6 mL min^{-1}. The temperature of the oven at the injection was 80 °C and was kept constant for 1 min. The linear increase in temperature to 230 °C was set by 5 °C min^{-1} and was kept constant at 230 °C for

7A – Cbz-*N*-3-amino-1,2-propanediol (racemic mixture), **7B** – (*S*)-3-Amino-1,2-propanediol,
7C – (*R*)-3-Amino-1,2-propanediol, **7D** – (*S*)-Cbz-*N*-3-amino-1,2-propanediol, **7E** – (*R*)-Cbz-*N*-3-amino-1,2-propanediol,
7F – Cbz-*N*-3-amino-2-hydroxypropanal, **7G** – Cbz-*N*-6-amino-1,3,4,5-tetrahydroxy-hexan-2-one
7H – 3-Chloro-1,2-propanediol (racemic mixture), **7I** – (*S*)-3-Chloro-1,2-propanediol, **7J** – (*R*)-3-Chloro-1,2-propanediol

another 4 minutes. The injector temperature was set at 280 °C and the detector temperature at 240 °C. The retention time of **7H** was 20.05 min and its peak is presented in Appendix (Figure 10.9).

Oxidations and cascade reactions were followed by HPLC. Since potentially evolving molecules in the cascade have aldehyde group, samples were derivatized according to procedure given in Chapter 5.2.3.1. Analysis details can be found in Table 5.2 – Method B. LC-MS analysis was performed using the method described in Chapter 5.3.6.

7A – Cbz-*N*-3-amino-1,2-propanediol (racemic mixture), **7B** – (*S*)-3-Amino-1,2-propanediol,
7C – (*R*)-3-Amino-1,2-propanediol, **7D** – (*S*)-Cbz-*N*-3-amino-1,2-propanediol, **7E** – (*R*)-Cbz-*N*-3-amino-1,2-propanediol,
7F – Cbz-*N*-3-amino-2-hydroxypropanal, **7G** – Cbz-*N*-6-amino-1,3,4,5-tetrahydroxy-hexan-2-one
7H – 3-Chloro-1,2-propanediol (racemic mixture), **7I** – (*S*)-3-Chloro-1,2-propanediol, **7J** – (*R*)-3-Chloro-1,2-propanediol

7.3 Experimental procedures – Approach I

7.3.1 Screening for the most suitable oxido-reductase

Activities of all oxido-reductases as biocatalysts for alcohol **7A** oxidation were determined spectrophotometrically by following NADH concentration change during time at 340 nm. Plate assay containing 192 oxido-reductases received from Prozomix Ltd (UK) were screened on substrates **7D** and **7E**. The aim was to find enzymes from the plate that are active towards investigated substrates. 0.05g of substrate was dissolved in 10 mL of 0.25 mg mL^{-1} INT solution. 10 µL of INT/substrate solution was added to each well of the panel. According to the assay, wells that contain enzymes active on tested alcohols as substrates turn red. KREDs with activity towards **7D** and **7E** were further tested with spectrophotometric assay to determine their exact activity. Activities are calculated from the change in NADH concentration with time, followed at 340 nm (Equations 7.1 and 7.2).

$$V.A. = \frac{\frac{\mathrm{d}ABS}{\mathrm{d}t} V_{\text{total}}}{V_{\text{enzyme}} \cdot d \cdot \varepsilon_{340,\text{NADH}}} \tag{7.1}$$

$$S.A. = \frac{V.A.}{\gamma_{\text{enzyme}}} \tag{7.2}$$

7.3.2 pH dependence of HLADH

pH dependence of HLADH activity was measured with four different buffers: phosphate, TEA HCl, Tris HCl and glycine NaOH buffers at pH 5.5, 6, 6.5, 7, 7.5, 8 and 9 in order to find the pH with highest enzyme activity.

7.3.3 Cbz protection group

Cbz-protection of **7B** and **7C** was carried out according to the procedure described in the literature (Sugiyama et al., 2007) in order to obtain enantiomerically pure Cbz-protected substrates **7D** and **7E**. The reaction was followed by TLC (Figure 7.1). Mobile phase for TLC was chloroform and methanol in 5:1 ratio. Protected alcohol **7A** was used as standard dissolved in methanol (25 mM) and 5 µL of this dilution was applied to TLC plate.

7A – Cbz-*N*-3-amino-1,2-propanediol (racemic mixture), **7B** – (*S*)-3-Amino-1,2-propanediol,
7C – (*R*)-3-Amino-1,2-propanediol, **7D** – (*S*)-Cbz-*N*-3-amino-1,2-propanediol, **7E** – (*R*)-Cbz-*N*-3-amino-1,2-propanediol,
7F – Cbz-*N*-3-amino-2-hydroxypropanal, **7G** – Cbz-*N*-6-amino-1,3,4,5-tetrahydroxy-hexan-2-one
7H – 3-Chloro-1,2-propanediol (racemic mixture), **7I** – (*S*)-3-Chloro-1,2-propanediol, **7J** – (*R*)-3-Chloro-1,2-propanediol

Concentration detection range for these compounds was 10-25 mM. The purity of obtained products was determined by HPLC on chiral column.

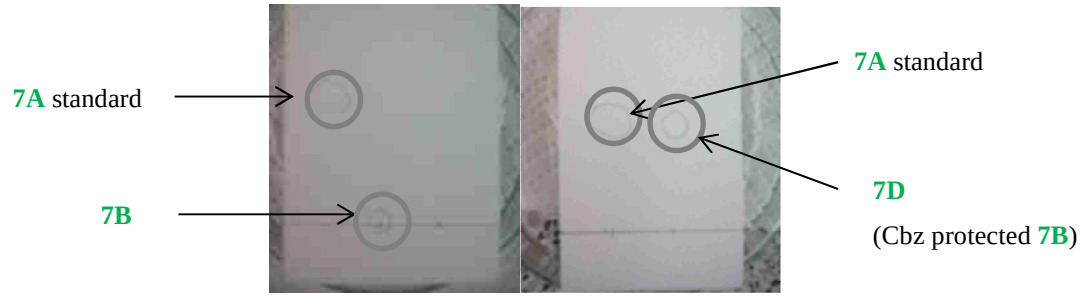

Figure 7.1 TLC plates during Cbz-protection reaction (the first and the last sample).

7.3.4 HLADH kinetic measurements

HLADH kinetics was determined spectrophotometrically. The data were collected by using the standard ADH assay (Boehringer Mannheim GmbH, 1975) at 340 nm by following NADH formation. From the experimental results kinetic parameters were estimated by using non-linear regression analysis implemented in SCIENTIST software.

7.3.5 NADH oxidase isolation from Lactococcus lactis

NADH oxidase is an enzyme required for coenzyme (NAD^+) regeneration in oxidation catalysed by HLADH. *Lactococcus lactis* bacteria cells are cultivated for the purpose of production and isolation of NADH oxidase. The used procedure is described in the literature (Sudar et al., 2014). Cells were disrupted by ultrasound by using MS 73 probe. Protein was precipitated by ammonium sulfate. Protein fractions were separated and collected on Äkta prime plus system for protein purification (GE Healthcare, Sweden) (Figure 7.2) by gel filtration (Sephadex G-50 column, 12 x 2,5cm) and ion exchange chromatography (Sepharose Q column, 17 x 1,5cm).

7A – Cbz-*N*-3-amino-1,2-propanediol (racemic mixture), **7B** – (*S*)-3-Amino-1,2-propanediol,
7C – (*R*)-3-Amino-1,2-propanediol, **7D** – (*S*)-Cbz-*N*-3-amino-1,2-propanediol, **7E** – (*R*)-Cbz-*N*-3-amino-1,2-propanediol,
7F – Cbz-*N*-3-amino-2-hydroxypropanal, **7G** – Cbz-*N*-6-amino-1,3,4,5-tetrahydroxy-hexan-2-one
7H – 3-Chloro-1,2-propanediol (racemic mixture), **7I** – (*S*)-3-Chloro-1,2-propanediol, **7J** – (*R*)-3-Chloro-1,2-propanediol

Figure 7.2 Protein purification on Äkta prime plus system.

7.3.6 Chemical oxidation of alcohol 7A

Compound **7F** was synthesised from**7A** by chemical oxidation in order to have an authentic standard and establish the analytic conditions by HPLC analysis. The oxidation reaction of **7A** was carried out using 2-iodoxybenzoic acid (IBX). IBX is an oxidation agent with application in chemical reactions where aldehydes are formed from primary alcohols and ketones from secondary alcohols (More & Finney, 2002). Procedure was as follows. 0.61 g of **7A** was dissolved in 58 mL of ethyl acetate and 1.47 g of IBX was added to reaction. Reaction took place in water bath (Figure 7.3). When temperature of 77 °C was reached, the oxidation started. The reaction took place for 4 hours. The samples were analysed by HPLC and TLC (mobile phase chloroform:methanol 5:1 ratio, *TLC Silica gel 60 F254* plates).

Figure 7.3 Experimental set-up for performing chemical oxidation of **7A**.

7A – Cbz-*N*-3-amino-1,2-propanediol (racemic mixture), **7B** – (*S*)-3-Amino-1,2-propanediol,
7C – (*R*)-3-Amino-1,2-propanediol, **7D** – (*S*)-Cbz-*N*-3-amino-1,2-propanediol, **7E** – (*R*)-Cbz-*N*-3-amino-1,2-propanediol,
7F – Cbz-*N*-3-amino-2-hydroxypropanal, **7G** – Cbz-*N*-6-amino-1,3,4,5-tetrahydroxy-hexan-2-one
7H – 3-Chloro-1,2-propanediol (racemic mixture), **7I** – (*S*)-3-Chloro-1,2-propanediol, **7J** – (*R*)-3-Chloro-1,2-propanediol

7.3.7 Preliminary experiments conducted in the batch reactor

The preliminary cascade reaction of **7A** oxidation and following aldol addition was carried out in 1.2 mL batch reactor. Substrates and enzymes concentrations were as follows: $c_{\mathbf{7A}}$ = 20 mM, c_{NAD+} = 1 mM c_{DHA} = 50 mM, γ_{HLADH}= 10 mg mL^{-1}, $\gamma_{NOX\ 009}$= 0.01 mg mL^{-1}, $\gamma_{FSA\ A129S}$ = 2 mg mL^{-1}. 0.1 M TEA HCl buffer pH 8.0 was used.

7.3.8 LC-MS analysis of the aldol product

Since there is no commercially available aldol adduct **7G** that can be used as an analytical standard, two peaks evolving during cascade reactions were assumed to be aldol peaks at RT 10.5 min and RT 11.2 min. They were analysed by LC-MS to confirm their molecular mass of 314 g mol^{-1}. The column and the conditions for LC-MS analysis were the same as for HPLC, except the use of formic acid instead of TFA. HPLC with DAD and MS detection was used. The selected ion monitoring method was used to confirm the molecular weight of the derivatized product peak. The mass spectrometer was equipped with electrospray ionization (ESI) source and operated in positive polarity mode. ESI+ conditions: capillary voltage 0.85 kV, nebulizing gas flow 1.5 L·min^{-1}, drying gas flow 15 L·min^{-1}, 250 °C.

7.3.9 The influence of NAD$^+$ concentration on the substrate conversion in the cascade

The influence of NAD$^+$ concentration on **7A** conversion was evaluated at 25 °C and pH 8.0 in 50 mM TEA HCl buffer. Reactor volume was 1.0 mL. Concentration of DHA, HLADH, NOX 009, FSA^{A129S}, and **7A** were 200 mM, 5 mg mL^{-1}, 1.0 mg mL^{-1}, 5.0 mg mL^{-1} and 100 mM, respectively. The tested concentration range of NAD$^+$ was from 0.05 to 1.00 mM.

7.3.10 The influence of different initial substrate concentrations on the conversion in the cascade

In the second series of cascade reactions different initial concentrations of diol **7A** were used to see which initial substrate concentration gives the highest conversion. Initial concentrations tested were 10, 20, 40, 60 and 100 mM. Reactions were performed at 25 °C in 50 mM TEA HCl buffer pH 8.0. Reactor volume was 1.2 mL. Concentration of DHA was 2.5

7A – Cbz-*N*-3-amino-1,2-propanediol (racemic mixture), **7B** – (*S*)-3-Amino-1,2-propanediol,
7C – (*R*)-3-Amino-1,2-propanediol, **7D** – (*S*)-Cbz-*N*-3-amino-1,2-propanediol, **7E** – (*R*)-Cbz-*N*-3-amino-1,2-propanediol,
7F – Cbz-*N*-3-amino-2-hydroxypropanal, **7G** – Cbz-*N*-6-amino-1,3,4,5-tetrahydroxy-hexan-2-one
7H – 3-Chloro-1,2-propanediol (racemic mixture), **7I** – (*S*)-3-Chloro-1,2-propanediol, **7J** – (*R*)-3-Chloro-1,2-propanediol

times **7A** initial concentration. Concentrations of NAD^+, HLADH, NOX 009 and FSA^{A129S} were 1 mM, 100 mg mL^{-1}, 0.01 mg mL^{-1} and 2.0 mg mL^{-1}, respectively.

7.3.11 The influence of HLADH/NOX activity ratio on the aldol adduct evolving

The next step was re-testing the influence of alcohol dehydrogenase and NADH oxidase activity ratio on diol **7A** conversion and product **7G** concentration. Reactions were performed at 25 °C in 50 mM TEA HCl buffer pH 8.0. Reactor volume was 0.4 mL. Concentrations of **7A**, NAD^+, DHA and FSA^{A129S} were 20 mM, 1 mM, 50 mM and 2.0 mg mL^{-1}, respectively. Tested HLADH/NOX ratios were 0.3, 0.6, 3, 6, 9, 12, 30, 48 and 60.

7.3.12 Operational stability of HLADH, NOX and FSA during the cascade reaction

To investigate whether the activity of HLADH, NOX and FSA decreases over time, their activities were followed during cascade reaction.

Test for NOX activity measurement contained 100 µL of 1 mM NADH (0.1 mM in test), 500 µL 50 mM TEA HCl pH 8.0 and 400 µL buffer with diluted enzyme. Once the buffer with diluted NOX was introduced to cuvette, spectrophotometric measurement started.

HLADH activity test contained 90 µL 50 mM TEA HCl pH 8.0, 333 µL of 25 mM NAD^+, 167 µL of 2 mM ethanol and 400 µL of buffer containing diluted enzyme. Once the buffer with diluted HLADH was introduced to cuvette, spectrophotometric measurement started. From the change in NADH concentration *vs* time, initial reaction rate was calculated. From this value, specific activity of enzyme was calculated according to Equations 7.1 and 7.2 in Chapter 7.2.4.1.

FSA^{A129S} activity during cascade reaction was followed by using filtrated FSA in an independent reaction activity test. Since **7F** is not commercially available, it could not be used as substrate for activity tests. Thus, an alternative substrate, Cbz-*N*-3-aminopropanal, was chosen based on previous experience working with this enzyme. Hence, the reaction used for the activity assay to determine FSA^{A129S} activity was aldol addition of dihydroxyacetone to Cbz-*N*-3-aminopropanal. The initial concentrations of *N*-Cbz-3-aminopropanal and dihydroxyacetone in the assay were always 100 mM, and the assay overall volume was 500 µL. The reaction was carried out in an Eppendorf tube at 25 °C and on an Eppendorf shaker at 1000 rpm in 50 mM TEA HCl buffer, pH 8.0. 10% of ethyl acetate has to be added to the

7A – Cbz-*N*-3-amino-1,2-propanediol (racemic mixture), **7B** – (*S*)-3-Amino-1,2-propanediol,
7C – (*R*)-3-Amino-1,2-propanediol, **7D** – (*S*)-Cbz-*N*-3-amino-1,2-propanediol, **7E** – (*R*)-Cbz-*N*-3-amino-1,2-propanediol,
7F – Cbz-*N*-3-amino-2-hydroxypropanal, **7G** – Cbz-*N*-6-amino-1,3,4,5-tetrahydroxy-hexan-2-one
7H – 3-Chloro-1,2-propanediol (racemic mixture), **7I** – (*S*)-3-Chloro-1,2-propanediol, **7J** – (*R*)-3-Chloro-1,2-propanediol

stock solution of Cbz-*N*-3-aminopropanal (500 mM) due to its limited solubility in buffer. 100 µL of aldehyde solution (100 mM in the test), 125 µL of DHA stock solution (400 mM, 100 mM in the test) and 75 µL of 50 mM TEA HCl buffer, pH 8.0 are mixed in an Eppendorf tube. Once 200 µL of diluted FSA was introduced to reaction mixture, the test started. Approximately six samples were taken during the initial 30 minutes of the assay reaction, and reaction was followed by HPLC. 10 µL of samples were diluted in 190 µL of methanol to precipitate the enzyme and centrifuged (2 min, 5000 g). Supernatant was used for the HPLC analysis. From the change in product concentration *vs* time, initial reaction rate was calculated. From this value specific activity of enzyme was calculated by dividing the initial reaction rate with the enzyme concentration in the assay as presented in Equation 7.3 where where *S.A.* designates the specific activity (U mg^{-1}). Change in product concentration in time is presented as $dc_{product}/dt$. V_r stands for reactor volume (cm^{-3}), V_{enzyme} stands for enzyme volume (cm^{-3}) and γstands for enzyme concentration (mg cm^{-3}).

$$S.A. = \frac{dc_{product}}{dt} \cdot \frac{V_r}{V_{enzyme}} \cdot \frac{1}{\gamma_{enyzme}} \qquad \left[\frac{U}{mg}\right] \tag{7.3}$$

7.3.13 Effect of aeration on the activity of the enzyme

Since low oxygen concentration in the reaction solution can be the reason for low reaction rate, aeration of the reaction was considered since it might improve the reaction outcome. Therefore, the influence of aeration on enzymes activity was tested. Reactions were conducted 25 °C in 50 mM TEA HCl buffer pH 8.0. Reactor was 30 mL flask. Enzyme solutions were stirred on a shaker at 250 rpm. Concentrations of HLADH, NOX 009 and FSA^{A129S} were 2 mg mL^{-1}, 0.5 mg mL^{-1} and 2 mg mL^{-1}, respectively. Airflow was 2 L h^{-1} and current oxygen content was measured by oxygen electrode. At known exact oxygen concentration, spectrophotometric activity assay was performed and enzyme's activity was measured.

7.3.14 Cascade reactions in batch reactor with multiple enzymes and substrates additions

Cascade reaction was performed. Enzymes and substrates were re-added to the reaction mixture during the experiment at a certain time. The aim of this experiment was

7A – Cbz-*N*-3-amino-1,2-propanediol (racemic mixture), **7B** – (*S*)-3-Amino-1,2-propanediol,
7C – (*R*)-3-Amino-1,2-propanediol, **7D** – (*S*)-Cbz-*N*-3-amino-1,2-propanediol, **7E** – (*R*)-Cbz-*N*-3-amino-1,2-propanediol,
7F – Cbz-*N*-3-amino-2-hydroxypropanal, **7G** – Cbz-*N*-6-amino-1,3,4,5-tetrahydroxy-hexan-2-one
7H – 3-Chloro-1,2-propanediol (racemic mixture), **7I** – (*S*)-3-Chloro-1,2-propanediol, **7J** – (*R*)-3-Chloro-1,2-propanediol

maximizing product **7G** concentration and diol **7A** conversion. The reaction volume was 1.2 mL. Reaction mixture contained alcohol **7A** (260.2 µL of 92.3 mM stock solution, 20 mM in the reaction), NAD^+ (56.1 µL of 21.4 mM stock solution, 1 mM in the reaction), DHA (186.4 µL of 321.9 mM stock solution, 50 mM in the reaction) and 517.5 µL of 50 mM triethanolamine HCl pH 8 buffer. The reaction was started by adding NADH oxidase (17.7 µL of 1 mg mL^{-1} stock solution, 0.01 mg mL^{-1} in the reaction), HLADH (120 µL of 100 mg mL^{-1} stock solution, 10 mg mL^{-1} in the reaction) and FSA^{A129S} (42.1 µL of 57 mg mL^{-1} stock solution, 2 mg mL^{-1} in the reaction). Extra additions of fresh enzymes and substrates were performed as listed in Table 7.2.

Table 7.2 Additions of fresh HLADH, NOX, FSA, DHA and NAD^+ during the cascade.

Reaction time [h]	Addition
42	HLADH (11.7 mg) and NOX (17.7 µL stock solution, 1 mg mL^{-1} in the reaction)
98	HLADH (2.2 mg) and NOX (17.7 µL stock solution, 1 mg mL^{-1} in the reaction)
211	HLADH (13.3 mg), NOX (17.7 µL stock solution, 1 mg mL^{-1} in the reaction), FSA (2.3 mg), DHA (5.9 mg) and NAD^+ (0.9 mg)
360	HLADH (12.0 mg), NOX (17.7 µL stock solution, 1 mg mL^{-1} in the reaction), FSA (2.3 mg), DHA (5.4 mg) and NAD^+ (1.1 mg)

7A – Cbz-*N*-3-amino-1,2-propanediol (racemic mixture), **7B** – (*S*)-3-Amino-1,2-propanediol,
7C – (*R*)-3-Amino-1,2-propanediol, **7D** – (*S*)-Cbz-*N*-3-amino-1,2-propanediol, **7E** – (*R*)-Cbz-*N*-3-amino-1,2-propanediol,
7F – Cbz-*N*-3-amino-2-hydroxypropanal, **7G** – Cbz-*N*-6-amino-1,3,4,5-tetrahydroxy-hexan-2-one
7H – 3-Chloro-1,2-propanediol (racemic mixture), **7I** – (*S*)-3-Chloro-1,2-propanediol, **7J** – (*R*)-3-Chloro-1,2-propanediol

7.4 Results and discussion – Approach I

7.4.1 Screening for the most suitable oxido-reductase

Enzymes with known potential for amino alcohol oxidation are tested spectrophotometrically to find the ones with highest activity toward **7A**, substrate of interest. Spectrophotometrically measured activities of tested enzymes are presented in Table 7.3.

Table 7.3 Activities of HLADH (Sigma Aldrich), YADH (Sigma Aldrich) and HLADH (FZ Jülich).

Substrate	Enzyme	*S.A.* [U mg^{-1}]
7D	HLADH Sigma Aldrich	0.126
7D	YADH Sigma Aldrich	0.006
7D	HLADH FZ Jülich	0.129
7E	HLADH Sigma Aldrich	0.165
7E	YADH Sigma Aldrich	n.a.
7E	HLADH FZ Jülich	0.178

Plate assay containing 192 ketoreductases (KREDs) showed that some enzymes are active towards **7D** and **7E** (tested separately) as substrates. The ones with strongest colouring were selected and tested spectrophotometrically (Figure 7.4).

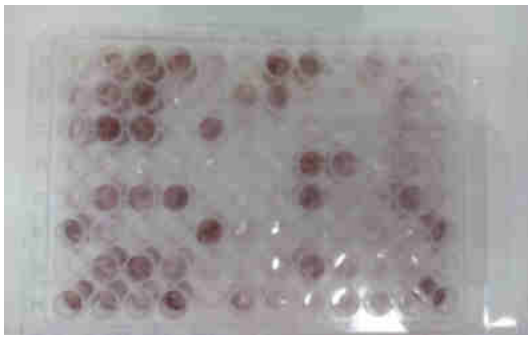

Figure 7.4 KRED plate activity test.

Since it is unknown whether activity of a certain plate enzyme is higher by using coenzyme NAD^+ or $NADP^+$, tests were made separately with both coenzymes. These results are presented in Table 7.4.

7A – Cbz-*N*-3-amino-1,2-propanediol (racemic mixture), **7B** – (*S*)-3-Amino-1,2-propanediol,
7C – (*R*)-3-Amino-1,2-propanediol, **7D** – (*S*)-Cbz-*N*-3-amino-1,2-propanediol, **7E** – (*R*)-Cbz-*N*-3-amino-1,2-propanediol,
7F – Cbz-*N*-3-amino-2-hydroxypropanal, **7G** – Cbz-*N*-6-amino-1,3,4,5-tetrahydroxy-hexan-2-one
7H – 3-Chloro-1,2-propanediol (racemic mixture), **7I** – (*S*)-3-Chloro-1,2-propanediol, **7J** – (*R*)-3-Chloro-1,2-propanediol

Table 7.4 Activities of selected KREDs on **7A**.

Enzyme (KRED)	*S.A.* [U mg^{-1}] with NAD^+	*S.A.* [U mg^{-1}] with $NADP^+$
4	0.00180	0.09464
6	0.00178	0.02380
30	0.00051	0.00547
54	0.00088	0.01169
83	0.00047	0.00168
84	0.00079	0.00285
291	0.00035	0.00072
296	0.00019	0.00965
303	0.00056	0.00219
314	0.00043	0.00186
315	0.00047	0.00107
353	0.00051	0.00278
362	0.00010	0.00051
376	0.00087	0.00898
51	0.00794	0.00070
61	0.00155	0.00449
307	0.00546	0.02345
373	0.00257	0.00181

Horse liver alcohol dehydrogenase (both from Sigma and FZ Jülich) showed the highest activity toward alcohol enantiomers, **7D** and **7E** (Table 7.3). No ketoreductase (KRED) showed higher activity than HLADH. Thus, the research of iminosugar precursor synthesis (Approach I) continued with using HLADH from Sigma Aldrich as a catalyst for the first reaction step of the investigated cascade.

7.4.2 pH dependence of HLADH

pH dependence of HLADH activity was measured and the results presented in Figure 7.5 show that the optimum activity for oxidation is at pH 8.0 in TEA HCl buffer.

7A – Cbz-*N*-3-amino-1,2-propanediol (racemic mixture), **7B** – (*S*)-3-Amino-1,2-propanediol,
7C – (*R*)-3-Amino-1,2-propanediol, **7D** – (*S*)-Cbz-*N*-3-amino-1,2-propanediol, **7E** – (*R*)-Cbz-*N*-3-amino-1,2-propanediol,
7F – Cbz-*N*-3-amino-2-hydroxypropanal, **7G** – Cbz-*N*-6-amino-1,3,4,5-tetrahydroxy-hexan-2-one
7H – 3-Chloro-1,2-propanediol (racemic mixture), **7I** – (*S*)-3-Chloro-1,2-propanediol, **7J** – (*R*)-3-Chloro-1,2-propanediol

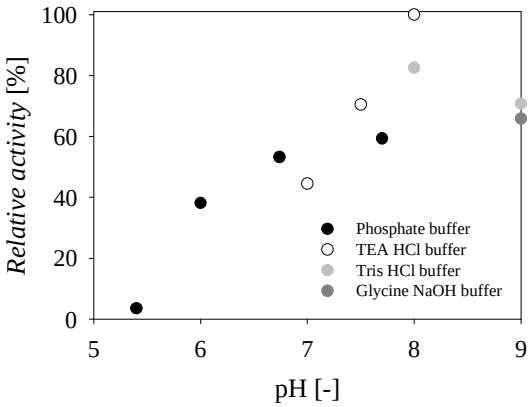

Figure 7.5 pH dependence of HLADH activity (25 °C, 340 nm, 50 mM buffer, γ_{HLADH} = 0.5 mg mL^{-1}, c_{7A} = 11.37 mM, c_{NAD+} = 4.71 mM).

7.4.3 Cbz protection group

Cbz protection of **7B** and **7C** was done to prepare the substrate for the reaction according to the procedure described in Chapter 7.3.3. The obtained product after putting a Cbz protection group on **7B** and **7C** is presented in Figure 7.6, and was used in further experiments.

Figure 7.6 Cbz-protected (*R*)-3-amino-1,2-propanediol.

By preparing different concentrations of synthesised compounds and by its comparison to the standard compound, their purities were determined and are presented in Table 7.5. These compounds, as well as the unprotected alcohols **7B** and **7C** were tested as substrates for horse liver ADH.

7A – Cbz-*N*-3-amino-1,2-propanediol (racemic mixture), **7B** – (*S*)-3-Amino-1,2-propanediol,
7C – (*R*)-3-Amino-1,2-propanediol, **7D** – (*S*)-Cbz-*N*-3-amino-1,2-propanediol, **7E** – (*R*)-Cbz-*N*-3-amino-1,2-propanediol,
7F – Cbz-*N*-3-amino-2-hydroxypropanal, **7G** – Cbz-*N*-6-amino-1,3,4,5-tetrahydroxy-hexan-2-one
7H – 3-Chloro-1,2-propanediol (racemic mixture), **7I** – (*S*)-3-Chloro-1,2-propanediol, **7J** – (*R*)-3-Chloro-1,2-propanediol

Table 7.5 The purity of the synthesised Cbz-protected (*R*) and (*S*)-3-amino-1,2-propanediol.

Compound	Purity [%]
7E	76.34 ± 3.76
7D	73.17 ± 1.72

7.4.4 HLADH kinetic measurements

The kinetics of the HLADH was determined by using single enantiomers (both with and without Cbz protection), to determine if the enzyme is enantioselective towards different enantiomers. The results are presented in Figure 7.7 to Figure 7.10.

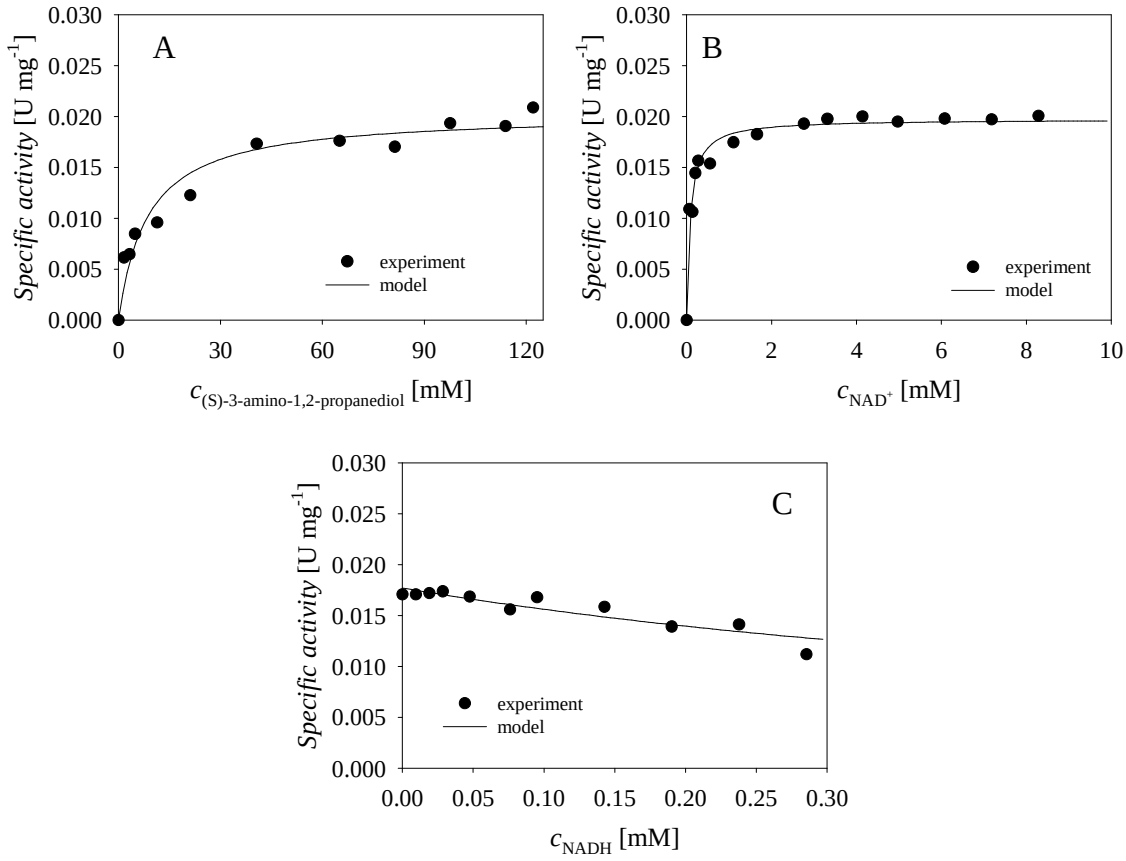

Figure 7.7 Kinetics of **7B** (unprotected (*S*)-3-amino-1,2-propanediol) oxidation catalysed by HLADH (25 °C, 50 mM TEA HCl buffer pH 8.0, γ_{HLADH}= 1.0 mg mL^{-1}, A. c_{NAD+} = 9.14 mM, B. c_{7B} = 150.53 mM, C. c_{NAD+} = 9.14 mM, c_{7B} = 136.83 mM).

7A – Cbz-*N*-3-amino-1,2-propanediol (racemic mixture), **7B** – (*S*)-3-Amino-1,2-propanediol,
7C – (*R*)-3-Amino-1,2-propanediol, **7D** – (*S*)-Cbz-*N*-3-amino-1,2-propanediol, **7E** – (*R*)-Cbz-*N*-3-amino-1,2-propanediol,
7F – Cbz-*N*-3-amino-2-hydroxypropanal, **7G** – Cbz-*N*-6-amino-1,3,4,5-tetrahydroxy-hexan-2-one
7H – 3-Chloro-1,2-propanediol (racemic mixture), **7I** – (*S*)-3-Chloro-1,2-propanediol, **7J** – (*R*)-3-Chloro-1,2-propanediol

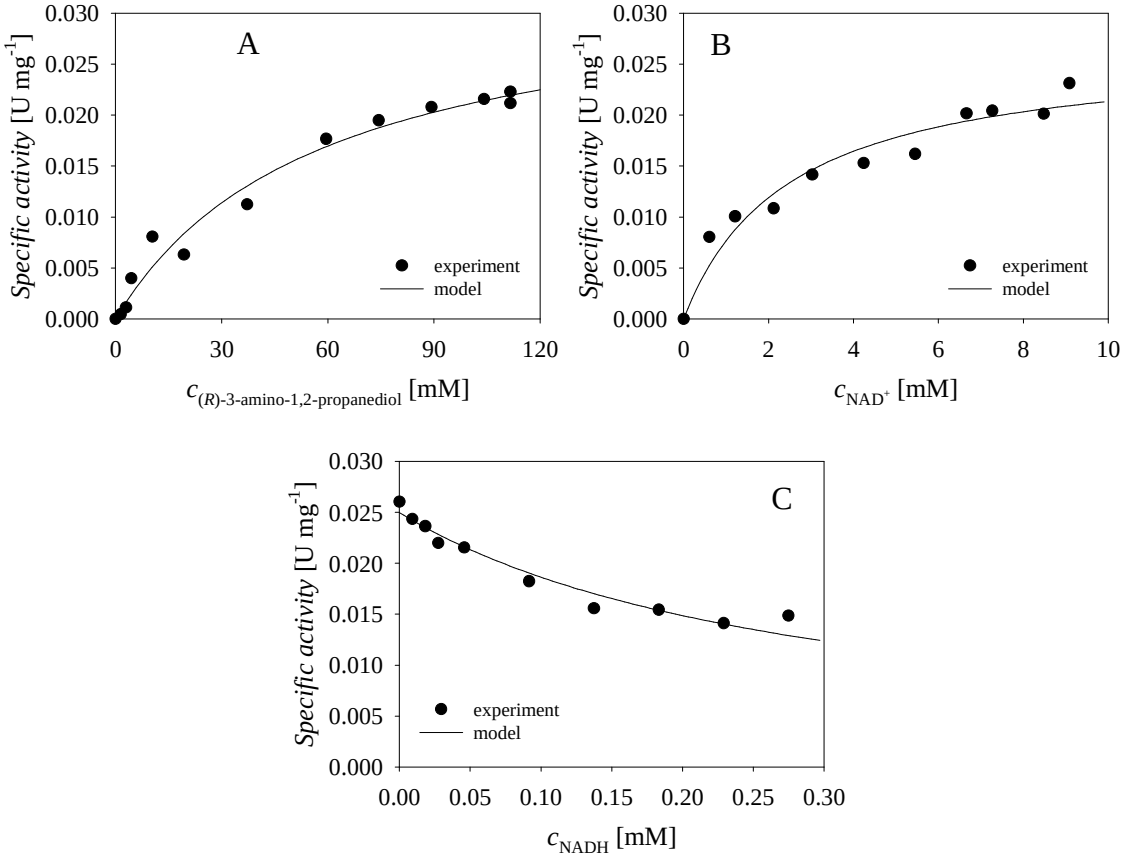

Figure 7.8 Kinetics of **7C** (unprotected (*R*)-3-amino-1,2-propanediol) oxidation catalysed by HLADH (25 °C, 50 mM TEA HCl buffer pH 8.0, γ_{HLADH}= 1.0 mg mL^{-1}, A. c_{NAD+} = 9.14 mM, B. c_{7C} = 150.53 mM), C. c_{NAD+} = 9.50 mM, c_{7C} = 157.90 mM).

7A – Cbz-*N*-3-amino-1,2-propanediol (racemic mixture), **7B** – (*S*)-3-Amino-1,2-propanediol,
7C – (*R*)-3-Amino-1,2-propanediol, **7D** – (*S*)-Cbz-*N*-3-amino-1,2-propanediol, **7E** – (*R*)-Cbz-*N*-3-amino-1,2-propanediol,
7F – Cbz-*N*-3-amino-2-hydroxypropanal, **7G** – Cbz-*N*-6-amino-1,3,4,5-tetrahydroxy-hexan-2-one
7H – 3-Chloro-1,2-propanediol (racemic mixture), **7I** – (*S*)-3-Chloro-1,2-propanediol, **7J** – (*R*)-3-Chloro-1,2-propanediol

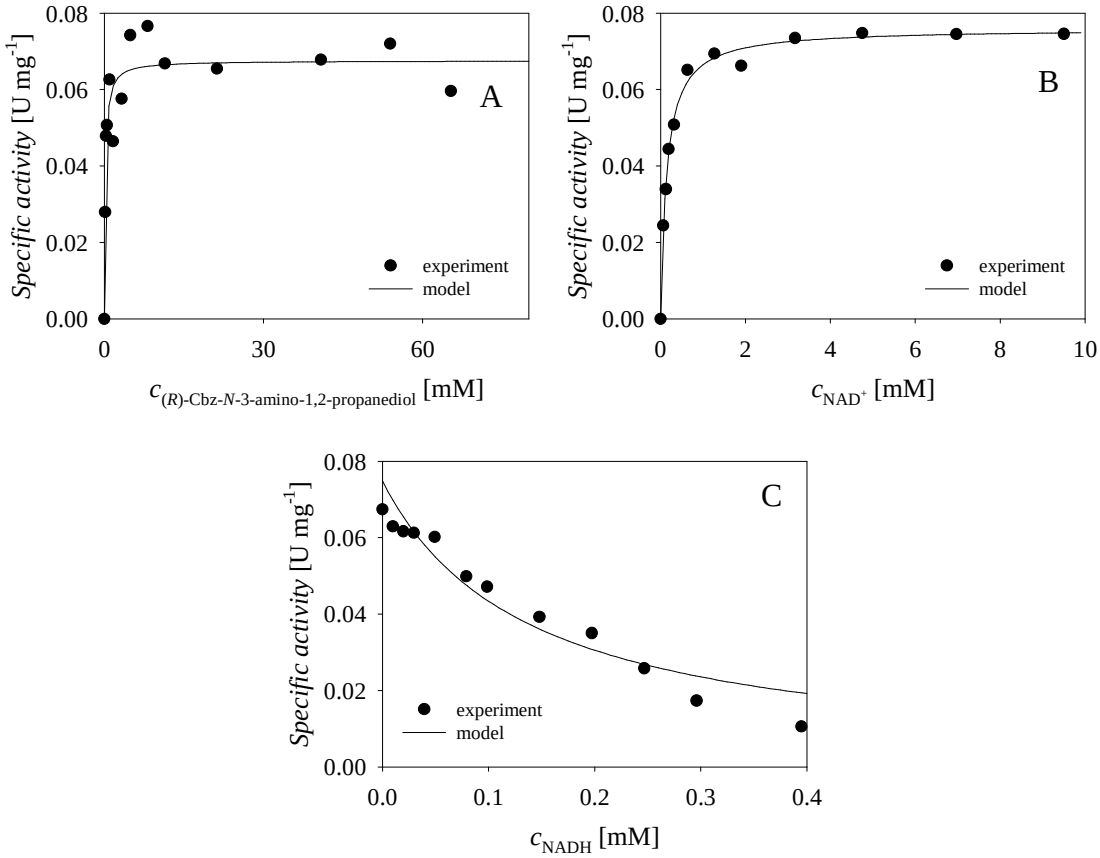

Figure 7.9 Kinetics of **7E** (protected (*R*)-Cbz-*N*-3-amino-1,2-propanediol) oxidation catalysed by HLADH (25 °C, 50 mM TEA HCl buffer pH 8.0, γ_{HLADH}= 0.5 mg mL^{-1}, A. c_{NAD+} = 9.5 mM, B. c_{7E} = 24.48 mM, C. c_{NAD+} = 9.5 mM, c_{7E} = 24.48 mM).

7A – Cbz-*N*-3-amino-1,2-propanediol (racemic mixture), **7B** – (*S*)-3-Amino-1,2-propanediol,
7C – (*R*)-3-Amino-1,2-propanediol, **7D** – (*S*)-Cbz-*N*-3-amino-1,2-propanediol, **7E** – (*R*)-Cbz-*N*-3-amino-1,2-propanediol,
7F – Cbz-*N*-3-amino-2-hydroxypropanal, **7G** – Cbz-*N*-6-amino-1,3,4,5-tetrahydroxy-hexan-2-one
7H – 3-Chloro-1,2-propanediol (racemic mixture), **7I** – (*S*)-3-Chloro-1,2-propanediol, **7J** – (*R*)-3-Chloro-1,2-propanediol

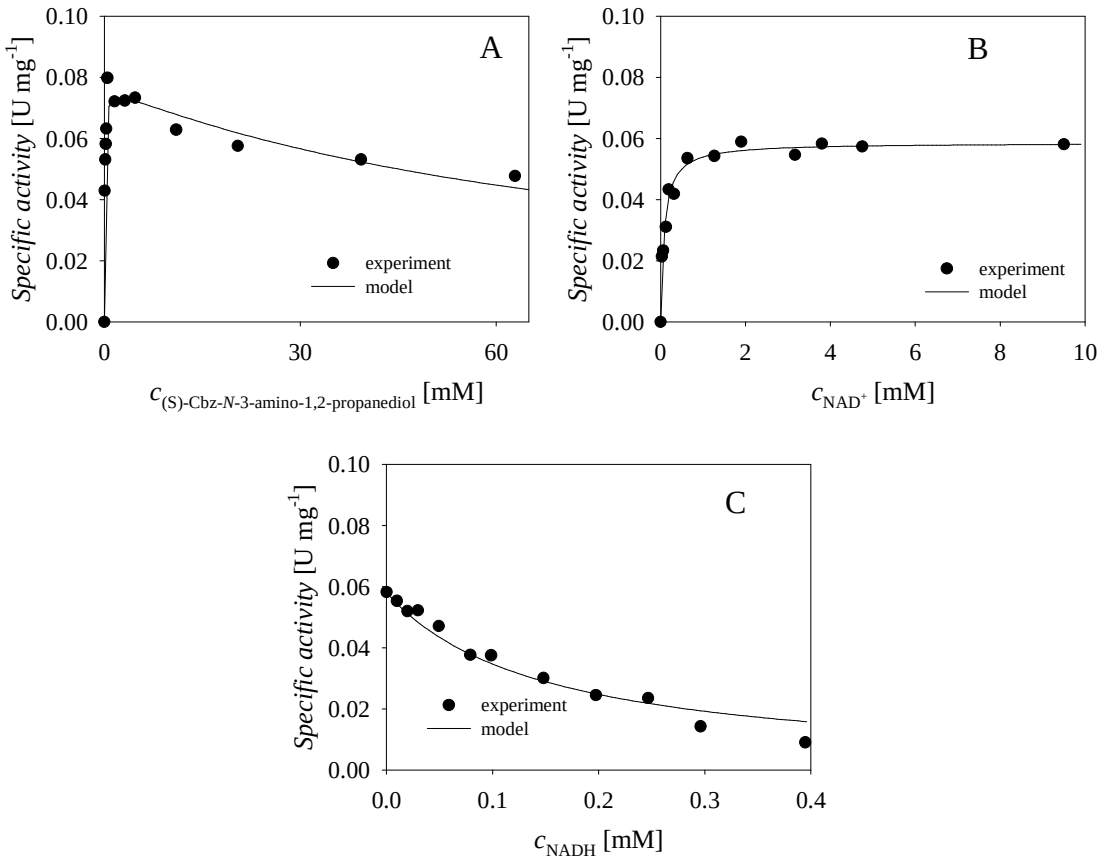

Figure 7.10 Kinetics of **7D** (protected (*S*)-Cbz-*N*-3-amino-1,2-propanediol) oxidation catalysed by HLADH (25 °C, 50 mM TEA HCl buffer pH 8.0, γ_{HLADH}= 0.5 mg mL^{-1}, A. c_{NAD^+} = 9.5 mM, B. c_{7D} = 15.72 mM, C. c_{NAD^+} = 9.5 mM, c_{7D} = 15.72 mM).

It can be concluded from the collected data (Figure 7.7) that HLADH is active towards the unprotected (*S*)-3-amino-1,2-propanediol (**7B**) and that the reaction is inhibited by NADH as a product. That is why coenzyme regeneration is important in this reaction system, while it will provide low concentration of NADH in the system, and minimize the inhibition. Figure 7.8 presents the influence of (*R*)-enantiomer concentration on the reaction rate. Similar results as in the previous case are obtained, and from the collected data kinetic parameters were estimated (Table 7.6). Figure 7.9 presents the results for **7E**. It can be seen that the activities are approximately doubled in comparison to the unprotected substrate. The situation is similar for **7D** (Figure 7.10). The kinetic parameters presented in (Table 7.6) show that HLADH has higher affinity towards (*S*)-enantiomer (lower estimated Michaelis constant). They also show that enzyme has similar activities towards unprotected substrates (V_m =0.033 and 0.020 U mg^{-1}), as well as for the protected ones (V_m =0.068 and 0.077 U mg^{-1}). It was shown that **7D**

7A – Cbz-*N*-3-amino-1,2-propanediol (racemic mixture), **7B** – (*S*)-3-Amino-1,2-propanediol,
7C – (*R*)-3-Amino-1,2-propanediol, **7D** – (*S*)-Cbz-*N*-3-amino-1,2-propanediol, **7E** – (*R*)-Cbz-*N*-3-amino-1,2-propanediol,
7F – Cbz-*N*-3-amino-2-hydroxypropanal, **7G** – Cbz-*N*-6-amino-1,3,4,5-tetrahydroxy-hexan-2-one
7H – 3-Chloro-1,2-propanediol (racemic mixture), **7I** – (*S*)-3-Chloro-1,2-propanediol, **7J** – (*R*)-3-Chloro-1,2-propanediol

slightly inhibits the enzyme as a substrate. In all cases, NADH was shown to be an inhibiting product.

Tables 7.6 and 7.7 present the calculated catalytic constants as well as k_{cat}/K_m values for all substrates. It can be seen that these values are the highest for (*S*)-Cbz-*N*-3-amino-1,2-propanediol. Hence, the enzyme is the most efficient in converting Cbz-protected (*S*)-enantiomer, but is not enantioselective.

Table 7.6 Kinetic parameters of horse liver ADH in the reaction of oxidation of protected and unprotected (*R*)- and (*S*)-3-amino-1,2-propanediol.

Parameter	Substrate	Unit	Value
V_m	**7C**	U mg^{-1}	0.033 ± 0.003
K_m^{7C}	**7C**	mM	57.816 ± 14.672
K_m^{NAD+}	**7C**	mM	2.476 ± 0.662
K_i^{NADH}	**7C**	mM	0.070 ± 0.006
V_m	**7B**	U mg^{-1}	0.020 ± 0.001
K_m^{7B}	**7B**	mM	8.571 ± 1.967
K_m^{NAD+}	**7B**	mM	0.083 ± 0.011
K_i^{NADH}	**7B**	mM	0.0064± 0.0007
V_m	**7E**	U mg^{-1}	0.068 ± 0.002
K_m^{7E}	**7E**	mM	0.182 ± 0.050
K_m^{NAD+}	**7E**	mM	0.142 ± 0.009
K_i^{NADH}	**7E**	mM	0.0023± 0.0002
V_m	**7D**	U mg^{-1}	0.077 ± 0.003
K_m^{7D}	**7D**	mM	0.062 ± 0.014
K_i^{7D}	**7D**	mM	82.649 ±18.143
K_m^{NAD+}	**7D**	mM	0.086 ± 0.011
K_i^{NADH}	**7D**	mM	0.0013± 0.0001

Table 7.7 Catalytic constants of HLADH for all used substrates.

Substrate	k_{cat} [min^{-1}]	k_{cat}/K_m [min^{-1} mM^{-1}]
7C	2.64	0.045662
7B	1.6	0.186676
7E	5.44	29.89011
7D	6.16	99.35484

7.4.5 Isolation of NADH oxidase from Lactococcus lactis

Several fermentations of *Lactococcus lactis* were carried out during this research to produce sufficient amount of cells for NADH oxidase isolation and purification. The concentration of proteins in purified protein suspension obtained by the end of purification

7A – Cbz-*N*-3-amino-1,2-propanediol (racemic mixture), **7B** – (*S*)-3-Amino-1,2-propanediol,
7C – (*R*)-3-Amino-1,2-propanediol, **7D** – (*S*)-Cbz-*N*-3-amino-1,2-propanediol, **7E** – (*R*)-Cbz-*N*-3-amino-1,2-propanediol,
7F – Cbz-*N*-3-amino-2-hydroxypropanal, **7G** – Cbz-*N*-6-amino-1,3,4,5-tetrahydroxy-hexan-2-one
7H – 3-Chloro-1,2-propanediol (racemic mixture), **7I** – (*S*)-3-Chloro-1,2-propanediol, **7J** – (*R*)-3-Chloro-1,2-propanediol

process was determined by the Bradford method (Bradford, 1976). The overall measured activity of 12.5 mL of protein suspension (Figure 7.11) obtained during one fermentation and purification was 21.2 U.

Figure 7.11 Isolated and purified NADH oxidase.

7.4.6 Chemical oxidation of alcohol 7A

Since aldehyde **7F** is not commercially available, it was synthesised by chemical oxidation of **7A** with IBX in order to establish the analytic protocol on HPLC. Chemical oxidation of alcohol **7A** was monitored by HPLC. The retention times of aldehyde **7F** and alcohol **7A** peaks are detected. Chromatogram is presented in Figure 7.12.

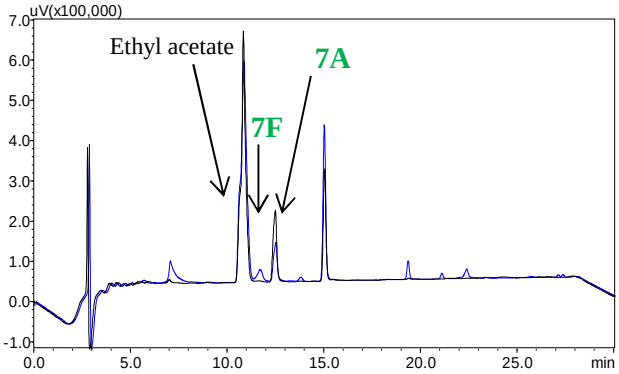

Figure 7.12 Example of chromatogram during IBX oxidation of racemic diol IBX oxidation in the batch reactor ($m_{\mathbf{7A}}$ = 0.61 g, m_{IBX} = 1.47 g IBX, V_{EtAc} 58 mL, t = 80 °C, reflux of EtAc) (black line - initial sample, blue line – sample after 4 hours).

7.4.7 Preliminary experiments carried out in batch reactor

The preliminary cascade reaction was carried out in 1.2 mL batch reactor. After approximately two days of reaction, aldol **7G** concentration started to decrease (degradation)

7A – Cbz-*N*-3-amino-1,2-propanediol (racemic mixture), **7B** – (*S*)-3-Amino-1,2-propanediol,
7C – (*R*)-3-Amino-1,2-propanediol, **7D** – (*S*)-Cbz-*N*-3-amino-1,2-propanediol, **7E** – (*R*)-Cbz-*N*-3-amino-1,2-propanediol,
7F – Cbz-*N*-3-amino-2-hydroxypropanal, **7G** – Cbz-*N*-6-amino-1,3,4,5-tetrahydroxy-hexan-2-one
7H – 3-Chloro-1,2-propanediol (racemic mixture), **7I** – (*S*)-3-Chloro-1,2-propanediol, **7J** – (*R*)-3-Chloro-1,2-propanediol

and alcohol **7A** conversion slows down. Therefore, fresh HLADH and NOX were added (5 mg mL^{-1} ADH and 0.01 mg mL^{-1} NOX after 2 and 9 days of reaction). In this way, substrate conversion of 50 % was achieved after 11 days (Figure 7.13).

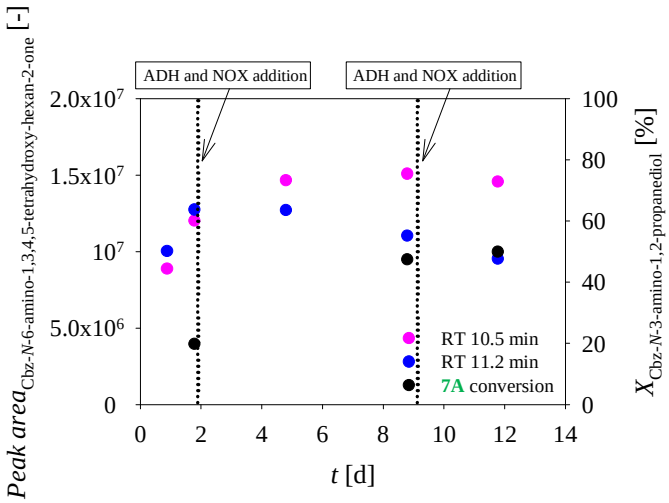

Figure 7.13 Cascade reaction with **7A** as starting substrate (50 mM TEA HCl buffer, pH 8.0, 25 °C, 1000 rpm , $V_{reactor}$ = 1.2 mL, c_{NAD^+} = 1 mM, c_{DHA} = 50 mM, γ_{HLADH} = 10.0 mg mL^{-1}, γ_{NOX} = 0.01 mg mL^{-1}, $\gamma_{FSA\ A129S}$ = 2.0 mg mL^{-1}, c_{7A} = 20 mM).

7.4.8 LC-MS analysis of the aldol product

The LC-MS analysis of the aldol adduct **7G** that evolves in the cascade reaction was performed. When cascade reactions were performed with pure alcohol enantiomers, one aldol peak evolved per reaction (Figure 7.14). When alcohol racemic mixture was used as cascade substrate, both peaks appeared (Figure 7.15), as they correspond to different diastereoisomers. LC-MS analysis confirmed both peaks are aldol adduct (Appendix, Figure 10.10) with molecular mass of 314 g mol^{-1}.

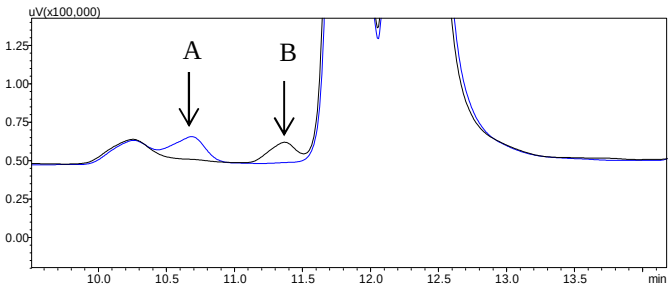

Figure 7.14 Chromatograms of aldol adducts produced separately in reactions with both enantiomers **7D** and **7E** (aldol peak A corresponds to reaction with (*R*)- and aldol peak B to (*S*)-enantiomer).

7A – Cbz-*N*-3-amino-1,2-propanediol (racemic mixture), **7B** – (*S*)-3-Amino-1,2-propanediol,
7C – (*R*)-3-Amino-1,2-propanediol, **7D** – (*S*)-Cbz-*N*-3-amino-1,2-propanediol, **7E** – (*R*)-Cbz-*N*-3-amino-1,2-propanediol,
7F – Cbz-*N*-3-amino-2-hydroxypropanal, **7G** – Cbz-*N*-6-amino-1,3,4,5-tetrahydroxy-hexan-2-one
7H – 3-Chloro-1,2-propanediol (racemic mixture), **7I** – (*S*)-3-Chloro-1,2-propanediol, **7J** – (*R*)-3-Chloro-1,2-propanediol

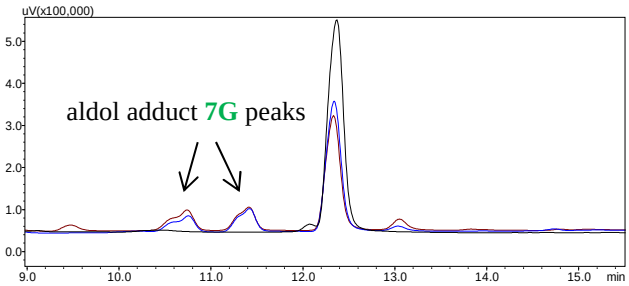

Figure 7.15 Chromatograms of aldol adducts in reactions with racemic mixture **7A**.

7.4.9 The influence of NAD$^+$ concentration on substrate conversion in the cascade

Preliminary cascade reactions showed that the presented cascade system works but needs optimization, because diol **7A** conversion up to only 50.5% was achieved with 20 mM substrate concentration. In order to find the reason behind this, more cascade experiments were carried out in different series. In the first series of experiments, the influence of NAD$^+$ concentration on the diol conversion was evaluated (Figure 7.16).

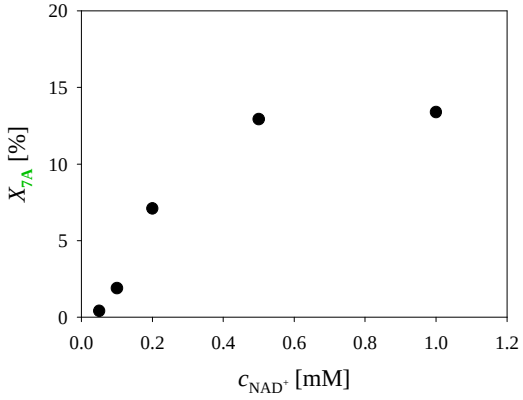

Figure 7.16 The influence of NAD$^+$ concentration on the diol conversion in the cascade reaction (50 mM TEA HCl buffer, pH 8.0, 25 °C, $V_{reactor}$ = 1.0 mL, c_{NAD^+} = 0.05 - 1.00 mM, c_{DHA} = 200 mM, γ_{HLADH} = 5 mg mL^{-1}, $\gamma_{NOX\ 009}$ = 1.0 mg mL^{-1}, $\gamma_{FSA\ A129S}$ = 5.0 mg mL^{-1}, c_{7A} = 100 mM).

It was found that NAD$^+$ concentration of 1 mM used in preliminary cascade experiments is also the optimal one. However, lower concentration can also be applied starting from 0.5 mM.

7A – Cbz-*N*-3-amino-1,2-propanediol (racemic mixture), **7B** – (*S*)-3-Amino-1,2-propanediol,
7C – (*R*)-3-Amino-1,2-propanediol, **7D** – (*S*)-Cbz-*N*-3-amino-1,2-propanediol, **7E** – (*R*)-Cbz-*N*-3-amino-1,2-propanediol,
7F – Cbz-*N*-3-amino-2-hydroxypropanal, **7G** – Cbz-*N*-6-amino-1,3,4,5-tetrahydroxy-hexan-2-one
7H – 3-Chloro-1,2-propanediol (racemic mixture), **7I** – (*S*)-3-Chloro-1,2-propanediol, **7J** – (*R*)-3-Chloro-1,2-propanediol

7.4.10 The influence of different initial substrate concentrations on the conversion in the cascade

In the second series of experiments, different initial concentrations of diol **7A** were used (Figure 7.17). All other experimental conditions were the same in all experiments. Experiments were followed for 14 days to achieve maximum conversion in all cases because this cascade reaction in general is very slow.

The results show an optimum, *i.e.* the highest diol **7A** conversion and aldol adduct(s) **7G** concentrations when 20 mM diol starting concentration was used. It was found that by increasing the diol concentration up to 100 mM the reaction slows down severely. These results cannot be explained by substrate inhibition with (*S*)-enantiomer **7D**, because of high value of inhibition constant 82.6 mM. At this substrate concentration, HLADH has significant activity. By-product formation was observed in all experiments. It is possible that by-product causes inhibition and negatively affects the cascade outcome. Further experiments were carried out by using 20 mM diol **7A** concentration.

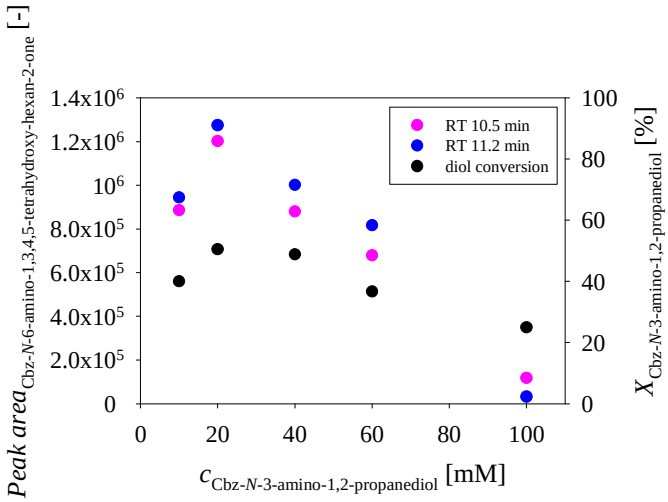

Figure 7.17 The influence of the **7A** initial concentration on the formation on aldol adduct **7G** in the cascade reaction (50 mM TEA HCl buffer, pH 8.0, 25 °C, $V_{reactor}$ = 1.2 mL, c_{NAD^+} = 1 mM, c_{DHA} = 50 mM, γ_{HLADH} = 10 mg mL^{-1}, $\gamma_{NOX\ 009}$ = 0.10 mg mL^{-1}, $\gamma_{FSA\ A129S}$ = 2.0 mg mL^{-1}, c_{7A} = 10, 20, 40, 60 and 100 mM). Legend: pink circles – aldol peak at RT 10.5 min, blue circles – aldol peak at RT 11.2.

7.4.11 The influence of HLADH/NOX activity ratio on the aldol adduct evolving

The next step was evaluation of the influence of enzyme activity ratio on diol **7A** conversion and product concentration (Figure 7.18). The results show the best results at the

7A – Cbz-*N*-3-amino-1,2-propanediol (racemic mixture), **7B** – (*S*)-3-Amino-1,2-propanediol,
7C – (*R*)-3-Amino-1,2-propanediol, **7D** – (*S*)-Cbz-*N*-3-amino-1,2-propanediol, **7E** – (*R*)-Cbz-*N*-3-amino-1,2-propanediol,
7F – Cbz-*N*-3-amino-2-hydroxypropanal, **7G** – Cbz-*N*-6-amino-1,3,4,5-tetrahydroxy-hexan-2-one
7H – 3-Chloro-1,2-propanediol (racemic mixture), **7I** – (*S*)-3-Chloro-1,2-propanediol, **7J** – (*R*)-3-Chloro-1,2-propanediol

activity ratio 30, which means 30-fold higher activity of ADH in comparison to NOX (50 mg mL^{-1} ADH in the reactor). At these conditions 50% substrate conversion was achieved.

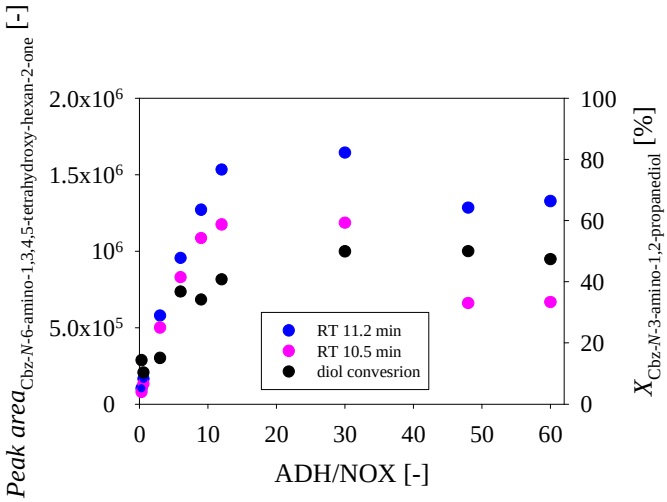

Figure 7.18 Influence of activity ratio of HLADH and NOX on the product formation and diol **7A** conversion in the cascade reaction (50 mM TEA HCl buffer, pH 8.0, 25 °C, $V_{reactor}$ = 0.4 mL, c_{NAD^+} = 1 mM, c_{DHA} = 50 mM, γ_{HLADH} = 0.5 - 100 mg mL^{-1}, $\gamma_{NOX\ 009}$ = 0.10 mg mL^{-1}, $\gamma_{FSA\ A129S}$ = 2.0 mg mL^{-1}, c_{7A} = 20 mM).

7.4.12 Operational stability of HLADH, NOX and FSA during the cascade reaction

Activities of HLADH and NOX were followed spectrophotometrically by following the NADH concentration. Activity of FSA^{A129S} was measured by performing the activity tests followed by HPLC. For each of the three enzymes, activity test started by taking 10 µL of cascade reaction sample and filtrating it by centrifugation of *Amicon ® Ultra filter unit* (5 min, 5000 g). Enzymes were diluted in buffer (400 µL for HLADH and NOX tests and 200 µL for FSA test) and used for activity test.

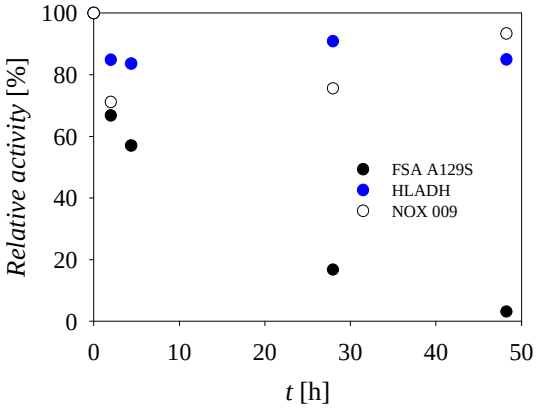

7A – Cbz-*N*-3-amino-1,2-propanediol (racemic mixture), **7B** – (*S*)-3-Amino-1,2-propanediol,
7C – (*R*)-3-Amino-1,2-propanediol, **7D** – (*S*)-Cbz-*N*-3-amino-1,2-propanediol, **7E** – (*R*)-Cbz-*N*-3-amino-1,2-propanediol,
7F – Cbz-*N*-3-amino-2-hydroxypropanal, **7G** – Cbz-*N*-6-amino-1,3,4,5-tetrahydroxy-hexan-2-one
7H – 3-Chloro-1,2-propanediol (racemic mixture), **7I** – (*S*)-3-Chloro-1,2-propanediol, **7J** – (*R*)-3-Chloro-1,2-propanediol

Figure 7.19 The change of FSA^{A129S}, HLADH and NOX009 relative activity during a cascade experiment (50 mM TEA HCl buffer, pH 8.0, 25 °C, $V_{reactor}$ = 1.2 mL, c_{NAD^+} = 1 mM, c_{DHA} = 50 mM, γ_{HLADH} = 10 mg mL^{-1}, $\gamma_{NOX\ 009}$ = 0.10 mg mL^{-1}, γ_{FSA} = 2.0 mg mL^{-1}, $c_{\mathbf{7A}}$ = 20 mM).

A slow negative change in activities of HLADH and NOX during 50 hours of a cascade experiment was noticed, whereas FSA activity almost vanished (Figure 7.19).

It was estimated that FSA half-life time was approx. 5.26 hours. Considering that this cascade is usually carried out for many days, it was expected that the activity of all enzymes would eventually drop to zero. It was assumed that poor operational stability of FSA and slow deactivations of other enzymes were not the only reason for the poor results in the cascade reaction.

7.4.13 Effect of aeration on enzymes' activity

Since low oxygen concentration in the reaction solution can be the reason for low reaction rate, aeration of the reaction was considered since it might improve the reaction outcome. Results of previously reported kinetics of NADH oxidation catalysed by NOX 009 are presented in Figure 7.20 and Table 7.8.

Table 7.8 Kinetic parameters of NADH oxidation catalysed by NOX 009.

Parameter	Unit	Value
V_m	U mg^{-1}	1.76 ± 0.11
K_m^{NADH}	mM	0.07 ± 0.01
K_i^{NAD+}	mM	0.47 ± 0.03
$K_m^{O_2}$	mM	0.09 ± 0.07

7A – Cbz-*N*-3-amino-1,2-propanediol (racemic mixture), **7B** – (*S*)-3-Amino-1,2-propanediol,
7C – (*R*)-3-Amino-1,2-propanediol, **7D** – (*S*)-Cbz-*N*-3-amino-1,2-propanediol, **7E** – (*R*)-Cbz-*N*-3-amino-1,2-propanediol,
7F – Cbz-*N*-3-amino-2-hydroxypropanal, **7G** – Cbz-*N*-6-amino-1,3,4,5-tetrahydroxy-hexan-2-one
7H – 3-Chloro-1,2-propanediol (racemic mixture), **7I** – (*S*)-3-Chloro-1,2-propanediol, **7J** – (*R*)-3-Chloro-1,2-propanediol

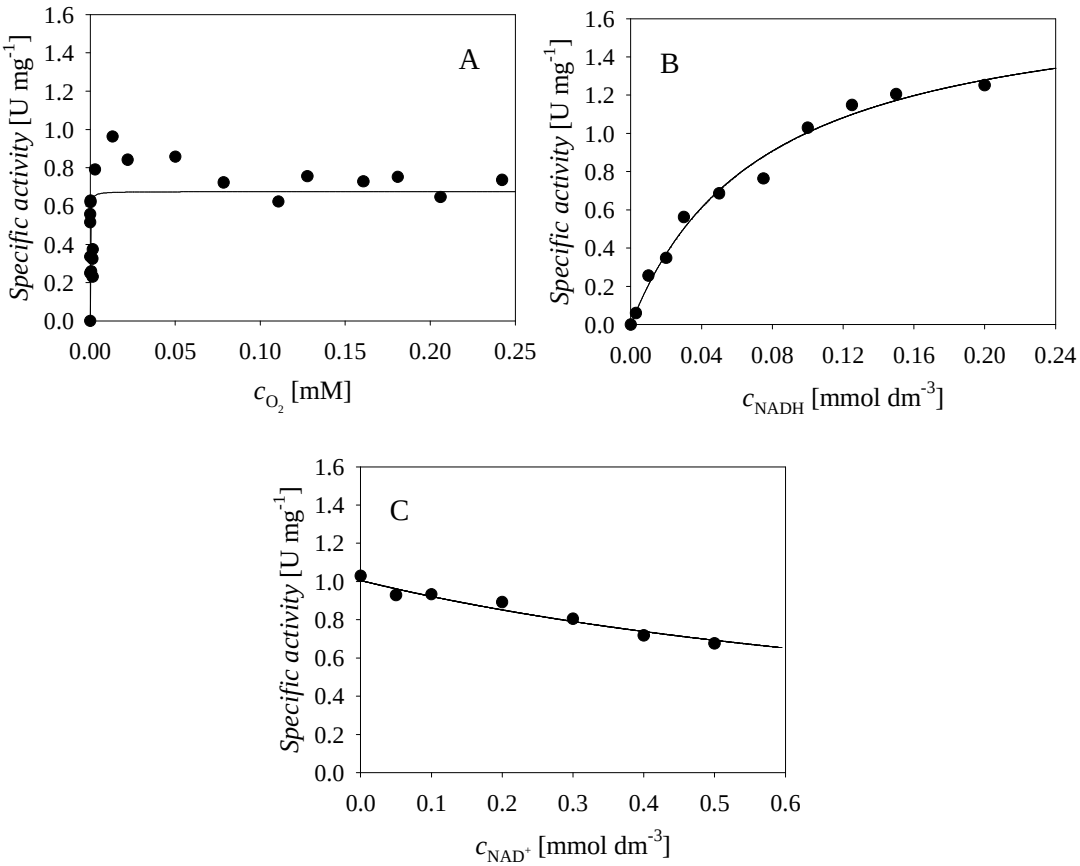

Figure 7.20 Kinetics of NADH oxidation catalysed by NOX 009 (25 °C, 50 mM TEA HCl buffer pH 8.0, $\gamma_{NOX\ 009}$= 3 mg mL^{-1}, A. c_{NADH} = 0.15 mM, B. c_{NADH} = 0 – 0.2 mM, C. c_{NADH} = 0.1 mM, c_{NAD+} = 0 – 0.5 mM). Legend: black circles – experimental data, line – model.

Even though NOX 009 has low Michaelis constant for oxygen estimated to be K_m^{O2} = 0.0904 μM, after a while oxygen concentration drops to zero (experimentally confirmed with oxygen probe), and the reaction rate is limited by slow oxygen transfer from air to solution. That is why it was assumed that aeration might improve the reaction outcome. However, first the influence of aeration on enzymes was tested. It was found that aeration has a negative influence on NOX (Figure 7.21 A), but has no negative effect on HLADH and FSA^{A129S} (Figures 7.21B and 7.21C).

7A – Cbz-*N*-3-amino-1,2-propanediol (racemic mixture), **7B** – (*S*)-3-Amino-1,2-propanediol,
7C – (*R*)-3-Amino-1,2-propanediol, **7D** – (*S*)-Cbz-*N*-3-amino-1,2-propanediol, **7E** – (*R*)-Cbz-*N*-3-amino-1,2-propanediol,
7F – Cbz-*N*-3-amino-2-hydroxypropanal, **7G** – Cbz-*N*-6-amino-1,3,4,5-tetrahydroxy-hexan-2-one
7H – 3-Chloro-1,2-propanediol (racemic mixture), **7I** – (*S*)-3-Chloro-1,2-propanediol, **7J** – (*R*)-3-Chloro-1,2-propanediol

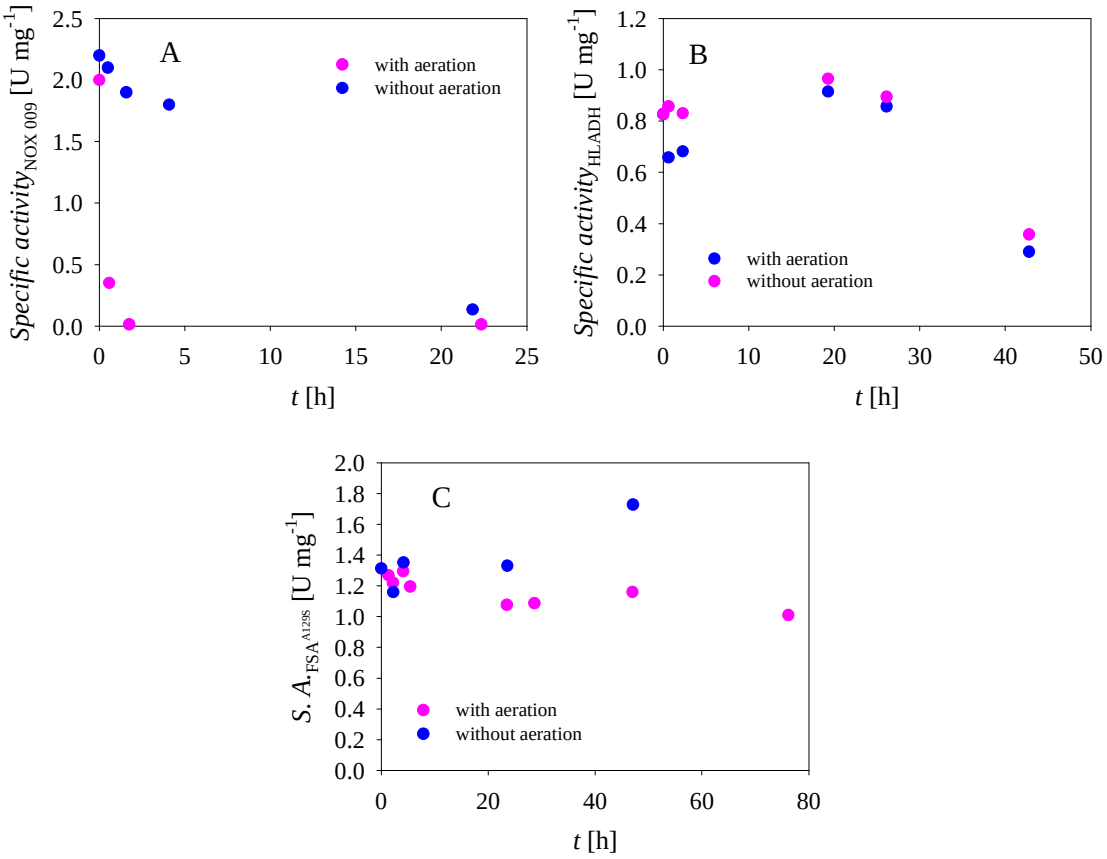

Figure 7.21 The influence of aeration (50 mM TEA HCl buffer, pH 8.0, 25 °C, 250 rpm, V = 30 mL, $q_{V,air}$ = 2 L h^{-1}) on A. NOX ($\gamma_{NOX\ 009}$ = 0.5 mg mL^{-1}), B. HLADH (γ_{HLADH} = 2.0 mg mL^{-1}) and C. FSA^{A129S} activity ($\gamma_{FSA\ A129S}$ = 2.0 mg mL^{-1}).

7.4.14 Cascade reactions in the batch reactor

Cascade reaction was performed where enzymes and substrates were re-added to the reaction mixture during the experiment. The aim of this experiment was maximizing product **7G** concentration and diol **7A** conversion. Evolving aldol **7G** and alcohol **7A** conversion are shown in Figure 7.22. Chromatographs of **7A**, **7F** and **7G** are presented in Figure 10.7.

7A – Cbz-*N*-3-amino-1,2-propanediol (racemic mixture), **7B** – (*S*)-3-Amino-1,2-propanediol,
7C – (*R*)-3-Amino-1,2-propanediol, **7D** – (*S*)-Cbz-*N*-3-amino-1,2-propanediol, **7E** – (*R*)-Cbz-*N*-3-amino-1,2-propanediol,
7F – Cbz-*N*-3-amino-2-hydroxypropanal, **7G** – Cbz-*N*-6-amino-1,3,4,5-tetrahydroxy-hexan-2-one
7H – 3-Chloro-1,2-propanediol (racemic mixture), **7I** – (*S*)-3-Chloro-1,2-propanediol, **7J** – (*R*)-3-Chloro-1,2-propanediol

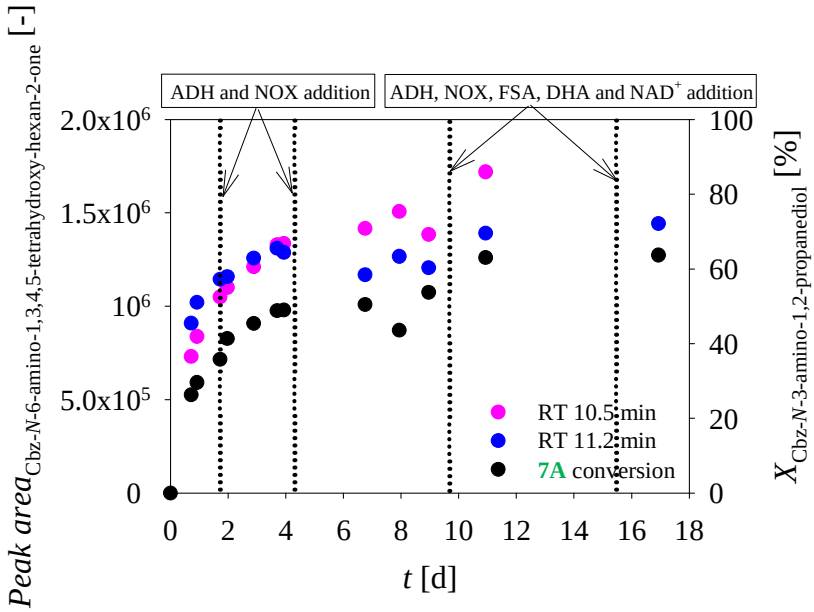

Figure 7.22 Addition of enzyme(s), DHA and NAD^+ in the cascade reaction to improve substrate conversion (50 mM TEA HCl buffer, pH 8.0, 25 °C, 1000 rpm , $V_{reactor}$ = 1.2 mL, $c_{NAD^+,0}$ = 1 mM, $c_{DHA,0}$ = 50 mM, $\gamma_{HLADH,0}$ = 10.0 mg mL^{-1}, γ_{NOX} = 0.10 mg mL^{-1}, γ_{FSA} = 2.0 mg mL^{-1}, c_{7A} = 20 mM).

It was shown that by using this approach diol **7A** conversion was increased up to 64% (from max. 50% in earlier experiments), and accordingly the increase in aldol adduct(s) **7G** concentration was noticed. These conditions, however, do not meet the necessary requirements for an industrial development. Efforts to optimize the HLADH/NOX/FSA^{A129S} cascade reaction were shown to be unsuccessful due to operational stability decay of enzymes.

7A – Cbz-*N*-3-amino-1,2-propanediol (racemic mixture), **7B** – (*S*)-3-Amino-1,2-propanediol,
7C – (*R*)-3-Amino-1,2-propanediol, **7D** – (*S*)-Cbz-*N*-3-amino-1,2-propanediol, **7E** – (*R*)-Cbz-*N*-3-amino-1,2-propanediol,
7F – Cbz-*N*-3-amino-2-hydroxypropanal, **7G** – Cbz-*N*-6-amino-1,3,4,5-tetrahydroxy-hexan-2-one
7H – 3-Chloro-1,2-propanediol (racemic mixture), **7I** – (*S*)-3-Chloro-1,2-propanediol, **7J** – (*R*)-3-Chloro-1,2-propanediol

7.5 Experimental procedures – Approach II

7.5.1 Screening for the most suitable oxido-reductase

For the second approach regarding iminosugar synthesis, several enzymes were tested for the use in first reaction step of 3-chloro-1,2-propanediol (**7H**) oxidation. These enzymes include horse liver alcohol dehydrogenase, yeast alcohol dehydrogenase, galactose oxidase and plate containing 192 oxido-reductases from Prozomix Ltd.

Activities of horse liver alcohol dehydrogenase and yeast alcohol dehydrogenase toward racemic **7H** were tested with standard NAD^+ dependent spectrophotometrical assay. Plate assay containing 192 oxido-reductases received from Prozomix (UK) were screened on **7H**.

Galactose oxidase (GOD) activity assay with 3,3′-dimethoxybenzidine (*o*-Dianisidine) as peroxidase substrate at 436 nm was firstly used (Boehringer Mannheim GmbH, 1973; Findrik & Vasić-Rački, 2007). The assay was not appropriate for this reaction due to brown color of enzyme solution. Therefore, another assay found in literature (Boehringer Mannheim GmbH, 1973; Pedersen et al., 2015) that uses ABTS (2,2'-azino-bis(3-ethylbenzothiazoline-6-sulphonic acid)) as peroxidase substrate at 420 nm was tested. This assay was appropriate and therefore the activity of GOD was measured this way that is described in detail in the next chapter.

7.5.2 Kinetics of 7H oxidation catalysed by galactose oxidase

Buffer used for kinetic measurements and reactions was 100 mM sodium phosphate buffer, pH 7.0. The content of the cuvette for spectrophotometric measurement of galactose oxidase activity is presented in Table 7.9.

Table 7.9 The content of the cuvette for spectrophotometric measurement of galactose oxidase activity.

Compound	Value	Unit
7H	0 - 800	mM
ABTS	8.7	mM
Cu^{2+}	0.015	mM
Galactose oxidase	1	mg mL^{-1}
Peroxidase	1990	U mg^{-1}

7A – Cbz-*N*-3-amino-1,2-propanediol (racemic mixture), **7B** – (*S*)-3-Amino-1,2-propanediol,
7C – (*R*)-3-Amino-1,2-propanediol, **7D** – (*S*)-Cbz-*N*-3-amino-1,2-propanediol, **7E** – (*R*)-Cbz-*N*-3-amino-1,2-propanediol,
7F – Cbz-*N*-3-amino-2-hydroxypropanal, **7G** – Cbz-*N*-6-amino-1,3,4,5-tetrahydroxy-hexan-2-one
7H – 3-Chloro-1,2-propanediol (racemic mixture), **7I** – (*S*)-3-Chloro-1,2-propanediol, **7J** – (*R*)-3-Chloro-1,2-propanediol

The influence of (*S*)-3-chloro-1,2-propanediol (**7I**) and (*R*)-3-chloro-1,2-propanediol (**7J**) concentration on galactose oxidase activity was measured separately to determine if the enzyme is enantioselective, and to estimate the values of kinetic constants.

Since oxidation requires oxygen (Scheme 7.3), the influence of oxygen concentration on galactose oxidation activity was measured. 58 mM solution of **7I** in buffer was prepared and mixed on magnetic stirrer at 300 rpm. Its volume was 20 mL. The concentration of oxygen in the solution was regulated by nitrogen and airflow and followed by oxygen probe. 856 μL of alcohol solution is taken from the solution at known oxygen concentration and put in the cuvette. 144 μL of previously prepared mixture that contains all compounds according to assay (Table 7.9) was introduced in cuvette when spectrophotometric measurement immediately started at 420 nm. Enzyme activity was calculated from the linear slope at the beginning of the reaction according to the Equations 7.1 and 7.2.

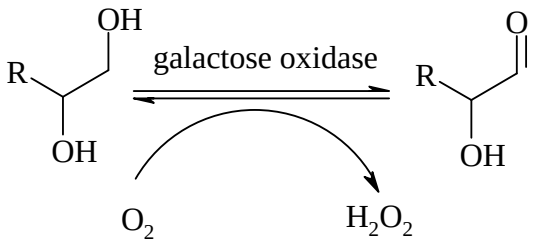

Scheme 7.3 Oxidation of diol catalysed by galactose oxidase.

7.5.3 Enzymatic 3-chloro-1,2-propanediol oxidation and cascade reaction

Oxidation reaction alone and cascade reaction (Scheme 7.4) were performed and followed by HPLC. Evolving peaks were detected in both reactions. Samples from cascade reactions were analysed by LC-MS as well to see if any of the evolving peaks correspond to targeted aldol adduct.

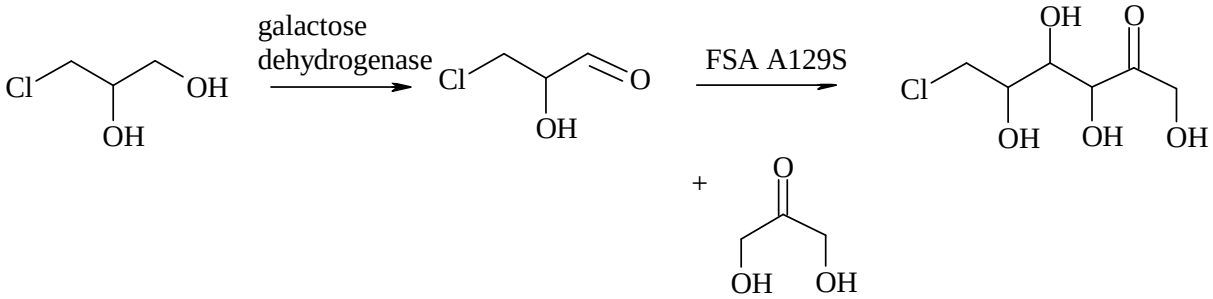

Scheme 7.4 Reaction scheme of the cascade iminosugar precursor synthesis – Approach II.

7A – Cbz-*N*-3-amino-1,2-propanediol (racemic mixture), **7B** – (*S*)-3-Amino-1,2-propanediol,
7C – (*R*)-3-Amino-1,2-propanediol, **7D** – (*S*)-Cbz-*N*-3-amino-1,2-propanediol, **7E** – (*R*)-Cbz-*N*-3-amino-1,2-propanediol,
7F – Cbz-*N*-3-amino-2-hydroxypropanal, **7G** – Cbz-*N*-6-amino-1,3,4,5-tetrahydroxy-hexan-2-one
7H – 3-Chloro-1,2-propanediol (racemic mixture), **7I** – (*S*)-3-Chloro-1,2-propanediol, **7J** – (*R*)-3-Chloro-1,2-propanediol

The conditions of the oxidation were as follows. Oxidation reaction volume was 1 mL. Reaction contained **7I** (189.6 µL of 1.055 M stock solution, 200 mM in the reaction), Cu^{2+} (10 µL of 5 mM stock solution, 0.05 mM in the reaction), galactose oxidase (100 µL of 100 mg mL^{-1} stock solution, 10 mg mL^{-1} in the reaction) and 717.6 µL of 100 mM sodium phosphate pH 7 buffer.

The conditions of the cascade reaction were as follows. First reaction step of a cascade was **7I** oxidation catalysed by galactose oxidase. Second reaction step is the aldol addition catalysed by FSA^{A129S} where dihydroxyacetone was introduced. Cascade reaction volume was 1 mL. Reaction contained **7I** (189.6 µL of 1.055 M stock solution, 200 mM in the reaction), Cu^{2+} (10 µL of 5 mM stock solution, 0.05 mM in the reaction), galactose oxidase (100 µL of 100 mg mL^{-1} stock solution, 10 mg mL^{-1} in the reaction), dihydroxyacetone (500 µL of 400 mM stock solution, 200 mM in the reaction), FSA^{A129S} (150 µL of 33.33 mg mL^{-1} stock solution, 5 mg mL^{-1} in the reaction), 50 µL of catalase from bovine liver (aqueous suspension, 10,000-40,000 units mg^{-1} protein). All solutions were made in 100 mM sodium phosphate pH 7.0 buffer. Catalase was added to the cascade with the purpose of eliminating evolved hydrogen peroxide.

7.5.4 3-Chloro-1,2-propanediol chemical oxidation and enzymatic aldol addition

Combination of chemical alcohol oxidation coupled with enzymatic aldol addition was the next approach in finding the pathway to synthesise the precursor of the iminosugar (Scheme 7.5). Chemical oxidation used 2-iodoxybenzoic acid (IBX) as oxidation agent.

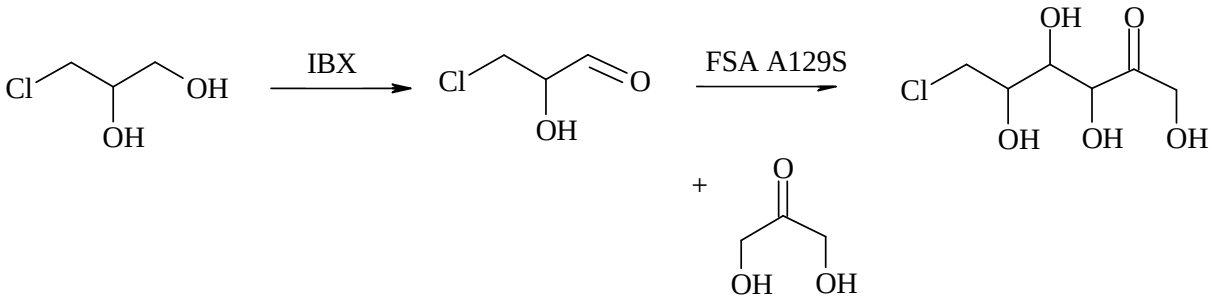

Scheme 7.5 Chemical **7H** oxidation coupled with enzymatic aldol addition reaction scheme.

7A – Cbz-*N*-3-amino-1,2-propanediol (racemic mixture), **7B** – (*S*)-3-Amino-1,2-propanediol,
7C – (*R*)-3-Amino-1,2-propanediol, **7D** – (*S*)-Cbz-*N*-3-amino-1,2-propanediol, **7E** – (*R*)-Cbz-*N*-3-amino-1,2-propanediol,
7F – Cbz-*N*-3-amino-2-hydroxypropanal, **7G** – Cbz-*N*-6-amino-1,3,4,5-tetrahydroxy-hexan-2-one
7H – 3-Chloro-1,2-propanediol (racemic mixture), **7I** – (*S*)-3-Chloro-1,2-propanediol, **7J** – (*R*)-3-Chloro-1,2-propanediol

The protocol was as follows. **7H** was diluted in 48 mL of ethyl acetate (192 mM alcohol in the reaction). 2.5 g of IBX (44.5 % purity of commercial chemical was taken into account) was added to the solution. At the point of reaching the temperature of 77°C the oxidation started. Reaction was performed in water bath with magnetic stirring. Samples were taken during reaction and analysed by GC monitoring alcohol concentration. Reaction was stopped after 9 hours by filtration where crude IBX was removed. Acidic residues of IBX in the solution were removed by adding 1 g of sodium bicarbonate. Reaction mixture was stirred and again filtrated. Afterwards, the two-phase aldol addition was started. Organic phase was ethyl acetate containing evolved aldehyde and unconverted alcohol. Water phase contained 2 mg mL^{-1} of FSA^{A129S} and 250 mM of dihydroxyacetone dissolved in 37.5 mL of 50 mM TEA HCl buffer pH 7.5. The idea was that during ethyl acetate evaporation on rotary evaporator aldehyde crosses to water phase where aldol addition occurs. During the reaction samples were withdrawn from water phase, derivatized with $BnONH_2 \cdot HCl$ (details in Chapter 5.2.3.1) for HPLC and LC-MS analysis.

7A – Cbz-*N*-3-amino-1,2-propanediol (racemic mixture), **7B** – (*S*)-3-Amino-1,2-propanediol,
7C – (*R*)-3-Amino-1,2-propanediol, **7D** – (*S*)-Cbz-*N*-3-amino-1,2-propanediol, **7E** – (*R*)-Cbz-*N*-3-amino-1,2-propanediol,
7F – Cbz-*N*-3-amino-2-hydroxypropanal, **7G** – Cbz-*N*-6-amino-1,3,4,5-tetrahydroxy-hexan-2-one
7H – 3-Chloro-1,2-propanediol (racemic mixture), **7I** – (*S*)-3-Chloro-1,2-propanediol, **7J** – (*R*)-3-Chloro-1,2-propanediol

7.6 Results and discussion – Approach II

7.6.1 Screening for the most suitable oxido-reductase

Horse liver alcohol dehydrogenase (Sigma Aldrich) and yeast alcohol dehydrogenase showed no activity toward **7H** during standard NAD^+ spectrophotometrical assay. Therefore, these enzymes were excluded from further research of iminosugar precursor synthesis from **7H** as starting substrate.

Two enzymes (KRED 6 and KRED 30) from tested oxido-reductase panel containing 192 enzymes were further investigated due to positive test outcomes. The influence of alcohol concentration and NAD^+ concentration on reaction rate was measured and kinetic parameters were estimated and presented in Table 7.10.

Table 7.10 Maximum specific activities of tested oxido-reductase KRED 6 and KRED 30 for the oxidation of **7H**.

Parameter	Unit	Value
$V_m^{\text{KRED 6}}$	U mg^{-1}	0.0028 ± 0.0001
$K_m^{\text{KRED 6}}$	mM	7.74 ± 1.62
$K_m^{\text{NAD+ (KRED 6)}}$	mM	0.32 ± 0.06
$V_m^{\text{KRED 30}}$	U mg^{-1}	0.0016 ± 0.00004
$K_m^{\text{KRED 30}}$	mM	9.41 ± 0.94
$K_m^{\text{NAD+ (KRED 30)}}$	mM	0.059 ± 0.012
$K_i^{\text{NAD+ (KRED 30)}}$	mM	26.38 ± 9.12

Since the activity of galactose oxidase was two orders of magnitude higher than activity of both selected KREDs (Table 7.11), detailed **7H** oxidation kinetic measurements were performed by using galactose oxidase (GOD).

Table 7.11 Maximum specific activities of tested enzymes for the oxidation of **7H**.

Enzyme	V_m [U mg^{-1}]
HLADH	0
YADH	0
KRED 6	0.0028
KRED 30	0.0016
GOD	0.27

7A – Cbz-*N*-3-amino-1,2-propanediol (racemic mixture), **7B** – (*S*)-3-Amino-1,2-propanediol,
7C – (*R*)-3-Amino-1,2-propanediol, **7D** – (*S*)-Cbz-*N*-3-amino-1,2-propanediol, **7E** – (*R*)-Cbz-*N*-3-amino-1,2-propanediol,
7F – Cbz-*N*-3-amino-2-hydroxypropanal, **7G** – Cbz-*N*-6-amino-1,3,4,5-tetrahydroxy-hexan-2-one
7H – 3-Chloro-1,2-propanediol (racemic mixture), **7I** – (*S*)-3-Chloro-1,2-propanediol, **7J** – (*R*)-3-Chloro-1,2-propanediol

7.6.2 Kinetics of the oxidation of 7H catalysed by galactose oxidase

Kinetics of the oxidation of both 3-chloro-1,2-propanediol enantiomers catalysed by galactose oxidase are shown on Figure 7.23. Figure 7.24 presents the influence of oxygen concentration on galactose oxidase activity.

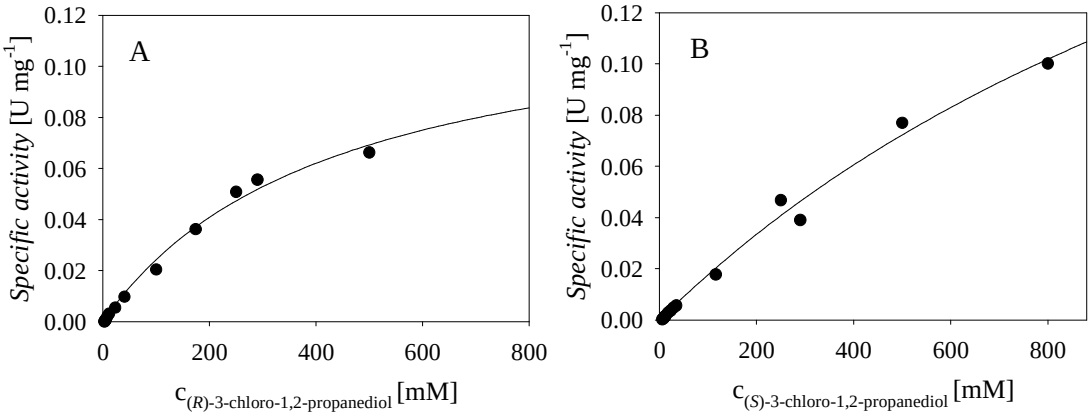

Figure 7.23 Kinetics of A. (*R*)-3-chloro-1,2-propanediol (**7J**) and B. (*S*)-3-chloro-1,2-propanediol (**7I**) oxidation catalysed by galactose oxidase (0.1 M sodium-phosphate buffer pH 7.0, 25 °C, γ_{GOD} = 1 mg mL^{-1}, $\gamma_{peroxidase}$ = 0.027 mg mL^{-1}, c_{CuCl2} = 0.015 mM, c_{ABTS} = 8.7 mM). Legend: black circles – experimental data, line – model.

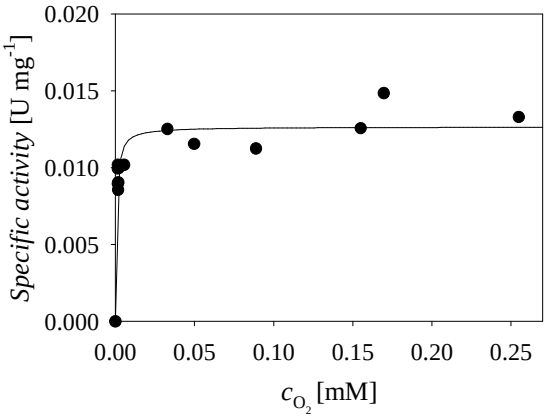

Figure 7.24 Influence of oxygen concentration on galactose oxidase specific activity (0.1 M sodium-phosphate buffer pH 7.0, 25 °C, γ_{GOD} = 1 mg mL^{-1}). Legend: black circles – experimental data, line – model.

Although the enzyme contains copper in its structure, the literature (Pedersen et al., 2015) suggests it is possible that it is lost from the structure during reaction. The influence of copper ions (Cu^{2+}) on reaction rate was therefore tested. The results are presented in Figure

7A – Cbz-*N*-3-amino-1,2-propanediol (racemic mixture), **7B** – (*S*)-3-Amino-1,2-propanediol,
7C – (*R*)-3-Amino-1,2-propanediol, **7D** – (*S*)-Cbz-*N*-3-amino-1,2-propanediol, **7E** – (*R*)-Cbz-*N*-3-amino-1,2-propanediol,
7F – Cbz-*N*-3-amino-2-hydroxypropanal, **7G** – Cbz-*N*-6-amino-1,3,4,5-tetrahydroxy-hexan-2-one
7H – 3-Chloro-1,2-propanediol (racemic mixture), **7I** – (*S*)-3-Chloro-1,2-propanediol, **7J** – (*R*)-3-Chloro-1,2-propanediol

7.25. It was found that in the concentration range from 0.002 mM to 0.05 mM it has no effect on oxidation rate.

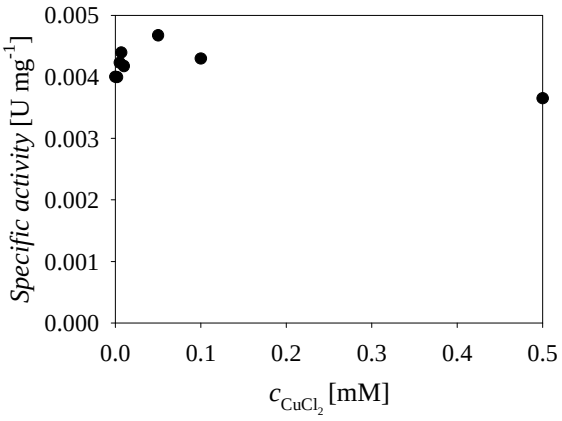

Figure 7.25 Influence of copper ions concentration on galactose oxidase specific activity (0.1 M sodium-phosphate buffer pH 7.0, 25 °C, γ_{GOD} = 1 mg mL^{-1}).

Estimated kinetic parameters for **7A** oxidation by GOD are presented in Table 7.12. It can be seen from presented data that the enzyme is not enantioselective and has low affinity toward substrate (K_m [7I] and K_m [7J]). The enzyme has high affinity toward oxygen so only a small concentration of oxygen in the reaction solution is sufficient for achieving maximum enzyme activity.

Table 7.12 Estimated kinetic parameters for **7A** oxidation catalysed by galactose oxidase.

Parameter	Unit	Value
V_m [7I]	U mg^{-1}	0.320 ± 0.068
K_m [7I]	mM	1716.1 ± 486.8
V_m [7J]	U mg^{-1}	0.275 ± 0.038
K_m [7J]	mM	1146.3 ± 192.1
$K_m^{O_2}$	mM	0.613± 0.131

7.6.3 Enzymatic 3-chloro-1,2-propanediol oxidation and cascade reaction

Oxidation reaction alone and cascade reaction (Scheme 7.25) were performed and followed by HPLC. Several unidentified peaks evolving were detected in both reactions.

LC-MS analysis had not confirmed the presence of aldol adduct in analysed samples. Since the concentration of dihydroxyacetone decreases during cascade, additional kinetic measurement was performed to see if galactose oxidase shows activity toward

7A – Cbz-*N*-3-amino-1,2-propanediol (racemic mixture), **7B** – (*S*)-3-Amino-1,2-propanediol,
7C – (*R*)-3-Amino-1,2-propanediol, **7D** – (*S*)-Cbz-*N*-3-amino-1,2-propanediol, **7E** – (*R*)-Cbz-*N*-3-amino-1,2-propanediol,
7F – Cbz-*N*-3-amino-2-hydroxypropanal, **7G** – Cbz-*N*-6-amino-1,3,4,5-tetrahydroxy-hexan-2-one
7H – 3-Chloro-1,2-propanediol (racemic mixture), **7I** – (*S*)-3-Chloro-1,2-propanediol, **7J** – (*R*)-3-Chloro-1,2-propanediol

dihydroxyacetone. The results of that measurement are shown in Figure 7.26 and estimated kinetic parameters in Table 7.13.

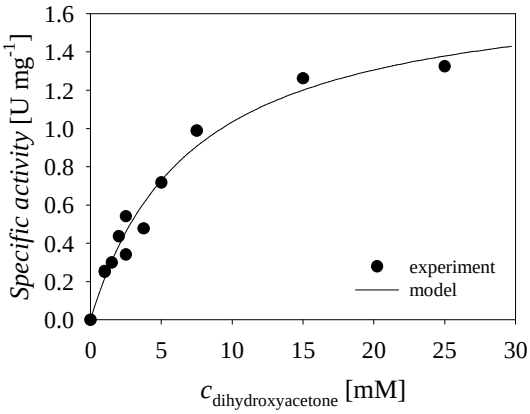

Figure 7.26 Influence of dihydroxyacetone on galactose oxidase activity (pH 7.0, 25 °C, γ_{GOD}= 20 mg/mL).

Table 7.13 Estimated kinetic parameters for DHA oxidation catalysed by galactose oxidase.

Parameter	**Unit**	**Value**
V_m	U mg^{-1}	1.774 ± 0.130
K_m^{DHA}	mM	7.167 ± 1.137

The results of kinetic measurements of DHA (Table 7.13) oxidation catalysed by galactose oxidase showed that enzyme has higher activity in reaction with DHA compared to both chloropropanediol enantiomers **7I** and **7J**. In addition, enzyme's affinity (lower K_m value) is much higher toward DHA. Hence, DHA that acts as an oxidation substrate makes proposed cascade (Schemes 7.2 and 7.4) ineffective and explains why desired aldol cannot evolve.

Consecutive reactions approach where chloropropanediol oxidation would finish and afterward FSA and DHA would be introduced to reaction to start second step of aldol addition also cannot work based on HPLC and LC-MS peaks analysis. Namely, no aldehyde peak was detected in oxidation and that confirmed that oxidation reaction alone is not successful.

These findings suggested that by using combination of chemical alcohol oxidation and enzymatic aldol addition discovered challenges could be resolved in order to synthesise iminosugar precursor.

7A – Cbz-*N*-3-amino-1,2-propanediol (racemic mixture), **7B** – (*S*)-3-Amino-1,2-propanediol,
7C – (*R*)-3-Amino-1,2-propanediol, **7D** – (*S*)-Cbz-*N*-3-amino-1,2-propanediol, **7E** – (*R*)-Cbz-*N*-3-amino-1,2-propanediol,
7F – Cbz-*N*-3-amino-2-hydroxypropanal, **7G** – Cbz-*N*-6-amino-1,3,4,5-tetrahydroxy-hexan-2-one
7H – 3-Chloro-1,2-propanediol (racemic mixture), **7I** – (*S*)-3-Chloro-1,2-propanediol, **7J** – (*R*)-3-Chloro-1,2-propanediol

7.6.4 3-Chloro-1,2-propanediol chemical oxidation and enzymatic aldol addition

Conversion of alcohol in chemical oxidation with IBX was 51% after 8.5 hours of reaction at 77°C. The reaction did not progress anymore.

Evaporation lasted for 3 hours and 45 minutes during which samples are taken for HPLC and LC-MS analysis. HPLC analysis showed different peaks evolving. However, LC-MS analysis confirmed none of the peaks corresponded to targeted aldehyde (molecular mass of derivatized aldehyde is 214 g mol^{-1}) or aldol (molecular mass of derivatized aldol is 304 g mol^{-1}) molecular masses. On the other hand, peak of dihydroxyacetone (196 g mol^{-1}) is clearly confirmed by MS.

There are several possible explanations why performed synthesis did not result in aldol adduct formation. Ethyl acetate dissolves in water up to 8% that can have a negative impact on FSA activity (Sudar et al., 2013). In addition, since aldehyde and aldol molecules are not commercially available, kinetic measurements could not be done. Therefore, there is a possibility that aldehyde inhibits aldol addition in higher concentrations. Aldehyde can be instable in organic and/or water phase, too. Furthermore, unconverted alcohol from oxidation step could cause FSA inhibition. Data from analogue system show that concentration of 80 mM Cbz protected aminoalcohol caused approx. 50% FSA^{A129S} activity loss. In addition, it is possible that 2 mg mL^{-1} of FSA was insufficient for successful aldol addition. Finally, FSA may not be active on this substrate because this or similar molecules have not been tested as FSA substrates (Clapés et al., 2010).

7A – Cbz-*N*-3-amino-1,2-propanediol (racemic mixture), **7B** – (*S*)-3-Amino-1,2-propanediol,
7C – (*R*)-3-Amino-1,2-propanediol, **7D** – (*S*)-Cbz-*N*-3-amino-1,2-propanediol, **7E** – (*R*)-Cbz-*N*-3-amino-1,2-propanediol,
7F – Cbz-*N*-3-amino-2-hydroxypropanal, **7G** – Cbz-*N*-6-amino-1,3,4,5-tetrahydroxy-hexan-2-one
7H – 3-Chloro-1,2-propanediol (racemic mixture), **7I** – (*S*)-3-Chloro-1,2-propanediol, **7J** – (*R*)-3-Chloro-1,2-propanediol

7.7 Conclusions

Two strategies for biocatalytic production of iminosugars *Miglustat* and *Miglitol* precursor are examined within this doctoral thesis. One approach suggested Cbz-*N*-3-amino-1,2-propanediol as a starting oxidation substrate. Second approach involved 3-chloro-1,2-propanediol as substrate for oxidation.

In the first approach, from all tested oxido-reductases, horse liver alcohol dehydrogenase showed highest activity toward suggested substrate. Detailed kinetic investigation showed that this enzyme is not enantioselective. The highest k_{cat}/K_m value was achieved with (*S*)-Cbz-*N*-3-amino-1,2-propanediol. For the aldol addition, FSA^{A129S} variant was used and NADH oxidase for coenzyme regeneration. Since suggested reaction system includes intermediate and target product, which are not commercially available, LC-MS analysis was performed and confirmed that formed aldol adduct is the expected molecule. Initial cascade substrate concentration, initial NAD^+ concentration and HLADH/NOX ratios are independently tested in order to investigate its influence on product yield. It was found that the highest substrate conversion was achieved with 20 mM initial alcohol concentration. Concentration of 1 mM NAD^+ and HLADH/NOX ratio of 30 showed the best results. Cascade reaction was performed with the aim of achieving the highest alcohol conversion by adding fresh amounts of enzymes and reaction compounds during the reaction. It was shown that by using this approach Cbz-*N*-3-amino-1,2-propanediol conversion was increased up to 64% (from max. 50% in earlier experiments), and accordingly the increase in aldol adduct concentration was noticed. Still, an increase was not that significant when the amount of enzymes re-added to the reactor is considered. These conditions, however, do not meet the necessary requirements for an industrial development. It can be concluded that impossibility of detailed kinetic measurement due to lack of pure intermediate and aldol adduct was the main issue of this proposed biocatalytic synthesis of the iminosugar precursor.

Second iminosugar precursor synthesis strategy considered 3-chloro-1,2-propanediol as cascade starting substrate. Galactose oxidase from *Dactylium dendroides* had the highest activity toward this substrate from all considered oxido-reductases. Kinetic measurements with (*S*)- and (*R*)-3-chloro-1,2-propanediol showed that the enzyme is not enantioselective. In this case, detailed kinetic measurements could not be performed as well due to unavailability of intermediate and product that could be used for kinetic experiments. This research can be continued once these compounds become available. By performing biocatalytic cascade of

7A – Cbz-*N*-3-amino-1,2-propanediol (racemic mixture), **7B** – (*S*)-3-Amino-1,2-propanediol,
7C – (*R*)-3-Amino-1,2-propanediol, **7D** – (*S*)-Cbz-*N*-3-amino-1,2-propanediol, **7E** – (*R*)-Cbz-*N*-3-amino-1,2-propanediol,
7F – Cbz-*N*-3-amino-2-hydroxypropanal, **7G** – Cbz-*N*-6-amino-1,3,4,5-tetrahydroxy-hexan-2-one
7H – 3-Chloro-1,2-propanediol (racemic mixture), **7I** – (*S*)-3-Chloro-1,2-propanediol, **7J** – (*R*)-3-Chloro-1,2-propanediol

oxidation by galactose oxidase and aldol addition by FSA^{A129S} no expected results were collected because the targeted molecules were not detected by LC-MS analysis. Another approach was tested that included chemical oxidation of alcohol coupled with enzymatic aldol addition. Aldol peak was not detected by LC-MS analysis and no further research was done regarding this precursor synthesis approach.

It is important to emphasize that both approaches major drawbacks are caused by incomplete kinetic measurements due to the unavailability of intermediates and final product molecules in the time the research was conducted. In addition, due to instability of such molecules, the attempts of their isolation within this research failed. Results obtained in research of Approach I could be completed once needed chemicals become commercially available. In this case, with mathematical model development, better understanding of the process would be possible and it could be used for process optimization that would increase so far the best result of 64% substrate conversion in a cascade reaction.

7A – Cbz-*N*-3-amino-1,2-propanediol (racemic mixture), **7B** – (*S*)-3-Amino-1,2-propanediol,
7C – (*R*)-3-Amino-1,2-propanediol, **7D** – (*S*)-Cbz-*N*-3-amino-1,2-propanediol, **7E** – (*R*)-Cbz-*N*-3-amino-1,2-propanediol,
7F – Cbz-*N*-3-amino-2-hydroxypropanal, **7G** – Cbz-*N*-6-amino-1,3,4,5-tetrahydroxy-hexan-2-one
7H – 3-Chloro-1,2-propanediol (racemic mixture), **7I** – (*S*)-3-Chloro-1,2-propanediol, **7J** – (*R*)-3-Chloro-1,2-propanediol

8 THESIS CONCLUSIONS

Biocatalysis is in focus due to its use for the synthesis of pharmaceuticals making manufacturing processes more sustainable. In recent years, much interest has been shown in the use of multi-enzyme cascades as a tool in organic synthesis. Reaction engineering methodology was used in this thesis for describing and optimizing three separate biocatalytic cascade reaction systems. The link between all cascades is the use of carbon–carbon bond forming enzyme in one reaction step per cascade.

Cascade reaction where three enzymes were involved, is a novel approach for synthesis of 3-hydroxyisobutyric acid, a methacrylic acid precursor used as important intermediate for the preparation of polymers. Proposed biocatalytic synthesis of 3-hydroxyisobutyric acid can be performed by an aldolase-catalysed aldol addition of propanal to formaldehyde followed by an enzymatic oxidation of the resulting 3-hydroxy-2-methylpropanal to 3-hydroxyisobutyric acid. From three tested aldolases FSA variants, FSA variant D6Q was chosen as the most suitable enzyme to continue the optimization of aldol addition with since it has high activity towards both substrates in large concentration range. It was found that the kinetics of the aldol addition catalysed by FSA^{D6Q} can be described by double substrate Michaelis-Menten kinetics. Because of enzyme inhibitions and operational stability decay, fed-batch was chosen as the best reactor choice for this reaction. Mathematical model that was developed for the first reaction step of aldol addition was used for the reaction optimization. At the optimal process conditions, the product concentration after 5.5 hours was 814 mM (72 g L^{-1}), product yield was 88.5% and volume productivity was 313.7 g L^{-1} d^{-1}. Since aldehyde dehydrogenase accepts propanal and formaldehyde as substrates, this cascade could not be performed in a one-pot synthesis, but consecutive, by starting oxidation after aldol addition was completed. Detailed oxidation kinetics was measured with aldehyde dehydrogenase 003 as catalyst and developed mathematical model of oxidation with coenzyme regeneration by NADH oxidase described the experimental data well. The yield on product 3-hydroxy-2-methylpropanoic acid depended on concentration of formaldehyde and propionaldehyde left in the produced aldol. The higher initial concentration, the lower was the product yield. With the increase of enzyme concentration, reaction rate increases as well, but it also accelerates by-product formation. It is therefore possible to achieve 100% conversion of substrate but not 100% of product yield. Performed one-pot consecutive enzymatic oxidation catalysed by AlDH 003 where complete consumption of 3-hydroxy-2-

methylpropanal occured, resulted in final concentration of 3-hydroxy-2-methylpropanoic acid of 24 mM. A panel of 24 different aldehyde dehydrogenases was tested and it was found that five of them gave higher product yield than AlDH 003. The highest potential for future oxidation investigation and optimization gives aldehyde dehydrogenase 41. At this point, the highest product yield corresponds to 66.5% and product concentration of 26.32 mM was obtained. Future research should be focused on the optimization of this reaction. It was confirmed by NMR analysis that proposed enzymatic cascade scheme produced desired product, 3-hydroxy-2-methylpropanoic acid, a methacrylic acid precursor. Therefore, this research proposed and demonstrated a functional new biocatalytic pathway that undoubtedly produces targeted precursor as final product.

The synthesis of L-homoserine in the reaction system consisting of transaminase and aldolase starting from pyruvate, formaldehyde and L-alanine was studied. Detailed kinetic measurements and parameters estimation was done separately for reactions catalysed by CFE enzymes and for reactions catalysed by *E. coli* cells that contained both enzymes and their comparison is made. Reactions catalysed by separate enzymes (cell free extracts) and *E. coli* cells containing the same co-expressed enzymes were optimized using mathematical model. Optimized reaction in the fed-batch reactor with continuous formaldehyde feed and two additions of L-alanine and pyruvate up to their initial concentrations produced 672 mM (80.1 g L^{-1}) of L-homoserine after 25 hours of reaction with volume productivity of 3.2 g L^{-1} h^{-1} and yield of 60% when cell free extract enzymes were used as biocatalysts. Optimized reaction with same initial conditions resulted in 640.74 mM (76.3 g L^{-1}) of L-homoserine after 29.25 hours with volume productivity of 2.6 g L^{-1} h^{-1} and yield of 65% when whole cell biocatalyst was used. Obtained process metrics presents a result that fulfils minimum industrial requirements and therefore has the potential for up-scale and industrial use. These two results are similar and confirm the same system behaviour. They also show that by determing enzyme kinetics of CFEs conclusions can be drawn for the whole-cell system. Industrial project partners confirmed that optimized process set-up and approach presented within this research produces expected results on a larger scale that can be considered as external confirmation of mathematical model development and process optimization.

Research of both approaches for iminosugar precursor synthesis was limited due to inability of measuring all kinetics. Mathematical model that would describe these systems well could not be developed due to unknown reaction components interactions. Nevertheless, approach using Cbz–protected amino alcohol as substrate can be considered as a solid proof

of concept due to MS confirmation of produced target molecule with 64% substrate conversion in the most successful attempt of cascade reaction. Approach with 3-chloro-1,2-propanediol as starting substrate was tested by enzymatic cascade reaction and chemo-enzymatic process. Both trials did not produce product of interest and this approach was abandoned.

Overall, it can be concluded that from three investigated novel enzymatic cascade systems, two of them were successfully performed and described by mathematical models and afterwards optimized toward reaching set goals. The third system's potential was not fulfilled due to previously mentioned obstacles. This thesis can be used as a basis for process scale-up for L-homoserine and methacrylic acid precursor synthesis since developed validated models give valuable information for process scale-up.

9 REFERENCES

1. Abu R., Gundersen M., Woodley J. M., Thermodynamic calculations for systems biocatalysis, *Comput.-Aided. Chem. En.*, 2015, 37, 233-238, doi: https://doi.org/10.1016/B978-0-444-63578-5.50034-7.
2. Abu R., Woodley J. M., Application of enzyme coupling reactions to shift thermodynamically limited biocatalytic reactions, *ChemCatChem.*, 2015 7(19), 3094-3105, doi: https://doi.org/10.1002/cctc.201500603.
3. Adrio J.-L., Demain A. L., Recombinant organisms for production of industrial products, *Bioengineered Bugs*, 2009, 1(2), 166-161, doi: https://doi.org/10.4161/bbug.1.2.10484.
4. Agudo R., Reetz M. T., Designer cells for stereocomplementary *de novo* enzymatic cascade reactions based on laboratory evolution, *Chem. Commun.*, 2013, 49(93), 10914-10916, doi: https://doi.org/10.1039/C3CC46229C.
5. Asano N., et al., Sugar-mimic glycosidase inhibitors: natural occurrence, biological activity and prospects for therapeutic application, *Tetrahedron.-Asymmetr.* 2000, 11(8), 1645-1680, doi: https://doi.org/10.1016/S0957-4166(00)00113-0.
6. Bailey J., et al., Biochemical Engineering Fundamentals, New York : McGraw-Hill Inc., 1977, 132-135.
7. Barnicki S. D., Bommaraju T. V., Kent J. A., Handbook of industrial chemistry and biotechnology, Cham : Springer International Publishing AG, 2017.
8. Berg J. M., Tymoczko J. L., Stryer L., Biochemistry, 5. ed., New York : W. H. Freeman, 2002.
9. Boehringer Mannheim GmbH, Biochemica information I, Mannheim : Boehringer Mannheim GmbH, 1973, 41.
10. Boehringer Mannheim GmbH, Biochemica information II, Mannheim : Boehringer Mannheim GmbH, 1975, 25-26.
11. Bradford M. M., A rapid and sensitive method for the quantitation of microgram quantities of protein utilizing the principle of protein-dye binding, *Anal. Biochem.*, 1976, 72(1-2), 248-254, doi: https://doi.org/10.1016/0003-2697(76)90527-3.
12. Brass J. M., Hoeks F. W. J. M. M., Rohner M., Application of modelling techniques for the improvement of industrial bioprocesses, *J. Biotechnol.*, 1997, 59(1-2), 63-72, doi: https://doi.org/10.1016/S0168-1656(97)00165-X.

13. Breuer M., Bonnekessel M., Schneider N., 9.14 Industrial Applications of Asymmetric Biocatalytic C–C Bond Forming Reactions, IN: Cerreira E. M., Yamamoto H. (ed.), *Comprehensive Chirality*, 2012, 9, 342-352, doi: https://doi.org/10.1016/B978-0-08-095167-6.00915-0.
14. Bruggink A., Schoevaart R., Kieboom T., Concepts of nature in organic synthesis: cascade catalysis and multistep conversions in concert, *Org. Process Res. Dev.,* 2003, 7(5), 622-640, doi: https://doi.org/10.1021/op0340311.
15. Busto E., Recent developments in the preparation of carbohydrate derivatives from achiral building blocks by using aldolases, *ChemCatChem.*, 2016, 8(16), 2589-2598, doi: https://doi.org/10.1002/cctc.201600366.
16. Campbell A., Le Châtelier's principle, temperature effects, and entropy, *J. Chem. Educ.*, 1985, 62(3), 231, doi: https://doi.org/10.1021/ed062p231.
17. Cavani F., et al., Main aspects of the selective oxidation of isobutane to methacrylic acid catalyzed by Keggin-type polyoxometalates, *Catal. Today,* 2001, 71(1-2), 97-110, doi: https://doi.org/10.1016/S0920-5861(01)00435-7.
18. Chautarf H., et al., An activity-independent selection system of thermostable protein variants, *Nat. Methods*, 2007, 4, 919-921.
19. Chenault H. K., Whitesides G. M., Regeneration of nicotinamide cofactors for use in organic synthesis, *Appl. Biochem. Biotech.,* 1987, 14(2), 147-197, doi: https://doi.org/10.1007/BF02798431.
20. Clapés P., Enzymatic C-C bond formation, IN: Goswami A., Stewart J. D. (ed.), Organic synthesis using biocatalysis, Elsevier, 2015, 285-335.
21. Clapés P., et al., Recent progress in stereoselective synthesis with aldolases, *Curr. Opin. Chem. Biol.*, 2010, 14(2), 154-167, doi: https://doi.org/10.1016/j.cbpa.2009.11.029.
22. Clapés P., Recent advances in enzyme-catalyzed aldol addition reactions, IN: Patel R. N. (ed.), Green biocatalysis, Hoboken, New Jersey : John Wiley & Sons, Inc., 2016, 267-306, doi: https://doi.org/10.1002/9781118828083.ch10.
23. Concia A. L., et al., D-fructose-6-phosphate aldolase in organic synthesis: cascade chemical-enzymatic preparation of sugar-related polyhydroxylated compounds, *Chem.-Eur. J.*, 2009, 15(15), 3808-3816, doi: https://doi.org/10.1002/chem.200802532.
24. Darabi Mahboub, M. J., et al., Gas phase oxidation of 2-methyl-1,3-propanediol to methacrylic acid over heteropolyacid catalysts, *Catal. Sci. Technol.*, 2016, 6(17), 6525-6535, doi: https://doi.org/10.1039/C6CY01025C.

25. Donati G., Paludetto R., Batch and semibatch catalytic reactors (from theory to practice), *Catal. Today*, 1999, 52(2-3), 183-195, doi: https://doi.org/10.1016/S0920-5861(99)00075-9.
26. D'Souza S. F., Microbial biosensors, *Biosens. Bioelectron.*, 2001, 16(6), 337-353.
27. Dunn I. J., et al., Biological reaction engineering: principles, applications and modelling with PC simulation, Weinheim : VCH Verlagsgesellschaft mbH, 1992, 67-109.
28. Fessner W. D., Systems Biocatalysis: development and engineering of cell-free "artificial metabolisms" for preparative multi-enzymatic synthesis, *New Biotechnol.*, 2015, 32(6), 658-664, doi: https://doi.org/10.1016/j.nbt.2014.11.007.
29. Findrik Blažević Z., et al., Kinetic models and optimization of enzymatic processes, IN: Fessner W. D., Theodoridou A. (ed.), *6th Novel Enzymes 2018*, 2018, 14.
30. Findrik Z., et al., Kinetic modeling of acetophenone reduction catalyzed by alcohol dehydrogenase from *Thermoanaerobacter* sp., *Biotechnol. Lett.*, 2005, 27(15), 1087-1095, doi: https://doi.org/10.1007/s10529-005-8455-y.
31. Findrik Z., Vasić-Rački Đ., Biotransformation of D-methionine into L-methionine in the cascade of four enzymes, *Biotechnol. Bioeng.*, 2007, 98(5), 956-967, doi: https://doi.org/10.1002/bit.21501.
32. Findrik Z., Vasić-Rački Đ., Overview on reactions with multi-enzyme systems, *Chem. Biochem. Eng. Q.*, 2009, 23(4), 545-553.
33. Garcia V., et al., Constrained optimization for fine chemical productions in batch reactors, *Chem. Eng. J. Bioch. Eng.*, 1995, 59(3), 229-241, doi: https://doi.org/10.1016/0923-0467(94)02949-0.
34. Garrabou X., et al., Asymmetric self- and cross-aldol reactions of glycolaldehyde catalyzed by D-fructose-6-phosphate aldolase, *Angew. Chem. Int. Edit.*, 2009, 48(30), 5521-5525, doi: https://doi.org/10.1002/anie.200902065.
35. Gomzi Z., Kemijski reaktori, Zagreb : Hinus, 1998, 48-96.
36. Grayson I., Kessler C., Modern applications of amino acids and dipeptides in pharmaceuticals and biopharmaceuticals, *Chim. Oggi.*, 2015, 33(5), 46-51.
37. Gundersen M. T., et al., A rapid selection procedure for simple commercial implementation of ω-transaminase reactions, *Org. Process Res. Dev.*, 2016, 20(3), 602-608, doi: https://doi.org/10.1021/acs.oprd.5b00159.
38. Gutierrez M., et al., Structure-guided redesign of D-fructose-6-phosphate aldolase from *E. coli*: remarkable activity and selectivity towards acceptor substrates by two-point

mutation, *Chem. Chommun.*, 2011, 47(20), 5762-5764, doi: https://doi.org/10.1039/C1CC11069A.

39. Hass, T., et al., Biotechnological preparation of 3-hydroxyisobutyric acid, 2015, US patent 2015/0218600 A1. Available at: https://patentimages.storage.googleapis.com/51/af/4a/d3335f1b5a3bce/US20150218600A1.pdf (21.3.2019.).
40. Hattori K., Sajiki H., Hirota K., Pd/C(en)-catalyzed chemoselective hydrogenation with retention of the N-Cbz protective group and its scope and limitations, *Tetrahedron*, 2000, 56(43), 8433-8441, doi: https://doi.org/10.1016/S0040-4020(00)00771-7.
41. Heiden St., et al., ChemBioTec – linking chemistry, biology and engineering, *J. Mol. Catal. B-Enzym.*, 2014, 103, 1, doi: https://doi.org/10.1016/j.molcatb.2014.02.011.
42. Heitzig M., et al., A computer-aided framework for development, identification and management of physiologically-based pharmacokinetic models, *Comput. Chem. Eng.*, 2014, 71, 677-698, doi: https://doi.org/10.1016/j.compchemeng.2014.07.016.
43. Hermann T., Industrial production of amino acids by coryneform bacteria, *J. Biotechnol.*, 2003, 104(1-3), 155-172, doi: https://doi.org/10.1016/S0168-1656(03)00149-4.
44. Hernández K., et al., Combining aldolases and transaminases for the synthesis of 2-amino-4-hydroxybutanoic acid, *ACS Catal.*, 2017a, 7(3), 1707-1711, doi: https://doi.org/10.1021/acscatal.6b03181.
45. Hernández K., et al., 2-keto-3-deoxy-L-rhamnonate aldolase (YfaU) as catalyst in aldol additions of pyruvate to amino aldehyde derivatives, *Adv. Synth. Catal.*, 2017b, 359(12), 2090-2100, doi: https://doi.org/10.1002/adsc.201700360.
46. Hirasawa T., Shimizu H., Recent advances in amino acid production by microbial cells, *Curr. Opin. Biotech.*, 2016, 42, 133-146, doi: https://doi.org/10.1016/j.copbio.2016.04.017.
47. Höhne M., et al., Efficient asymmetric synthesis of chiral amines by combining transaminase and pyruvate decarboxylase, *ChemBioChem*, 2008, 9(3), 363-365, doi: https://doi.org/10.1002/cbic.200700601.
48. Illanes A., et al., Recent trends in biocatalysis engineering, *Bioresource Technol.*, 2012, 115, 48-57, doi: https://doi.org/10.1016/j.biortech.2011.12.050.
49. Ishii N., et al., Dynamic simulation of an *in vitro* multi-enzyme system, *FEBS Lett.*, 2007, 581(3), 413-420, doi: https://doi.org/10.1016/j.febslet.2006.12.049.

50. Jana S., Deb J. K., Strategies for efficient production of heterologous proteins in *Escherichia coli*, *Appl. Microbiol. Biot.*, 2005, 67(3), 289-298, doi: http://dx.doi.org/10.1007/s00253-004-1814-0.
51. Jia X., Liu Y., Han Y., A thermophilic cell-free cascade enzymatic reaction for acetoin synthesis from pyruvate, *Scientific Reports*, 2017, 7, article number: 4333 (2017), doi: https://doi.org/10.1038/s41598-017-04684-8.
52. Johannes T., Simurdiak M. R., Zhao H., Biocatalysis, IN: Lee S. (ed.), Encyclopedia of chemical processing, Boca Raton : CRC Press, 2005, 101-101.
53. Jones D. W. C., et al., Identification of the 2-hydroxymethyl-3, 4-dihydroxypyrrolidine (or 1,4-dideoxy-1,4-iminopentitol) from *Angylocalyx boutiqueanus* and from *Arachniodes standishii*as the (2R, 3R, 4S)-isomer by the synthesis of its enantiomer, *Tetrahedron Lett.*, 1985, 26(26), 3125-3126, doi: https://doi.org/10.1016/S0040-4039(00)98635-0.
54. Junker S., et al., Complete switch of reaction specificity of an aldolase by directed evolution in vitro: Synthesis of generic aliphatic aldol products, *Angew. Chem. Int. Ed.*, 2018, 57, 10153–10157.
55. Kalyanam N., et al., L- and D-homoserine and related C_4-chiral blocks, *PharmaChem*, 2008, 7(7-8), 10-11.
56. Kapoor S., Rafiq A., Sharma S., Protein engineering and its applications in food industry, *Crit. Rev. Food. Sci.*, 2017, 57(11), 2321-2329, doi: https://doi.org/10.1080/10408398.2014.1000481.
57. Karau A., Grayson I., Amino acids in human and animal nutrition, *Adv. Biochem. Eng. Biot.*, 2014, 143, 189-228, doi: https://doi.org/10.1007/10_2014_269.
58. Koszelewski D., et al., Deracemisation of α-chiral primary amines by a one-pot, two-step cascade reaction catalysed by ω-transaminases, *Eur. J. Org. Chem.*, 2009, 2009(14), 2289-2292, doi: https://doi.org/10.1002/ejoc.200801265.
59. Kragl U., Vasić-Rački Đ., Wandrey C., Continuous production of L-tert-leucine in series of two enzyme membrane reactors, *Bioprocess eng.*, 1996, 14, 291-297
60. Kunjapur A. M., Tarasova Y., Prather K. L. J., Synthesis and accumulation of aromatic aldehydes in an engineered strain of *Escherichia coli*, *J. Am. Chem. Soc.*, 2014, 136(33), 11644-11654, doi: https://doi.org/10.1021/ja506664a.
61. Laidler K. J., Bunting, P. S., Chemical kinetics of enzyme action, Oxford : Calderon Press, 1973, 93-97.

62. Lang, K., Buehler K., Schmid A., Multistep synthesis of (*S*)-3-hydroxyisobutyric acid from glucose using *Pseudomonas taiwanensis* VLB120 B83 T7 catalytic biofilms, *Adv. Synth. Catal.*, 2015, 357(8) spec. issue: Biocatalysis, 1919-1927, doi: https://doi.org/10.1002/adsc.201500205.
63. Leuchs S., et al., Reaction engineering of biocatalytic enantioselective reduction: a case study for aliphatic ketones, *Org. Process Res. Dev.*, 2013, 17(8), 1027-1035, doi: https://doi.org/10.1021/op400117t.
64. Li C.-J., Organic reactions in aqueous media with a focus on carbon−carbon bond formations: a decade update, *Chem. Rev.* 2005, 105(8), 3095-3166, doi: https://doi.org/10.1021/cr030009u.
65. Li S., et al., Technology prospecting on enzymes: application, marketing and engineering, *Comput. Struct. Biotechnol. J.*, 2012, 2(3), e201209017, doi: https://doi.org/10.5936/csbj.201209017.
66. Liese A., Filho M. V., Production of fine chemicals using biocatalysis, *Curr. Opin. Biotech.*, 1999, 10(6), 595-603, doi: https://doi.org/10.1016/S0958-1669(99)00040-3.
67. Marx A., et al., Process for preparing methacrylic acid or methacrylic esters, 2010, US patent 2010/0291644 A1. Available at: https://patentimages.storage.googleapis.com/pdfs/9b394977f4a6b426a578/US20100291644A1.pdf (21.3.2019.).
68. McArthur IV, G. H., Fong S. S., Toward engineering synthetic microbial metabolism, *J. Biomed. Biotechnol.*, 2010, 2010, doi: http://dx.doi.org/10.1155/2010/459760.
69. Mehta A., Oeser A. M., Carlson M. G., Rapid quantitation of free fatty acids in human plasma by high-performance liquid chromatography, *J. Chromatogr. B.*, 1998, 719(1-2), 9-23, doi: https://doi.org/10.1016/S0378-4347(98)00403-4.
70. Meyer A., Pellaux R., Panke S., Bioengineering novel *in vitro* metabolic pathways using synthetic biology, *Curr. Opin. Microbiol.* 2007, 10(3), 246-253, doi: https://doi.org/10.1016/j.mib.2007.05.009.
71. Milker S., et al., Kinetic modeling of an enzymatic redox cascade *in vivo* reveals bottlenecks caused by cofactors, *ChemCatChem*, 2017, 9(17), 3420-3427, doi: https://doi.org/10.1002/cctc.201700573.
72. Molla G. S., et al., Bioreaction engineering leading to efficient synthesis of L-glyceraldehyd-3-phosphate, *Biotechnol. J.*, 2017, 12(3), 1600625, doi: https://doi.org/10.1002/biot.201600625.

73. More J. D., Finney N. S., A simple and advantageous protocol for the oxidation of alcohols with o-iodoxybenzoic acid (IBX), *Org. Lett.*, 2002, 4(17), 3001-3003, doi: https://doi.org/10.1021/ol026427n.
74. Nash R. J., et al., Iminosugars as therapeutic agents: recent advances and promising trends, *Future Med. Chem.*, 2011, 3(12), 1513-1521, doi: https://doi.org/10.4155/fmc.11.117.
75. Nestl B. M., Nebel B. A., Hauer B., Recent progress in industrial biocatalysis, *Curr. Opin. Chem. Biol.*, 2011, 15(2), 187-193, doi: https://doi.org/10.1016/j.cbpa.2010.11.019.
76. Otte K. B., Hauer B., Enzyme engineering in the context of novel pathways and products, *Curr. Opin. Biotech.*, 2015, 35, 16-22, doi: https://doi.org/10.1016/j.copbio.2014.12.011.
77. Park E.-S., Dong J.-Y., Shin J.-S., ω-Transaminase-catalyzed asymmetric synthesis of unnatural amino acids using isopropylamine as an amino donor, *Org. Biomol. Chem*., 2013, 11(40), 6929-6933, doi: https://doi.org/10.1039/C3OB40495A.
78. Park E.-S., et al., One-pot production of enantiopure alkylamines and arylalkylamines of opposite chirality catalyzed by ω-transaminase, *ChemCatChem*, 2013, 5(7), 1734-1738, doi: https://doi.org/10.1002/cctc.201300052.
79. Patel R. N., Synthesis of chiral pharmaceutical intermediates by biocatalysis, *Coordin. Chem. Rev.*, 2008, 252(5-7), 659-701, doi: https://doi.org/10.1016/j.ccr.2007.10.031.
80. Pedersen A. T., et al., Process requirements of galactose oxidase catalyzed oxidation of alcohols, *Org. Process Res. Dev.*, 2015, 19(11), 1580-1589, doi: https://doi.org/10.1021/acs.oprd.5b00278.
81. Pollard D. J., Woodley J. M., Biocatalysis for pharmaceutical intermediates: the future is now, *Trends Biotechnol.*, 2007, 25(2), 66-73, doi: https://doi.org/10.1016/j.tibtech.2006.12.005.
82. Posorske L. H., Industrial-scale application of enzymes to the fats and oil industry, *J. Am. Oil Chem. Soc.*, 1984, 61(11), 1758-1760, doi: https://doi.org/10.1007/BF02582143.
83. Price J., et al., Application of uncertainty and sensitivity analysis to a kinetic model for enzymatic biodiesel production, *IFAC Proceedings Volumes*, 2013, 46(31), 149-156, doi: https://doi.org/10.3182/20131216-3-IN-2044.00060.
84. Przybylski D., et al., Exploiting mixtures of H_2, CO_2, and O_2 for improved production of methacrylate precursor 2-hydroxyisobutyric acid by engineered *Cupriavidus necator* strains, *Appl. Microbiol. Biot*. 2018, 99(5), 2131-2145, doi: https://doi.org/10.1007/s00253-014-6266-6.

85. Pyo S.-H., et al., A new route for the synthesis of methacrylic acid from 2-methyl-1,3-propanediol by integrating biotransformation and catalytic dehydration, *Green Chem.*, 2012, 14(7), 1942-1948, doi: https://doi.org/10.1039/C2GC35214A.
86. Pyo S.-H., et al., Self- and cross-aldol condensation of propanal catalyzed by anion-exchange resins in aqueous media, *Org. Process Res. Dev.*, 2011, 15(3), 631-637, doi: https://doi.org/10.1021/op200004p.
87. Raran-Kurussi S., Waugh D.S., The ability to enhance the solubility of its fusion partners is an intrinsic property of maltose-binding protein but their folding is either spontaneous or chaperone-mediated, PloS one, 2012, 7, e49589.
88. Resch V., et al., Novel carbon–carbon bond formations for biocatalysis, *Curr. Opin. Biotech.*, 2011, 22(6), 793-799, doi: https://doi.org/10.1016/j.copbio.2011.02.002.
89. Ringborg R. H., Woodley J. M., The application of reaction engineering to biocatalysis, *Reaction Chemistry & Engineering*, 2016, 1(1), 10-22, doi: https://doi.org/10.1039/C5RE00045A.
90. Ringborg R. H., Woodley J. M., The application of reaction engineering to biocatalysis, *React. Chem. Eng.*, 2016, 1, 10-22, doi: https://doi.org/10.1039/c5re00045a.
91. Rios-Solis L., et al., Modelling and optimisation of the one-pot, multi-enzymatic synthesis of chiral amino-alcohols based on microscale kinetic parameter determination, *Chem. Eng. Sci.* 2015, 122, 360-372, doi: https://doi.org/10.1016/j.ces.2014.09.046.
92. Rocha-Martin J., et al., New biotechnological perspectives of a NADH oxidase variant from *Thermus thermophilus* HB27 as NAD^+-recycling enzyme, *BMC Biotechnol.*, 2011, 11:101, doi: https://doi.org/10.1186/1472-6750-11-101.
93. Santacoloma P. A., et al., Multienzyme-catalyzed processes: next-generation biocatalysis, *Org. Process Res. Dev.*, 2011, 15(1), 203-212, doi: https://doi.org/10.1021/op1002159.
94. Savile C. K., et al., Biocatalytic asymmetric synthesis of chiral amines from ketones applied to sitagliptin manufacture, *Science*, 2010, 329(5989), 305-309, doi: https://doi.org/10.1126/science.1188934.
95. Scherkus C., et al., Kinetic insights into ϵ-caprolactone synthesis: improvement of an enzymatic cascade reaction, *Biotechnol. Bioeng.*, 2017, 114(6), 1215-1221, doi: https://doi.org/10.1002/bit.26258.
96. Schmid F., Baro A., Laschat S., Strategies for the synthesis of deoxypropionates, *Synthesis*, 2017, 49, 237-251.

97. Schmidt N. G., Eger E., Kroutil W., Building bridges: biocatalytic C–C-bond formation toward multifunctional products, *ACS Catalysis*, 2016, 6(7), 6286-4311, doi: https://doi.org/10.1021/acscatal.6b00758.
98. Schoemaker H. E., Mink D., Wubbolts M. G., Dispelling the myths–biocatalysis in industrial synthesis, *Science*, 2003, 299(5613), 1694-1697, doi: https://doi.org/10.1126/science.1079237.
99. Schrittwieser J. H., et al., Artificial biocatalytic linear cascades for preparation of organic molecules, *Chem. Rev.*, 2018, 118(1), 270-348, doi: https://doi.org/10.1021/acs.chemrev.7b00033.
100. Scofield A. M., et al., Castanospermine and other polyhydroxy alkaloids as inhibitors of insect glycosidases, *Comparative Biochemistry and Physiology Part A: Physiology*, 1995, 112(1), 187-196, doi: https://doi.org/10.1016/0300-9629(95)00070-N.
101. Segel I. H., Enzyme kinetics: behavior and analysis of rapid equilibrium and steady-state enzyme systems, New York, USA : Wiley – Interscience, 1975, 465-473.
102. Sheldon R. A., Woodley J. M., Role of biocatalysis in sustainable chemistry, *Chem. Rev.*, 2018, 118(2), 801-838, doi: https://doi.org/10.1021/acs.chemrev.7b00203.
103. Sivashanmugam A., et al., Practical protocols for production of very high yields of recombinant proteins using *Escherichia coli*, *Protein Sci*. 2009, 18(5), 936-948, doi: http://doi.org/10.1002/pro.102.
104. Sudar M., et al., A new concept for production of (3*S*,4*R*)-6-[(benzyloxycarbonyl)amino]-5,6-dideoxyhex-2-ulose, a precursor of D-fagomine, *RSC Adv.*, 2015, 5(85), 69819-69828, doi: http://doi.org/10.1039/C5RA14414K.
105. Sudar M., et al., Aldol addition of dihydroxyacetone to N-Cbz-3-aminopropanal catalyzed by two aldolases variants in microreactors, *Enzyme Microb. Tech.*, 2013, 53(1), 38-48, doi: https://doi.org/10.1016/j.enzmictec.2013.03.013.
106. Sudar M., et al., Coenzyme regeneration catalyzed by NADH oxidase from *Lactococcus lactis*, *Biochem. Eng. J.*, 2014, 88, 12-18, doi: https://doi.org/10.1016/j.bej.2014.04.001.
107. Sudar M., et al., Mathematical model of the MenD-catalyzed 1,4-addition (Stetter reaction) of α-ketoglutaric acid to acrylonitrile, *J. Biotechnol.*, 2018, 268, 71-80, doi: https://doi.org/10.1016/j.jbiotec.2018.01.013.

108. Sugiyama M., et al., D-fructose-6-phosphate aldolase-catalyzed one-pot synthesis of iminocyclitols, *J. Am. Chem. Soc.*, 2007, 129(47), 14811-14817, doi: https://doi.org/10.1021/ja073911i.

109. Sun H., et al., Biocatalysis for the synthesis of pharmaceuticals and pharmaceutical intermediates, *Bioorgan. Med. Chem.*, 2018, 26(7), 1275-1284, doi: https://doi.org/10.1016/j.bmc.2017.06.043.

110. Truppo M. D., Turner N. J., Rozzell J. D., Efficient kinetic resolution of racemic amines using a transaminase in combination with an amino acid oxidase, *Chem. Commun.*, 2009, 0(16), 2127-2129, doi: https://doi.org/10.1039/B902995H.

111. Tufvesson P., et al., Experimental determination of thermodynamic equilibrium in biocatalytic transamination, *Biotechnol. Bioeng.*, 2012, 114(6), 2159-62, doi: https://doi.org/10.1002/bit.24472.

112. Vasić-Rački Đ., et al., Modeling of reaction kinetics for reactor selection in the case of L-erythrulose synthesis, *Bioproc. Biosyst. Eng.*, 2003, 25(5), 285-290, doi: https://doi.org/10.1007/s00449-002-0312-y.

113. Vasić-Rački, Đ., Findrik Z., Vrsalović Presečki A., Modelling as a tool of enzyme reaction engineering for enzyme reactor development, *Appl. Microbiol. Biot.*, 2011, 91, 845-857, doi: https://doi.org/10.1007/s00253-011-3414-0.

114. Vasić-Rački, Đ., Kragl U., Liese A., Benefits of enzyme kinetics modelling, *Chem. Biochem. Eng. Q.*, 2003, 17(1), 7-18.

115. Watson A. A., et al., Polyhydroxylated alkaloids - natural occurrence and therapeutic applications, *Phytochemistry*, 2001, 56(3), 265-295, doi: https://doi.org/10.1016/S0031-9422(00)00451-9.

116. Weckbecker A., Gröger H., Hummel W., Regeneration of nicotinamide coenzymes: principles and applications for the synthesis of chiral compounds, *Adv. Biochem. Eng. Biot.* 2010, 120, 195-242, doi: https://doi.org/10.1007/10_2009_55.

117. Wendisch V. F., et al., The flexible feedstock concept in industrial biotechnology: metabolic engineering of *Escherichia coli, Corynebacterium glutamicum, Pseudomonas, Bacillus* and yeast strains for access to alternative carbon sources, *J. Biotechnol.*, 2016, 234, 139-157, doi: https://doi.org/10.1016/j.jbiotec.2016.07.022.

118. Wichmann R., Vasić-Rački Đ., Cofactor regeneration at the lab scale, IN: Kragl U., Scheper T. (ed.), *Technology Transfer in Biotechnology*, *Adv. Biochem. Eng. Biot*., 2005, 92, 225-260, doi: https://doi.org/10.1007/b98911.

119. Willke T., Methionine production - a critical review, *Appl. Microbiol. Biot.*, 2014, 98(24), 9893-9914, doi: https://doi.org/10.1007/s00253-014-6156-y.

120. Windle C. L., et al., Engineering aldolases as biocatalysts, *Curr. Opin. Chem. Biol.*, 2014, 19(100), 25-33, doi: https://doi.org/10.1016/j.cbpa.2013.12.010.

121. Wittmann C., Liao J., Industrial biotechnology : products and processes, Weinheim : Wiley-VCH Verlag GmbH, 2017.

122. Wohlgemuth R., Interfacing biocatalysis and organic synthesis, *J. Chem. Technol. Biot.*, 2007, 82(12), 1055-1062, doi: https://doi.org/10.1002/jctb.1761.

123. Woodley J. M., Integrating protein engineering with process design for biocatalysis, *Philos. T. Roy. Soc. A.*, 2018, 376(2110), doi: https://doi.org/10.1098/rsta.2017.0062.

124. Woodley J. M., Protein engineering of enzymes for process applications, *Curr. Opin. Chem. Biol.*,2013, 17(2), 310-316, doi: https://doi.org/10.1016/j.cbpa.2013.03.017.

125. Woodyer R. D., Johannes T. W., Zhao H., Regeneration of cofactors for enzyme biocatalysis, IN: Pandey A., et al. (ed.), Enzyme technology, Springer Science + Business Media, Inc.; Asiatech Publishers : Delhi, 2006, 85-105.

126. Yokota A., Ikeda M. (ed.), Amino acid fermentation, Tokyo : Springer Verlag, 2017.

127. Zaks A., Industrial biocatalysis, *Curr. Opin. Chem. Biol.*, 2001, 5(2), 130-136, doi: https://doi.org/10.1016/S1367-5931(00)00181-2.

128. Zhong C., Wei P., Percival Zhang Y.-H., A kinetic model of one-pot rapid biotransformation of cellobiose from sucrose catalyzed by three thermophilic enzymes, *Chem. Eng. Sci.*, 2017, 161, 159-166, doi: https://doi.org/10.1016/j.ces.2016.11.047.

10 APPENDIX

Table 10.1 Apparatus used in this doctoral thesis.

SYNTHESIS OF METHACRYLIC ACID PRECURSOR	SYNTHESIS OF L-HOMOSERINE	SYNTHESIS OF IMINOSUGAR PRECURSOR
Laboratory shaker (Vibromix 203 EVT, Tehtnica, Slovenia)	Laboratory shaker (Vibromix 203 EVT, Tehtnica, Slovenia)	Äkta prime plus system for protein purification (GE Healthcare, Sweden)
Orbital shaker (PSU-10i, Biosan, Latvia)	Laboratory shaker (Thermomixer C, Eppendorf, Germany)	Cleanroom Technology (Klimaoprema, Croatia)
Ultra-low freezer (Simon, Croatia)	Ultra-low freezer (Simon, Croatia)	Ultra-low freezer (Simon, Croatia)
Lyophilizer (FreeZone 1, Labconco, USA)	Lyophilizer (FreeZone 1, Labconco, USA)	Orbital shaker (PSU-10i, Biosan, Latvia)
Ultrasound (Sonopuls HD 3100, horn type SH 70G, 20 kHz, Bandelin GmbH, Germany) and ultrasound probes (MS 73, 3 mm tip)	Ultrapure water system (NIRO-VV-UV-UF, Nirosta, Croatia)	Refrigerated Incubator Shaker (Innova 4330, New Brunswick Scientific, USA)
High performance liquid chromatography (HPLC) (degasser DGU-20A3; pumps LC-20AT and LC-10AT; injector SIL-20AC; UV-VIS detector SPD-10A; communications bus module CBM-20A; column oven CTO-20AC, Shimadzu, Japan)	High performance liquid chromatography (HPLC) (degasser DGU-20A3; pumps LC-20AT and LC-10AT; injector SIL-20AC; UV-VIS detector SPD-10A; communications bus module CBM-20A; column oven CTO-20AC, Shimadzu, Japan)	High performance liquid chromatography (HPLC) (degasser DGU-20A3; pumps LC-20AT and LC-10AT; injector SIL-20AC; UV-VIS detector SPD-10A; communications bus module CBM-20A; column oven CTO-20AC, Shimadzu, Japan)
Liquid chromatography mass spectrometry (LCMS-2020, single quadrupole instrument, Shimadzu, Japan)	Centrifuge with cooling (Hettich Universal 320R, Germany)	Gas chromatograph (GC) (GC-2014; autoinjector AOC-20i, Shimadzu, Japan; gas generator 9150, Parker, USA)
Homogenizer (MS2 Minishaker, Ika-Combing, Germany; V-1 plus, Biosan, Latvia)	Homogenizer (MS2 Minishaker, Ika-Combing, Germany; V-1 plus, Biosan, Latvia)	Homogenizer (MS2 Minishaker, Ika-Combing, Germany; V-1 plus, Biosan, Latvia)
Spectrophotometers (UV 1601 and UV 1800, Shimadzu, Japan)	pH meter (Lab 860, Schott Instruments Analytics, Germany)	Laboratory shaker (Vibromix 203 EVT, Tehtnica, Slovenia)
Pump (PHD 4400 Syringe Pump Series, Harvard Apparatus, USA) and pump syringes (PHD 4400 Syringe Pump Series 8 cm^3, Harvard Apparatus, USA)	Pump (PHD 4400 Syringe Pump Series, Harvard Apparatus, USA) and pump syringes (PHD 4400 Syringe Pump Series 8 cm^3, Harvard Apparatus, USA)	Liquid chromatography mass spectrometry (LCMS-2020, single quadrupole instrument, Shimadzu, Japan)
Analytical balance (AUW120, Shimadzu, Japan)	Analytical balance (AUW120, Shimadzu, Japan)	Analytical balance (AUW120, Shimadzu, Japan)
Rotary evaporator (Hei-VAP Value, Heidolph, Germany)		Rotary evaporator (Hei-VAP Value, Heidolph, Germany)
Centrifuge with cooling (Hettich Universal 320R, Germany)		Centrifuge with cooling (Hettich Universal 320R, Germany)
High pressure steam sterilizer (Sutjeska, Yugoslavia)		High pressure steam sterilizer (Sutjeska, Yugoslavia)
pH meter (Lab 860, Schott Instruments Analytics, Germany)		pH meter (Lab 860, Schott Instruments Analytics, Germany)
Ultrapure water system (NIRO-VV-UV-UF, Nirosta, Croatia)		Ultrapure water system (NIRO-VV-UV-UF, Nirosta, Croatia)
		Ultrasound (Sonopuls HD 3100, horn type SH 70G, 20 kHz, Bandelin GmbH, Germany) and ultrasound probes (MS 73, 3 mm tip)
		Oxygen electrode (FireSting O2, PyroScience GmbH, Aachen, Germany)
		Thermostat water bath (Termomix 1420, Braun, Germany)
		Spectrophotometers (UV 1601 and UV 1800, Shimadzu, Japan)

A

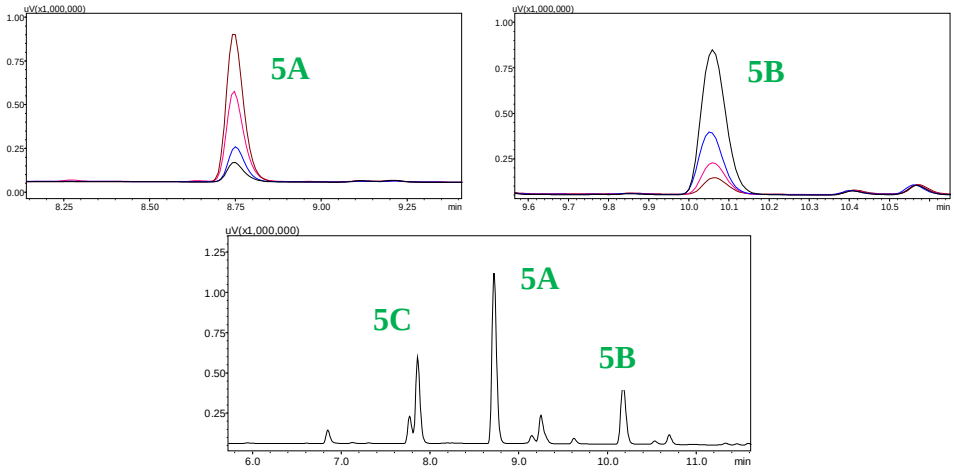

B

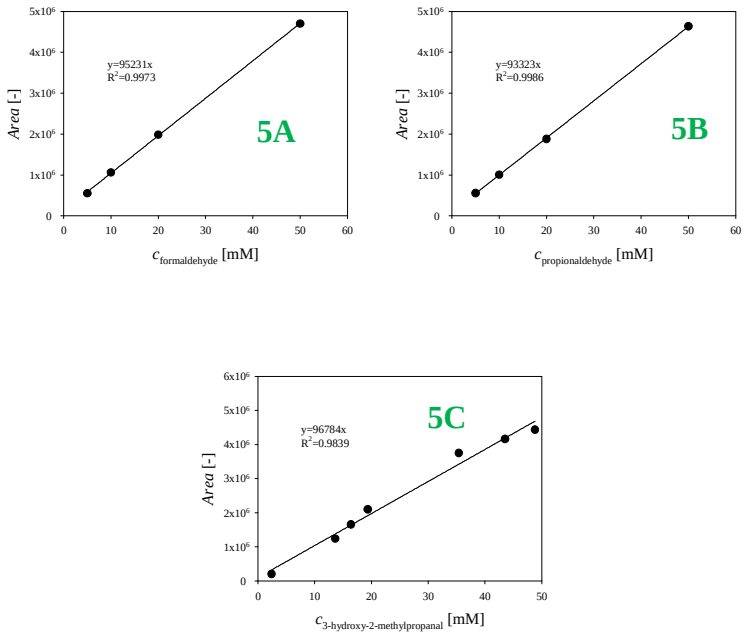

Figure 10.2 HPLC analysis (method B from Table 5.2): A. chromatograms of **5A**, **5B** and **5G**, B. calibration curves for **5A**, **5B** and **5G**.

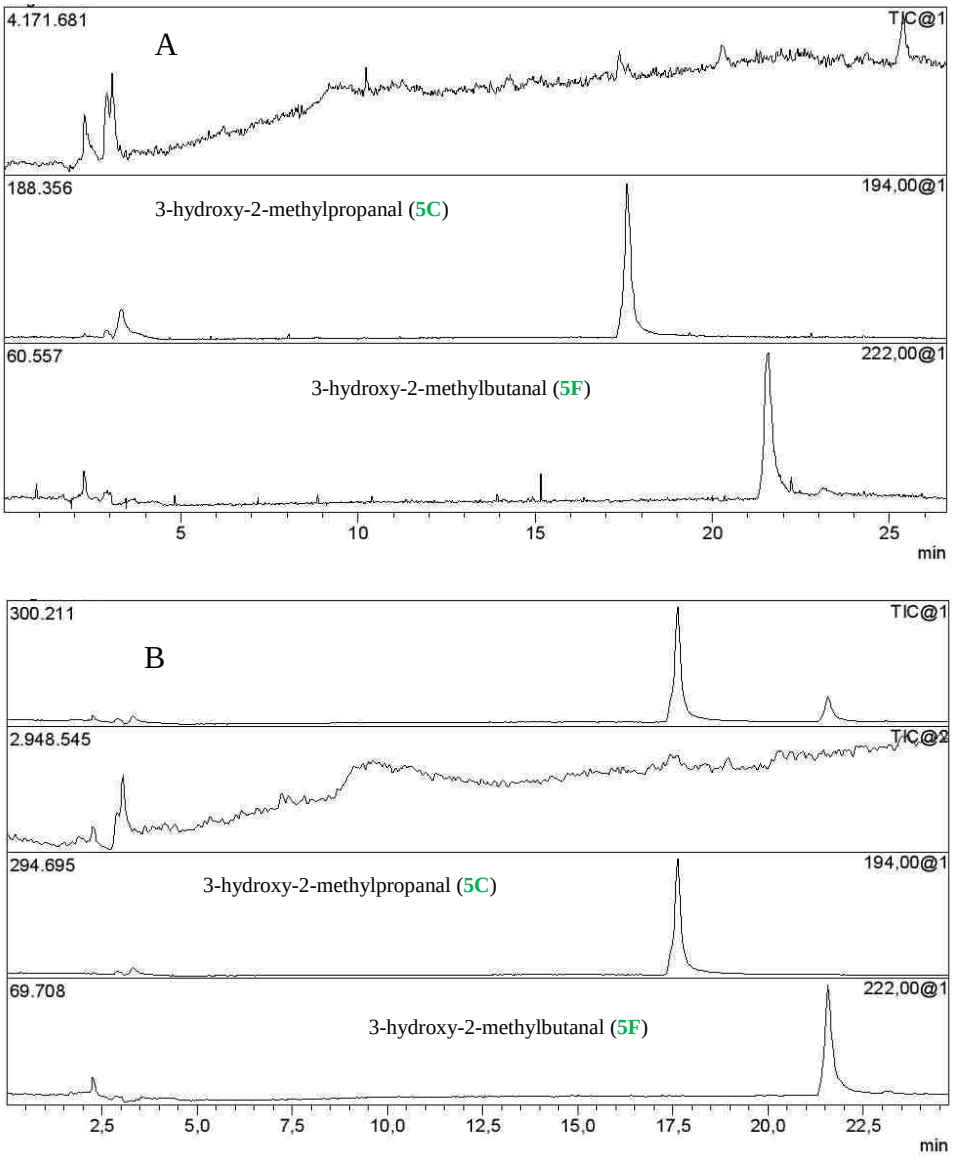

Figure 10.3 Chromatograms of **5C** and **5F** analysed by LC-MS. A. TIC chromatogram, B. SIM chromatogram.

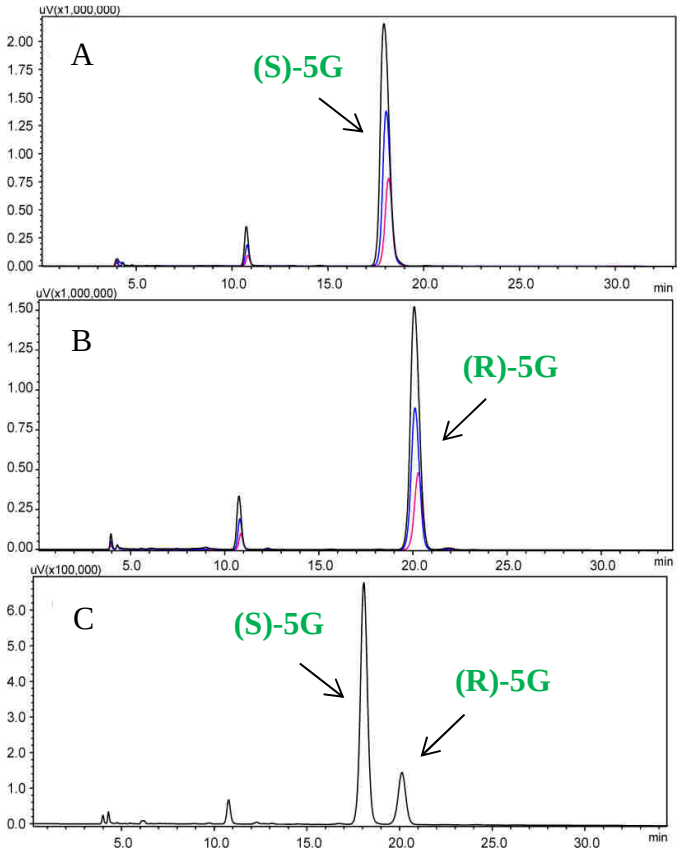

Figure 10.4 Analysis of 4-bromophenacyl-*β*-hydroxyisobutyrate on chiral HPLC column A. Standard solutions of (*S*)-4-bromophenacyl-*β*-hydroxyisobutyrate (RT 17.966 min), B. Standard solutions of (*R*)-4-bromophenacyl-*β*-hydroxyisobutyrate (RT 20.413 min), C. Analysis of a sample obtained by enzymatic oxidation (ee 51%).

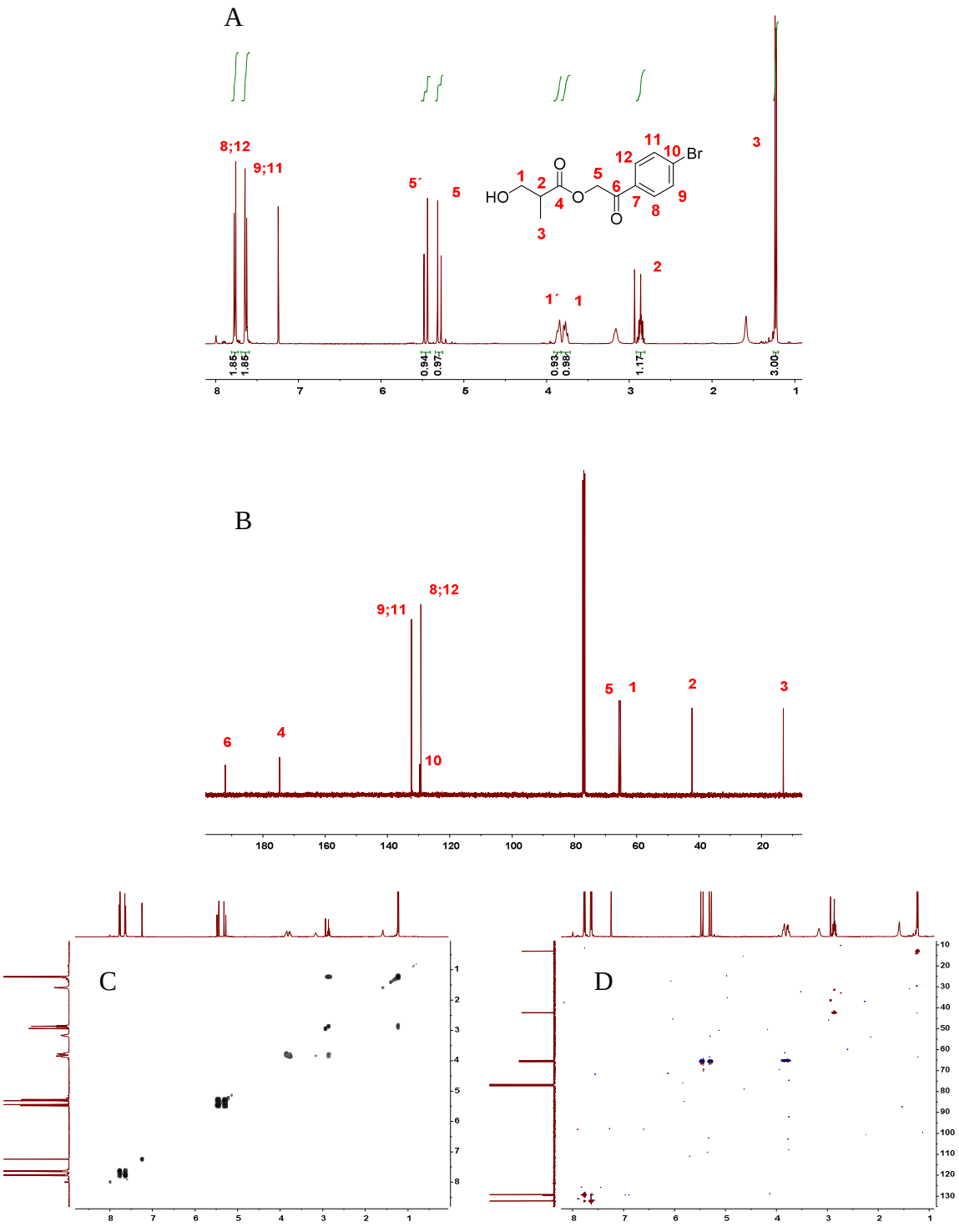

Figure 10.5 NMR analysis of **5G** results. A. ^{1}H NMR spectrum. B. ^{13}C spectrum. C. 2D COSY spectrum. D. 2D HSQC spectrum.

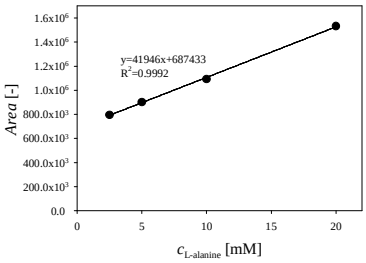
y=41946x+687433
R²=0.9992
Area [-]
c L-alanine [mM]

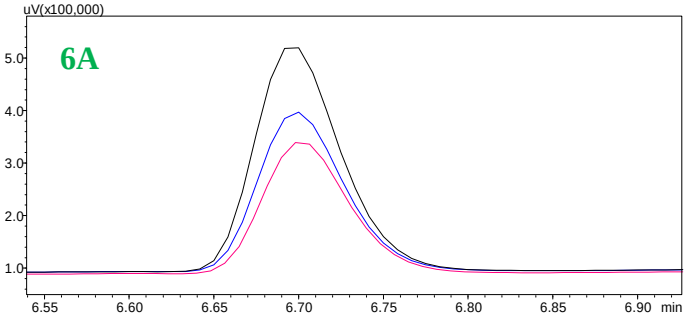
uV(x100,000)
6A
min

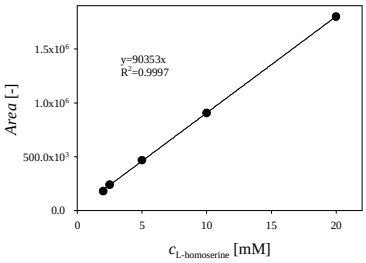
y=90353x
R²=0.9997
Area [-]
c L-homoserine [mM]

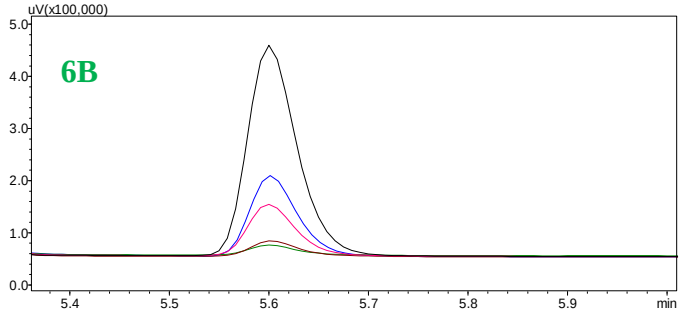
uV(x100,000)
6B
min

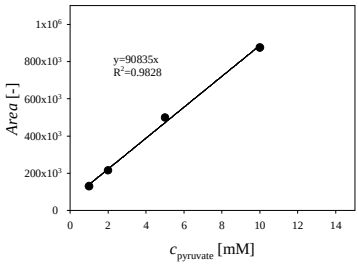
y=90835x
R²=0.9828
Area [-]
c pyruvate [mM]

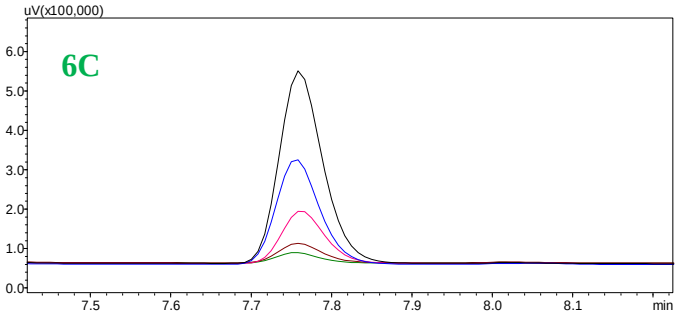
uV(x100,000)
6C
min

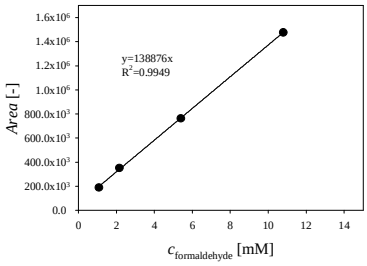
y=138876x
R²=0.9949
Area [-]
c formaldehyde [mM]

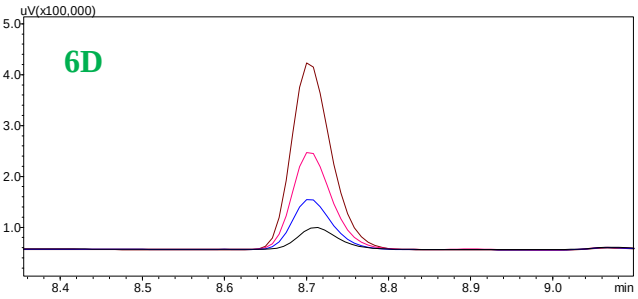
uV(x100,000)
6D
min

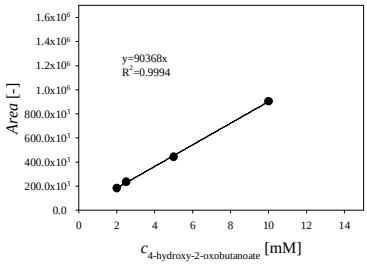
y=90368x
R²=0.9994
Area [-]
c 4-hydroxy-2-oxobutanoate [mM]

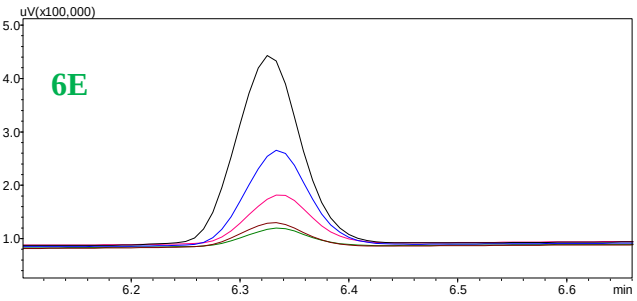
uV(x100,000)
6E
min

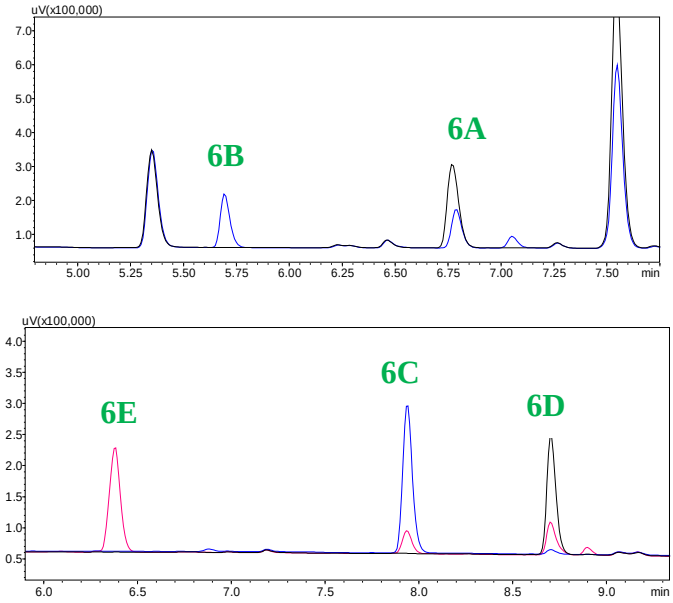

Figure 10.6 Chromatograms of **6A**, **6B**, **6C**, **6D** and **6E** analysed by HPLC using Method B from Table 6.2.

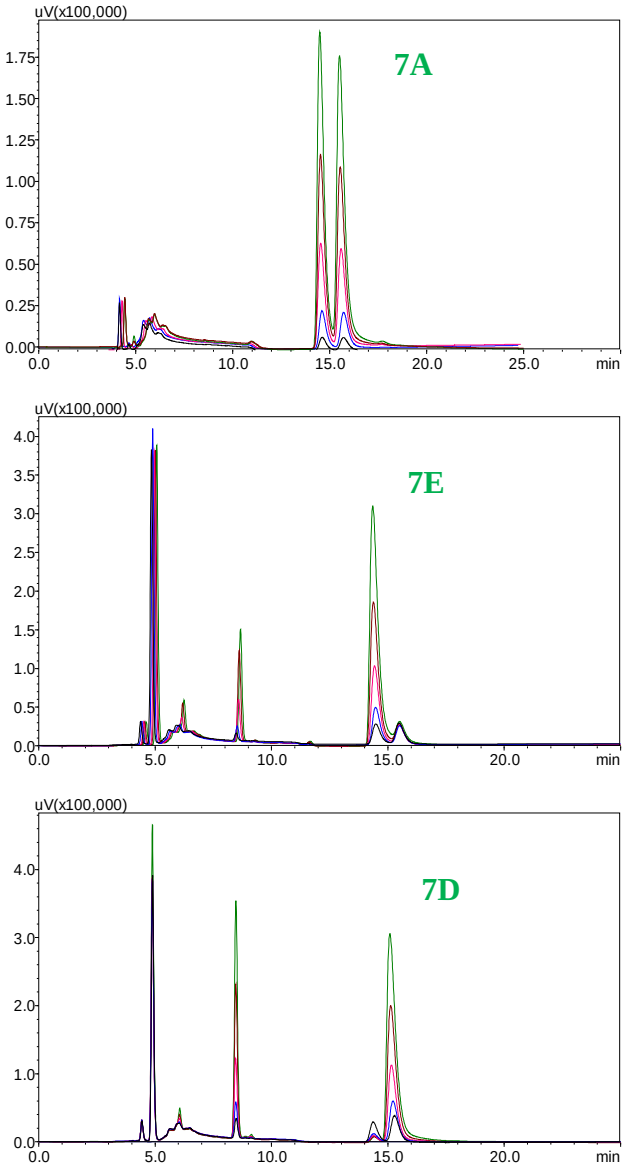

Figure 10.7 Chromatograms of **7A**, **7E** and **7D** analysed on chiral HPLC column with UV detection.

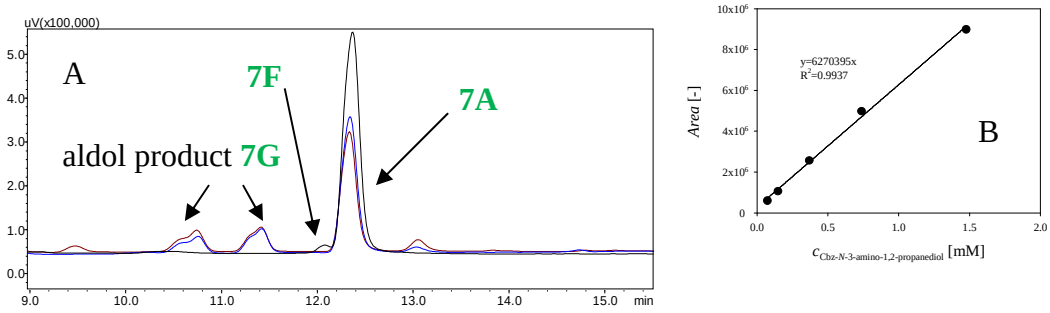

Figure 10.8 Chromatograms from the cascade reaction: **7G**, **7F**, **7A** analysed by HPLC with LiChrospher (Phenomenex) column (A) and calibration curve for **7A** (B).

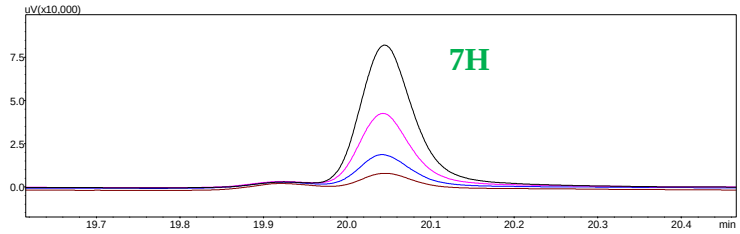

Figure 10.9 Chromatograms from the cascade reaction: **7H** analysed by GC.

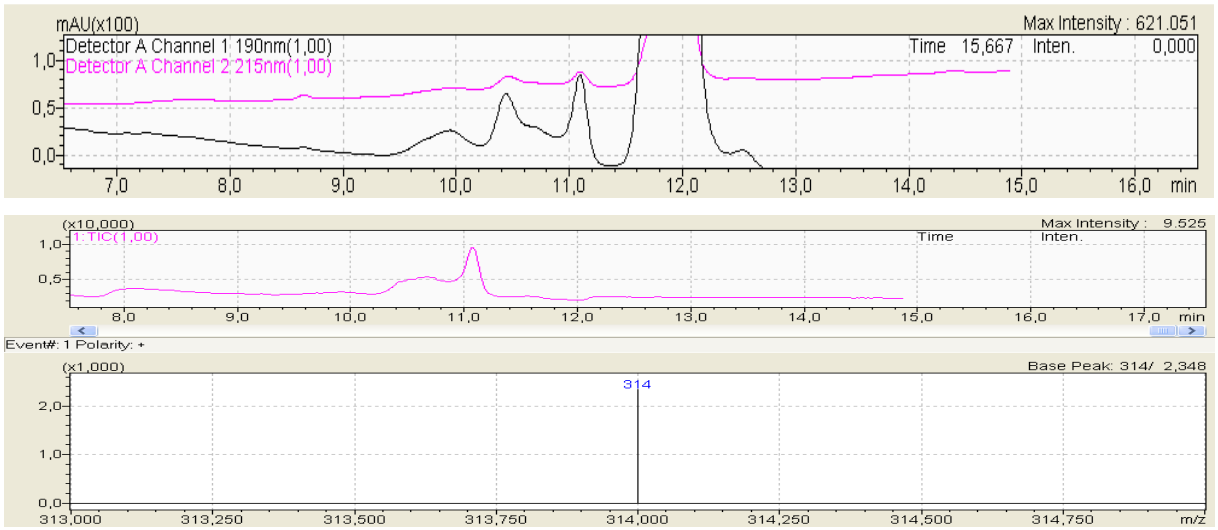

Figure 10.10 LC-MS analysis and confirmation of aldol adduct **7G** peaks (Single Ion Monitoring mode: M = 314 gmol^{-1}).

SYMBOLS

ABS	absorbance, -
c	molar concentration, mmol dm^{-3} (mM)
d	diameter, mm
k_d	operational stability decay rate constant, h^{-1}
k	kinetic constant of the first order, min^{-1}
K_i	inhibition constant, mmol dm^{-3} (mM)
K_m	Michaelis constant, mmol dm^{-3} (mM)
m	mass, g
Q_v	volume productivity in the fed-batch reactor, g dm^{-3} d^{-1}
q	volume flow rate, cm^3 h^{-1}
r	reaction rate, mmol dm^{-3} min^{-1}
$S.A.$	specific activity, U mg^{-1}
t	reaction time, min
$t_{1/2}$	half-life time, h
$V.A.$	volume activity, U cm^{-3} (U mL^{-1})
V_{enz}	enzyme volume, cm^3
V_m	maximum reaction rate, U mg^{-1}
V_r	reactor volume, cm^3 (mL)
X	substrate conversion, % or –
Y	reaction yield, %
γ	mass concentration, mg cm^{-3} (mg mL^{-1})

BIOGRAPHY

Morana Česnik [redacted] After finishing gymnasium Lucijan Vranjanin in 2006, she attended undergraduate study Environmental Engineering at the Faculty of Chemical Engineering and Technology, University of Zagreb. In 2009 she enrolled the same graduate study. In 2011 she spent a month at Veszprém, Hungary working on a project Industrial Biotransformation in Unconventional Media at the University of Pannonia. The same year she won Dean's award for notable scientific work and was acknowledged as the most successful student of her Master Study presented at Faculty 92. anniversary celebration. After finishing her study, she received *magna cum laude* diploma and gained academic title Master Engineer of Environmental Engineering.

After graduation, she started working at INA oil industry as an Engineer of Technology in oil refinery in Sisak. She spent almost 4 years in Operational Production Management Department mainly coordinating process unit capacities, controlling quality of process flows and blending final refinery products.

In 2014 she enrolled university specialist postgraduate study programme MBA at the Faculty of Economics and Business, University of Zagreb, which she successfully completed in 2018 and got academic title of University Specialist in Business Administration – MBA. She published her thesis results as a review article in Proceedings of the Faculty of Economics and Business in Zagreb.

In May 2015 she started working at the Department of Reaction Engineering and Catalysis at the Faculty of Chemical Engineering and Technology, University of Zagreb as an assistant in the Horizon 2020 project Carbazymes. The same year she enrolled postgraduate doctoral study Chemical Engineering and Applied Chemistry at the Faculty of Chemical Engineering and Technology, University of Zagreb under the mentorship of prof. Zvjezdana Findrik Blažević. During her research, she has published the results of her work in one scientific paper in a journal cited in Current Contents data base, one paper in a Journal cited in tertiary database and has one paper in the publication process. Additionally, she published one review paper in a journal cited in the Web of Science database non-related to the topic of doctoral work. She participated in five international and national scientific conferences, three international summer schools and four workshops. In 2016 she spent one and a half month at the Institute for the Advanced Chemistry in Barcelona, Spain where she worked under the mentorship of prof. Pere Clapés.

Scientific papers

Česnik M., Sudar M., Roldan R., Hernandez K., Parella T., Clapés P., Charnock S., Vasić-Rački Đ., Findrik Blažević Z., Model-based optimization of the enzymatic aldol addition of propanal to formaldehyde; a first step towards enzymatic synthesis of 3-hydroxybutyric acid, *Chem. Eng. Res. Des.*, 2019, 150, 140-152, doi: https://doi.org/10.1016/j.cherd.2019.06.025.

Milčić N., **Česnik M.**, Sudar M., Findrik Blažević Z., Primjena matematičkog modeliranja u razvoju enzimskih kaskadnih reakcija, *Kem. Ind.*, 2019 (accepted for publishing), doi: https://doi.org/10.15255/KUI.2019.035.

Česnik M., Sudar M., Hernandez K., Clapés P., Charnock S., Vasić-Rački Đ., Findrik Blažević Z., Cascade enzymatic synthesis of L-homoserine – mathematical modeling as a tool for process optimization and design (in review).

Review

Česnik M., Findrik Blažević Z., Vuković Domanovac M., Povećanje učinkovitosti bioremedijacije na razini gena, *Kem. Ind.*, 2019, 68(1-2), 23-30, doi: https://doi.org/10.15255/KUI.2018.031.

Scientific conferences

1. **Česnik M.**, Švarc A., Sudar M., Vrsalović Presečki A., Vasić-Rački Đ., Findrik Blažević Z., Intermediate isolation in the synthesis of statin side chains, XI Meeting of Young Chemical Engineers, Zagreb, 2016.
2. Švarc A., **Česnik M.**, Sudar M., Vrsalović Presečki A., Vasić-Rački Đ., Findrik Blažević Z., The investigation of the stability of 2- deoxyribose-5-phosphate aldolase, XI Meeting of Young Chemical Engineers, Zagreb, 2016.
3. Findrik Blažević Z., **Česnik M.**, Vasić-Rački Đ., Hernández K., Clapés P., Optimization of enzyme catalysed aldol addition of propanal and formaldehyde, 13th International Symposium on Biocatalysis and Biotransformations, Budapest, 2017.
4. **Česnik M.**, Sudar M., Vasić-Rački Đ., Clapés P., Findrik Blažević Z., Enzymatic cascade reaction for the synthesis of imino sugar precursors, 13th International Symposium on Biocatalysis and Biotransformations, Budapest, 2017.

5. **Česnik M.**, Sudar M., Vasić-Rački Đ., Clapés P., Findrik Blažević Z., Enzymatic cascade reaction for the synthesis of an imino aldol adduct: oxido-reduction coupled with aldol addition, 25th Croatian Meeting of Chemists and Chemical Engineers, Poreč, 2017.
6. Findrik Blažević Z., Sudar M., Müller M., **Česnik M.**, Clapés P., Vasić-Rački Đ., Kinetic models and optimization of enzymatic processes, 6th Novel Enzymes, Darmstadt, 2018.
7. **Česnik M.**, Sudar M., Roldan R., Hernández K., Clapés P., Vasić-Rački Đ., Findrik Blažević Z., Mathematical model based optimization of enzymatic aldol addition of propanal to formaldehyde, European congress of Biotechnology, Gemeve, 2018.
8. **Česnik M.**, Skendrović D., Sudar M., Vasić-Rački Đ., Roldan R., Hernández K., Clapés P., Szekrenyi A., Fessner W-D., Findrik Blažević Z., Aldolase comparison in enzymatic aldol addition, XII Meeting of Young Chemical Engineers, Zagreb, 2018.

International summer schools

1. **Česnik M.**, Sudar M., Vasić-Rački Đ., Romo J. M., Clapés P., Findrik Blažević Z., Cbz-*N*-3-amino-1,2-propanediol oxidation with horse liver alcohol dehydrogenase, Systems Biocatalysis, Siena, 2016.
2. **Česnik M.**, Sudar M., Vasić-Rački Đ., Roldan R., Hernández K., Clapés P., Findrik Blažević Z., Mathematical model development of enzyme catalysed aldol addition, Technical approaches to the study of extremophiles, Alicante, 2017.
3. **Česnik M.**, Vasić-Rački Đ., Roldan R., Hernández K., Clapés P., Findrik Blažević Z., Enzyme catalysed aldol addition of propanal and formaldehyde, Biocatalysis as key enabling technology, Siena, 2017.